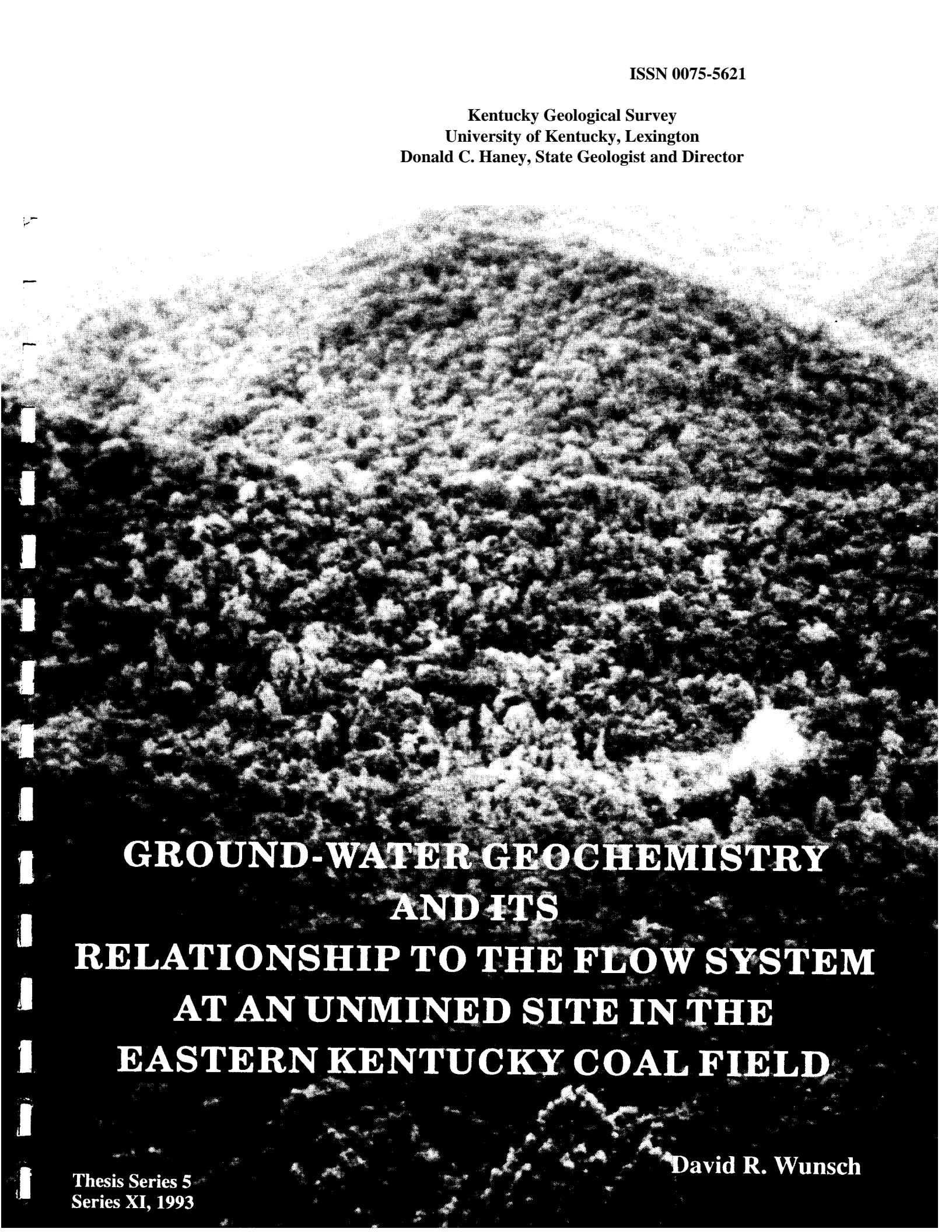


ISSN 0075-5621

Kentucky Geological Survey
University of Kentucky, Lexington
Donald C. Haney, State Geologist and Director



**GROUND-WATER GEOCHEMISTRY
AND ITS
RELATIONSHIP TO THE FLOW SYSTEM
AT AN UNMINED SITE IN THE
EASTERN KENTUCKY COAL FIELD**

David R. Wunsch

Thesis Series 5
Series XI, 1993

ISSN 0075-5621

**Kentucky Geological Survey
University of Kentucky, Lexington
Donald C. Haney, State Geologist and Director**

**GROUND-WATER GEOCHEMISTRY AND ITS
RELATIONSHIP TO THE FLOW SYSTEM AT AN
UNMINED SITE IN THE EASTERN KENTUCKY
COAL FIELD**

David R. Wunsch

**Thesis Series 5
Series X1, 1993**

DISCLAIMER

The Kentucky Geological Survey provides online versions of its publications as a public service. Publications are provided as Adobe PDF (portable document format) files. Hard-copy versions are available for purchase by contacting the Survey at:

Kentucky Geological Survey
Publication Sales Office
228 Mining and Mineral Resources Building
University of Kentucky
Lexington, Kentucky 40506-0107

Phone: 606-257-5500

Fax: 606-257-1147

Selected KGS reports published before 1999 have been scanned and converted to PDF format. Scanned documents may not retain the formatting of the original publication. In addition, color may have been added to some documents to clarify illustrations; in these cases, the color does not appear in the original printed copy of the publication. Every effort has been made to ensure the integrity of the text. KGS maps and charts are supplied either whole or in part and some are too large to be printed on most plotters. Open-file reports are reproduced from the best available copy provided by the author, and have not undergone KGS technical or editorial review.

The Kentucky Geological Survey disclaims all warranties, representations, or endorsements, expressed or implied, with regard to the information accessed from, or via, this server or the Internet.

UNIVERSITY OF KENTUCKY

Charles T. Wethington, Jr., President
Linda J. Magid, Vice President for Research and
Graduate Studies
Jack Supplee, Director, Fiscal Affairs and Sponsored
Project Administration

KENTUCKY GEOLOGICAL SURVEY ADVISORY BOARD

Steve Cawood, Chairman, Pineville
Larry R. Finley, Henderson
Hugh B. Gabbard, Richmond
Kenneth Gibson, Madisonville
Wallace W. Hagan, Lexington
Phil M. Miles, Lexington
W. A. Mossbarger, Lexington
Ralph Palmer, Winchester
Henry A. Spalding, Hazard
Ralph N. Thomas, Owensboro
George H. Warren, Jr., Owensboro
David A. Zegeer, Lexington

KENTUCKY GEOLOGICAL SURVEY

Donald C. Haney, State Geologist and Director
John D. Kiefer, Assistant State Geologist for Administration
James C. Cobb, Assistant State Geologist for Research

ADMINISTRATIVE DIVISION

Personnel and Finance Section:

James L. Hamilton, Administrative Staff Officer II
Roger S. Banks, Account Clerk V

Clerical Section:

Jody L. Fox, Staff Assistant VI
Regina A. Gibson, Staff Assistant VII
Shirley D. Dawson, Staff Assistant V
Eugenia E. Kelley, Staff Assistant V
Juanita G. Smith, Staff Assistant V, Henderson Office

Publications Section:

Donald W. Hutcheson, Head
Margaret Luther Smath, Geologic Editor III
Terry D. Hounshell, Chief Cartographic Illustrator
Richard A. Smath, Geologist III, ESIC Coordinator
Robert C. Holladay, Principal Drafting Technician
Michael L. Murphy, Drafting Technician
William A. Briscoe, III, Publication Sales Supervisor
Kenneth G. Otis, Stores Worker

GEOLOGICAL DIVISION

Coal and Minerals Section:

James C. Cobb, Head
Garland R. Dever, Jr., Geologist VII

Donald R. Chesnut, Jr., Geologist V
Cortland F. Eble, Geologist V
David A. Williams, Geologist V, Henderson Office
Warren H. Anderson, Geologist IV
Gerald A. Weisenfluh, Geologist IV
Stephen F. Greb, Geologist III
Robert Andrews, Geologist I
Dean D. Sheets, Assistant Geologist

Petroleum and Stratigraphy Section:

James A. Drahovzal, Head
Martin C. Noger, Geologist VII
Terence Hamilton-Smith, Geologist V
Patrick J. Gooding, Geologist IV
David C. Harris, Geologist IV
Brandon C. Nuttall, Geologist IV
Joseph F. Meglen, Geologist II
Matthew Humphreys, Geologist I
Mara Chen, Post-Doctoral Scholar
James B. Harris, Post-Doctoral Scholar
Robert R. Daniel, Laboratory Technician B
David E. McFadden, Senior Laboratory Assistant
Robyn A. Johnson, Staff Assistant IV
Anna E. Watson, Staff Assistant IV
Frances A. Benson, Staff Assistant IV
Luanne Davis, Staff Assistant IV
Theola L. Evans, Staff Assistant IV

Water Resources Section:

James S. Dinger, Head
James A. Kipp, Geologist V
Daniel I. Carey, Hydrologist IV
James C. Currens, Geologist IV
David R. Wunsch, Geologist IV
Alex W. Fogle, Hydrologist III
Philip G. Conrad, Geologist II
O. Barton Davidson, Geologist II
David L. Harmon, Geologist II
Dwayne M. Keagy, Geologist II
Shelley A. Minns, Research Assistant
Ed Fortner, Jr., Geological Technician
C. Douglas R. Graham, Geological Technician
Joyce Belcher, Staff Assistant IV

Computer and Laboratory Services Section:

Steven J. Cordiviola, Head
Richard E. Sergeant, Geologist V
Joseph B. Dixon, Systems Programmer
Henry E. Francis, Associate Scientist
Zhalet Baharestan, Senior Research Analyst
Xenia P. Culbertson, Research Analyst
Steven R. Mock, Senior Laboratory Technician
Mark F. Thompson, Research Analyst

CONTENTS

	Page
Abstract	1
Introduction	1
Statement of Purpose	2
Location of Study Area	2
Geography and Climate	2
Geology and Hydrogeology	2
Previous Investigations	3
Ground-Water Geochemistry in Coal-Bearing Strata	5
Controls on Barium in Ground Water	6
Fluoride in Ground Water	6
Methods	7
Site Selection	7
Ground-Water Monitoring Objectives	9
Monitoring-Well Locations	9
Piezometer Installation	9
Drill Cuttings	9
Geologic Core	9
Water-Injection Packer Tests	9
Downhole Camera Investigations	12
Geophysical Logging	12
Ground-Water-Level Measurements	12
Precipitation Measurements	12
Water Sampling	12
Tritium Analysis	12
Quality Control	13
Laboratory Experiments	13
Water-Quality Effects from Well Construction Materials	13
Barium Exchange Experiments	13
Statistical Analyses	13
Geochemical Modeling	13
Results	13
Geologic Core	13
Drill Cuttings	13
Water-Injection Packer Tests	13
Downhole Camera Investigations	13
Geophysical Logging	15
Zones Monitored by Piezometers	15
Precipitation Data	15
Ground-Water Levels	15
Chemical Analyses	15
Quality of Analyses	15
Tritium Analyses	20
Water Samples	20
Fluoride in Ground Water	21
Barium in Ground Water	21
Barium-Sodium Exchange Experiments	21
Total Organic Carbon	23
Discussion	24
The Ground-Water Flow System	24

CONTENTS (Continued)

	Page
Piezometers Monitoring Fracture Zones	24
Piezometers Monitoring Coal Seams	26
Piezometers in the Below Drainage/Ridge Interior	29
Evaluation of Ground-Water Recharge Using Tritium	33
Conceptual Model of Ground-Water Flow in the Ridge	37
Ground-Water Geochemistry	38
Variation in Water Types	38
Geochemical Reactions Controlling Ground-Water Types	41
Geochemical Controls on Fluoride in Ground Water	55
Geochemical Controls on Barium in Ground Water	56
Reaction-Path Modeling Using Geochemical Models	61
Conceptual Model of Hydrochemical Facies	67
Description of Hydrochemical Model Fields	67
Conclusions	70
Acknowledgments	72
References Cited	73
Appendix 1: Discussion on the mineral weathering reactions in the Appalachian coal-bearing strata	76
Appendix 2: Geologic core description, piezometer construction specifications, piezometer construction diagrams	78
Appendix 3: Analytical laboratory methods, methods for tritium collection, description of geochemical models ..	88
Appendix 4: Description of drill cuttings, borehole diagnostics from downhole camera investigations, geophysical logs	91
Appendix 5: Daily precipitation data, Robinson Forest precipitation data	107
Appendix 6: QA/QC chemical data, water-quality tests of well construction materials, water-sample chemical analyses	109
Appendix 7: Geochemical modeling data	124
Vita	128

ILLUSTRATIONS

Figure	Page
1. Location of the Star Fire Mine	3
2. Relationship between barium, sulfate, and sulfur fractionation ($S^{34}(SO_4^{2-})$) within the sulfate molecule in water samples from eastern Kentucky (from Wunsch, 1988)	7
3. Location of study site showing assumed drainage features	8
4. Location of piezometers at the study site	10
5. Profile of the site from the valley bottom to the top of the ridge through each piezometer location	11
6. Range of hydraulic conductivity values determined in 5-foot increments in core hole 1066	14
7. Photographs showing collapse of borehole along a fractured zone in well 14	16
8. Vertical fracture encountered in well 11	17
9. Infilled fracture encountered in well 13	18
10. Water entering the borehole from the Hazard No. 8 coal	19
11. Monthly precipitation totals	21
12. Charge-balance error determined for all inorganic analyses	23

ILLUSTRATIONS (Continued)

Figure	Page
13. Contoured profile of piezometric head measured in February 1991	25
14. Contoured profile of piezometric head measured in November 1991	26
15. Hydrograph for piezometer 12A	27
16. Hydrograph for piezometer 14A	28
17. Hydrograph for piezometer 31B	29
18. Hydrograph for piezometer 11C	30
19. Hydrograph for piezometer 11B	31
20. Hydrograph for piezometer 13B	32
21. Hydrograph for piezometer 13A	33
22. Hydrograph for piezometer 21A	34
23. Water-level fluctuation with depth below the surface in piezometers monitoring coal seams	35
24. Hydrograph for piezometer 22B	36
25. Hydrograph for piezometer 11A	37
26. Hydrograph for piezometer 22A	38
27. Hydrograph for piezometer 31A	39
28. Hydrograph for piezometer 41B	40
29. Potentiometric surface for piezometers screened below the Magoffin Member	41
30. Hydrographs for piezometers 11A, 22A, 31A, and 41B	42
31. Hydrograph for piezometer 41A	43
32. Contoured profile of tritium data	44
33. Conceptual model of ground-water flow occurring at the site	45
34. Conceptualized ground-water flow system in the coal fields of southwestern Virginia	46
35. Chemical analyses from piezometer 12A shown on a Piper diagram	47
36. Chemical analyses from piezometer 14A shown on a Piper diagram	48
37. Chemical analyses from piezometer 31B shown on a Piper diagram	49
38. Chemical analyses from piezometer 11B shown on a Piper diagram	50
39. Chemical analyses from piezometer 13A shown on a Piper diagram	51
40. Chemical analyses from piezometer 21A shown on a Piper diagram	52
41. Chemical analyses from piezometer 11C shown on a Piper diagram	53
42. Chemical analyses from piezometer 22B shown on a Piper diagram	54
43. Chemical analyses from piezometer 11A shown on a Piper diagram	55
44. Chemical analyses from piezometer 22A shown on a Piper diagram	56
45. Chemical analyses from piezometer 31A shown on a Piper diagram	57
46. Chemical analyses from piezometer 41B shown on a Piper diagram	58
47. Chemical analyses from piezometer 41A shown on a Piper diagram	59
48. Water samples from each piezometer plotted on the stability fields of albite, gibbsite, sodium-montmorillonite, and kaolinite at 25°C and 1 atmosphere	60
49. Saturation indices for calcite for all piezometers	61

ILLUSTRATIONS (Continued)

Figure	Page
50. Profile of changes in selected chemical parameters in piezometers 31A and 31B	62
51. Contoured profile of chloride data	63
52. Saturation indices for fluorite for all piezometers	64
53. Contoured profile of fluoride data	66
54. Saturation indices for barite for all piezometers	67
55. Trends in the activities of selected parameters along the flow path from piezometer 11A to 41B	68
56. Temporal changes in the concentrations of selected parameters in piezometer 12A	69
57. Reaction path of ground water modeled using using PHREEQE and BALANCE, and mixing model HC-GRAM	70
58. Conceptualized model of hydrochemical-facies zones present in the unmined ridge	71

TABLES

Table	Page
1. Major Cations, Anions, and Range of pH Found in Ground Water Derived from Coal or Coal- Bearing Rocks	5
2. Piezometer Identification, Total Depth, and Zone to be Monitored	20
3. Water Level Elevations for All Piezometers	22
4. Results of Tritium Analyses	23
5. Results of Barium Exchange and Extraction Experiments Using Deionized Water, 10 Mmol NaCl, and 100 Mmol NaCl Solutions, and 100 Mmol Na-EDTA	24
6. Tritium Data with Estimates of Age Based on Interpretation from Hendry (1988)	43
7. Pierson Correlation Coefficients Calculated for Selected Constituents from All Piezometers Using July 1991 Data	65

GROUND-WATER GEOCHEMISTRY AND ITS RELATIONSHIP TO THE FLOW SYSTEM AT AN UNMINED SITE IN THE EASTERN KENTUCKY COAL FIELD

ABSTRACT

A comprehensive hydrogeologic and hydrogeochemical study was conducted at an unmined site in the Eastern Kentucky Coal Field. Sixteen piezometers were installed to approximate a vertical grid in a ridge that is characteristic of the geologic and hydrologic conditions of the region. Piezometer placement was based on data collected from geologic core description, geophysical logs, water-injection packer tests, and downhole camera investigations. Water levels were measured on approximately 10-day intervals. Water samples were collected monthly to evaluate temporal variation in water chemistry. A one-time sampling for tritium analysis was performed to aid in the determination of recharge and discharge areas.

Piezometers monitoring shallow, fractured bedrock and coal beds showed the greatest temporal water-level fluctuation and hydrochemical variation. These effects decreased with depth below the surface. Coal beds of the Hazard series probably act to dewater the upper portion of the ridge by laterally transmitting water that discharges as springs or seeps. Interpretation of the tritium data indicates that a significant amount of recharge enters the ridge along the hillslope where fractures, along with a break in the degree of slope, allow for the greatest infiltration of ground water.

Temporal variation in ground-water chemistry was minimal at the site except for a few specific cases. Ground water derived from coal seams contained the lowest pH and was predominantly a Ca-Mg-HCO₃ water type. Water derived from fractured zones varied between CaHCO₃ and Mg-SO₄ water types. Ground water from the ridge interior is a Na-HCO₃ type, which contained a high pH and characteristically high F⁻. Barium was found in significant concentrations in piezometers near the discharge area (valley bottom) where Na-Cl water types were encountered, although ground water with elevated barium concentrations was shown to exist in other locations. Sulfate reduction and cation exchange appear to control the occurrence of barium.

Reaction path modeling of the geochemical evolution of ground water at the site showed excellent agreement with observed trends. A conceptual model is presented that shows the location of hydrochemical facies zones within the ridge and outlines a set of plausible water-rock reactions for their occurrence.

INTRODUCTION

The bedrock of eastern Kentucky consists of relatively flat-lying, alternating layers of coal, sandstone, shale, clay, and to a lesser extent, limestone, which vary dramatically in thickness, as well as laterally. The hydraulic properties of these rock types can vary considerably, but at shallow depths (generally less than 100 feet) the movement of water is predominantly controlled by shallow fracture systems. It has been suggested that these fractures have resulted from external unloading, or stress relief (Wyrick and Borchers, 1981).

Conceptual models have been proposed to describe the ground-water flow that occurs in coal-bearing rocks in eastern Kentucky and neighboring states in the Appalachian Plateau Province. The primary emphasis of these models was to define the flow system, with little or no regard to the geochemistry of the ground water. Water quality can vary greatly within an area, and particular ground-water facies appear to correlate with the location of water-producing zones or with respect to the elevation of the local surface drainage. For example, wells bottoming below major drainage in eastern Kentucky tend to be Na-HCO₃ or Na-Cl water types, whereas

ground water from wells or springs found along hillsides above drainage tend to be dominated by Ca-HCO₃ or Ca-SO₄.

Approximately 90 percent of rural Kentucky households use ground water as their source of water. Barium concentrations in ground water greater than the U.S. EPA maximum contaminant level of 1.0 mg/L have been documented in areas of eastern Kentucky. It is suspected that other minor and trace elements are present in concentrations exceeding U.S. Environmental Protection Agency (EPA) drinking-water standards. Undesirable trace elements may have a considerable impact on the health of many Kentucky residents.

Ground-water monitoring schemes for mining and other industries located in these areas have also been complicated by the fact that the background geochemical conditions have not been accurately defined or described.

This study documents the relationship between groundwater geochemistry and the flow system that controls the movement of ground water. The flow system is described by conceptual models and confirmed by field investigation in a control area representative of the Eastern Kentucky Coal Field.

This task was accomplished by installing piezometer/monitoring wells at a relatively undisturbed site typical of the area. The wells were drilled using air-rotary methods while maintaining tight environmental protocol during well installation to insure well integrity and minimize any potential contamination. Methods employed to obtain stratigraphic control included the collection of drill cuttings and the examination of geologic core. Geophysical logging of the boreholes was performed to aid in stratigraphic positioning of piezometer screens. The holes were examined with a downhole camera to document specific features such as water-producing horizons and fractures.

Data collection included an intensive schedule for collection of water-level measurements, detailed chemical analyses of water samples, and pressure testing of a borehole to determine the hydraulic characteristics of the water-bearing rocks. Other facets of the study include water sample collection for radioisotopic analyses (tritium) for relative age dating and the delineation of recharge zones, laboratory studies of water-rock reactions, and geochemical modeling.

A conceptual model describing the geochemical evolution of ground water in eastern Kentucky is presented, which will be useful in understanding the relationship of the groundwater flow system to the chemistry of ground water in other areas with a similar setting.

Statement of Purpose

This investigation represents one of the most intensive ground-water studies to be performed in the Eastern Kentucky Coal Field. Presently there exists a deficiency of post 1970's ground-water chemical data that include measurements of major cations and anions, stable isotopes, radionuclides, and trace metals. Also, the fresh water-saline water interface is not well defined in the eastern area of the state (Sprinkle and others, 1983). This study contributes to abating this lack of data by generating chemical and isotopic data from ground water.

Mandatory monitoring of ground water in the Appalachian coal field has only been required since the Surface Mining Control and Reclamation Act (PL 95-87) was implemented in 1977. The results of this study should prove valuable to individuals, industry, and regulatory agencies because it provides a major contribution to the understanding of the hydrogeology and chemistry of ground water in the region.

Location of Study Area

The goal for site selection for this study was to find an unmined area in the Eastern Kentucky Coal Field that was reasonably representative of the geology and geomorphology throughout the region. This proved to be a difficult task. Much of the land in eastern Kentucky that has not been deemed unsuitable for mining usually exhibits some signs of mining-related disturbance.

The location of the control site that was chosen for this study is on property owned or leased by the Star Fire Mining Company in Perry County, Kentucky (Figure 1). The site is contained on the Noble 7.5-minute quadrangle (Hinrichs, 1978).

Geography and Climate

The Eastern Kentucky Coal Field lies in the maturely dissected Appalachian Plateau Province and experiences a humid continental climate. The southeastern region of the coal field may receive up to 50 inches of precipitation a year and has an average annual temperature of approximately 57°F. The dominant cation and anion found in precipitation are typically H^+ and SO_4^{2-} , respectively, with a pH range that is typically between 4.3 and 4.5 (Coltharp and Brooks, 1991). The coldest month of the year is January, where temperatures may fall below zero. The warmest temperatures occur in July, where they may occasionally exceed 100°F (Price and others, 1962).

Active coal mining occurs near the study area in the form of both surface and deep mines. Active oil and gas fields, along with isolated abandoned wells, are also located throughout the region. The majority of the area that has not been recently mined is covered by forests consisting of broadleaf deciduous hardwood trees and conifers.

Geology and Hydrogeology

The study area is located in the dissected Appalachian Plateau Province, which is characterized by irregular, steeply sloping ridges separated by narrow valleys. The most common lithologies are interbedded sandstones, siltstones, shales, underclays, and coals (Spengler, 1977). Some units are locally calcareous, or may contain lenticular limestones or limy concretions. The major soil group in the area of study is Jefferson-Shelocta, which is a well-drained soil formed primarily from the siltstones, shales, and sandstones. The soil cover is generally thin on the steep slopes common to the area, with the thickest accumulations in the valley bottoms and flood plains (Quinones and others, 1981).

The majority of ground water in eastern Kentucky is obtained from shallow bedrock wells generally less than 100 feet deep and from very shallow dug wells in alluvium or regolith. Salty water and brines are commonly encountered at depths greater than 100 feet below major drainage (Price and others, 1962). The largest yields are usually derived from wells in valley bottoms and generally decrease up slope (Price and others, 1962). Private residences in the area tend to be located in valley bottoms because of the greater availability of water and the preference people have for flat land over mountain slopes for home sites.

Sandstone aquifers are responsible for most of the water produced, but in most cases water is also contributed from the various other lithologies penetrated by the well, especially coal seams (Kiesler, 1986). The relatively impermeable underclays and shales that typically underlie coal act as aquitards to the vertical movement of water, which may result in horizontal flow through coal seams and other highly conductive layers. The vast majority of water wells in the area are shallow, but encounter several different lithologies.

The effects of fracture-related flow in the Appalachian Plateau (Wyrick and Borchers, 1981) and the Eastern Kentucky Coal Field (Kipp and others, 1983; Kipp and Dinger, 1987) have been documented. Fracture flow usually occurs through joints, partings along bedding planes, and near-surface frac-

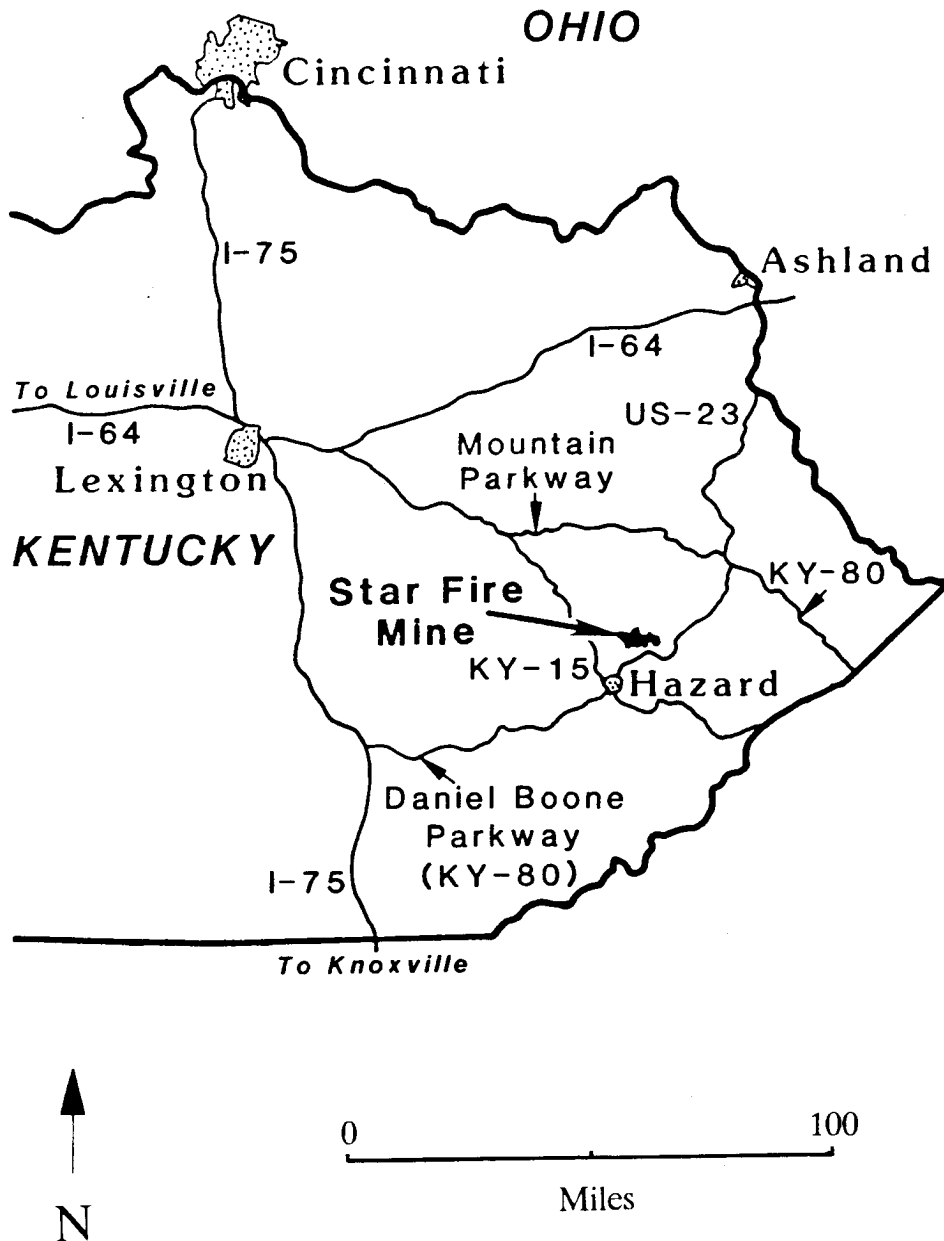


Figure 1. Location of the Star Fire Mine, which includes the study site.

turing. These forms of secondary permeability probably control shallow ground-water flow, with intergranular and confined flow gradually increasing in importance with depth.

Previous Investigations

The importance of fractures, joints, and bedding planes as avenues for enhanced ground-water flow was mentioned in early published reports concerning coal-field hydrology and ground-water resource evaluation in the Eastern Kentucky Coal Field (Price, 1962). Wyrick and Borchers (1981) postulated that ground-water flow in an area in West Virginia was controlled by shallow fracture systems. They concluded that vertical fracture systems caused by unloading and slumping predominate along the valley walls, whereas horizontal fractures along bedding planes are more prevalent in the valley

bottoms. Their study did not discuss any geochemical aspects of ground water; neither did they confirm their postulations concerning the presence of fractures along valley sides.

Kipp and others (1983) suggested that a complex flow system exists in the Eastern Kentucky Coal Field. Their findings suggest water is stored in intergranular space within clastic rocks in the hill interiors, but that a relatively small amount of water is produced from the intergranular storage. Shallow fracture systems (generally less than 50 feet deep) control most of the flow within the small drainage basins characteristic of eastern Kentucky. A cascading type of flow may occur along hillsides, where local confining layers prevent vertical movement of ground water, causing its emergence as springs along the hillsides. No ground-water chemical data were reported in their findings, although it was ob-

served from a limited amount of samples that the water derived from hillsides was a calcium-bicarbonate or mixed-cation type, whereas sodium-bicarbonate-type waters were found in water-producing zones below local drainage (Jim Kipp, personal communication). Similar trends in water types have been observed in other areas of eastern Kentucky (Ron Yost, personal communication).

Hopkins (1966) published a salt-water interface map for eastern Kentucky. This document shows that salt water can be encountered at depths as little as 100 feet below major drainage in many areas of eastern Kentucky. One of the earliest references to fracture-dominated flow of ground water in eastern Kentucky is found in the text that accompanies the interface map.

Bienkowski (1990) delineated several aquifers in eastern Kentucky based on estimated and measured production data from monitoring- and domestic-water wells. Differences were noted in above- and below-drainage portions of aquifers, and decreasing yields in wells were most closely related to increasing depth. The chemical data used in this study to correlate water quality with the aquifers were limited to measurements of iron, manganese, and sulfate concentration, along with pH and electrical conductance data. The lack of data and other constituents precluded determination of the geochemical mechanisms related to the generation of specific water types encountered in the study.

Harlow and LeCain (1991) performed packer injection tests in several hundred coal exploration core holes in Virginia to determine the hydraulic characteristics of various strata, including coal. They found a pronounced decrease in hydraulic conductivity with depth in all lithologies except coal. This decrease is consistent with the fracture-dominated flow systems as described above, and the relatively constant hydraulic conductivity of the coal seams was probably a result of the cleating in the coal, which may be more regionally controlled than the localized near-surface fracturing dictated by the surface topography. Originally, Harlow and LeCain intended to take water samples from many of the various horizons studied. Unfortunately, many of the core holes had been left open for significant lengths of time, causing uncertainties in the quality of the data that would have been collected (Gary LeCain, personal communication). This circumstance, along with the factors of time and cost, did not allow for the collection of chemical data.

Little research has been performed in hydrogeologic systems to identify the cause of high barium concentrations in ground water (Moore and Staubitz, 1984). Studies performed at the Illinois State Water Survey by Gilkeson and others (1981, 1983) showed that deep Cambro-Ordovician and Pennsylvanian aquifers in northern Illinois contained high barium concentrations with anomalously low concentrations of sulfate. It was concluded that sulfur-reducing bacteria were responsible for the reduction of sulfate to hydrogen sulfide, thus lowering the dissolved sulfate content of the ground water and allowing high barium concentrations to remain in solution. Caithamer (1983) performed an additional study concerning the mineralogical sources for barium in this area. The data collected were not conclusive as to the source of

the barium, although accessory feldspar in sandstones was mentioned as a possibility.

Arora and Rodenbeck (1983) noted the occurrence of high barium concentrations in ground waters found in the Georgia coastal plain aquifers, but did not speculate as to the source or controls of barium in solution. Moore and Staubitz (1984) studied the occurrence of high barium concentrations in ground water on the Seneca Nation of Indians Reservation in southwestern New York State. Their report showed barium concentrations as high as 21.5 mg/L, and they claimed this number to be the highest reported concentration of barium from any natural ground-water system in the world. They concluded the source of barium was from the dissolution of the mineral barite. This conclusion would seem unlikely at the sulfate concentrations reported in their study due to the low solubility of barite ($K_{sp} = 10^{-10}$; Hem, 1985). Also, Moore and Staubitz (1984) sampled potable water that typically contains low dissolved solids. This suggests that the ionic strength effect imparted by the dissolved constituents on the dissolution of barite would probably be minimal.

Wunsch (1988a) studied the cause and occurrence of high barium concentrations in ground water in eastern Kentucky. This reconnaissance study of barium analyses from 130 wells in a two-county area showed that high-barium ground waters were restricted to drilled, bedrock wells bottoming in Pennsylvanian coal-bearing strata. A more detailed study included the collection of samples for major cation-anion and barium analyses from 46 of the 130 wells sampled in the reconnaissance stage. This sampling included wells known to have high barium concentrations as well as those with low barium concentrations. Analysis of these samples showed high correlations between barium and sodium, calcium, and chloride. Wells sampled in and around the town of Buckhorn, Kentucky, had the highest number of wells with barium concentrations greater than 1 mg/L, with the mean barium concentration of 3.11 mg/L. The Buckhorn samples were also predominantly Na-Cl type waters. Stable Isotopic Ratio Analysis (SIRA) of hydrogen and oxygen in the water molecule showed slight enrichment of both ^{18}O and deuterium, probably reflecting the influence of mixing with brines. Brines typically are enriched in ^{18}O and deuterium because of water-rock interactions over long periods of time (Hoefs, 1987).

Fleischer (1974) produced a map showing the distribution of fluoride in ground water on a county-wide basis for each county in Kentucky. The data in this report indicated that some counties in eastern Kentucky had fluoride values as high as 1.4 mg/L, while little or no data were available for others. Hopkins (1966) found fluoride as high as 2.6 mg/L and that concentrations frequently exceed 0.3 mg/L in ground water in eastern Kentucky. The occurrence of high fluoride content in ground water has been noted in northeastern Ohio (Wunsch, 1982; Corbett and Manner, 1984). The occurrence of fluoride in this area was related to wells penetrating the Pennsylvanian strata in northeastern Ohio. It was proposed that high fluoride was the result of anion exchange reaction where fluoride was exchanged for aqueous hydroxyl ions. Zack and Roberts (1988) found high fluoride concentrations

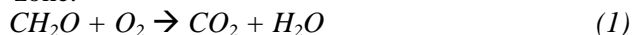
in ground water in the Atlantic Coastal Plain of South Carolina. The occurrence of fluoride was also attributed to anion exchange reactions. Robertson (1984) and Robertson and Garrett (1988) studied the occurrence of fluoride in alluvial deposits in the southwestern United States and included extensive work on the solubility controls of fluoride in ground water.

Ground-Water Geochemistry In Coal-Bearing Strata

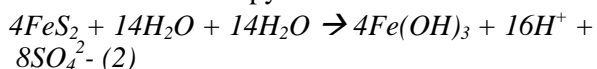
The literature does not contain a voluminous amount of geochemical data on ground waters derived from coal seams or coal-bearing rocks. The majority of work on this topic has been performed in the Western lignite coal fields. Table 1 shows the major cations and anions (in decreasing order), along with pH values listed by several researchers who conducted studies involving the geochemistry of ground waters derived from coal or coal-bearing strata. The studies shown represent analyses from the Western lignite coal fields (North Dakota and Wyoming), the Paleozoic bituminous coals of the Appalachian Basin (northeastern Ohio), and the Illinois Basin (southern Indiana). Although several water types could be found in each of these areas, all of the above examples, except for one, found that sodium and bicarbonate were the dominant cation and anion, respectively. It appears that geology and the setting of the coal basins play a primary role in determining the ground-water geochemistry in coal-bearing sediments.

Groenewold and others (1981) proposed a series of processes that generate high-pH, Na-HCO₃ ground waters. They can be summarized as follows:

1. CO₂ is produced in the organic horizons of the soil zone.



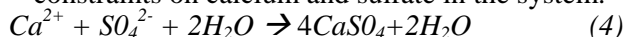
2. The oxidation of pyrite liberates H⁺.



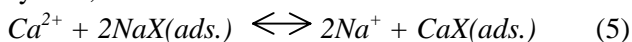
3. Dissolution of carbonate minerals produces bicarbonate.



4. Precipitation and dissolution of gypsum may place constraints on calcium and sulfate in the system.



5. Cation exchange reactions take calcium out of the system,



The shift in calcite equilibrium allows for more dissolution of calcite (eqn. 3), which consumes H⁺ and results in an increase in pH and bicarbonate concentration. Ground waters derived from coals from the Western coal fields often contain significant amounts of sulfate because of gypsum dissolution.

Foster (1950) and Winograd and Farlekas (1974) have suggested similar processes for the genesis of high-pH, NaHCO₃ waters in the Atlantic Coastal Plain, except that they proposed that CO₂ is produced at depth from either the coalification (diagenesis) of lignite or by sulfate reduction requiring sulfur-reducing bacteria. The reaction for the reduction of sulfate with the presence of organic matter is:

Table 1.—Major Cations, Anions, and Range of pH Found in Ground Water Derived from Coal or Coal-Bearing Rocks. Ions Listed in Order of Significance.

Location	Major Cations	Major Anions	pH	Source
South Dakota	Sodium, Calcium	Bicarbonate, Sulfate	7–9	Groenewold and others (1980)
Southern Indiana	Calcium, Sodium	Bicarbonate	up to 8	Banasczak (1980)
Wyoming	Sodium, Calcium	Bicarbonate	7.3–7.8	Stone and Snoeberger (1976)
Ohio	Sodium, Calcium	Bicarbonate	7.8–8.7	Wunsch (1982)



Sulfur-reducing bacteria require less than 0.1 mg/L of organic material to support their activity (Gilkeson and others, 1981). Ground water in which CO₂ has been generated by sulfate reduction typically has low sulfate concentrations; thus, it can be clearly distinguished from high-Na-HCO₃ water that has evolved only from the dissolution of calcite, oxidation of pyrite, and ion exchange processes (Freeze and Cherry, 1979). Other evidence for bacterially mediated sulfate reduction is the presence of hydrogen sulfide (H₂S). The unappealing smell of this gas is generally a detriment to water quality and is common in the Eastern Interior coal basins (Banasczak, 1980).

Ground waters derived from coal layers may also contain metals such as iron and manganese (Stone and Snoeberger, 1978; Banasczak, 1980). The presence of these elements is most likely the result of the oxidation of sulfide minerals. Secondary mineralization (e.g., barite, calcite) often exists in fractures and partings in coal, and may also be a source of trace metals (Stach, 1982). Banasczak (1980) also noted the presence of microscopic particles of coal suspended in ground waters from wells receiving their water from coal seams, often referred to as "black water."

Danilchik and Waldrop (1978) listed the following suite of minerals present in the stratigraphic section that encompasses the study site: quartz, feldspar, mica, calcite. Their data are limited in that they did not conduct detailed petrographic evaluations or determine the relative abundances of each mineral.

Weinheimer (1983) performed sedimentological and mineralogical analyses of thin sections from four cores representing the Breathitt Formation in eastern Kentucky. Two of the cores were taken from locations approximately 4 miles from the site chosen for this study, and represent the best mineralogical control available for understanding the geochemical reactions that may control the water chemistry at the site. Analyses of the cores revealed the following average percentages: quartz, 47 percent; feldspar, mainly K-spar, 29 percent; rock fragments, 11.9 percent; mica, 5.4 percent; and heavy minerals (pyrite, siderite), 0.5 percent. The majority of

the cement was determined to be ferroan calcite. Abundant authigenic kaolinite was found to fill pore spaces and form reaction rims around feldspar grains. Opaque minerals and accessory components included pyrite and detrital organic matter. Siderite and iron oxide were also common. Dolomite was rare. Shales and claystones in the Breathitt Formation contain illite, kaolinite, and chlorite (Papp, 1976). Diamond (1972) reported montmorillonite in the Magoffin Member.

Minerals that are the most abundant in rocks are not necessarily those that have the greatest control on the dissolved constituents that occur in the water. Also, some minerals, especially aluminum silicate minerals, dissolve incongruently (Freeze and Cherry, 1979). Although the carbonate minerals (e.g., calcite and siderite) are present in minor amounts, often they can exert a pronounced effect on the geochemistry of ground water, especially when the ground water is exposed to a high partial pressure of CO_2 .

Powell and Larson (1985) related the chemistry of ground water to the mineralogy of the Norton Formation of Virginia. Their report describes in detail a suite of reactions that may be responsible for the observed types of water quality encountered in the coal-bearing strata of southwestern Virginia. The Norton Formation of Virginia is very similar to the Breathitt Formation in Kentucky (Don Chesnut, personal communication). The study site used by Powell and Larson is near the Kentucky-Virginia border, approximately 65 miles from the present study site. The mineralogical determinations by Weinheimer (1983) also indicate a high degree of similarity between the rocks of the Norton and Breathitt Formations. Because the geology and hydrogeology of the two areas are similar, the chemical reactions relating the reactions of ground water with minerals in the rocks described by Powell and Larson (1985) are considered valid to describe the reactions that control the ground-water geochemistry in this study. Therefore, a discussion based on their work is included in this study and can be found in Appendix 1. Their discussion presents an excellent description of the probable weathering reactions taking place in or above the groundwater system found in Pennsylvanian coal-bearing rocks in the Appalachian Basin.

Controls on Barium in Ground Water

Barium is an alkali earth element found in a number of silicate minerals, mainly feldspars and micas. It often substitutes for potassium because of the nearly identical ionic radii of 1.59 Angstrom units for potassium, and 1.50 for barium. In sedimentary rocks, shales usually contain the greatest amounts of barium because it is commonly adsorbed onto clay minerals or incorporated in the clay-mineral structure (Levinson, 1980). Wunsch (1988a) found that barium content was the highest (1,180 ppm) in shales and lowest in coal (< 50 ppm) in cores from coal-bearing rocks of the Breathitt Formation in eastern Kentucky. These values are consistent with other values found in the literature (Levinson, 1980).

Two barium compounds, barite (BaSO_4) and witherite (BaCO_3), can impose solubility constraints on barium in natural waters. Witherite has a solubility product of $10^{-8.64}$ at 25°C , which is similar to calcite ($K = 10^{-8.48}$). Witherite solu-

bility is largely dependent on the carbon dioxide partial pressure in equilibrium with the solution. The amount of barium in solution is most likely controlled by the solubility of the mineral barite (BaSO_4) (Hem, 1985). The solubility product of barite at 25°C has been given as 10^{-10} (Hem, 1985) and 1.08×10^{-10} (Weast, 1975). Consistent with the law of mass action high activities of barium must correspond to low activities of sulfate. For example, at sulfate molar activities near 10^{-4} (~10 mg/L) or 10^{-3} (~100 mg/L) the corresponding equilibrium molar activities would be 10^{-6} or 10^{-7} (~0.14 mg/L or ~0.014 mg/L), respectively (Hem, 1985).

Collins (1975) confirmed that the solubility of barium sulfate increases with an increase in the ionic strength of solution. This important solubility effect is the probable reason for the high barium content in brines. Brines from the Appalachian Basin have been noted as containing significant amounts of barium (Heck, 1940). Brines high in barium are characteristically low in sulfate content, probably due to sulfate reduction (Hem, 1985). The resulting low sulfate concentrations allow for the barium concentration to increase, at least up to the point where the barium carbonate solubility limit is reached (Hem, 1985).

Wunsch (1988b) showed that the low concentrations of sulfate in ground water in areas of eastern Kentucky were due to sulfate reduction mitigated by sulfur-reducing bacteria. Stable Isotope Ratio Analysis (SIRA) of sulfur in the sulfate molecule showed that samples with low sulfate content had high S^{34} , suggesting that the activity of sulfur-reducing bacteria in the aquifer causes the reduction of sulfate to sulfide. Figure 2 shows the relationship of sulfate content and the degree of sulfur-isotope fractionation to barium content.

Microbial culture analyses confirmed the presence of sulfur-reducing bacteria in many of the wells from which the sulfur-isotope samples were drawn. The sulfur-reducing bacteria were found to be halophilic, and probably thrive in the shallow mixing zone where brines and fresh water produce optimum salinities for their growth. The process affects the chemical equilibria by keeping the concentrations of sulfate low, thus allowing for greater concentrations of barium to exist in solution (Wunsch, 1988b).

The effect of pH on barite solubility is thought to be minimal in natural waters. At pH values of less than about 4, the HSO_4^- ions become important, which would tend to increase the solubility of barite. However, most ground waters in undisturbed settings in eastern Kentucky have pH values above 4, and the effect of this complex would not be significant.

Fluoride in Ground Water

Fluorine is the most electronegative (tendency of an element to acquire a negative charge) member of the halogen group of elements. In solutions, fluorine is found in the form of F^- ions, and is generally found in natural waters in concentrations less than 1.0 mg/L. Fluoride also may form complexes with aluminum and ferric iron. Aluminum-fluoride complexes are most common at low pH values (Hem, 1985). At a pH below about 3.5, the form HF^0 could occur, although this value is below the pH range of most natural waters.

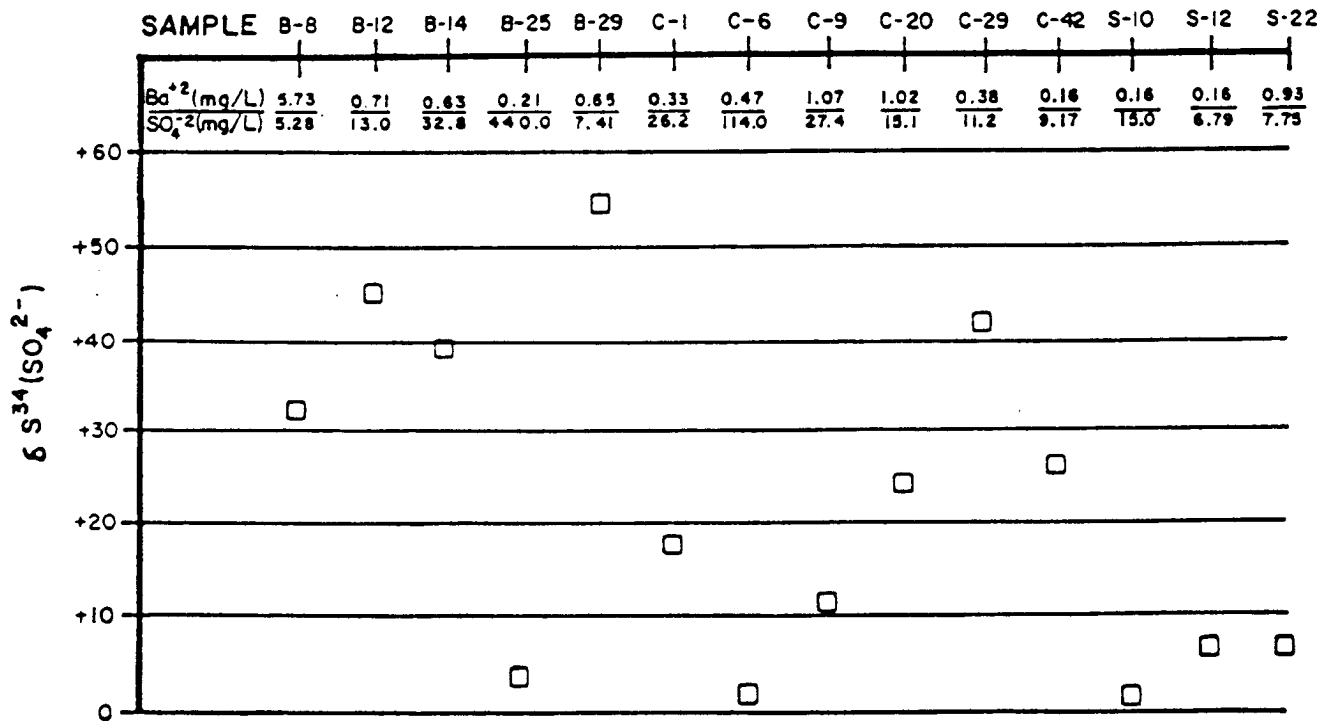


Figure 2. Relationship between barium, sulfate, and sulfur fractionation ($S^{34}(SO_4^{2-})$) within the sulfate molecule in water samples from eastern Kentucky (from Wunsch, 1988a).

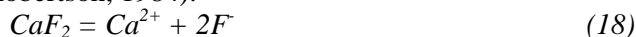
Fluoride ions have nearly the same ionic radius as the hydroxyl ion (ionic radius is 1.40 Angstroms; ionic radius of F⁻ is 1.36); therefore, these ions may replace each other in mineral structures (Hem, 1985).

In sedimentary rocks, fluorine is found in fluorite (CaF₂), amphiboles, and micas where it may also substitute for hydroxyl ions. Fluoride ions may also be exchanged with hydroxyl ions at mineral surfaces in pH-dependent reactions:



Bower and Hatcher (1967) studied fluoride adsorption on various soils and minerals. They found a high degree of adsorption on gibbsite, kaolinite, and halloysite.

In natural waters with fluoride concentrations -5 mg/L, the solubility of fluoride is probably controlled by fluorite, such that high dissolved fluoride concentrations would correspond to low calcium concentrations (Robertson, 1984):



$$K = [Ca^{2+}][F^-]^2 / [CaF_2]$$

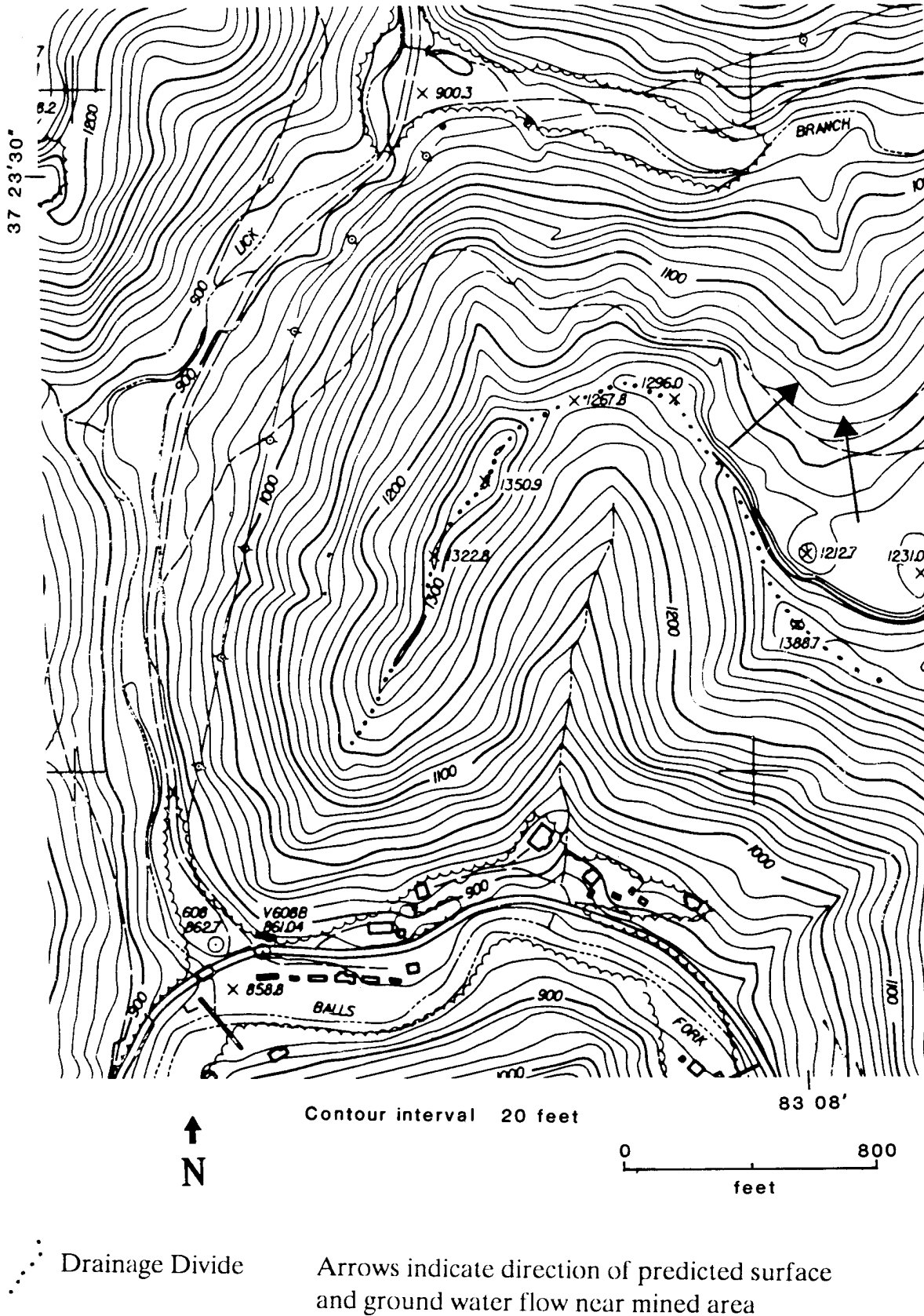
At 250C the solubility product for fluorite has been found to be near 10-11 (Hem, 1985). In ground waters that are undersaturated with respect to fluorite, hydroxyl-fluoride exchange appears to be the more important control on fluoride concentration (Robertson, 1984).

METHODS

Site Selection

The study site chosen for piezometer installation is shown on Figure 3. It is located on a ridge bounded on the northern and western sides by Lick Branch, a third-order stream, and on the south by Balls Fork, a fourth-order stream. Both of these streams drain large basins and maintain their flow throughout the year. Contour-cut mining to remove the Hazard Nos. 7 and 8 coals occurred to the east of the study site during the 1970's. The locations chosen for piezometer placement were selected to minimize any effects of this mining on the occurrence and chemistry of ground water encountered during the study. The western edge of the bench resulting from mining is approximately 500 feet from the nearest piezometer site, and it is also outside the apparent surface-water (and assumed ground-water) drainage divide as shown on Figure 3.

Access for drilling and subsequent sampling was made possible by the existence of a former coal-hauling road located on the northwestern side of the ridge. An access road that branches from the haul road was constructed to allow access to the top of the ridge. The effects, if any, on the shallow ground-water flow system due to the construction of this access road are unknown, but are believed to be minimal. Its construction was completed 3 months before the commencement of well drilling for this study, and it is assumed that any disturbance in the flow system would have declined. Kipp



and others (1983) showed that water levels in wells directly affected by contour-cut mining returned to pre-mining levels within 4 months. Additionally, the disturbance to the landscape due to the installation of a one-lane access road is much less than a hillside contour cut created for mining purposes.

Ground-Water Monitoring Objectives

The piezometers were located so that comparisons could be made between the head distribution and water chemistry of ground water from the ridge interior, near-surface fracture zone and sites adjacent to and below the major surface-water drainage adjacent to the site. In order to make these comparisons, detailed geologic and hydrogeologic information was collected to provide for an accurate monitoring scheme.

Monitoring Well Locations

Four locations along the access road on the northwestern side of the ridge were selected for well drilling and subsequent piezometer installation. Each of these locations were chosen on the following bases: (1) to maximize the monitoring of all the prevalent hydrogeologic conditions at the site, (2) to provide a fairly even spacing from the ridge top to the adjacent valley bottom, (3) to provide easy access for the drilling equipment, and (4) to be as close as practicable to the main road to ensure access for sample collection during wet weather conditions.

An 8-inch surface casing was set by drilling an 8-5/8-inch pilot hole to a depth that insured that the casing bottom was approximately 10 feet into the solid bedrock. The hole was then completed to the predetermined depth using a 7-7/8-inch roller-cone drill bit. A minimum amount of water was added during drilling for dust control.

The boreholes were drilled using a Schramm Rotodrig air-rotary drilling rig. The driller was required to keep the drilling rig and equipment clean to avoid contamination from synthetic byproducts used when drilling, such as hydraulic oils and fuel. All drilling rods and tools were kept on a flatbed truck or on plastic sheeting to avoid contamination. Steel drilling rods were decontaminated after the completion of a hole by washing them with chlorinated water to avoid cross-contamination between boreholes.

The location of the wells can be seen on Figure 4. A profile of the ridge that passes through the wells along the line shown on Figure 4 is shown in Figure 5. Four wells, numbered 11, 12, 13, and 14, are located at the top of the ridge, including a deep well (418 feet total depth) that penetrated the center of the ridge below the level of the surrounding major-surface drainage. Wells 21, 22, 31, and 41 are at descending locations on the access road along the slope of the ridge.

Piezometer Installation

Sixteen piezometers were installed in the eight holes during November and December of 1990. The installation of each piezometer was performed under the direct supervision of the author and staff from the Kentucky Geological Survey. The methods that were followed for the construction of multiple-level monitoring wells are described in the "Handbook of

Suggested Practices for the Design and Construction of Ground-Water Monitoring Wells" by Aller and others (1989).

Materials used in the installation of piezometers were factory sealed. Detailed well construction diagrams along with specifications for the installation of piezometers can be found in Appendix 2.

The units or water-producing zones to be monitored were chosen using data and observations from the examination of geologic core, drill cuttings, water-injection packer test data, downhole camera investigations, and geophysical logs.

Drill Cuttings

Samples of the rock cuttings produced while drilling the boreholes for piezometer emplacement were collected at 5-foot intervals for each hole. The cuttings were placed in plastic bags and labeled for identification. Borehole logging by field examination of the cuttings was performed in holes that bottomed at elevations below the level of CH 1066 so that a continuous record of the geology of the ridge could be obtained.

Geologic Core

A geologic core (Star Fire CH 1066) was drilled by the Star Fire Mining Company for exploration purposes on August 8, 1990. The core hole was taken from the ridge top and was located between the locations for well 12 and 13 (see Figure 4). The core was an NX hole (3-inch diameter) drilled to a depth of 210 feet. The depth was limited by the exploration needs of the mining company.

The core was described for lithology and features such as fractures that may be indicative of water-producing zones. The geologic column adjacent to the profile shown on Figure 5 is based on the geologic data obtained from CH 1066 and from the geologic quadrangle map (Danilchik and Waldrop, 1978) that encompasses the site, and from drill cuttings obtained from wells 11 and 41.

Water-Injection Packer Tests

Water-injection packer tests were performed to determine the hydraulic conductivities for the various lithologies encountered in core hole 1066. The tests were performed by using a packer setup in which a 5-foot perforated section of pipe was separated by two inflatable packers. The perforated pipe permitted the injection of water into the zone of interest, which was sealed off by the packers.

The method used for calculating hydraulic conductivities was taken from the U.S. Bureau of Reclamation (1974) technical publication, "The Design of Small Dams." The formula used is:

$$K = [Q / 2\pi LH] * [In / R] \quad \text{For } L > 10r$$

Where:

K = permeability

Q = constant rate of flow into the hole

L = length of the portion of the hole tested

H = gravity head + pressure head

r = radius of hole

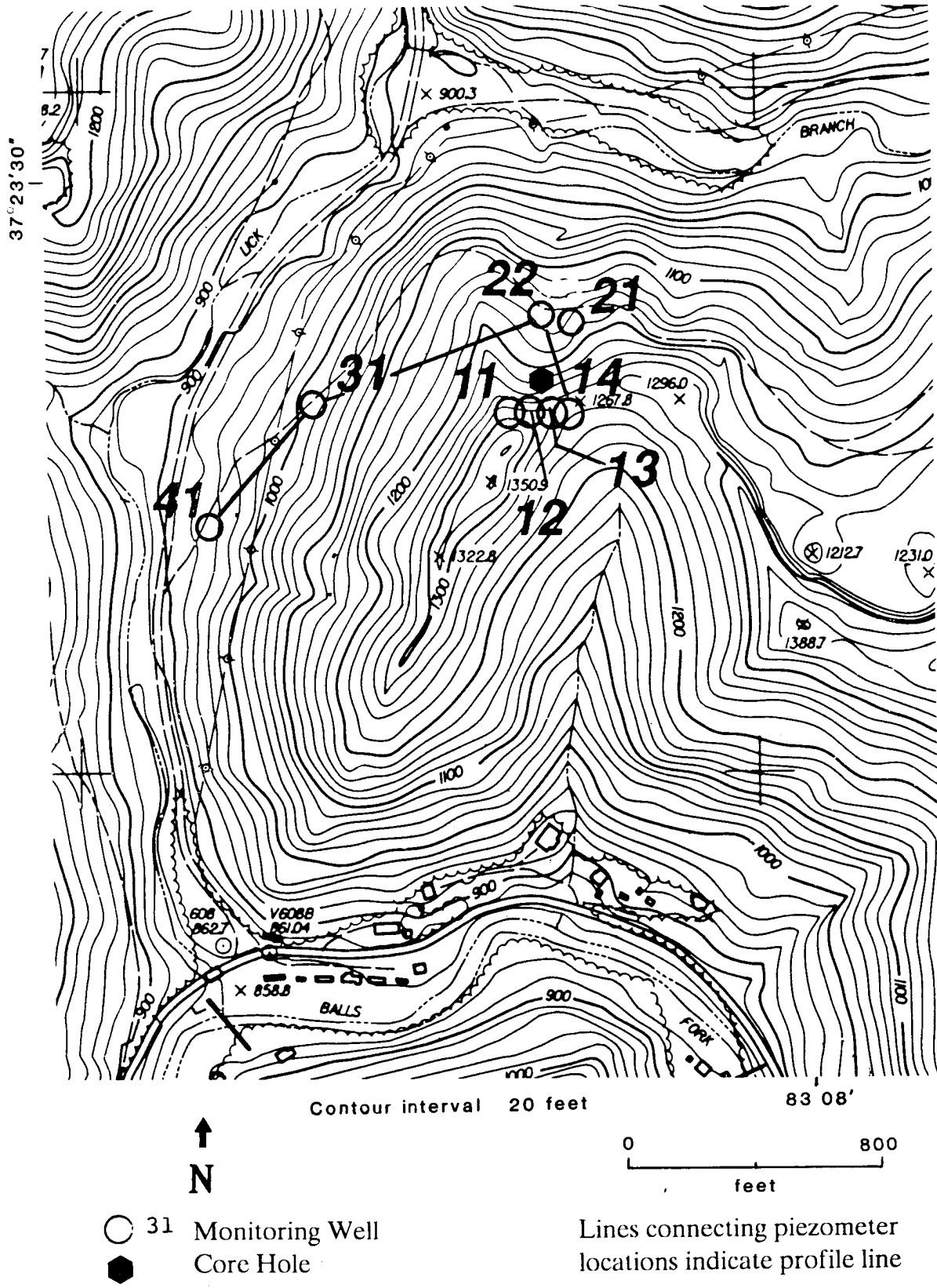


Figure 4. Location of piezometers at the study site.

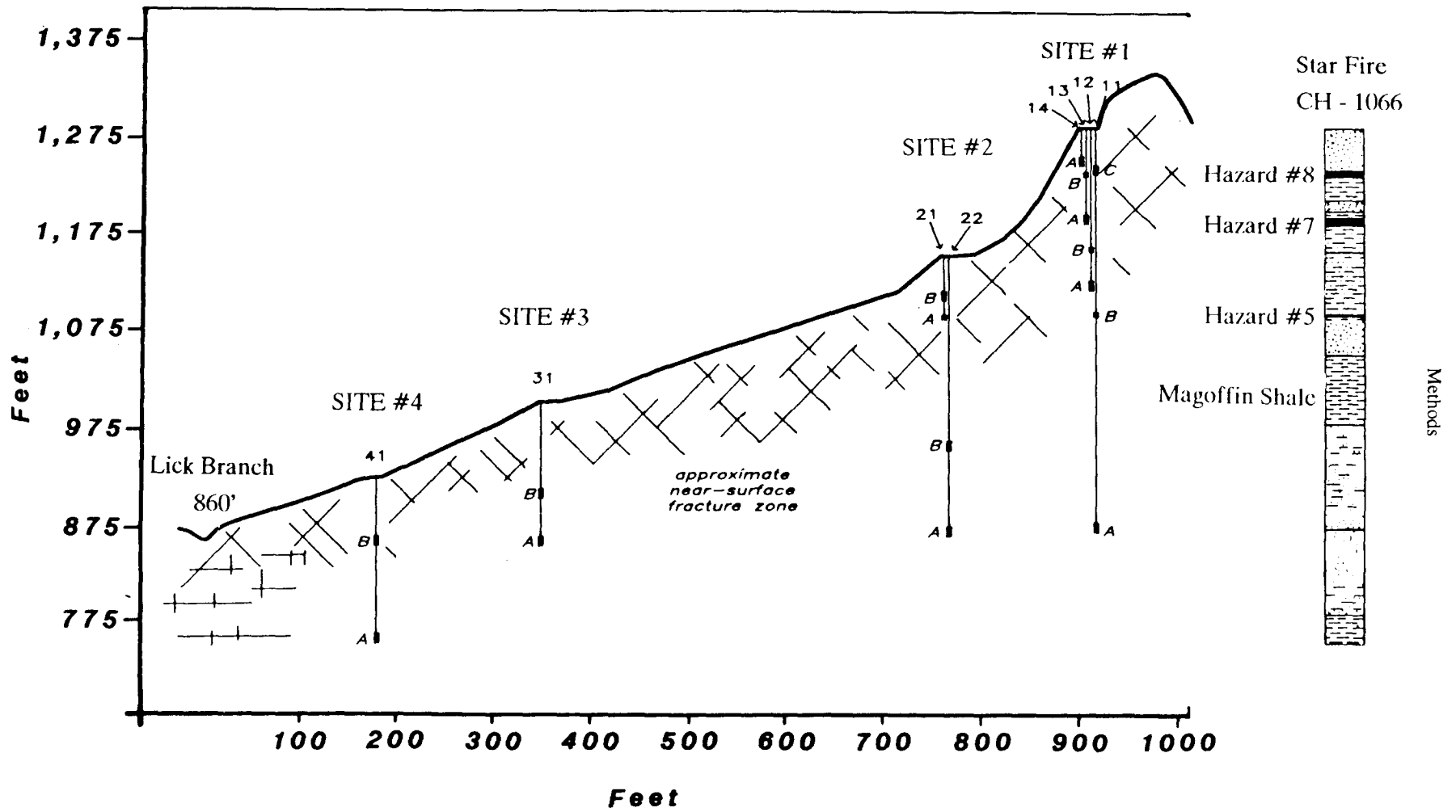


Figure 5. Profile of the site from the valley bottom to the top of the ridge through each piezometer location. The trace of the profile is shown on Figure 4.

Downhole Camera Investigations

A PLS International 8750 Portable Television Inspection System was used to view the open monitoring-well boreholes. The viewing of each borehole was videotaped using a VCR and recorded on standard VHS-format videotape for later viewing. The video recorder failed halfway through the tests, so recordings of the inspections are not available for two boreholes. In anticipation of this problem, written field notes were taken as the examination of each hole took place to insure the data would not be lost.

Geophysical Logging

Geophysical logging was performed by the staff of the Kentucky Geological Survey on November 29, 1990. Natural gamma, SP resistivity, and caliper logs were collected.

Ground- Water-Level Measurements

Ground-water levels were measured by using a Slope Indicator Co. Model 51453 electric water-level meter equipped with an indicator horn and light. The indicator probe and lead wire were rinsed with distilled water between each measurement and stored in a plastic bag during transport to and from each site to avoid contamination. Measurements were recorded to the nearest tenth of a foot.

Precipitation Measurements

Precipitation data were collected by a tipping bucket rain gage equipped with a continuous digital data recorder. The gage is located on the Star Fire Mine property approximately 1.8 miles from the study site.

Water Sampling

Water samples were collected on a monthly basis for the period of 1 year beginning in February of 1991 and ending in January of 1992. Purging and sampling for the deepest piezometer and other wells producing a limited amount of water was performed by using a stainless steel bailer with a Teflon ball and seat. The bailer was retrieved from the piezometer using a pump-hoist truck equipped with a sandline capable of lowering and retrieving the bailer at a rate of up to 400 feet per minute. The sandline cable is 3/8-inch nylon-coated steel wire, which allows for flexibility and easy decontamination. A polypropylene rope leader was used to secure the bailer. The pump-hoist truck is operated by the Water Resources Section of the Kentucky Geological Survey.

The remaining wells were routinely purged and sampled using a Grundfos Redi-Flo 2-inch submersible pump. Wells were purged of three well volumes before initiating sample collection. The handling of the bailers and the pump was performed while wearing latex disposable gloves to prevent contamination. All objects that were lowered into the hole were placed on plastic sheeting and covered when not in use.

Specific conductance, temperature, pH, and redox potential (Eh) were recorded in the field. A YSI 3500 flow-through meter was used to obtain the temperature, pH, and redox potential values. This device is an enclosed cell hosting the appropriate electrodes (pH and oxidation-reduction potential [ORP]). The cell was connected directly to the pump discharge hose or connected to the bailer by way of an emptying

valve and hose to allow for simultaneous monitoring of the stabilization of the field parameters while purging the well. The pH probe was standardized by calibrating to pH buffers of 4.01, 7.0, and 10.0 (standard pH units) before sampling each piezometer. The YSI meter is equipped with automatic temperature compensating probes (ATC) so that the pH values are automatically corrected for temperature. In order to check the integrity of the pH electrode and determine the amount of drift throughout the period of this study, the probe was checked periodically by measuring the millivolts of pH buffers to determine the slope of the best-fit line describing the relationship between pH and millivolts (mV). The ORP was checked periodically against a solution containing a known and stable redox couple (ZoBell's solution) to determine if electrode poisoning had occurred (Nordstrom, 1977).

Specific conductance was measured using a Cole-Parmer 1481-55 conductivity meter. The meter is equipped with an ATC probe that corrected all values to a temperature of 25°C. The conductance readings of water samples were corrected to the values of conductivity standard solutions by linear regression using the actual and observed reading from standards of 200, 2000, and 20,000 microsiemens measured in the field each day.

Water samples for chemical analyses were placed in 250-ml acid-rinsed polyethylene bottles. Water samples collected for dissolved metals were filtered by pumping water using a peristaltic pump through a 0.45-micron membrane filter housed in a Fisher stainless-steel and Teflon filtering device. Two ml of a 1:1 mixture of deionized/distilled water and double-distilled HNO₃ were added to each sample for preservation and to prevent the precipitation of solutes as hydroxides (Brown and others, 1970). Samples collected for total metals analysis were acidified but not filtered. Samples collected for dissolved anionic species were neither filtered or acidified.

Samples were collected on a few occasions for total organic carbon (TOC) and total metals. TOC samples were not filtered and were placed in a 250-ml bottle and acidified and preserved by adding 1 ml of concentrated H₂SO₄. Chemical analyses of water samples were performed by the Laboratory Services Section of the Kentucky Geological Survey. Analysis of metals was performed using a Thermal-Jarrell Ash Inductively Coupled Plasma Emission Spectrometer (ICAP). Bicarbonate analysis was performed using a Mettler autotitrator. Sulfate, chloride, and bromide analyses were performed using a Dionex ion chromatograph. Fluoride was determined using a specific ion electrode. Total organic carbon was determined using a Dorhmann total organic carbon analyzer. A description of the specific method used for each analysis is given in Appendix 3.

Tritium Analysis

Water samples were collected on one occasion to determine the relative age of the ground water at the site and to add insight to the rate of recharge. Tritium samples were placed in 125-ml boro-silicate glass bottles with conical inset caps to displace any air bubbles created when filling the bottles. The caps were double-tightened and tightly wrapped with electrical tape and sent to the University of Miami Tritium

Laboratory for analysis. Low level-proportional counting was performed on each sample for 1,000 minutes. This produced an accuracy and precision of ± 2 tritium units (TU) (Dr. Gote Ostlund, Tritium Laboratory, personal communication). Samples resulting in counts of less than 5 TU were recounted using enrichment and low-level direct counting, which allowed for precision of less than 0.5 TU. A detailed description of sample collection and preparation methods suggested by the lab can be found in Appendix 3.

Quality Control

A duplicate sample from a randomly chosen piezometer was taken during most sampling events and sent to the KGS analytical laboratory for analysis for comparison with the results of the original sample. A field blank was also prepared in the field during each sampling event to determine if any contamination was introduced to water samples during collection. This involved passing distilled/deionized water through the filtering device and acidifying the filtrate for total metals analysis. The analytical laboratory also performs detailed quality control/quality assurance procedures within the lab (Henry Francis, Laboratory Manager, personal communication).

Laboratory Experiments

Water-Quality Effects From Well Construction Materials

A gravel pack consisting of fine silica sand was used to create a filter pack around the piezometer well screens. Visual examination of the sand revealed that it consisted of mainly quartz sand with minor amounts of feldspar. In order to determine if any significant contribution of dissolved constituents found in water samples could be attributable to the gravel pack, an experiment was conducted where 200.0 grams of the sand used in well construction was placed in an acid-rinsed 1-gallon container and filled with deionized/distilled water. A 250-ml water sample was collected from the container three times throughout the duration of this study and analyzed for total metals by the lab.

Barium Exchange Experiments

Experiments were conducted to determine the amount of barium that could be removed from rock samples from drill cuttings collected during monitoring-well drilling. The tests for barium extraction consisted of mixing equal amounts (by weight) of drilling cuttings from within the stratigraphic interval to be tested. The rock chips were ground up to create fresh reactive surfaces and air dried. Ten grams of each sample were placed in a 250-ml polyethylene bottle and filled to volume. The solutions were a 10 and 100 mmol NaCl solution along with a distilled/deionized water blank. One set of samples were reacted with a disodium-EDTA (ethylenediaminetetraacetic acid) solution to solicit maximum extraction. Each sample set was run in triplicate to demonstrate reproducibility. The samples were agitated for 1/2 hour and allowed to react for 72 hours. The solutions were filtered using a 45-micron filter and analyzed.

Statistical Analyses

Statistical analyses of data were performed using the STSC Statgraphics statistical software on a Zeos 386-SX microcomputer. In some cases univariate statistics were performed using a hand calculator or a spreadsheet program.

Geochemical Modeling

Geochemical modeling of ground-water chemical data allowed for the determination of the speciation of ions and the degree of saturation with respect to several minerals. In some cases, reaction-path modeling was used to validate a conceptual model covering the evolution of ground water at the site. Ground-water mixing scenarios are also presented.

The geochemical model PHREEQE (Parkhurst and others, 1980) was used to perform the equilibrium calculations in this report. BALANCE (Parkhurst and others, 1982) was used for mass-balance calculations. Binary mixing of water samples was modeled using HC-GRAM (McIntosh and Miller, 1989). The models were operated on a 386-SX microcomputer equipped with an 80387 math co-processor chip. The reader is referred to Appendix 3 for a general discussion on the capabilities of each model.

RESULTS

Geologic Core

A total of 210 feet of NX core was examined and logged to evaluate potential monitoring zones. A lithologic description of this core is shown in Figure 6. Four major coal seams, the Hazard Nos. 5, 6, 7, and 8, were encountered in the cored section. Fractures were observed in the core intervals from 28.6 to 33.6, 58.6 to 63.6, and 153.6 to 158.6 feet.

Drill Cuttings

Samples of drill cuttings were collected generally at 5-foot intervals from monitoring-well boreholes to obtain control for the complete geologic column for the study site and for laboratory experiments. In some locations cuttings were collected from 10-foot intervals. A listing of the sampling interval and description of the cuttings is included in Appendix 4.

Water-Injection Packer Tests

Figure 6 shows the hydraulic conductivity values associated with each 5-foot test interval in Star Fire core hole 1066. A description of the core lithology of each interval along with any features of hydrogeologic significance is included. Eleven intervals out of a total of 39 took significant amounts of water; most of these intervals correlated to either a coal seam or a fracture zone (as revealed from the core removed from the borehole). Hydraulic conductivity ranged from 3.5×10^{-7} to 9.3×10^{-4} cm/sec. The highest hydraulic conductivity values were obtained from the Hazard Nos. 5, 7, and 8 coal seams.

Downhole Camera Investigations

Excellent resolution of the boreholes was observed for the portions of the holes that were not filled with water. Visibility was usually lost after the camera was lowered below the level of static water due to turbidity. The video examination provided great insight as to where water was entering the hole.

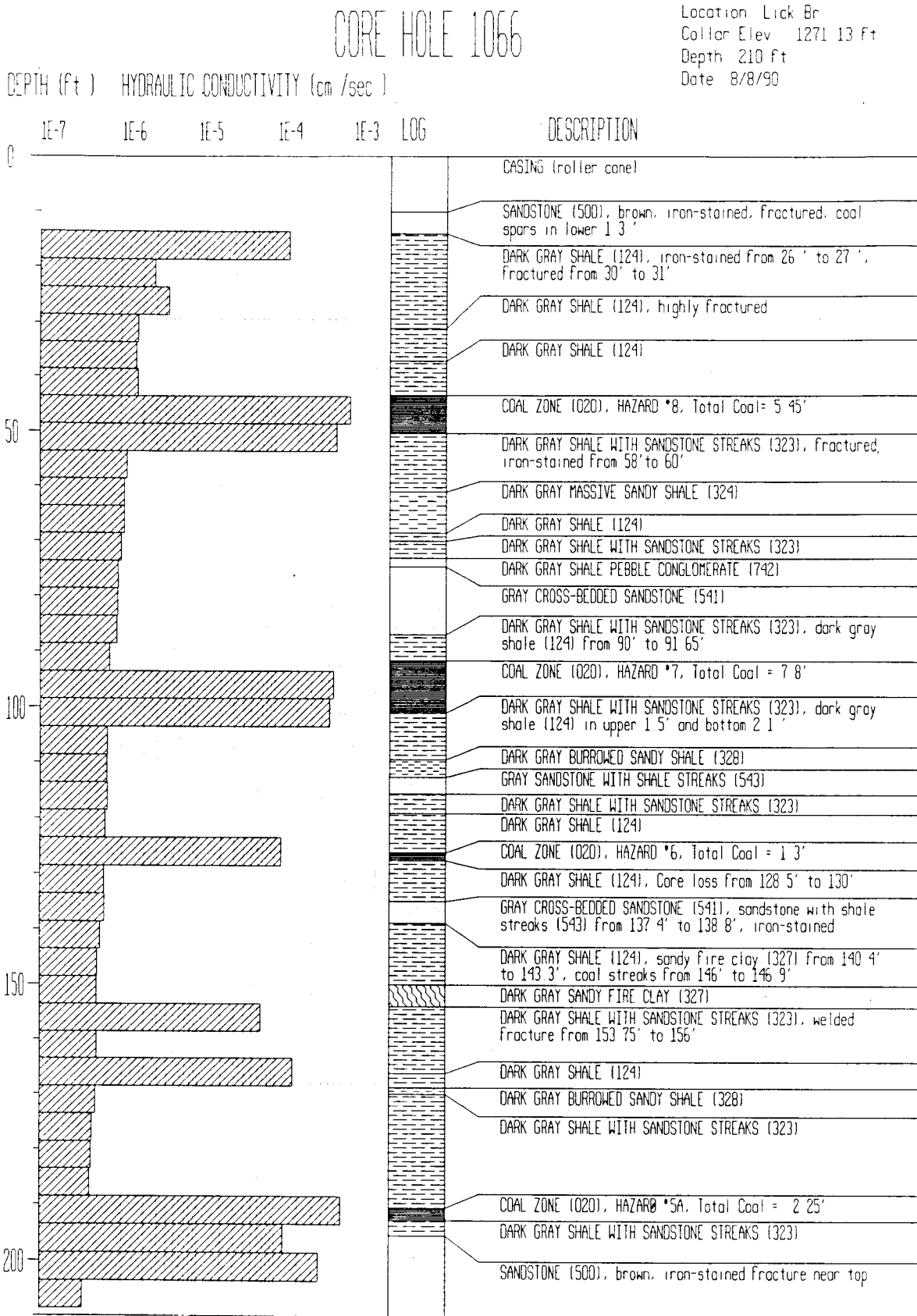


Figure 6. Range of hydraulic conductivity values determined in 5-foot increments in core hole 1066.

Fractures and coal seams were easily identifiable, and often water was observed flowing into the hole from these features. The camera viewing of each hole was recorded on videotape for close examination. Figure 7 shows photographs reproduced from the videotape and shows a fracture observed in well 14. The two photographs shown on each figure show either a close-up or an alternate viewing angle. Figure 8 shows a vertical fracture and collapse of fractured rock in well 11. A fracture plane that is infilled with clay or sediment is shown in Figure 9. The plane defined by the fracture is inclined to the borehole, so the outline of the fracture appears as an ellipse in the photograph. Water flowing from the Hazard No. 7 coal seam is shown in Figure 10. Diagnostics from each borehole were described and are included in Appendix 4.

Geophysical Logging

Caliper, natural gamma, and SP resistivity logs were run in wells 11 and 41. These wells were chosen because the geologic sequence encountered in these wells overlap, allowing for a continuous logging sequence to be recorded from the ridge top to below drainage. Profiles of these logs, including geologic contacts and units of interest, are presented in Appendix 4. The geophysical data, in conjunction with the geologic data, aided in determining the location of coals and lithology changes, which was important in accurately determining depths where piezometer screens were to be positioned.

Zones Monitored by Piezometers

Careful evaluation of the results of geologic, geophysical, and hydraulic data resulted in the selection of the discrete zones chosen for monitoring. The monitoring scheme resulted in a total of 16 piezometers being installed in the eight drilled holes. The piezometer with the deepest screened interval in each borehole was designated the "A" piezometer, followed by "B" and "C" for the other piezometers in order of decreasing depth from the surface.

Based on the data from the water-injection packer tests and downhole camera investigations, only coal seams and fractured bedrock, which includes vertical fractures, joints, and bedding-plane splits and partings, possessed sufficient hydraulic conductivities to transmit significant amounts of water. This observation is supported by the work of other researchers who studied the flow systems in nearby or similar settings (Wyrick and Borchers, 1981; Kipp and Dinger, 1987; Harlow and LeCain, 1991). Therefore, water-producing zones monitored in this study can be placed into three groups: (1) fractured bedrock, both near-surface and deep, (2) coal seams, and (3) solid bedrock zones monitored below the Magoffin Shale Member at or below major drainage. Table 2 lists the piezometer identification, the depth of each individual piezometer, and the hydrogeologic zone to be monitored.

Precipitation Data

Figure 11 shows the precipitation totals for each month in 1991. The highest recorded precipitation occurred in the summer months of June and July. The lowest monthly total occurred in October, when less than 1 inch of rain fell.

Examination of the daily precipitation data (Appendix 5) shows that precipitation in the winter and early spring months was relatively evenly distributed. The precipitation that occurred in the late spring and summer was from intense storm events. Because of the steep slope, and because maximum evapotranspiration occurs in the summer months, it is presumed that most of the intense rain that fell during the spring and summer left the site as surface runoff or was transpired by vegetation, leaving a smaller amount for infiltration and recharge to the ground-water system. The period of maximum ground-water recharge is most likely in the winter and spring because of the relatively even rate of precipitation and low evapotranspiration.

Ground-Water Levels

Static water levels were measured at roughly 10-day intervals during the 376-day period from January 11, 1991, through January 23, 1992. During this period, 14 of the 16 piezometers had water present in sufficient quantity to measure. Two of these piezometers, 13B and 14A, went dry at times during the period. Continuous water levels could thus be recorded from 12 piezometers.

Table 3 lists the water-level elevations of all the piezometers. The maximum, minimum, and range of water-level fluctuation are also given for each piezometer.

CHEMICAL ANALYSES

Quality of Analyses

Duplicate samples were collected to evaluate the precision of the analytical laboratory. A different sample was chosen for duplication so that a sample from almost every piezometer was duplicated throughout the sampling period. The results of analysis and the ID of the sample it duplicated are presented in Appendix 6. Overall, the results from the lab showed excellent precision.

An indication of the accuracy of water analyses data can be obtained by calculating the charge-balance error, which is the calculated difference between the sum of the cationic charges and the sum of the anionic charges divided by the sum of the cation and anion charges; it is represented by the expression

$$\text{Error} = \frac{\sum \text{MEQc} - \sum \text{MEQa}}{\sum \text{MEQc} + \sum \text{MEQa}} \times 100\%$$

where MEQc = cations in millequivalents and MEQa = anions in millequivalents (Freeze and Cherry, 1979). Many laboratories consider charge-balance error of less than 10 percent as acceptable, although advanced analytical equipment is making it possible to obtain results with errors less than this. Figure 12 is a bar graph with the distribution of charge-balance error and the corresponding percent of total analyses. The results achieved for this study are good, with 92 percent of the performed analyses with an error of less than 10 percent. The average charge-balance error for the 129 analyses was 5.36 percent.

Laboratory tests were performed to evaluate the chemical effects, if any, of the sand used as a filter pack around the piezometer screens. Samples were drawn from a 4-liter con-

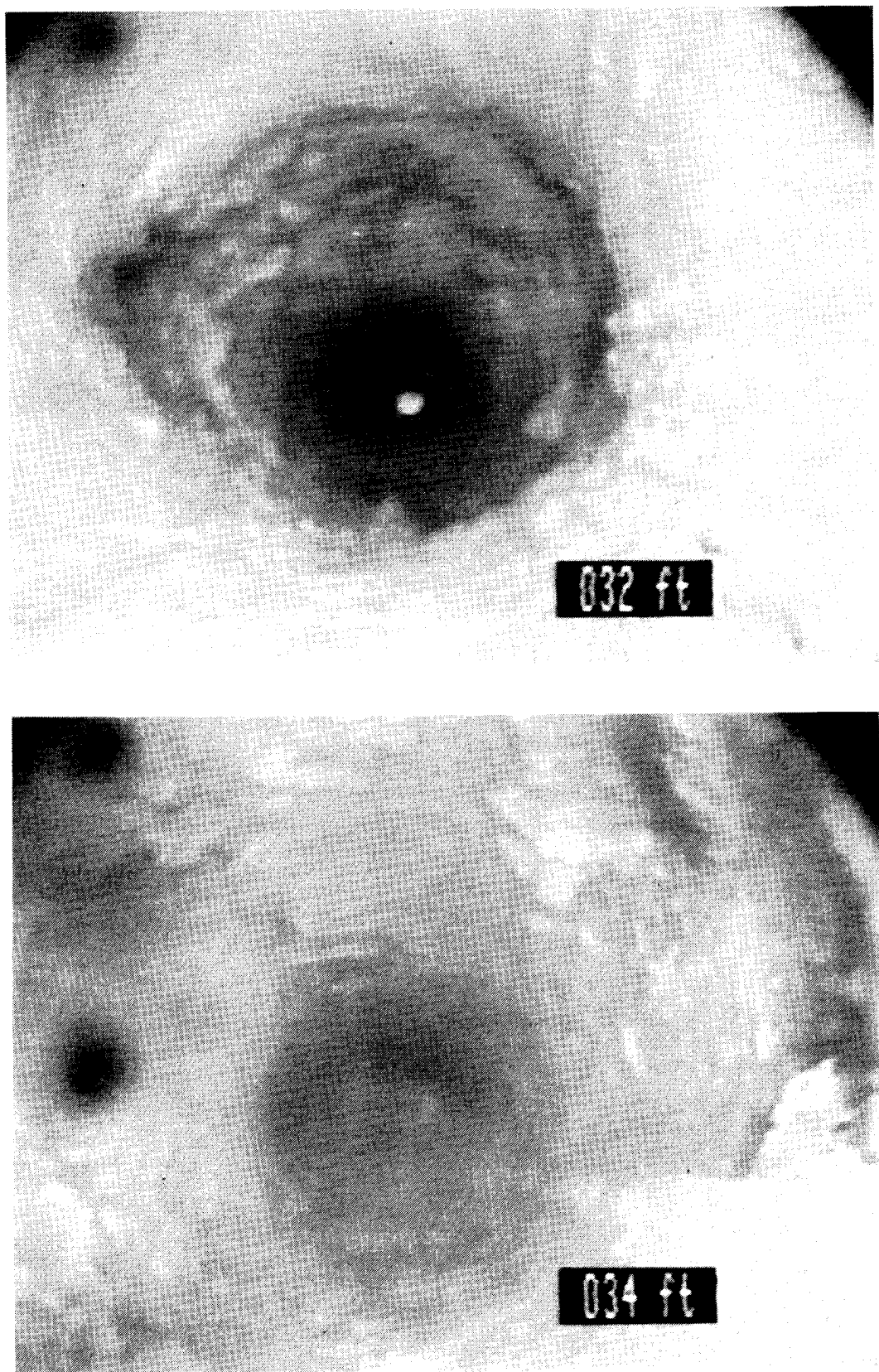


Figure 7. Photographs showing collapse of borehole along a fractured zone in well 14. To obtain color copies of these photographs, contact the Kentucky Geological Survey.

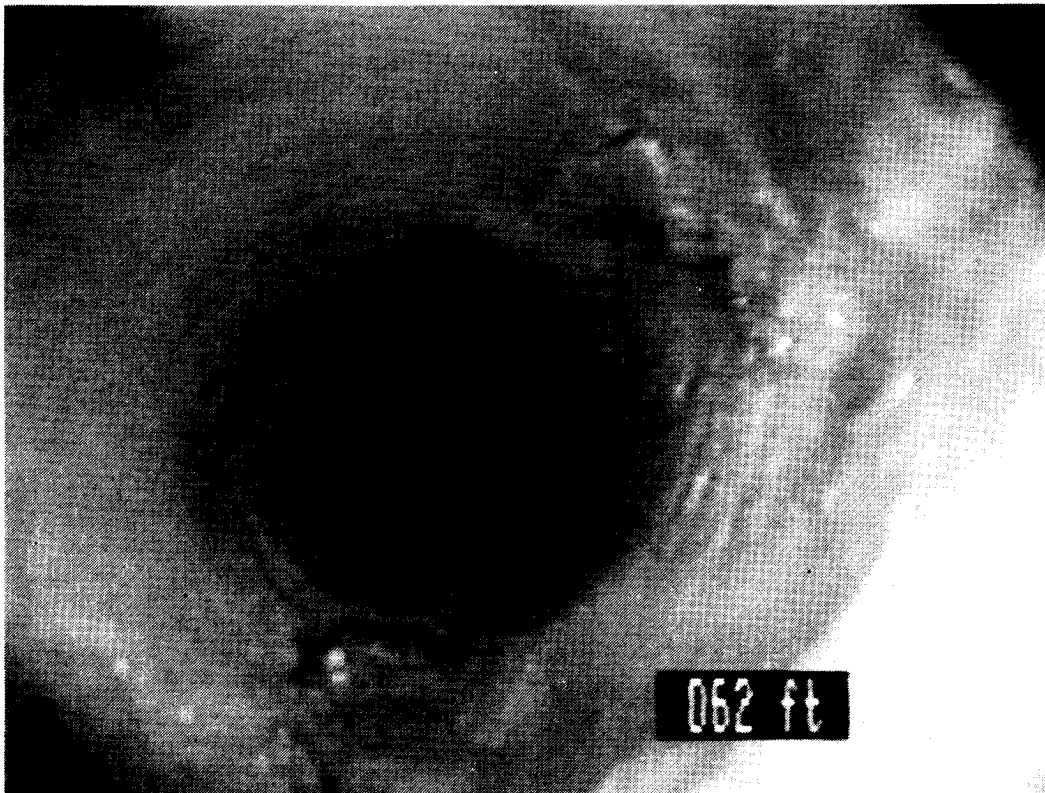


Figure 8. Vertical fracture encountered in well 11. To obtain color copies of these photographs, contact the Kentucky Geological Survey.

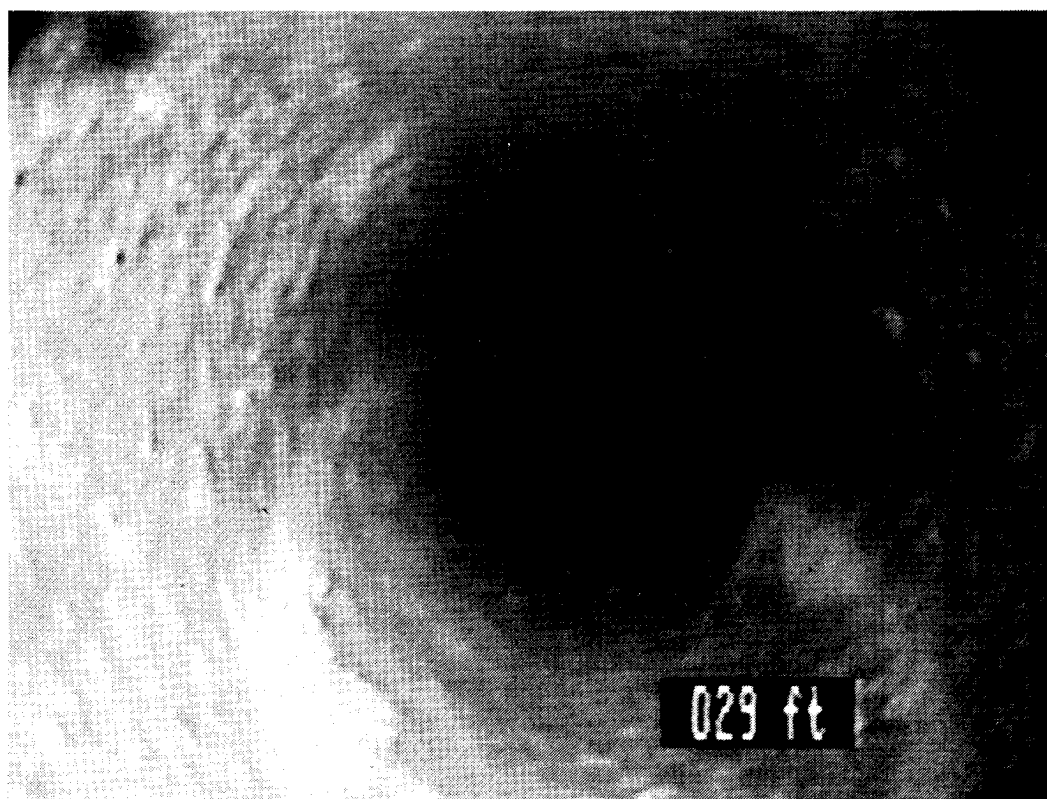
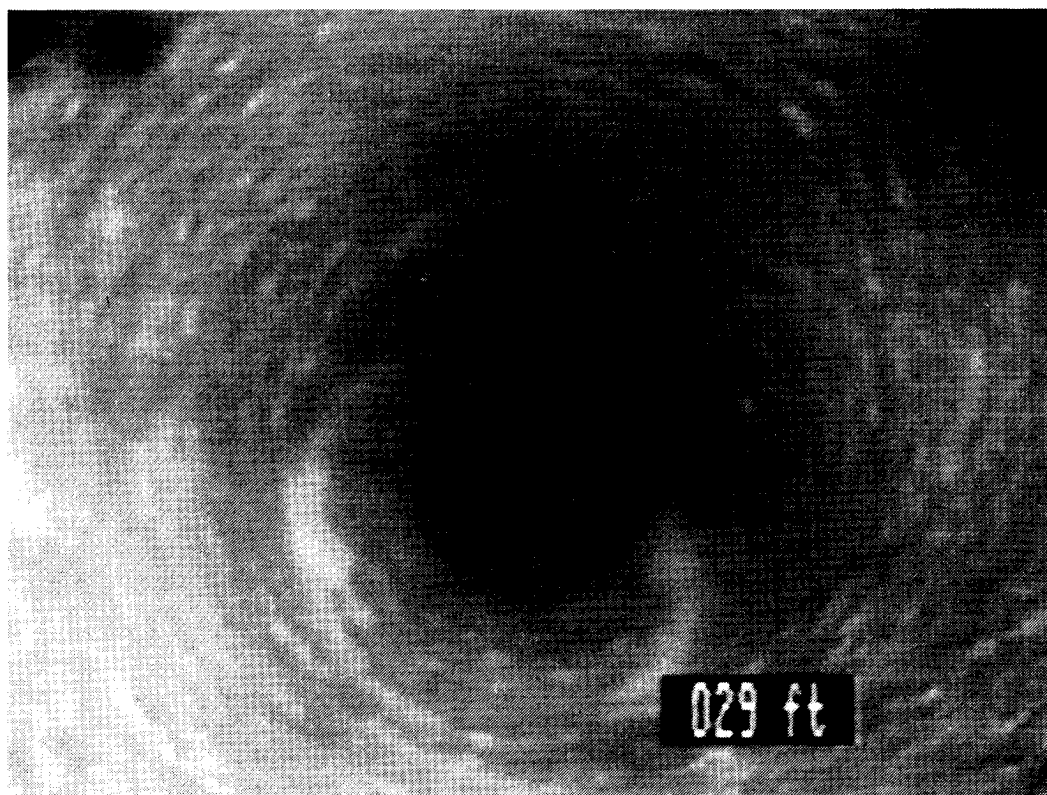


Figure 9. Infilled fracture encountered in well 13. Fracture plane is inclined to the vertical borehole, forming an elliptical pattern. Clay or sediment can be observed oozing from the fracture. To obtain color copies of these photographs, contact the Kentucky Geological Survey.

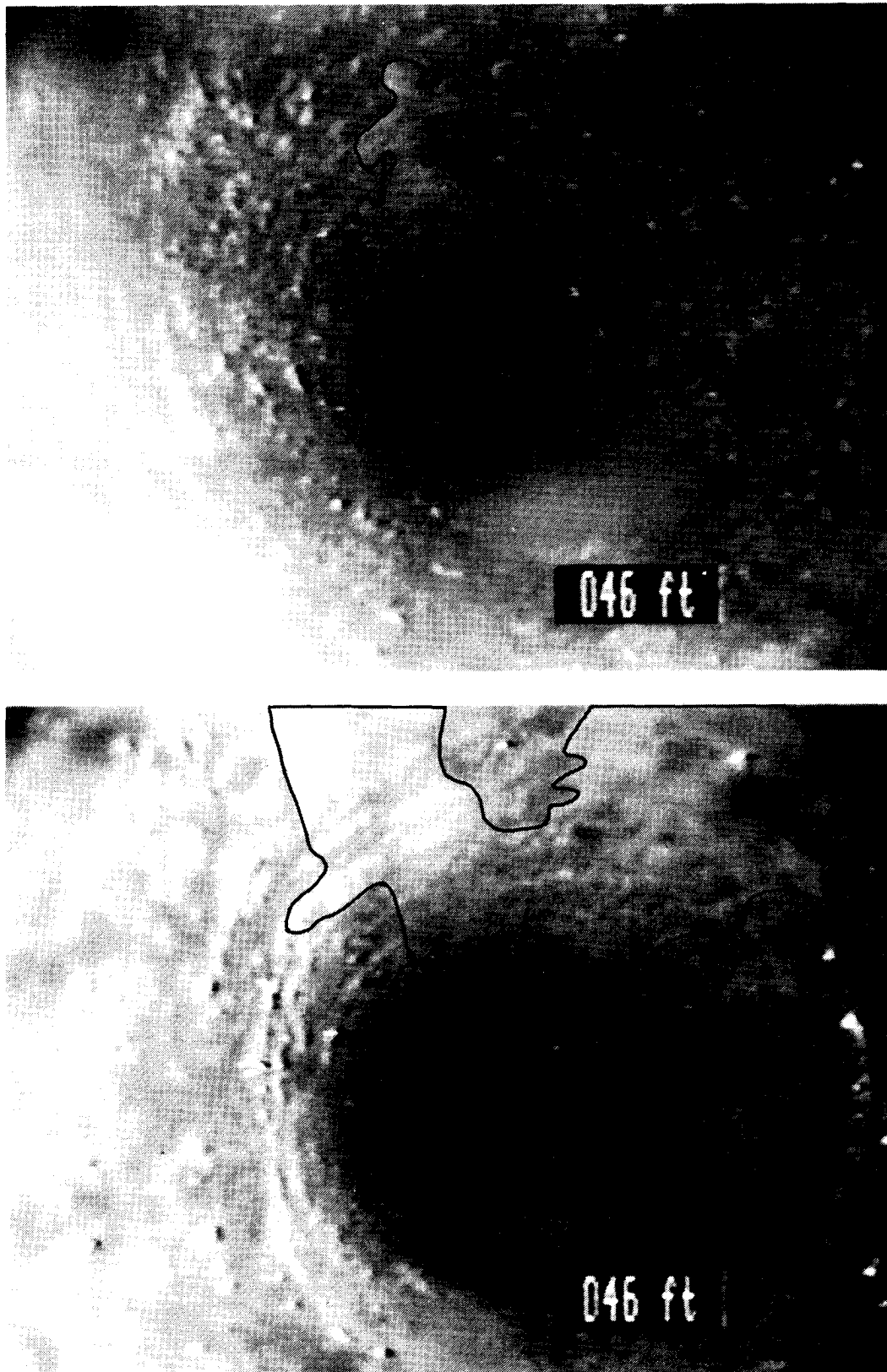


Figure 10. Water entering the borehole from the Hazard No. 8 coal in well 11. Bright areas on the left side of the photographs are caused by the reflection of the camera light where water is flowing out of the coal. Areas where Fe-oxides have precipitated are outlined. To obtain color copies of these photographs, contact the Kentucky Geological Survey.

Table 2.—Piezometer Identification, Total Depth, and Zone to be Monitored.

Piezometer	Total Depth (feet)	Zone Monitored
11A	418	Below drainage, ridge interior
11B	195	Hazard No. 5 coal
11C	48.5	Hazard No. 8 coal
12A	167	Fracture in shale
12B	131	Hazard No. 6 coal
13A	102	Hazard No. 7 coal
13B	50	Hazard No. 8 coal
14A	40	Fracture zone
21A	67	Hazard No. 5 coal
21B	47	Fracture zone
22A	290	Below drainage, ridge interior
22B	200	Base of Magoffin Shale
31A	140	Below drainage, hillslope
31B	100	Fracture zone
41A	172.7	Sandstone, deep below drainage
41B	70	Below drainage, valley bottom

tainer holding the sand and distilled water and analyzed for significant metal content at roughly quarterly intervals during the period of study. The results of analyses are included in Appendix 6. The test results reveal that no appreciable metals concentrations result from leaching or dissolution of minerals contained in the sand. The concentrations of all metals were below 0.5 mg/L. Only six metals out of an analytical suite of 30 were present in concentrations above the limit of detection of the ICAP instrument. Therefore, it is highly unlikely that the results of chemical analyses from water samples would be significantly affected by mineral-water reactions between formation water and the sand-pack material.

Tritium Analyses

The results of the tritium analyses for water samples collected in May of 1991 are listed in Table 4. Thirteen piezometers had sufficient water from which a sample could be collected for analysis. Water samples with tritium values below 6 TU were resampled in June of 1991 and analyzed using enrichment, which results in higher precision and accuracy.

Water Samples

Water samples were collected on a monthly basis for the period of 1 year beginning in February of 1991 and ending in January of 1992. All piezometers, with the exception of 12B, 13B, and 21B, produced sufficient water for samples to be drawn each month. Piezometers 13A and 14A had months when the water level dropped below a level where satisfactory samples could be taken, and samples were not collected during 8 of the 12 months for 13A; also, 14A is lacking 1 month of data.

Compilation of chemical data from field and laboratory analyses is contained in Appendix 6. Univariate statistics for each ion or applicable parameter, including the maximum and minimum value, mean, standard deviation, coefficient of variation, and the number of samples are shown.

Examination of the tabulated data revealed that the chemical data for the first suite of water samples collected for this study in February of 1991 may not be representative of the water chemistry for each of the piezometers from which samples were drawn. It can be seen from the tabulated data (Appendix 6) that the concentrations of several parameters are

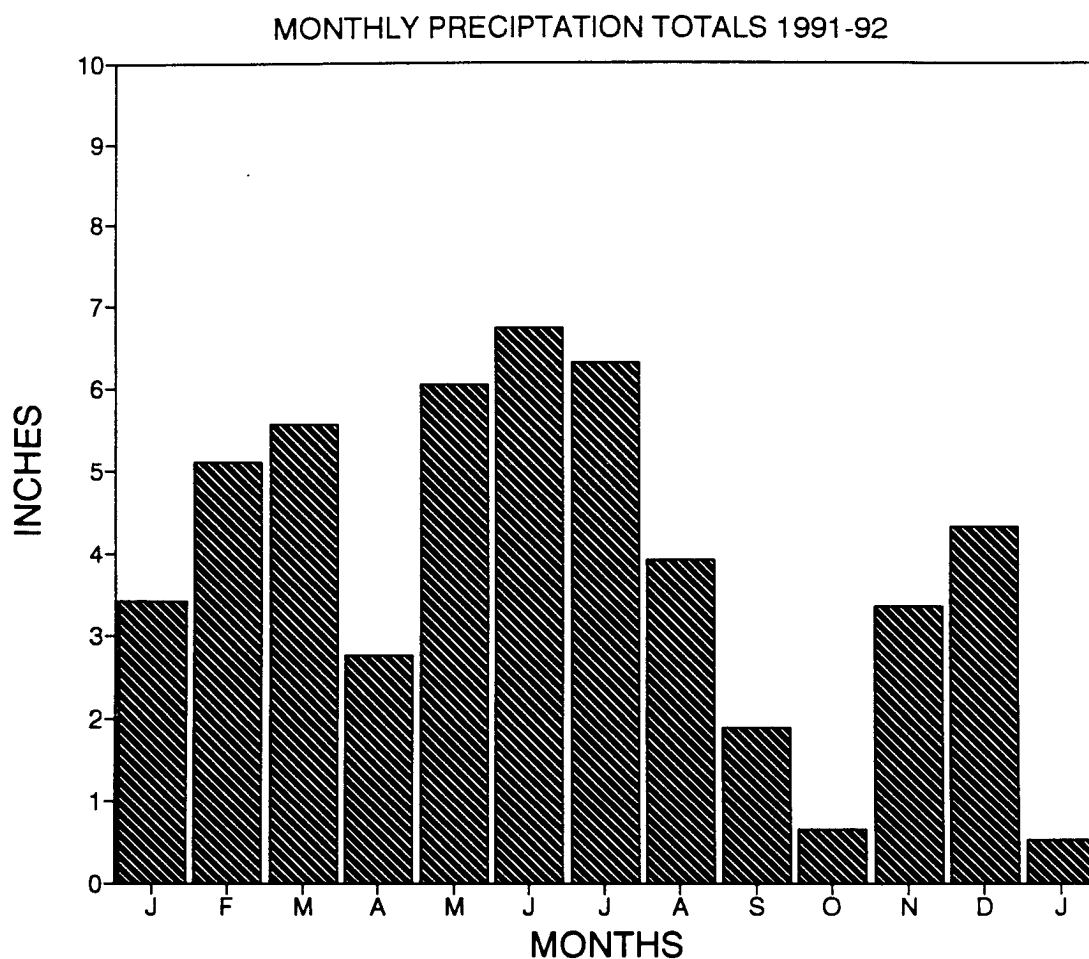


Figure 11. Monthly precipitation totals.

either considerably lower or higher when compared to the data from all subsequent analyses. This disparity in the data is most likely due to insufficient development after the piezometers were completed. It was noted that during the first sampling episode that water drawn from some piezometers still exhibited considerable turbidity, most likely a remnant of well construction. Therefore, the chemical data resulting from samples taken on February 5 and 6, 1991, will not be included in statistical calculations, graphical portrayal of data, or discussions in this study. The samples used for discussion in this report will therefore be those collected from March 1991 through January 1992.

Fluoride in Ground Water

The occurrence of significant fluoride (in this study concentrations above 1.0 mg/L are considered significant) in ground water at the site is restricted to piezometers 11A and 22A. Both of these piezometers monitor the same zone, which is the ridge interior at an elevation that is just below drainage. The mean value for fluoride in these two piezometers is 1.59 and 1.02 mg/L, respectively. All of the water samples from the other piezometers have maximum and mean fluoride concentrations below 1 mg/L.

Barium in Ground Water

Two piezometers, 41A and 41B, show maximum and mean values for barium exceeding 1.0 mg/L. This value is the maximum contaminant level (MCL) currently suggested by the U.S. Environmental Protection Agency (U.S. EPA, 1975). The mean value for barium concentration in piezometer 41A is 37.4 mg/L, and 1.72 mg/L in 41B. Piezometer 12A showed an increase in barium content with each subsequent sampling, and the concentration exceeded 1.0 mg/L during the period from September 1991 through January 1992.

Barium-Sodium Exchange Experiments

The results of laboratory experiments to determine the potential exchangeability of sodium for barium on rock particle surfaces from the study are shown in Table 5. A high linear correlation ($r = .99$) exists between the amount of barium extracted into solution and the concentration of the Na-Cl solution used. A 100-millimolar Na-EDTA solution was used to determine the maximum extractable barium from the samples. The samples derived from borehole 11 had a mean value of 1.43 mg/L of Ba (average based on triplicate samples) and 1.64 mg/L of Ba for samples from borehole 41.

Table 3.—Water-Level Elevations for All Piezometers.

Date:	MW#:11A	11B	11C	12A	12B*	13A	13B	14A	21A	21B*	22A	22B	31A	31B	41A	41B
1/11	905.0	1093.6	1245.7	1121.9		1185.7	1235.6	1251.7	1089.5		904.6	990.5	872.5	918.4	842.5	866.5
2/4	905.9	1093.8	1243.4	1122.3		1185.1	1235.2	1251.1	1089.9		905.2	990.4	871.7	917.1	841.8	867.8
2/13	904.0	1094.0	1244.9	1122.2		1185.4	1235.4	1250.7	1089.9		901.6	991.8	871.8	917.1	841.7	864.2
2/20	903.5	1093.7	1248.1	1122.2		1185.1	1236.1	1252.2	1090.0		901.2	991.6	871.4	916.9	843.3	864.5
2/27	903.6	1093.8	1245.3	1122.2		1185.7	1235.3	1251.3	1089.9		901.1	991.3	871.4	917.1	841.4	863.9
3/6	904.1	1093.9	1242.6	1122.3		1185.8	1235.4	1249.9	1090.2		901.8	991.2	871.9	917.2	841.8	863.9
3/13	903.9	1093.9	1239.5	1122.3		1185.5	1235.3	1250.4	1089.9		901.7	990.8	870.9	917.4	841.3	863.9
3/20	903.5	1093.7	1240.0	1122.2		1185.7	1235.5	1251.5	1090.1		901.1	990.3	870.9	917.3	841.2	863.8
3/26	903.9	1093.8	1240.3	1122.3		1185.7	1235.8	1251.5	1090.1		901.5	990.7	871.2	917.4	841.1	863.8
4/2	903.5	1093.7	1240.4	1122.1		1185.8	1235.7	1251.6	1090.1		901.1	990.4	870.9	917.3	841.3	863.8
4/17	903.9	1093.9	1240.2	1122.3		1185.8	1235.8	1251.6	1090.3		901.9	988.3	870.9	917.5	841.7	864.1
4/24	903.7	1093.7	1239.7	1122.2		1185.4	1235.6	1251.4	1089.9		901.6	989.0	871.0	917.4	840.9	863.7
5/3	903.3	1093.7	1239.3	1122.3		1185.0	1235.3	1250.8	1089.9		901.4	988.9	871.0	917.5	840.5	863.6
5/7	903.2	1093.7	1239.0	1122.3		1184.9	1235.2	1250.6	1089.8		901.1	988.6	870.8	917.3	840.2	863.4
5/15	903.5	1093.8	1239.3	1122.3		1184.7	1235.2	1248.5	1089.6		902.1	987.7	866.8	917.4	840.7	862.6
5/22	903.5	1093.8	1240.2	1122.2		1185.2	1235.6	1251.5	1089.9		902.0	988.9	868.9	917.5	841.2	863.9
5/30	903.5	1093.8	1239.6	1122.3		1184.8	1235.4	1251.6	1089.8		902.2	989.3	869.7	917.6	840.8	863.7
6/4	903.7	1093.7	1240.5	1122.2		1185.3	1235.6	1251.9	1089.9		902.1	989.6	869.8	917.5	840.7	863.8
6/12	903.5	1093.7	1239.0	1122.2		1184.8	1235.3	1250.9	1089.8		902.2	987.2	869.9	917.6	840.2	863.5
6/20	903.4	1093.8	1238.3	1122.2		1184.6	1235.0	1251.0	1089.7		902.3	987.8	870.0	917.4	840.4	863.5
6/27	903.0	1093.8	1238.9	1122.2		1184.5	1235.0	1251.7	1089.6		901.9	988.6	869.9	917.3	841.1	863.6
7/11	903.2	1093.6	1238.1	1122.2		1184.2	1234.1	1250.9	1089.3		901.9	988.3	870.0	917.0	840.4	863.6
7/18	903.0	1093.8	1238.6	1122.2		1184.5	1234.4	1250.5	1089.4		901.1	987.3	865.3	917.1	840.8	863.5
7/30	903.0	1093.6	1238.2	1122.2		1184.3	1233.9	1251.0	1089.2		901.0	988.1	869.1	917.1	840.4	863.4
8/6	902.7	1093.6	1238.0	1122.2		1184.2	1233.8	1250.7	1089.1		900.6	988.0	869.3	916.9	840.0	863.2
8/29	902.5	1093.5	1238.2	1122.1		1184.2		1248.3	1088.9		900.3	987.3	869.1	916.6	840.0	863.2
9/17	902.2	1093.4	1238.1	1122.1		1184.2		1248.5	1088.6		900.0	987.4	869.5	916.1	840.1	863.2
10/1	902.1	1093.5	1237.4	1122.1		1184.2		1245.6	1088.5		898.9	990.6	869.1	915.8	839.9	863.2
10/7	901.7	1093.5	1237.5	1122.0		1184.2		1245.6	1088.3		898.7	990.4	869.3	915.2	839.6	863.1
10/24	901.8	1093.6	1237.0	1122.1		1184.2			1088.0		899.0	990.4	869.2	915.0	839.9	863.2
11/5	901.7	1093.5	1237.1	1122.0		1184.2			1088.0		898.6	990.2	869.4	914.7	839.6	863.1
11/11	901.7	1092.4	1237.0	1122.0		1184.2			1087.9		898.6	990.2	869.5	914.4	839.5	863.1
11/25	901.5	1093.5	1237.1	1122.0		1184.2		1244.7	1087.7		898.5	990.2	869.7	914.0	839.7	863.3
12/10	901.8	1093.3	1236.5	1121.8		1185.0		1249.6	1088.2		898.4	990.6	869.2	914.7	840.3	863.7
01/09	903.2	1093.8	1240.0	1121.9		1185.1		1251.4	1089.3		898.8	990.4	870.0	915.8	839.8	863.5
01/23	903.2	1094.2	1239.7	1122.1		1184.9		1250.9	1089.7		898.8	990.6	870.4	916.3	839.7	863.7

*Dry Well

MAX	905.9	1094.0	1248.1	1122.3		1185.8	1236.1	1252.2	1090.3		905.2	991.8	872.5	918.4	843.3	867.8
MIN	901.7	1093.4	1237.0	1122.0		1184.2	1233.8	1245.6	1088.0		898.6	987.2	865.3	914.7	839.6	862.6
RANGE	4.2	0.6	11.1	0.3		1.6	2.3	6.6	2.3		6.6	4.6	7.2	3.7	3.7	5.2

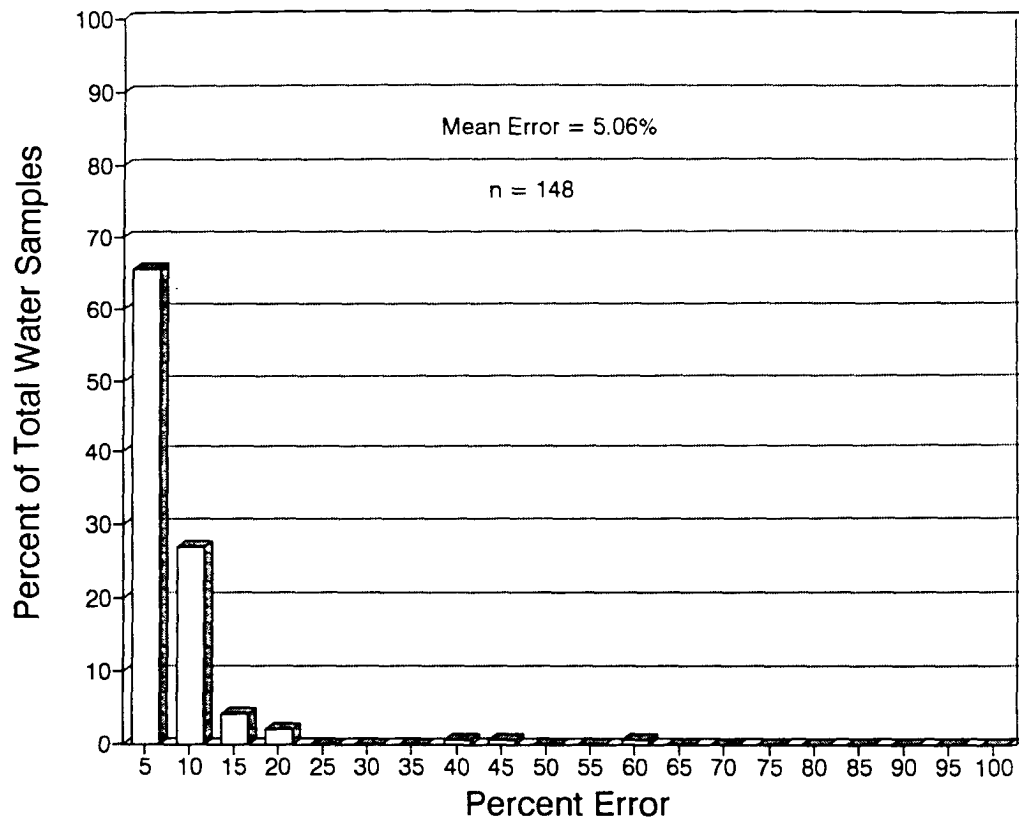


Figure 12. Charge-balance error determined for all inorganic analyses.

Table 4.—Results of Tritium Analyses.

Sample ID	Counting Method	TU	error (\pm TU)
11A	Enrichment	0.32	0.12
11B	Enrichment	2.19	0.30
11C	Direct	13	2
12A	Direct	13	2
13A	Direct	13	2
14A	Direct	23	2
21A	Direct	17	2
22A	Enrichment	4.64	0.35
22B	Direct	11	2
31A	Direct	10	2
31B	Direct	13	2
41A	Enrichment	0.53	0.10
41B	Enrichment	7.07	0.33

Total Organic Carbon

Samples were collected for the analysis of total organic carbon content (TOC) during September and October of 1991 (*see* Appendix 6). The results of analysis show that only

three piezometers, 14A, 22B, and 22A, contained significant amounts of TOC. The instrument used to determine TOC only has a resolution of 1 mg/L; therefore, these analyses do not preclude the occurrence of TOC concentrations less than

Table 5.—Results of Barium Exchange and Extraction Experiments Using Deionized Water, 10 Mmol NaCl, and 100 Mmol NaCl Solutions, and 100 Mmol Na-EDTA.

Sample ID	Sodium	Barium	Calcium	Sample ID	Sodium	Barium	Calcium
41B-DI-1	3.02	0.045	4.44	11A-DI-1	13.9	0.002	0.038
41B-DI-2	1.28	0.039	4.85	11A-DI-2	13.3	0.023	0.154
41B-DI-3	1.20	0.045	4.92	11A-DI-3	14.7	0.011	0.129
41B-10-1	210	0.126	7.41	11A-10-1	234	0.076	1.95
41B-10-2	229	0.135	7.97	11A-10-2	243	0.076	1.94
41B-10-3	232	0.143	8.07	11A-10-3	245	0.088	2.05
41B-100-1	1990	0.606	15.7	11A-100-1	2240	0.806	11.2
41B-100-2	2270	0.702	18.0	11A-100-2	2290	0.815	11.7
41B-100-3	2280	0.700	18.3	11A-100-3	2370	0.845	12.1
41B-EDTA-1	2230	1.32	80.7	11A-EDTA-1	2090	1.55	31.3
41B-EDTA-2	2340	1.44	85.1	11A-EDTA-2	2340	1.79	38.9
41B-EDTA-3	2200	1.52	106.0	11A-EDTA-3	2210	1.59	32.8

All Results in mg/L

1.0 mg/L. Piezometer 22B contained the highest concentration with 24 mg/L, followed by 8.0 mg/L in 22A, each in September of 1991. Piezometer 14A showed 4.0 mg/L in October of 1991.

DISCUSSION

The Ground-Water Flow System

Figures 13 and 14 show a traverse of the study site shown on Figure 1 with contours of potentiometric head conditions based on water-level readings from each of the piezometers that contained measureable water. Figures 13 and 14 show the head conditions based on the water levels for each piezometer recorded in February and November 1991, respectively. The equi-potential lines are generated by contouring the potentiometric head level corresponding to the elevation of the bottom of each piezometer. The resulting contours of the head levels are shown on the traverse along a line that passes through each cluster of piezometers.

This graphical representation of the potentiometric head conditions at the site is useful for examining the head gradient of ground water and defining the apparent ground-water flow system. However, the traverse on which the contours are shown is a two-dimensional representation and lacks lateral control where other components of flow could be defined. Therefore, flow lines or any other representation of actual ground-water flow are not shown on this illustration.

Water-level data from February and November were chosen for representation in order to evaluate the changes between the periods of maximum and minimum water levels throughout the year. Overall, the minimum and maximum water levels measured in each piezometer occurred during the same month for all piezometers. All but two piezometers, 13A and 21A, achieved the maximum head reading in February of 1991. Piezometers 13A and 21A reached their maximum lev-

els in April. All but three piezometers fell to their minimum level in November 1991.

Both figures show a consistent drop in head from the ridge top to an elevation below drainage (Lick Branch). The slightly closer spacing between contour lines in the upper area of the ridge indicates a higher vertical gradient than the lower section. The equal head contours in the upper interior section of the ridge correspond closely to their measured elevation (shown on the Y axis of both figures) within the ridge. This reveals that the total head levels in the wells in the upper reaches of the site are approximately equal to the elevation head, suggesting that the ground-water conditions near the ridge top are unconfined or semi-confined and are mostly a function of the elevation of where the piezometer is located. The presence of dry piezometers in this area indicates that portions of the upper part of the ridge are unsaturated. The nearly horizontal attitude of the contours in this area implies a downward, vertical movement of ground water.

The contour lines at lower elevations (920 feet and below) exhibit a moderate amount of downward deflection in the area from approximately 200 feet above drainage to the elevations below drainage (i.e., Lick Branch). The piezometric contours in this area are well below their corresponding elevation level, indicating that the pressure head at this level provides a significant contribution to the total head.

Figure 14 shows the contoured head elevations when the water levels were at their lowest conditions. There is very little noticeable change in the shape or intensity of the contours between Figure 13 and Figure 14, strongly suggesting a relatively consistent flow field remains throughout the year.

Piezometers Monitoring Fracture Zones

Four piezometers, 12A, 14A, 21B, and 31B, monitor fractured bedrock zones. Piezometer 21B did not accumulate water during the study period. Piezometer 12A is screened in

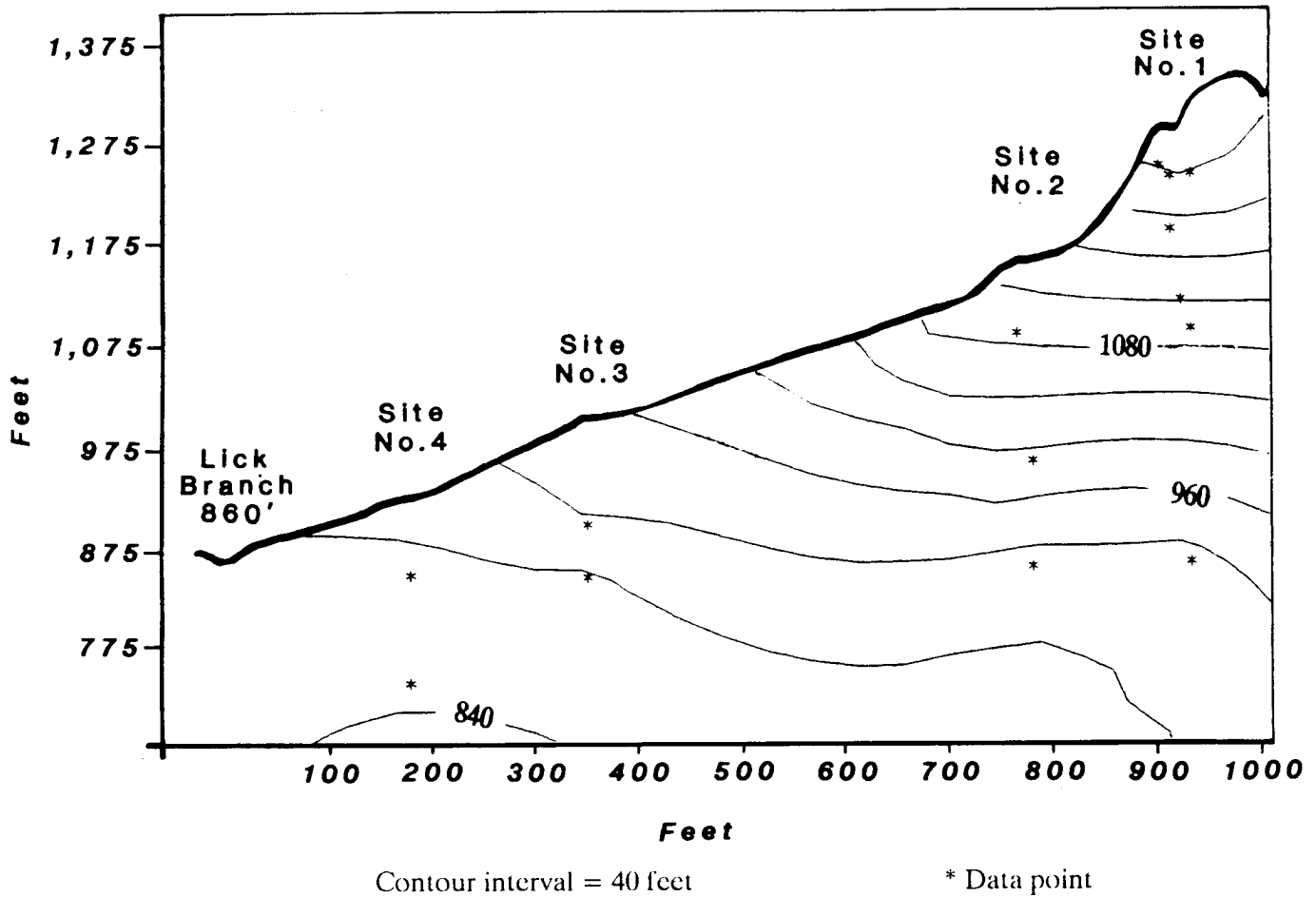


Figure 13. Contoured profile of potentiometric head measured in February 1991.

a sandy-shale zone above the Hazard No. 5 coal. No fractures in the rock were observed at this elevation by downhole camera observation because visibility was lost; however, examination of the geologic core indicated fractures in shale at this elevation (the location of the core hole, CH 1066, is approximately 20 feet from the borehole containing piezometer 12A). The hydrograph for piezometer 12A is shown on Figure 15. The hydrograph shows that the water level remains fairly consistent throughout the record period, with a subtle decline in water level from its maximum of 1,122.3 feet to its minimum of 1,122.0 feet in December. The hydrograph does not seem to correlate well with the trends in precipitation measured at the site. Apparently, the fractures present in CH 1066 either do not intersect the immediate area monitored by piezometer 12A, or fractures become ineffective in transmitting recharging water to this depth.

Piezometer 14A is open to the shallow fracture zone above the Hazard No. 8 coal. The hydrograph for this piezometer is shown in Figure 16. The range of water-level fluctuation is 7.7 feet. The hydrograph shows a fluctuating water level that remains between 1,248 and 1,252 feet from the beginning of the record period to August. The water level drops throughout the fall months, and the piezometer becomes dry

in October. Water accumulates in 14A again in late November and quickly rebounds up to near the level it had attained at the beginning of the study. The hydrograph exhibits a close correlation with the monthly precipitation data observed for the study period. The maximum water level of nearly 1,252.2 feet is reached in February of 1991. The dry period for this piezometer corresponds well to the period of lowest precipitation (October) measured at the site. Water once again accumulates in the piezometer following an increase in precipitation in November. This pattern indicates that the shallow fracture monitored by piezometer 14A is greatly influenced by atmospheric recharge and that the fractures maintain a good connection with the ground surface.

The hydrograph for piezometer 31B is shown in Figure 17. This piezometer is screened at a zone where fractures were observed at a depth of approximately 100 feet. The hydrograph reveals an initial drop in water level by over 1 foot. A slight rise in water level occurs from February through June, before falling to a minimum value in December. The hydrograph for this piezometer is generally smooth, more closely resembling the pattern exhibited by 12A than the erratic hydrograph displayed by 14A. This observation suggests that the rapid and pronounced effect of recharge in fractured bed

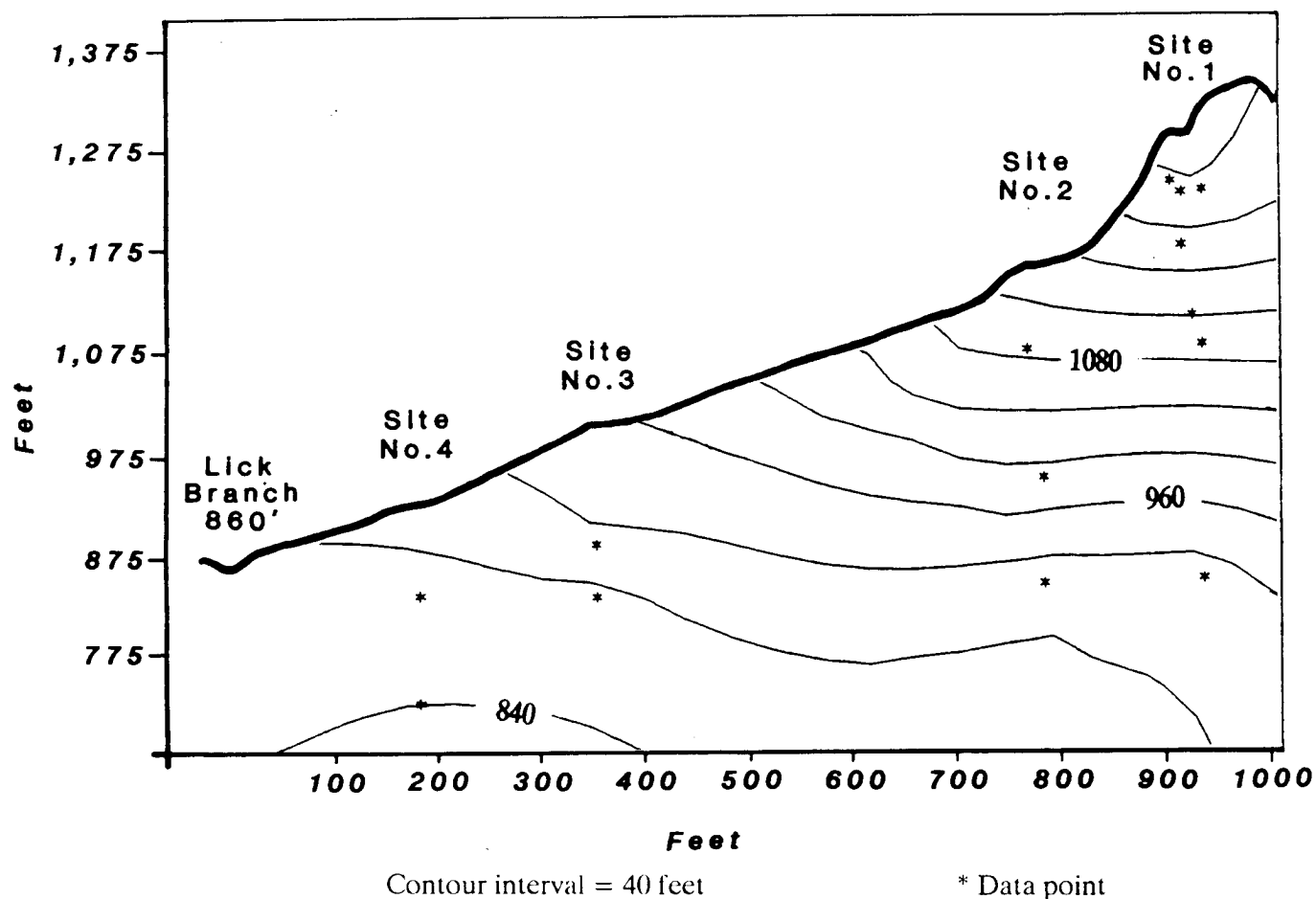


Figure 14. Contoured profile of potentiometric head measured in November 1991.

rock decreases with depth below the surface. Additionally, the hydrograph for piezometer 31B may be an indicator of the effect of the degree of saturation of the hillside fracture system compared to the system at the ridge top, which appears to exhibit saturated conditions only during wet periods. Piezometer 31B, representing the hillside system, remained saturated throughout the study period. The water present in the hillside fracture system may act to buffer the incident recharge, whereas piezometers monitoring fractures at the ridge top (e.g., 14A) would exhibit water-level pulses in response to rapid recharge entry because the unsaturated fractures would likely offer less resistance to rapid changes in ground-water movement.

Piezometer 21B was screened in the shallow near-surface zone where fractures were observed with the downhole camera. Piezometer 21B remained dry throughout the study period. The lack of water accumulation in this screened fracture zone indicates some shallow fracture zones remain unsaturated. The infilled fractures observed by the downhole camera (see Fig. 9) support this observation.

Piezometers Monitoring Coal Seams

Six piezometers, 11B, 11C, 12B, 13A, 13B, and 21A, were installed to monitor water in coal seams. Figure 18 shows the hydrograph for piezometer 11C, which monitors the Hazard No. 7 coal. The maximum water level was recorded in February and the minimum level recorded in December. The greatest fluctuations occurred in the winter months of February through March, with a steady decline in water level taking place for most of the remainder of the year. This piezometer exhibited the largest water-level fluctuation of all piezometers at the site (11.1 feet). A correlation of the water-level fluctuation with monthly precipitation is observed. The steep drop in the hydrograph that occurs during February and March is somewhat opposite the precipitation pattern observed at the site during the same period. One possibility is that the spring awakening of vegetation may have resulted in the sharp water-level drop due to increased vegetative demand on the shallow ground-water supply.

A gradual decline in water level is observed for most of the remaining months, which may be due to increased evapo-

Piezometer 12A

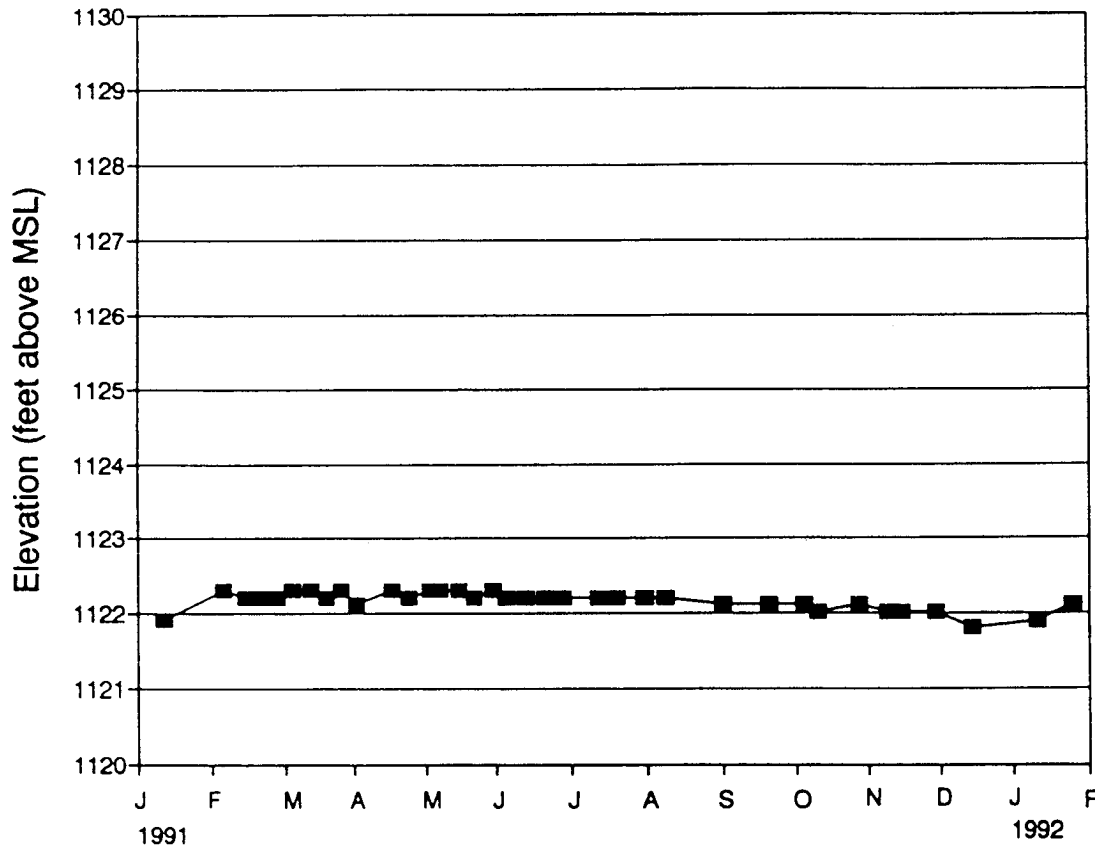


Figure 15. Hydrograph for piezometer 12A.

transpiration, along with the loss of recharge due to the high runoff usually associated with intense summer storms, which composed most of the precipitation during the period of May through August. The minor peaks in water level that seem to correspond to the increase in precipitation observed in May through July indicate that some water from these storm events is able to enter the coal seam during or after these events.

The hydrograph for piezometer 11B, which monitors the Hazard No. 5 coal, is shown on Figure 19. The water level in this piezometer remained relatively unchanged, and ranged between 1,093 and 1,094 feet. Very little correlation with the precipitation trends is observed, with the exception of the sharp drop in water level in November, which may be a delayed response to the low precipitation measured in October. Piezometer 11B is screened at a depth of 195 feet. A significant amount of rock mass lies between the coal and the ground surface, which probably acts to buffer the movement of water downward to this level, resulting in the stable hydrograph. Additionally, the occurrence and frequency of fractures that transmit water at depth tend to decrease with increasing depth from the surface (Wyrick and Borchers, 1981; Kipp and Dinger, 1987).

Piezometer 12B is open to an interval that included the Hazard No. 6 coal and accumulated no water during the re-

cord period. Water injection data (see Fig. 6) indicate that the interval that includes this coal had a higher hydraulic conductivity than the surrounding rock, suggesting that this zone should contain water if it is stored in adjacent rocks. It is possible that the No. 6 coal was inadvertently sealed by bentonite or drill cuttings during drilling or well construction, which would act to retard the production of water. This sealing could have occurred because the well is located in the near-surface fracture zone where bentonite and cuttings would be free to move into the fractures or coal cleats, thereby sealing them.

The hydrograph for piezometer 13B is shown in Figure 20. This piezometer exhibits a similar hydrograph pattern to piezometer 11C, but within a smaller range. The range of water level fluctuation in 13B is 2.3 feet. Both of these piezometers monitor the Hazard No. 8 coal. A comparison of the water-level data for each of these piezometers reveals that the difference in maximum water level between these two piezometers is 12 feet. Also, piezometer 13B became dry in August, whereas 11C did not. Apparently the screened interval for 11C may be in contact with a fracture system in which rapid recharge can enter that may not be present in 13B. Examination of the geologic core showed that the Hazard No. 8 coal also contained several splits consisting of fire clay and shale. A difference in the exact placement of the screens in

Piezometer 14A

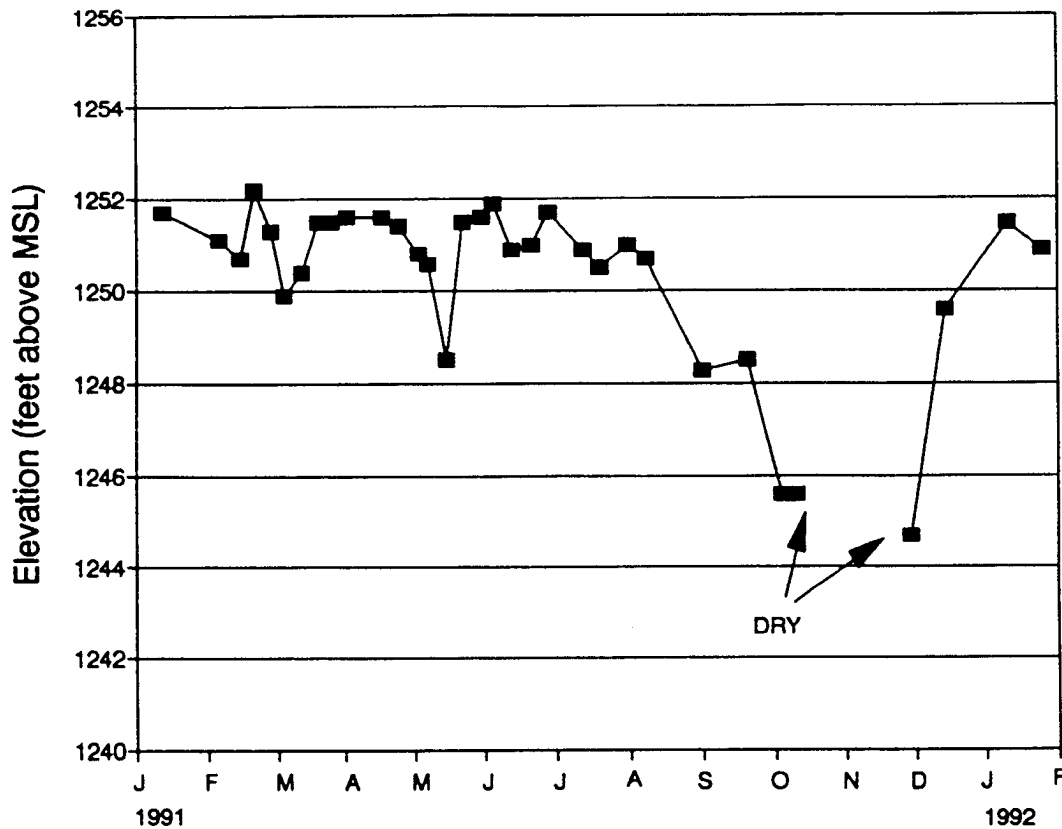


Figure 16. Hydrograph for piezometer 14A.

relation to the splits could also explain the difference in head if the coal layers contributing water to each piezometer are not in direct hydraulic connection. Piezometer 13B is set at a depth of 50 feet and 11C is set to a depth of 48.5 feet. The difference in depth (1.5 feet) may have resulted in sufficient offset to limit the hydraulic connection between the two piezometers. Additionally, blockage to water entry resulting from drill cuttings being injected into the cleat may have occurred in 13B, resulting in decreased flow. Piezometer 13B also became dry in August of 1991 and did not regain water for the duration of the study.

Piezometer 13A is screened into the Hazard No. 7 coal. The hydrograph shown on Figure 21 indicates a net decrease in water level for the record period before rebounding in December. The maximum water level of 1, 185.9 was reached in April, and the minimum of 1, 184.2 was observed in October and November, indicating a water-level range of only 1.7 feet. The Hazard No. 7 coal has approximately 100 feet of overburden above it in the location of piezometer 13A. The overlying bedrock, in conjunction with decreasing fractures with depth, probably acts to restrict the rapid influx of recharge into this coal seam.

Piezometer 21A is situated in the Hazard No. 5 coal. Figure 22 shows that the water level remains relatively constant for the first half of the year near an elevation of 1,090 feet,

until a gradual decrease begins in June and continues throughout the summer and fall months. Comparison of the hydrograph for this piezometer with the hydrograph of piezometer 11B, which is also screened in the Hazard No. 5 coal but in the ridge interior, shows that the water level in 21A is lower by an average of close to 4 feet. The water-level decrease observed in both 11B and 21A during the fall months occurs much sooner in 21A. The more rapid hydrograph response in 21A, along with the decreasing hydraulic gradient from 11B toward 21A, suggests that the water in the Hazard No. 5 coal is discharging along the side of the hill in the direction of 21A where the coal seam crops out. Water was observed discharging from the Hazard No. 5 coal where the access road intersects the exposed coal seam during the field reconnaissance for study-site selection. Because the Hazard No. 5 is the lowest significant coal seam (>1 foot thick is considered a significant coal seam) in the geologic section, it probably acts as a significant control to the amount of ground water that can migrate down into the ridge interior by laterally diverting the downward flow of ground water from the mass of rocks and coal above it.

Figure 23 shows the piezometers that monitor coal seams plotted as a function of increasing depth below the surface. A strong relationship is observed in the water-level fluctuation in each piezometer as a function of depth below the surface.

Piezometer 31B

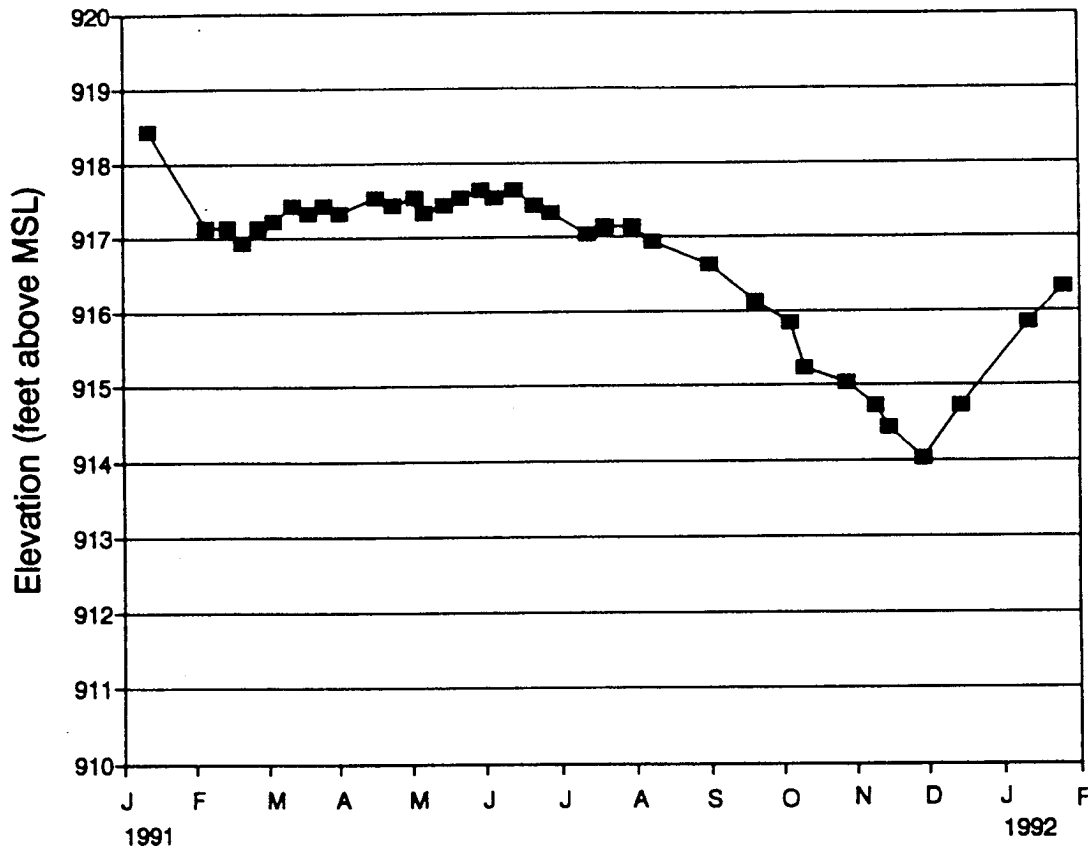


Figure 17. Hydrograph for piezometer 31B.

Coals that are nearest the surface exhibit the greatest amount of water-level fluctuation. Fluctuation decreases with increasing thickness of overburden, and is most likely attributable to the decrease in the movement of water through fractures, and an increased granular flow component with depth that would tend to buffer rapid ground-water infiltration. The shift from fracture flow to granular flow probably is caused by the decrease in the frequency and distribution of fractures, along with the infilling of fractures by sediment or mineral precipitation.

Piezometers in the Below Drainage Ridge Interior

Six piezometers were installed to monitor ground water in the ridge interior and valley bottom area where no near-surface fractures or coal seams were observed. All of these piezometers, with the exception of 22B, were set at an elevation that is at or below the elevation of the nearest major drainage (Lick Branch). Each of these piezometers contained measurable water throughout the period of study.

The hydrograph for piezometer 22B (Fig. 24) shows a roughly cyclic rise and fall of its water level, which is superimposed on a net decline that continues until September. The water level rebounds to above 990 feet in October and remains near this level for the remainder of the record period. The cyclicality exhibited by the graph may be related to the

well's recovery after purging and sampling. Examination of the individual water-level data reading indicates that the steep drop in water level was usually recorded on the first water-level measurement, which was usually several days after sampling (a minimum of three or more well volumes was purged from the piezometers before collecting samples for chemical analysis). Subsequent water-level readings show a gradual increase in water level until the next sampling event. Piezometer 22B could often be purged dry when sampling.

The net drop in water level during the months of maximum precipitation indicates that little or no direct recharge was entering the water-producing zone screened by piezometer 22B. The drop in water level, along with the drawdown-recovery cycle exhibited by this piezometer, suggest that the water is released from rocks with a low storage capacity. Fractures probably do not penetrate to this depth (200 feet); therefore, there is no route for direct recharge from the surface. Unfortunately, the downhole-camera examination was limited in this hole due to turbid water conditions, and the extent of fractures that intersect the hole was not qualified.

The screened interval for piezometer 11A penetrates to the center of the ridge interior. The hydrogeologic zone of interest is interbedded sandstone and siltstones below the Magoffin Shale. The hydrograph for this piezometer is shown on Figure 25. A drop in water level of nearly 2.5 feet occurred

Piezometer 11C

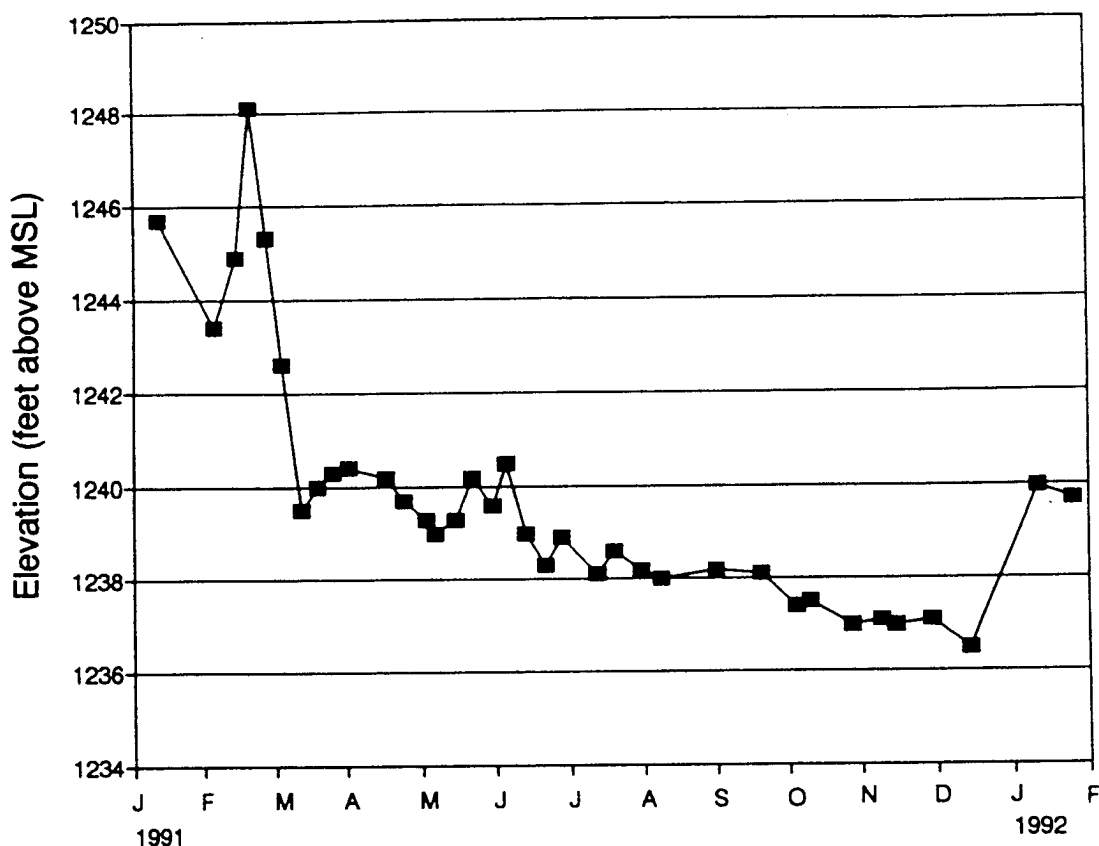


Figure 18. Hydrograph for piezometer 11C.

during February. This anomaly may be the result of water injected into the surrounding rock before construction of the piezometers had taken place, and subsequently discharging back into the hole. The water-level elevation measured in the open hole before piezometer 11A was installed was approximately 1,049 feet, which is nearly 150 feet higher than the observed water level after completion. After piezometer installation and development, the water level dropped to a level that seems more in line with subsequent measurements. The water level oscillated between 903 and 904 feet throughout most of the spring and early summer, before dropping steadily and reaching its lowest level in December. The oscillations in water level are all within a range of 1 foot and do not exhibit any obvious correlation with specific precipitation events except for the gradual decline in water level that began about August, and continued through the fall months.

The hydrograph for piezometer 22A is shown in Figure 26. Piezometer 22A is screened in the same interval as piezometer 11A, except that it is located downslope from 11A. The hydrograph shows a similar pattern to that exhibited by piezometer 11A. Piezometer 22A is second in total depth at 290 feet. The initial rise, then fall observed in 22A may also be a result of water stored in the rock above the saturated zone before completion. The range of water-level fluctuation during the study period was 6.6 feet.

The hydrograph for piezometer 31A is shown in Figure 27. Piezometer 31A is also screened into the same interval as piezometers 11A and 22A (*see* Fig. 1). The range of water-level fluctuation is 7.2 feet, which is largest of the four piezometers; set at this level. The hydrograph exhibits the same water-level decline throughout the year, with the addition of two significant drops in May and July. The hydrograph shows a 4-foot water-level drop in May, followed by a rise in water level to within a foot of the level before the drop occurred. The graph of the rebound resembles a pumping recovery curve, and this may represent drawdown induced by purging for water sampling on May 7, 1991, which occurred 8 days before the large drop in water level was recorded. A similar pattern was observed after the monthly sampling in July. However, this drop in water level was not observed in other months following monthly sampling, although approximately the same time interval had passed before the next water-level measurement was recorded. Another explanation for this hydrograph behavior can be related to the location and depth from the surface of 31A compared to 11A and 22A. Piezometer 31A is situated near the bottom of the ridge; thus, its depth (150 feet) from the surface is not as great as 11A and 22A (416 and 290 feet, respectively), which places 31A within the depth range where near-surface fractures commonly occur. Fractures could allow precipitation to recharge 31A more

Piezometer 11B

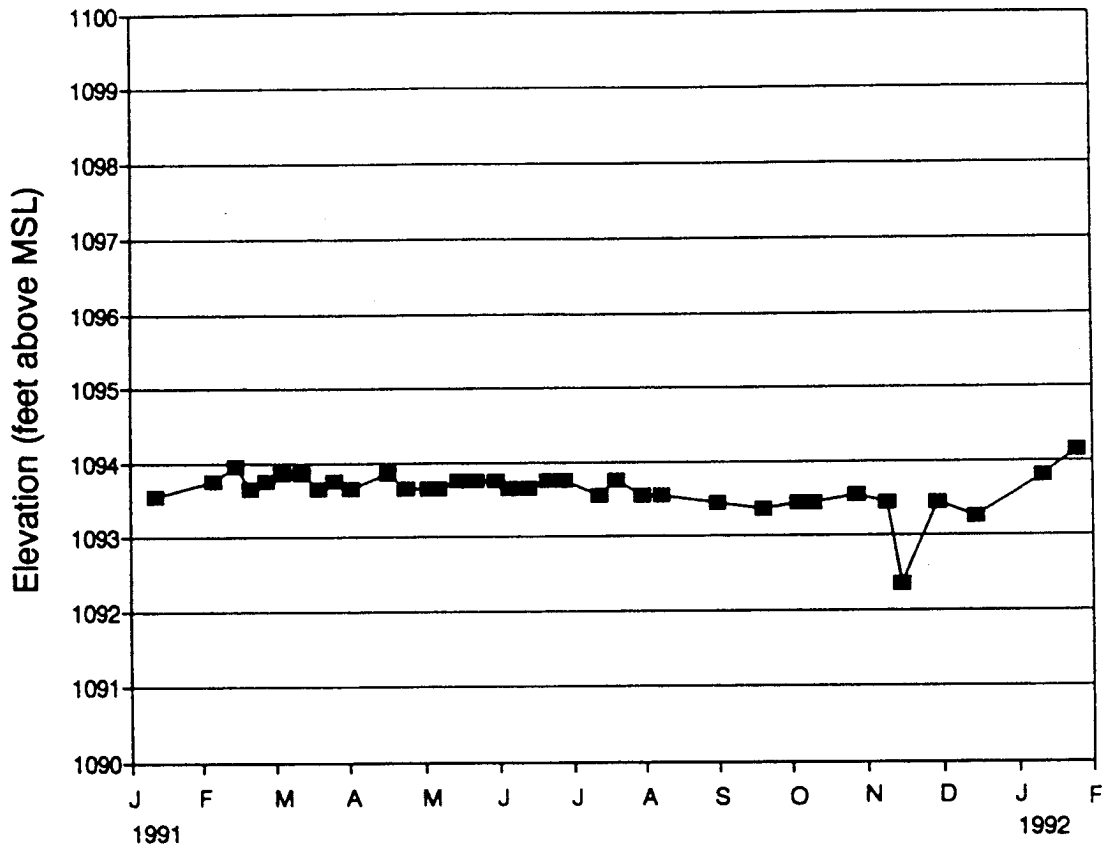


Figure 19. Hydrograph for piezometer 11B.

readily than the other piezometers screened at this level. Both of the large drops in water level in 31A occurred in the spring and summer when less recharge was probably entering the ground-water system, as evidenced by the gradual decline in hydrographs for all piezometers. Only 0.3 inch of precipitation fell during the 10-day period following the sampling event that took place on May 8, indicating that the lack of precipitation probably contributed to the rapid water-level declines, in addition to any effects induced by pumping.

Although the monthly precipitation total for May was nearly 6 inches, the daily precipitation data show that most of the rain fell as intense, short-term events (i.e., thunderstorms). With high evapotranspiration and runoff, it is likely that only small amounts of precipitation from intense events would move into the ground-water system as recharge during the summer months unless the precipitation is able to flow directly into highly conductive fractures that maintain a connection to the surface.

The hydrograph for piezometer 41B is shown in Figure 28. Piezometer 41B also reveals an initial sharp drop in water level similar to that observed in wells 11A, 22A, and 31A. The consistent occurrence of this pattern in each of the four piezometers set at the level below the Magoff in Shale suggests

that this response is probably real and not an artifact of pre-construction conditions.

Following an initial drop to approximately 864 feet, the water level in 41B remained consistent between 863 and 864 feet, with the exception of a decline of nearly 1 foot on May 15, 1991. This decline may correlate with the decline observed in 31A at approximately the same time. The graph of monthly precipitation (see Fig. 11) shows that the total for April was approximately 3 inches less than the precipitation total for the preceding and following months. Therefore, this decline in water level may represent a delayed response to precipitation shortfall.

Figure 29 shows the lateral placement of piezometers 11A, 22A, 31A, and 41B with the contoured equi-potential lines between the piezometers. The data indicate that the piezometric surface between these piezometers slopes from the ridge interior to the southwest toward the direction of where Lick Branch discharges into Balls Fork (see Fig. 1), indicating that water in the interior of the ridge flows toward 41B. An average hydraulic gradient of 0.037 was calculated along the inferred direction of flow, as indicated by the arrow on the figure. The piezometric surface, as represented by the contours, indicates that the area of highest head lies beneath the

Piezometer 13B

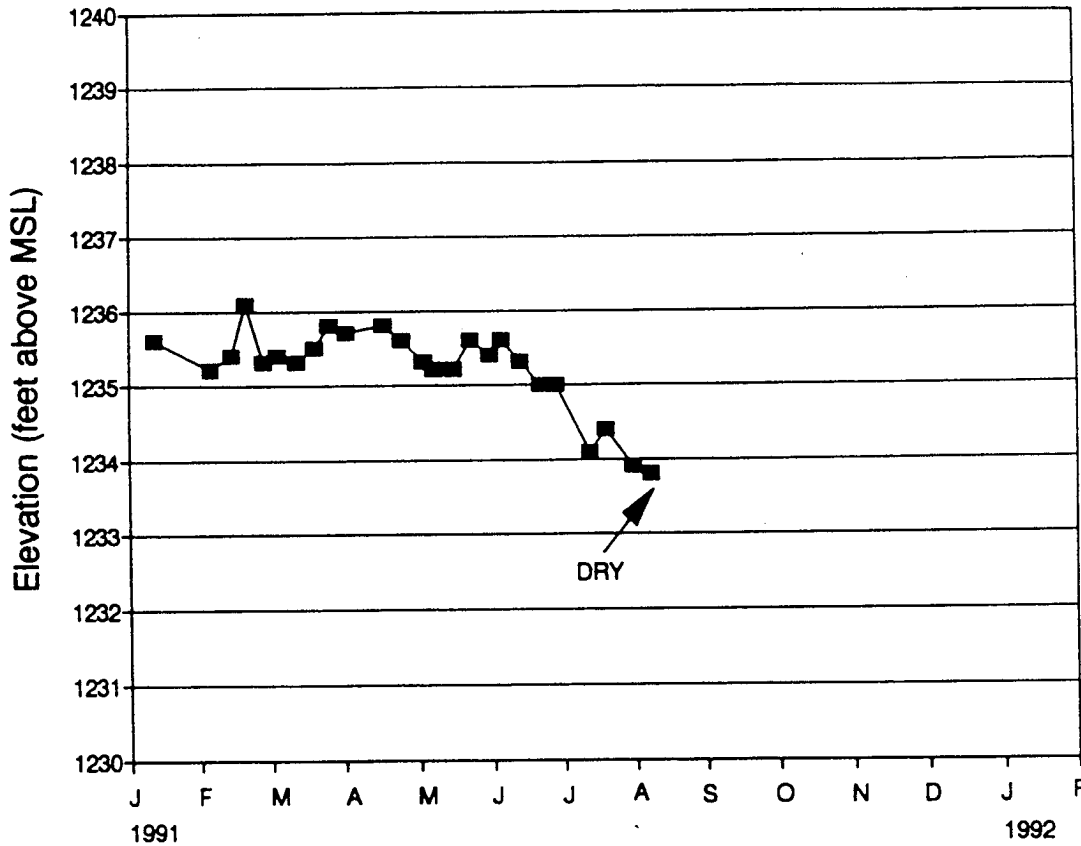


Figure 20. Hydrograph for piezometer 13B.

center of the ridge and that the potentiometric surface defined by the contour lines generally approximates the topography.

The water levels for each of the four piezometers open to the interval below the Magoffin Shale are plotted on Figure 30. Piezometer 11A maintains its water level at the highest elevation, followed by 22A, 31A, and 41B, which is the order of encounter from the ridge center (11 A) to the site adjacent to Lick Branch (41B). Each of these piezometers remained saturated throughout this study, indicating that saturated conditions exist deep within the ridge interior.

In general, the water levels in piezometers 11A, 22A, and 31A indicate that an increase in the amount of fluctuation occurs in the piezometers away from the center of the ridge (from 11 A toward 31 A). This most likely results from an increase in the influence of fractures at the lower elevations because the thickness of bedrock overlying the stratigraphic interval monitored by these piezometers decreases from the center of the ridge to the valley bottom. The consistency observed in 41B probably is related to its position in the discharge zone, where a consistent ground-water flux is maintained from ground water moving toward this area from higher elevations.

A strong correlation to specific precipitation events is not observed in any of these piezometers, although a gradual de-

cline in water level in each occurs for most of the observation period, with a slight increase observed in January. This trend probably reflects the lack of deep penetrating recharge during the summer months. The higher water levels observed in all piezometers during the winter months is probably related to cyclonic storms that produce soaking rains, which, in the absence of evapotranspiration, provide recharge water that can reach the deep bedrock zones below the fracture systems.

Piezometer 41A is screened to an interval at an elevation of 752.2 feet above MSL, which represents the lowest elevation monitored in this study. The hydrograph for 41A is shown on Figure 31. The borehole that contains both piezometer 41A and 41B is adjacent to the major drainage stream (Lick Branch). The water level in 41A (Fig. 2) rises to an elevation that ranges between 839.6 and 843.4 feet, yielding a total fluctuation of 3.8 feet. The maximum water-level elevation observed in 41A is below the level of the adjacent stream channel, which at its closest point lies west of the piezometer, approximately 150 feet away at an elevation of 860.9 feet. The head levels in 41B and 41A indicate that there is a vertical component of ground-water flow between the two. The head level in 41B is higher than that of Lick Branch, indicating that ground water from the interval monitored by 41B, and all intervals above this elevation, is discharging into the stream.

Piezometer 13A

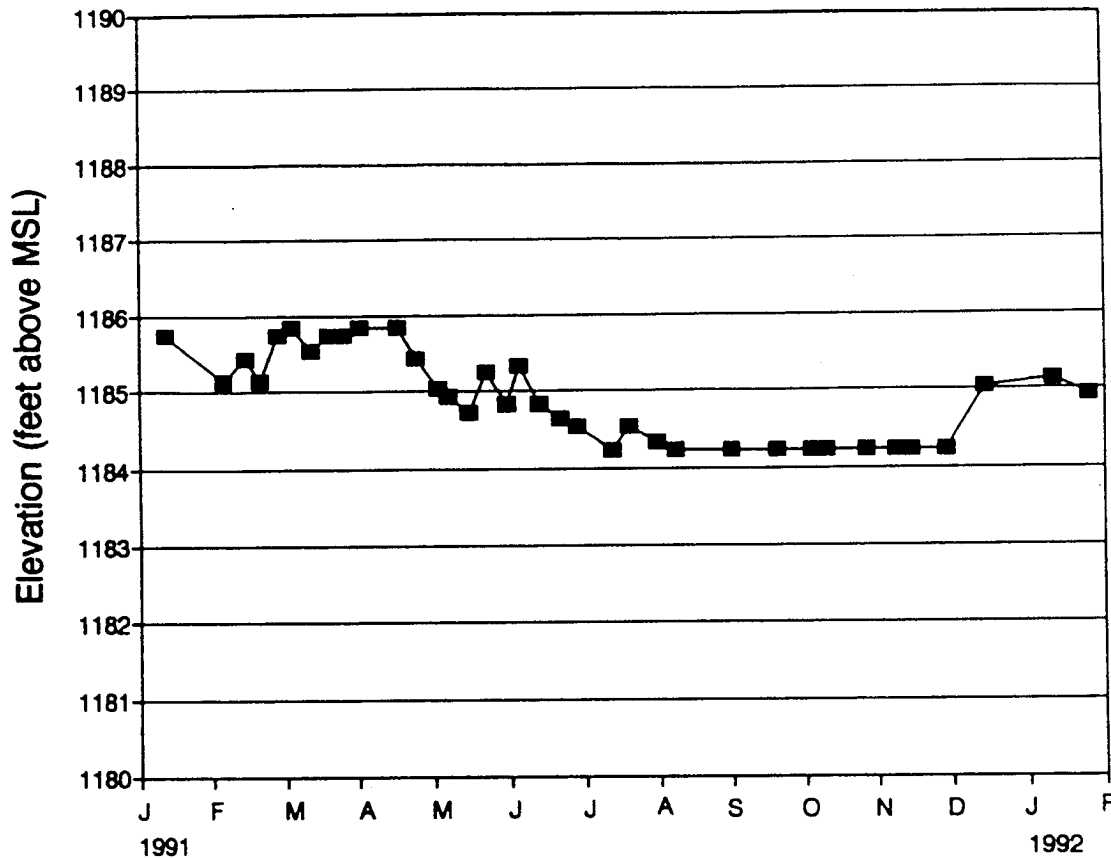


Figure 21. Hydrograph for piezometer 13A.

Field observations of Lick Branch during the study period indicate that it is a perennial stream that appears to gain flow before discharging into Balls Fork. Lick Branch remained flowing throughout the observation period for this study. Piezometer 41A apparently monitors a deeper, perhaps regional, flow system. Subsequent discussions on chemical characteristics of water samples derived from piezometer 41A will support this conclusion.

Evaluation of Ground-Water Recharge Using Tritium

Tritium is a radiogenic isotope of hydrogen with a half-life of 12.43 years (Ostlund, 1991). Tritium content is commonly reported in tritium units (TU), which represent one tritium atom in 10^{18} hydrogen atoms. The use of tritium in groundwater studies is a valuable tool for determining qualitative ages of ground water and in aiding in the delineation of ground-water flow paths and recharge rates (Davis, 1986; Hendry, 1988).

The amount of tritium present in the atmosphere has not been constant over time. It is estimated that tritium generation from cosmic radiation reactions in the atmosphere would be responsible for average tritium values in precipitation of approximately 10 TU (Davis, 1986). Atmospheric testing of thermonuclear devices in the early 1950's created a large in-

flux of tritium into the atmosphere. As a result, tritium concentrations of 10,000 TU's were measured in the northern hemisphere during the 1960's (Hendry, 1988). This large spike of tritium into the atmosphere has allowed tritium to be used as a tracer in ground-water studies during the past 50 years.

In using tritium in ground-water studies, the effects of unequal recharge rates and ground-water mixing must be acknowledged in order for the interpretations to be of high quality. The magnitude of these variables is not known for this study; therefore, the following ages of ground water based on tritium concentrations are derived from those listed in Table 6, which only provides a qualified age determination based on the tritium content.

Figure 32 shows the site profile with contours of the tritium data. With the exception of piezometer 12B, all of the piezometers situated in the upper section of the ridge (Fig. 11) or at shallow depths near the slope contained tritium values above 10 TU. The piezometer with the highest tritium content was 14A with a value of 23 TU and is interpreted as being recent recharge probably less than 35 years old. This piezometer is situated in the shallow fracture zone near the top of the ridge, and exhibited a large water-level fluctuation that correlated well with precipitation trends, indicating that recharge rapidly enters through fractures. A one-time tritium sampling of precipitation from a thunderstorm in the summer

Piezometer 21A

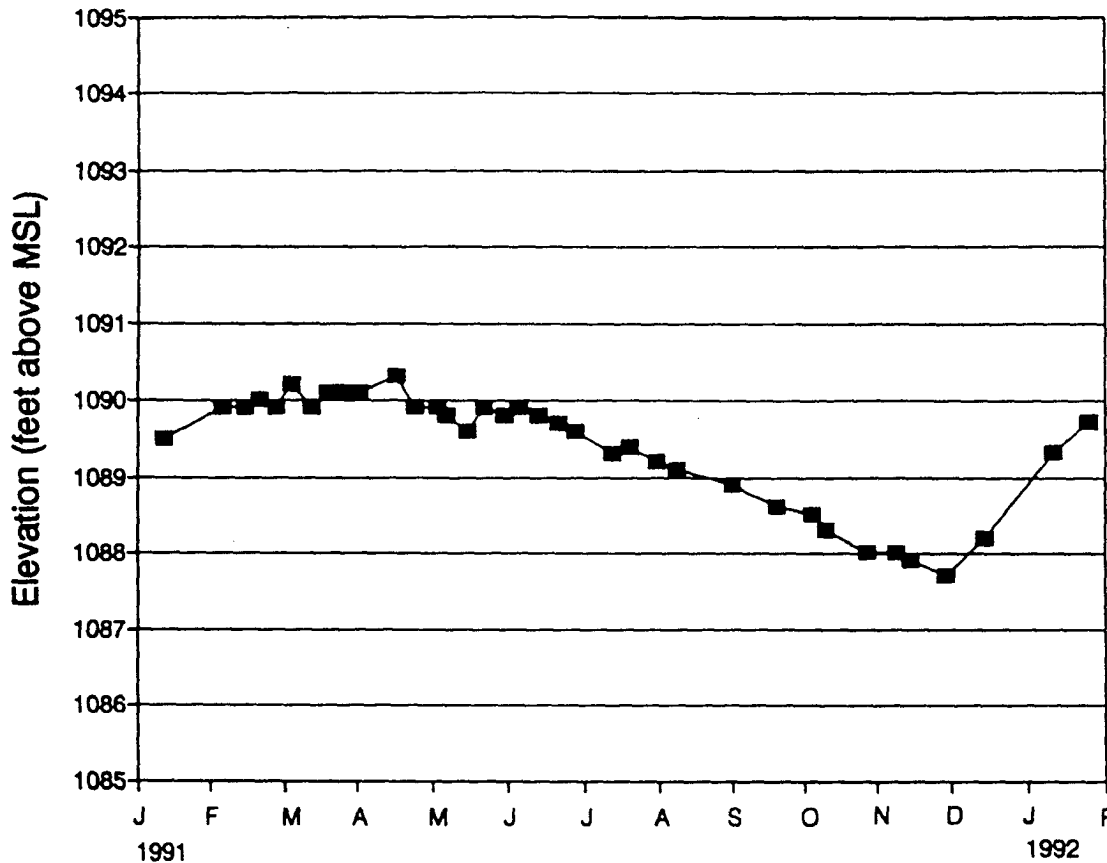


Figure 22. Hydrograph for piezometer 21A.

of 1991 near the site revealed that the tritium content for that event was 6 TU. However, tritium data obtained from the U.S. Geological Survey indicate that in the late 1970's the tritium content in rain in eastern Kentucky was nearly 60 TU. Most likely the water obtained from 14A is a mixture of recent precipitation and relatively young ground water stored in the rocks, which probably accumulated when tritium content in precipitation was substantially higher in the recent past.

Fractures could be observed in the steep, natural outcroppings of bedrock near the ridge top and in areas disturbed during road construction. Fractures exposed at the ground surface would allow for the easy entry of recharge water and probably result in the ground water in this area having the highest tritium content. The high degree of water-level fluctuation in the shallow piezometers (e.g., 11C and 14A) in this area would support this conclusion. However, the fractures, in conjunction with the coal seams, could also allow for the rapid discharge of ground water from the ridge top, which would act to "short circuit" the vertical migration of groundwater recharge into the ridge interior.

Evidence to support this interpretation is the depletion of tritium in the central area of the ridge. Figure 32 shows a zone of tritium-depleted (old) water beneath the core of the ridge, indicating very little recent penetration of recharge. For example, borehole 11 hosts three piezometers that are set at

increasing depths into the center of the ridge. The shallow piezometer, 11C, set at 48.5 feet below the surface, has a tritium value of 13 TU. Piezometer 11B, set at 200 feet, measured 2.19 TU, followed by 11A with 0.32 TU at a depth of 418 feet. Piezometer 11B is set into the Hazard No. 5 coal. The contours of the tritium data show an abrupt decrease in the gradient of tritium content below the elevation of the Hazard No. 5 coal (elevation of approximately 1,100 feet) in the ridge interior, which is reflected by the sharp break in the slope seen in the 4 TU contour line directly below 11B. The two piezometers that did not accumulate water (1213 and 21 B) during the entire record period are situated above the Hazard No. 5 coal seam, as are the other piezometers that went dry at times during this investigation (13B and 14A). The dry piezometers, the occurrence of old water below the 1,100-foot (No. 5 coal) elevation in the ridge interior, and the occurrence of springs that crop out on the surface at or near the elevation of the Hazard No. 5 and other coal seams indicate that the coal seams act to drain the ground water that infiltrates into the bedrock above it. Springs and seeps were observed at several locations at the site, and nearly all of them correspond to an elevation of one of the major coal seams present in the ridge.

It was also noted that water that accumulated in core hole 1066 after the core was removed was at an elevation that

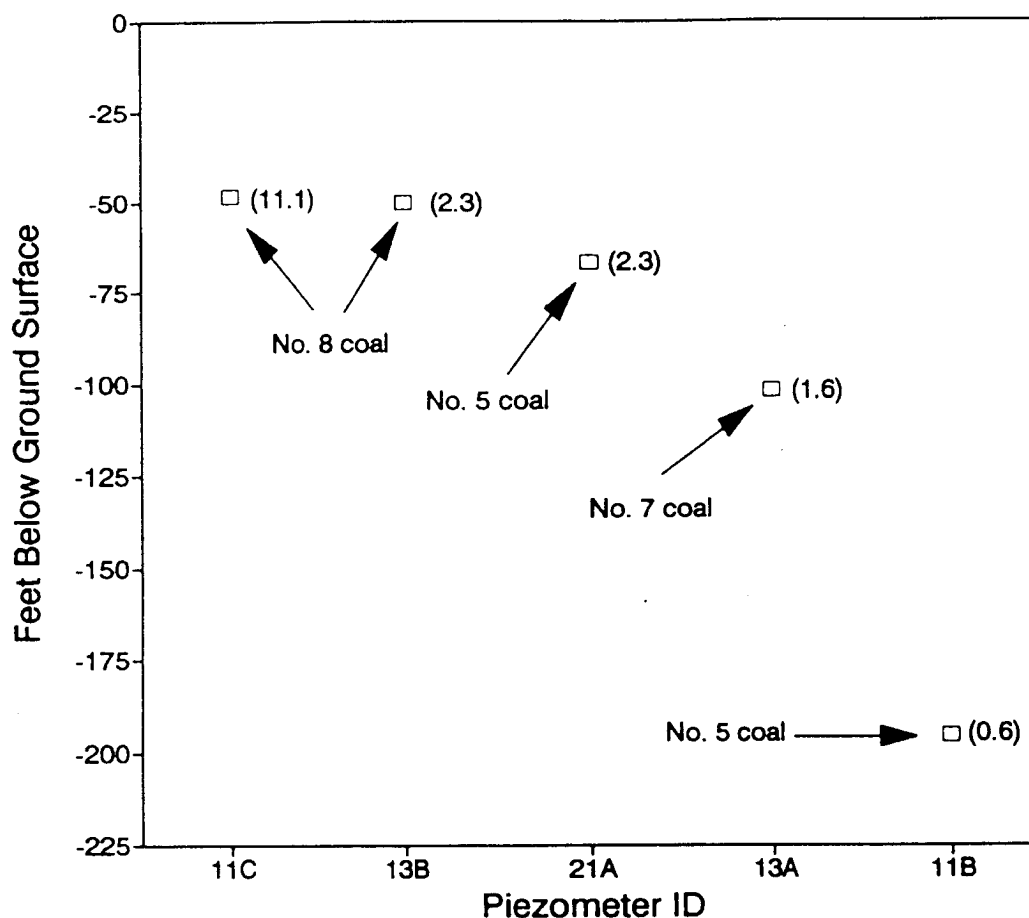


Figure 23. Water-level fluctuation with depth below the surface in piezometers monitoring coal seams. Number in parentheses is range of fluctuation in feet.

corresponded to the elevation of the Hazard No. 5 coal. It could not be determined at that time if the water was flowing into the hole from strata or fractures located above the coal, or rising from below, but it appears that the coal imparted a control on the elevation of the water in the hole. Each of the coal seams on the ridge top (the Hazard Nos. 5, 6, 7, and 8) may contribute to draining the ridge top, but the No. 5, being the lowest seam of significant thickness (greater than 1 foot thick), ultimately constrains the amount of ground water moving down into the ridge interior.

Piezometer 21A is situated at a lower surface elevation than 11B and also monitors the No. 5 coal. The coal seam is only 67 feet below the ground surface (*see* Figure 1 for piezometer placements with respect to lithologic units) in the location of 21A. The water obtained from 21A contains 17 TU of tritium, indicating that much younger water is able to flow into the coal near the outslope, probably because of fractures that can intersect the coal seam near the outcrop. This observation is consistent with the hydrographs for these two piezometers. The hydrograph for 11B, located in the interior of the ridge, indicated very little water-level fluctuation throughout the record period, whereas 21A exhibited some short-term fluctuations as well maintaining a water-level elevation that averages 4 feet lower than that observed in 11B. This hydraulic gradient within the coal indicates that water will flow

along the No. 5 coal seam from the interior region and toward 21A and probably discharge where the coal crops out. The steady hydrograph of piezometer 11B suggests that the water present in the Hazard No. 5 coal may be retarded on lithologies with low hydraulic conductivities that lie below it. Water contained in the No. 5 coal is probably in equilibrium with the small but steady amount of recharge that migrates from the leaky layers above.

The higher hydraulic conductivities for coal seams compared to the other lithologies present would suggest that the majority of water moving downward from the top of the ridge would be diverted laterally along the coal seams. No data were found in the literature where vertical hydraulic conductivity values for coal-bearing strata in eastern Kentucky are given. However, a net vertical hydraulic value can be calculated from the tritium data that support a lateral flow mechanism.

The amount of tritium in piezometer 11A, which penetrates the deepest into the ridge interior, is 0.32 TU, which is conservatively interpreted as being at least 30 years old. Tritium values this low are commonly referred to as dead water, and the water may be significantly older than this. Assuming recharge rates were relatively constant through time, this cor-

Piezometer 11A

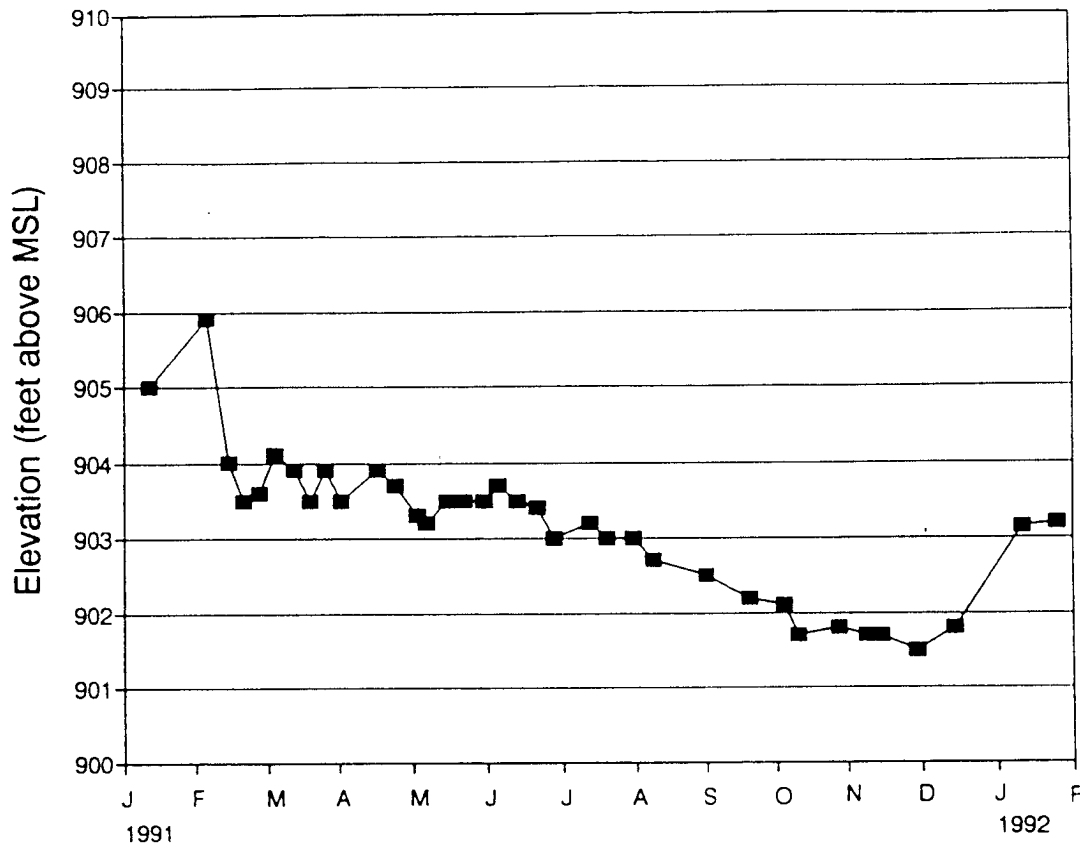


Figure 25. Hydrograph for piezometer 11A.

(mean = 3.8×10^{-4} cm/sec). The difference in these estimates supports the conclusion that the higher hydraulic conductivity of the coals would cause coals to exert the greater control in the transmission of ground water in the section of the ridge where they are present. The unsaturated or partially saturated conditions of the coals near the top of the ridge and their higher hydraulic conductivities would act to divert the downward movement of recharge water by promoting the horizontal movement of water. The less conductive rock layers beneath the coal seams would act to hinder the vertical movement of water and cause ground water to discharge from the coals as springs or seeps at or near the outslope.

A downward deflection in the tritium contours in the area between sites 2 and 4 indicates the penetration of relatively younger water to a greater depth than is observed at the same elevation below the ridge top or the valley bottom. This pattern probably is related to the movement of ground water through the near-surface fracture zone. Also, there are no significant coal seams present at this lower level to divert the vertical migration of ground water. Additionally, the break in the degree of slope below an elevation of approximately 1,200 feet may cause a decrease in the velocity of flowing surface water, allowing for a higher percentage of surface runoff to percolate into the soil and bedrock to recharge the ground-water system. This conclusion is supported by water-

level data for the piezometers that monitor the interval below the Magoff in Shale (11A, 22A, 31A, and 41B). These piezometers showed an increase in water-level fluctuation downslope, which corresponds to the area where the tritium data indicate the penetration of young ground water. The increased fluctuation in water levels is attributed to the increased effects of fractures. This area along the hill slope where the penetration of recent ground water is shown is interpreted as being the zone where the greatest amount of recharge enters the ground-water system.

Conceptual Model of Ground-Water Flow in the Ridge

Figure 33 presents a schematic view that summarizes the recharge and discharge relationships observed at the site, based on the previous discussion. The top of the ridge is shown as an area characterized as having a high surface runoff component because of the steepness of slope. The major coal seams of the Hazard group are concentrated in this area. The coals and fractures act to divert a significant amount of the recharge that infiltrates into the bedrock laterally to the outslope as seeps and springs. This water may (1) remain on the surface and move to lower elevations as runoff, (2) be transpired in the evapotranspirative process, or (3)

Piezometer 22A

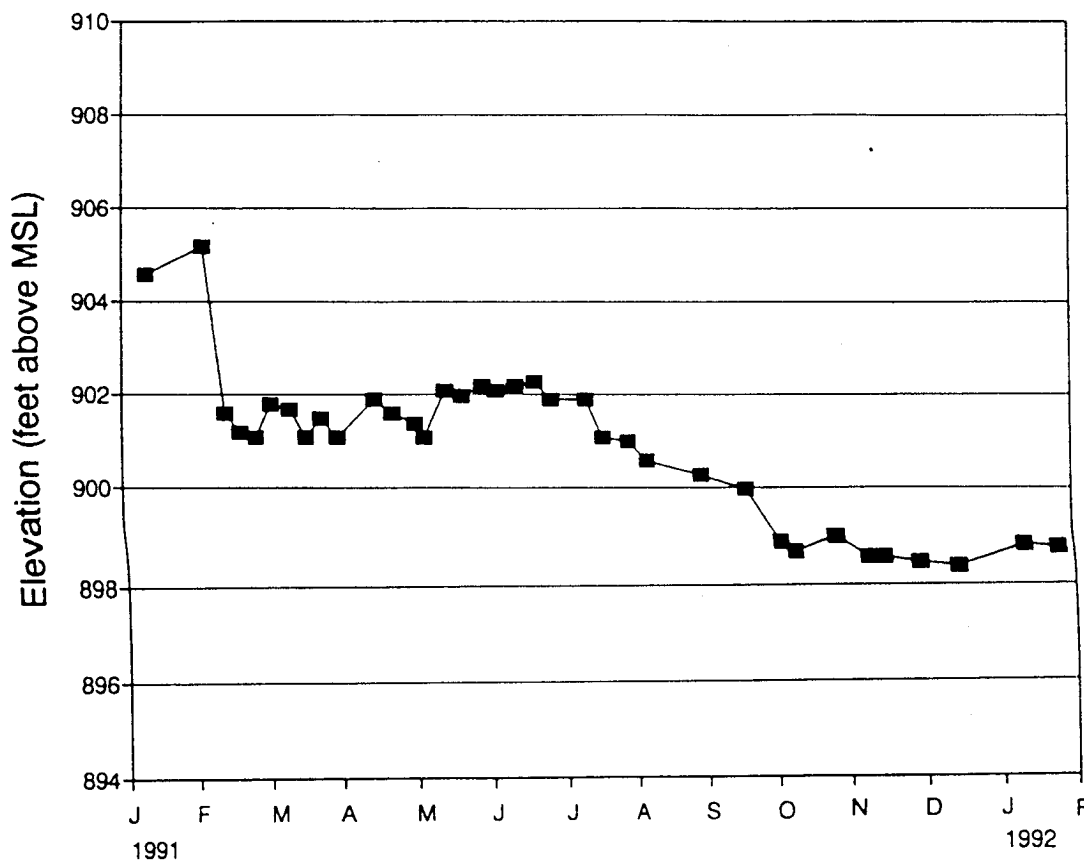


Figure 26. Hydrograph for piezometer 22A.

re-enter the ground-water system at or below the spring or seep.

The area between the location of site 2 and site 4 is shown as the area of maximum recharge. The break in slope and increased surface-area toward the base of the ridge allows for a higher percentage of precipitation to enter the groundwater system. This is reflected by the deeper penetration of relatively younger water, as indicated by the tritium data. The area below site 4 down to the channel of Lick Branch is shown as the discharge area. Water moving down-slope in the shallow fracture zone along with ground water that is flowing from the interior of the ridge (see Fig. 31) would discharge in this area. An area of ground-water mixing would be expected in the area where the shallow, fracture-controlled flow and the ground water from the ridge interior would converge. The significance of this hypothesis will become more evident in following discussions on chemical considerations.

Several researchers have presented conceptual models of flow that are applicable to the Appalachian Coal Field (Wyrick and Borchers, 1981; Kipp and Dinger, 1987; Harlow and LeCain, 1991). Harlow and LeCain (1991) have presented the most recent model, which was based on the previous investigations of others and a large assemblage of hydraulic data from borehole testing. Figure 34 shows their conceptualized flow system for the coal field in Virginia. The model

presented in this study is in agreement with the location and occurrence of the major features that control ground-water flow presented in their model.

The following discussion will address the observed geochemical trends in this study as they relate to the flow system defined here.

Ground-Water Geochemistry Variation in Water Types

The use of Piper diagrams (Piper, 1944) is a common, practical means of graphically portraying water composition. To create a Piper plot, the concentrations of major cations and anions from the chemical analysis of water are converted to milliequivalents per liter (meq/L) and plotted as a percentage of the total cation or anion concentration normalized to 100 percent on a triangular field. Each apex of the triangle represents 100 percent of an ion. Representative points from the cation and anion fields are then projected onto a diamond-shaped field. The point of intersection of the two projections represents the samples' water type. The following discussions will refer to water types that are named according to the dominant cation and anion (based on being greater than 50 percent of the total cation or anion equivalents). If no ion makes up more than 50 percent, the water type will be defined by using the two more abundant ions (in decreasing

Piezometer 31A

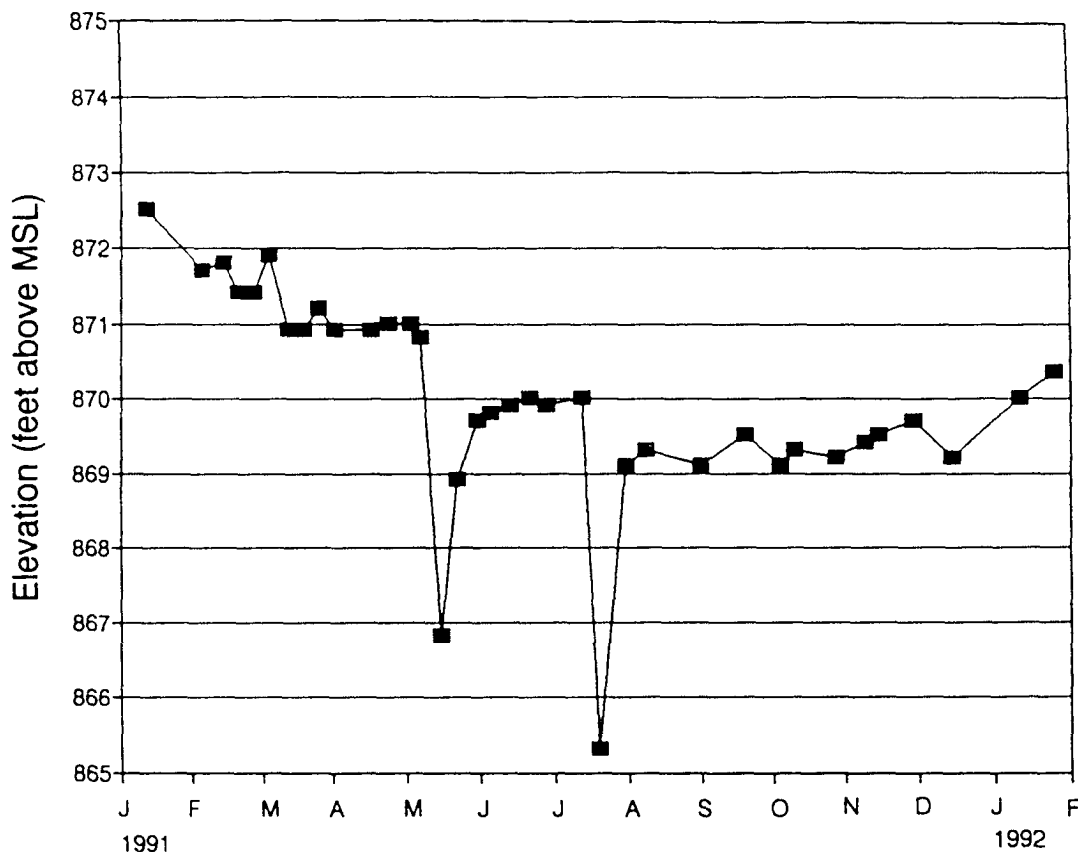


Figure 27. Hydrograph for piezometer 31A.

order) that together represent more than 50 percent of the total.

The Piper diagrams show that several water types are represented at the site. However, similarities in water types are observed among piezometers that obtain their water from similar water-producing zones.

Figure 35 shows the 11 water samples taken from piezometer 12A plotted on a Piper diagram. All of the samples plot as a Ca-HCO₃ water type. Water samples from piezometer 14A are a Mg-SO₄ type and are shown on Figure 36. All of the samples from both of these piezometers plot in nearly the same location on their respective diagrams, indicating that very little variation occurred within the percentages of major ions. The coefficient of variation (CV) for the total dissolved solids for piezometer 12A is 7.16 percent, indicating that the concentrations of dissolved constituents remained constant throughout the sampling period. A coefficient of variation of 20.04 percent for 14A indicates considerable variation in the concentration of dissolved constituents throughout the year and that it exhibited more variation than 12A. Piezometer 14A is shallow (40 feet) compared to 12A (167 feet), and the variation in piezometer 14A is probably due to dilution from fresh recharge after precipitation events. This conclusion is consistent with the hydrograph and tritium data for 14A, which showed a water-level response that correlated well

with precipitation measurements and also that 14A contained the highest tritium content (23 TU) of all piezometers sampled. The stability exhibited by piezometer 12A in both water quality and water level is probably related to its depth (167 feet), where the immediate effects of recharge events are minimized by the longer flow path the ground water must travel.

Piezometer 31B had Na⁺ and HCO₃⁻ as the dominant ions in the beginning of the sampling period, but gradually evolved to a Ca-Mg-HCO₃ water type (Fig. 37). Bicarbonate remained the major anion throughout the entire period. The total concentration remained very consistent, as indicated by the coefficient of variation (CV = 3.6 percent). A more detailed discussion on the changes in water type in this piezometer and one adjacent to it will be presented in following sections.

Three of the piezometers; monitoring the coal seams, 11B, 13A, and 21A, are shown in Figures 38, 39, and 40, and reveal that each of these piezometers yield a Ca-Mg-HCO₃ water, type. The coefficient of variation for these three piezometers is 5.01, 5.4, and 6.0 percent, respectively, indicating that very little variation occurred in the relative concentration of the total dissolved constituents. The Piper plot for piezometer 11C (Fig. 41) shows consistency in the total concentration of dissolved solids (CV = 10.01 percent), but exhibits a mi-

Piezometer 41B

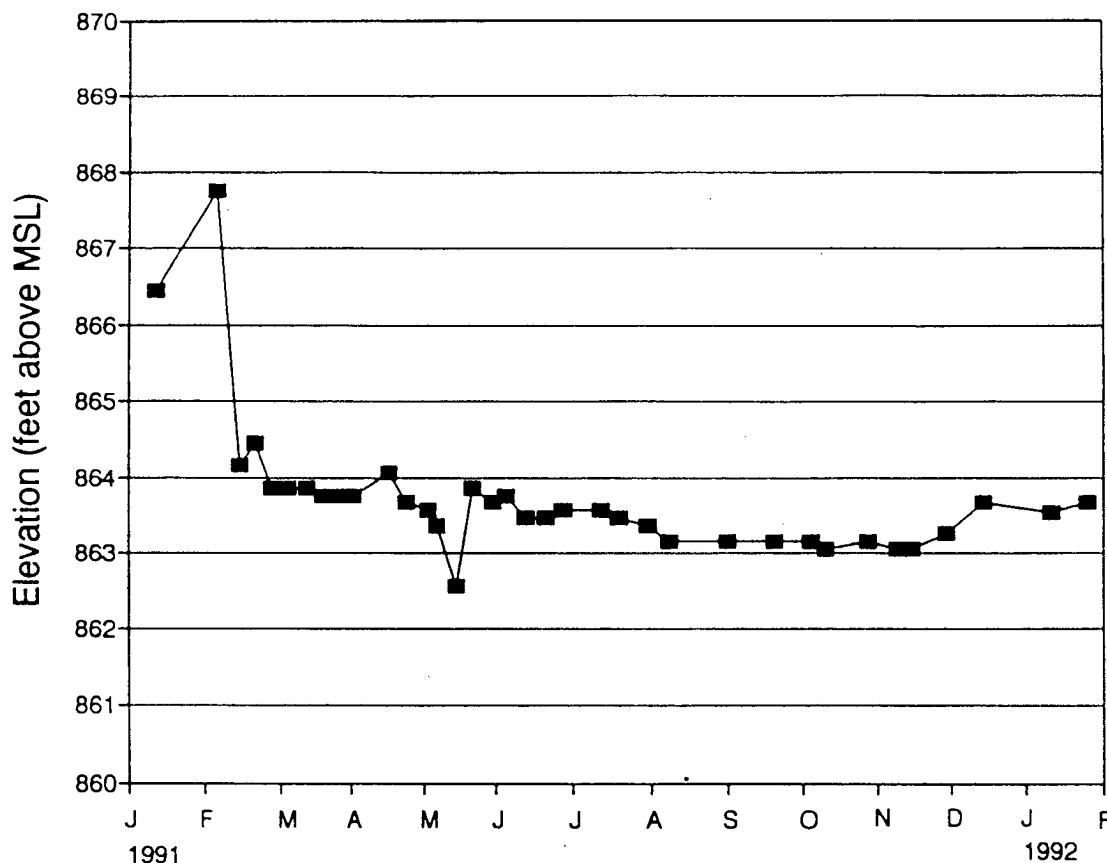


Figure 28. Hydrograph for piezometer 41B.

gration in the major cations from a calcium-magnesium type for most of the year to an Na-Ca-HCO₃ type in November of 1991. Piezometer 11C is set into the Hazard No. 8 coal seam, which is nearest to the surface at the top of the ridge. The fluctuating hydrograph in this piezometer indicates that the influx of recharge following precipitation events may be responsible for the chemical variation. A tritium content of 13 TU indicates that it is slightly older than water derived from the fracture system monitored above it (e.g., 14A). Cation exchange or older water entering the coal from the surrounding bedrock may also account for the major ion variation during times when recharge rates are low.

Figure 42 shows that piezometer 22B has an Na-SO₄ water type. The cluster of points on the Piper diagram indicates that the water quality for this piezometer remained consistent throughout the sampling period, but the coefficient of variation (CV = 23.2 percent) indicates significant variation in the amount of dissolved solids. This trend also may be explained by an addition of ground water to the zone monitored by piezometer 22B by more mineralized recharge. Comparing the piezometer hydrograph with the dissolved solids data (see Appendix 6) indicates that the dissolved solids content is the highest when the water levels are high, and low values correspond to low water levels.

Fractures were not observed at the depth of piezometer 22B by inspection, but the tritium content in ground water from this piezometer (11 TU) is more on the order of tritium content found in piezometers at much shallower depths (see Fig. 32). This piezometer contained water that typically contained dissolved solids concentrations greater than 1,000 mg/L, which is significantly higher than all other piezometers that monitor zones that are above the major drainage.

Three piezometers, 11A, 22A, and 31A, are Na-HCO₃ type waters and are shown in Figures 43, 44, and 45, respectively. These three piezometers monitor the same zone (below the Magoffin Shale) at an elevation of approximately 860 feet. The Piper plots for 11A and 22A are nearly identical. Both of these piezometers are situated near the core of the ridge, with 11A located in the center of the ridge, and 22A located downslope and slightly off center. The coefficient of variation for these piezometers is 4.11 and 15 percent, respectively, which indicates that slightly more variation in the dissolved constituents occurred in piezometer 22A. Piezometer 31A shows sodium to be the dominant cation, but 31A contained a higher percentage of calcium and sulfate compared to both 11A and 22A. The coefficient of variation in dissolved solids is 14.4 percent. Piezometers; 22A and 31A monitor locations that are progressively farther from the cen-

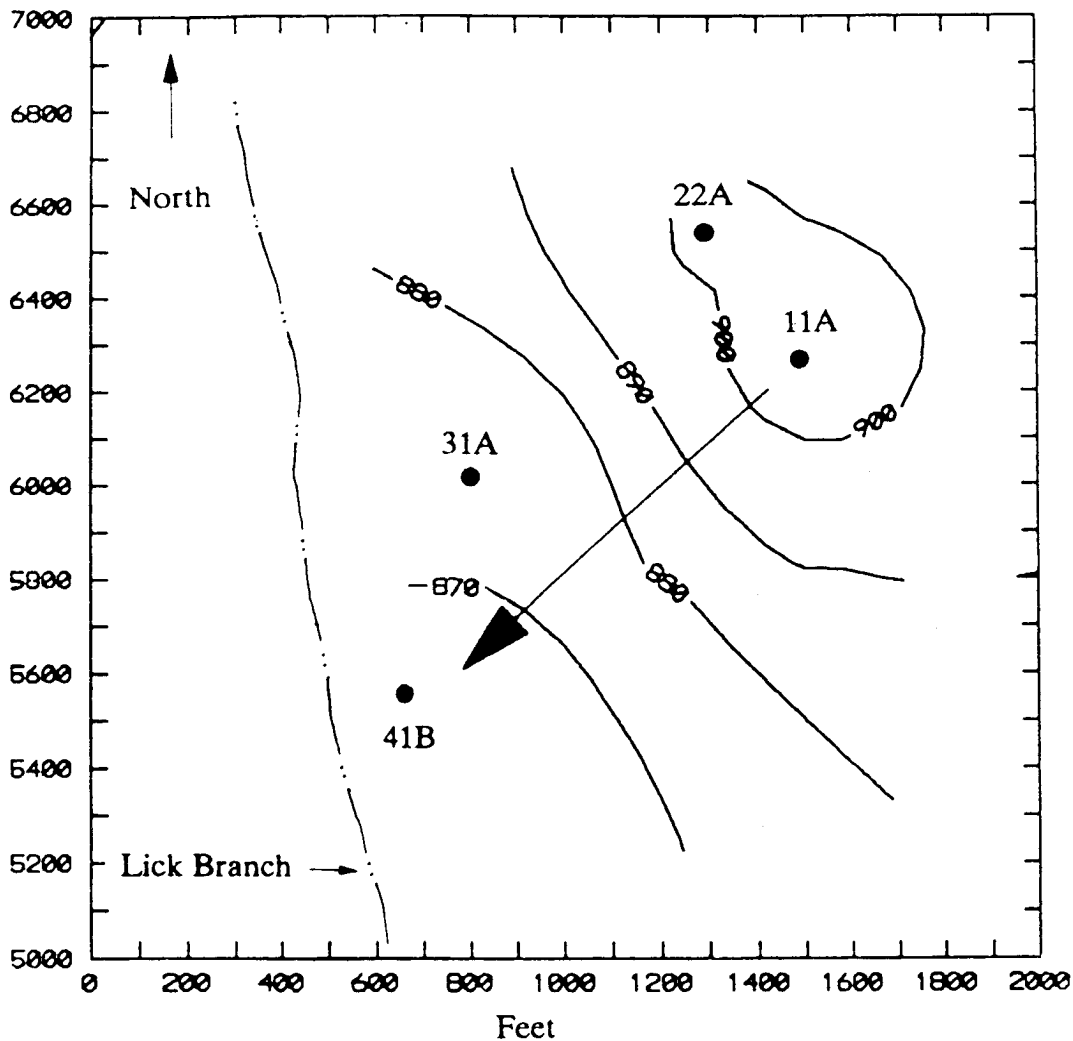


Figure 29. Potentiometric surface for piezometers screened below the Magoffin Member.

ter of the ridge monitored by 11A. A gradual increase in calcium and sulfate content, along with the increased variation in dissolved constituents moving from 11A toward 31A probably indicates the influx of ground water into the hillslope, piezometers (22A and 31A) through the near-surface fractures where calcium and sulfate are more prevalent, as shown previously. The zone monitored by these piezometers is covered by progressively less bedrock as one traverses from 11A to 31A, and fractures probably have an increasing effect. The tritium data support this conclusion by indicating the deeper penetration of younger water (recharge) in the area between the locations of piezometers 22A and 31A (see Fig. 32).

Piezometer 41B is also screened near the same elevation as 11A, 22A, and 31A. The Piper diagram showing data from this piezometer is shown on Figure 46. The water from this piezometer is an Na-Ca-HCO₃ type. The clustering of sample points and the small coefficient of variation (1.93 percent) indicate that the major ion chemistry remained consistent throughout the sampling period. The additional calcium content compared to the other piezometers screened to this level suggest a mixing of water from below the Magoffin zone with

water from the near-surface zone. This piezometer is near the presumed discharge zone, and the stable nature of the water quality probably results from a homogenization of various water types that blend as they move toward this location.

The water sampled from piezometer 41A plots as an Na-Cl water type high in dissolved solids (Fig. 47). The tight clustering of water samples indicates that the percentage of major ions has remained relatively consistent throughout the sampling period. The coefficient of variation (CV = 14 percent) indicates some variation has occurred in the quantity of dissolved constituents. This piezometer contained brine, and typically contained dissolved solids greater than 10,000 mg/L.

Overall, the temporal variation in water quality of ground water at the site was quite low, with the exception of the shallower piezometers screened in coal and fractured zones.

Geochemical Reactions Controlling Ground-Water Types

Of the various ground-water flow paths that exist in the ridge examined in this study, two can be defined with some

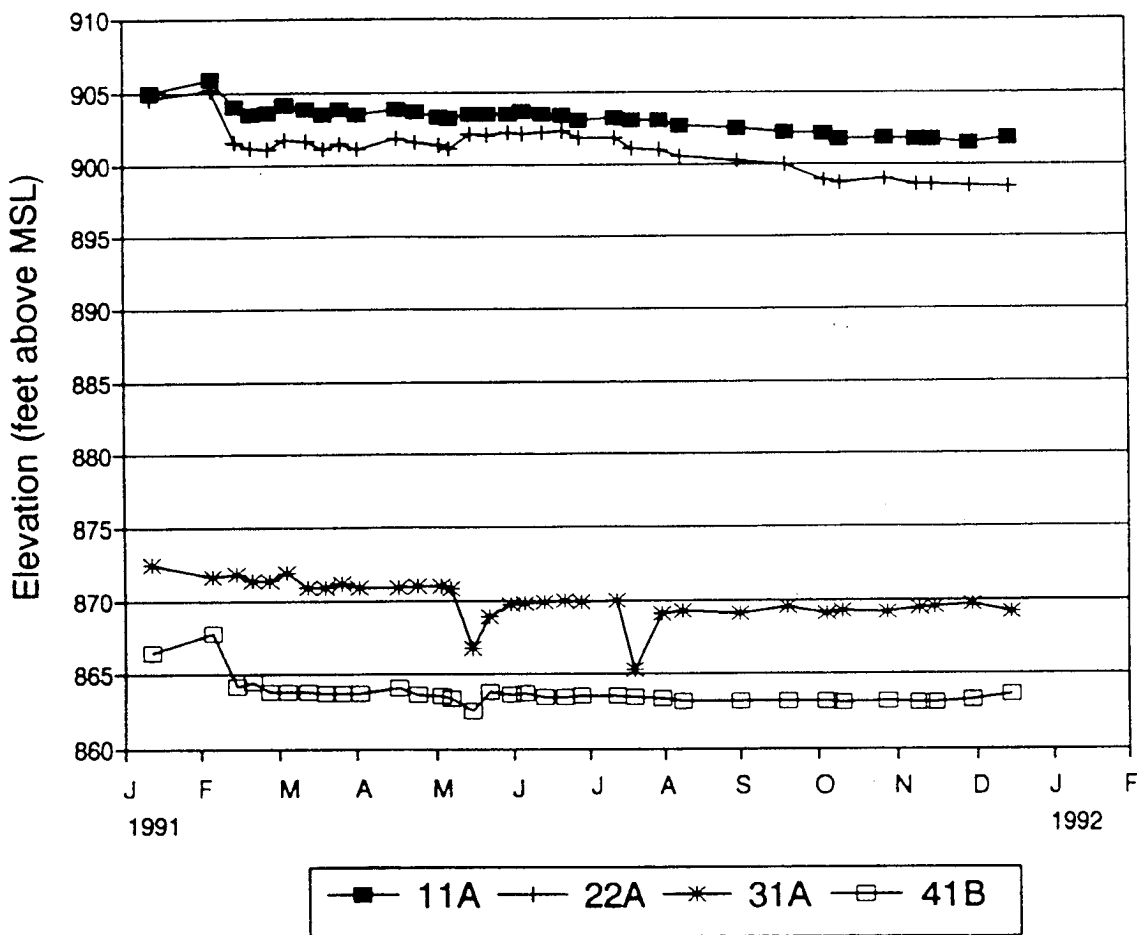


Figure 30. Hydrographs for piezometers 11A, 22A, 31A, and 41B.

certainty. The contours of the piezometric head (Figs. 13 and 14) and the tritium data indicate that (1) recharge that enters the ridge at the top migrates vertically downward into the ridge core, and that (2) water that accumulates in the ridge interior moves outward toward the discharge area at Lick Branch.

Piezometer 14A is screened at the shallowest depth of all the piezometers located on the ridge top and contains the youngest water. The major water type is an Mg-SO₄.

Because there is no common source of sulfate in the rocks in eastern Kentucky (i.e., gypsum is not commonly found in the strata nor is its presence observed in the core taken from the ridge), the most likely source of sulfate in shallow ground water is pyrite. The sulfate content in piezometer 14A most likely results from pyrite oxidation (Appendix 1, equation 14). Coal seams and rocks common to the area often contain pyrite (Danilchik and Waldrop, 1978), and pyrite was observed in the geologic core examined at the site. Powell and Larson (1985) found that in a similar setting in Virginia the presence of sulfate is generally a function of pyrite oxidation. The iron produced by this reaction (eqn. 11) often precipitates along fractures and in the cleat surfaces in coals. Iron-hydroxide, identified by its common orange coloration, was observed by downhole camera investigation entering the borehole in some places where fractures and coal seams

were encountered. Fractures observed in the geologic ore also showed iron stains and solid Fe-hydroxide. A total iron content of 114 mg/L was determined in piezometer 14A, with the dissolved content less than detectable limits (see Appendix 6). The high total iron content, and the relatively high Eh value (mean of 170 mV) suggests that the iron would occur as Fe³⁺, which is consistent with the presence of precipitated iron-hydroxide that was often observed when purging piezometer 14A.

The source of the magnesium in 14A may be from reactions with chlorite (eqn. 9) and/or the solution of magnesian-calcite. Dolomite does not appear to be a likely source of magnesium because it is not a common mineral in the rocks of the Breathitt Formation (Dafnilchik and Waldrop, 1978; Weinheimer, 1982).

Piezometer 12A maintained a Ca-HCO₃ water type. This most likely reflects the solution of calcium carbonate (eqn. 12) and, because of the long ground-water migration time due to depth, possibly plagioclase (eqn. 8). The major ion chemistry remained relatively constant throughout the sampling period with the exception of sulfate. The drop in sulfate content corresponds to a drop in Eh and an increase of barium concentration that exceeded 1.0 mg/L in the last 4 months of sampling. This behavior will be discussed in more detail in a later section.

Piezometer 41A

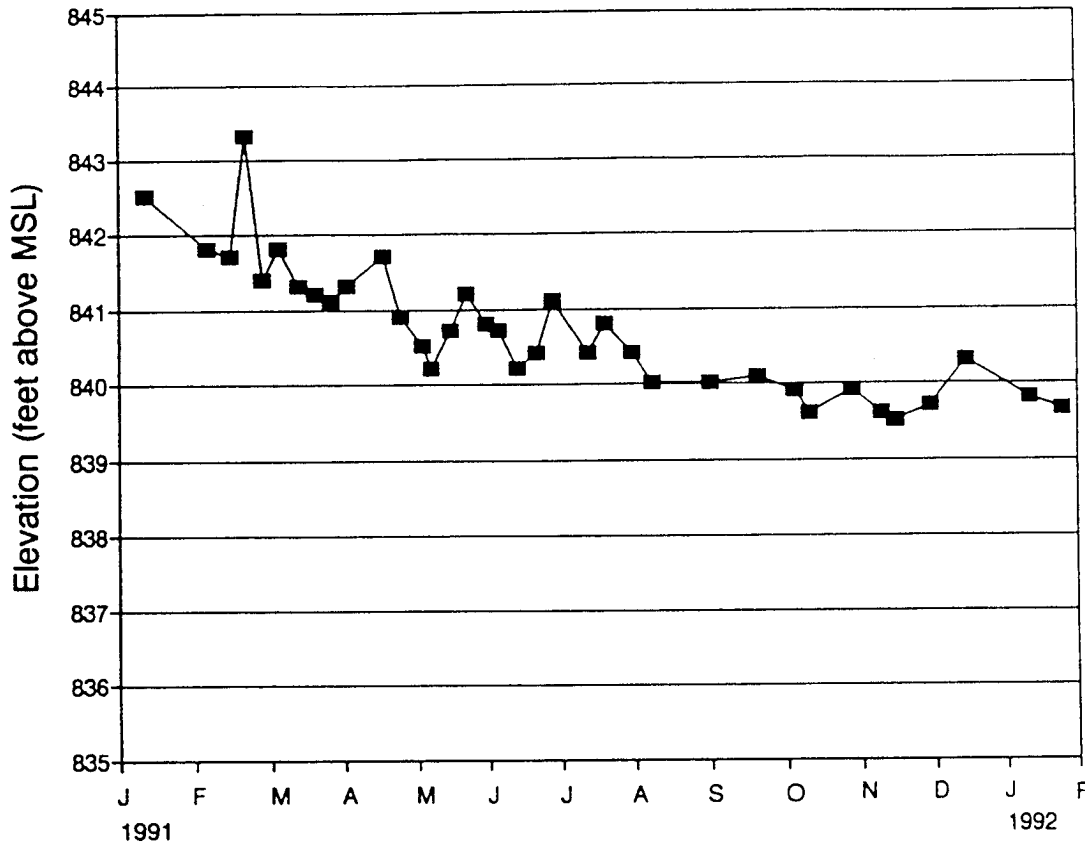


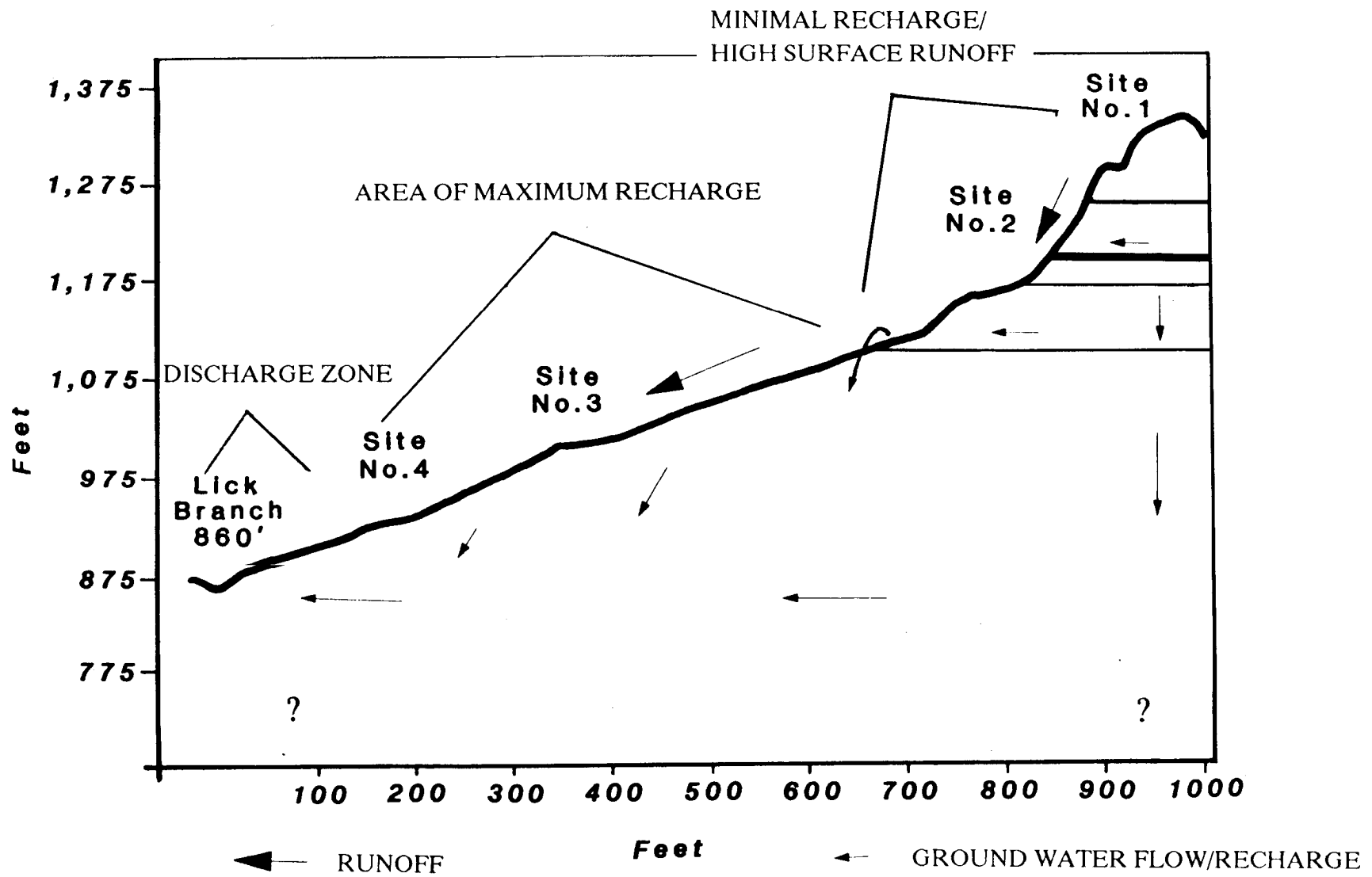
Figure 31. Hydrograph for piezometer 41A.

Table 6.—Tritium Data with Estimates of Age Based on Interpretation from Hendry (1988).

Sample ID	Counting Method	TU	error (\pm TU)	Estimated Age
11A	Enrichment	0.32	0.12	> 50 years old
11B	Enrichment	2.19	0.30	at least 20 years old
11C	Direct	13	2	< 35 years old
12A	Direct	13	2	< 35 years old
13A	Direct	13	2	< 35 years old
14A	Direct	23	2	< 35 years old
21A	Direct	17	2	< 35 years old
22A	Enrichment	4.64	0.35	at least 20 years old
22B	Direct	11	2	< 35 years old
31A	Direct	10	2	< 35 years old
31B	Direct	13	2	< 35 years old
41A	Enrichment	0.53	0.10	> 50 years old
41B	Enrichment	7.07	2	at least 20 years old

The water type observed in piezometer 31B began as Na-HCO₃, with calcium gradually replacing sodium as the major cation. The relative percentages of anions remained constant for the sampling period, which suggests that cation exchange has occurred where sodium is exchanged for calcium (eqn. 5). Calcium is probably derived from the dissolution of calcite. Alternatively, the disruption of the bedrock by drilling and

purging of water on a monthly basis may have induced flow from fractures or saturated zones in hydraulic connection with the open interval, allowing for addition of ground water with a higher calcium content. The low variance in dissolved solids (CV = 3.6 percent) would support a cation exchange explanation. However, the intrusion of water with a higher percentage of calcium could also explain this variation in the



Discussion

Figure 33. Conceptual model of ground-water flow occurring at the site.

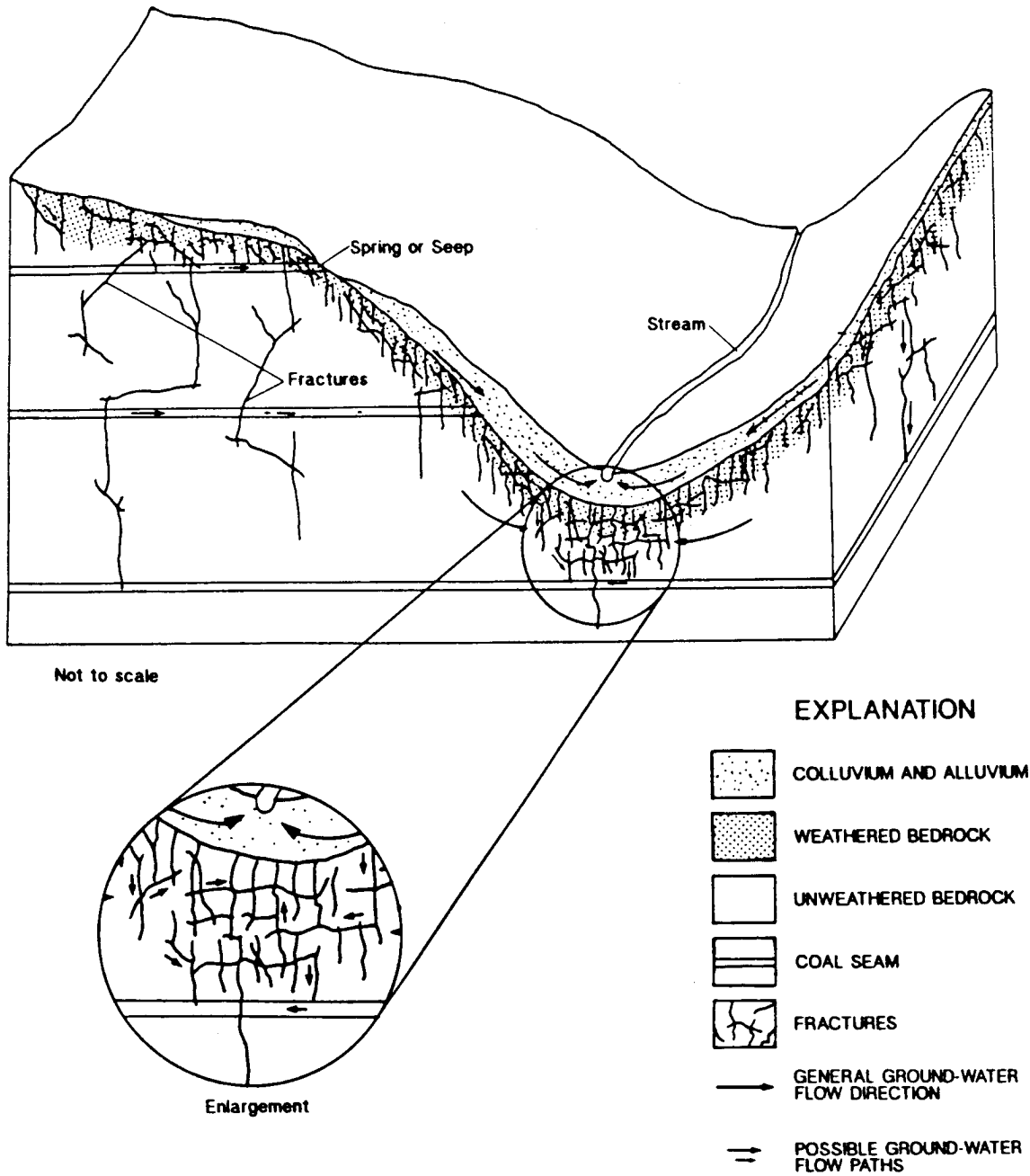


Figure 34. Conceptualized ground-water flow system in the coal fields of southwestern Virginia (from Harlow and LeCain, 1991).

source of the sulfate observed in 22B (mean = 447 mg/Q. Iron hydroxides were not observed in the purge water during sampling.

One explanation for this water type is that the location in the subsurface where the majority of the reactions that influence the water chemistry found in this piezometer are taking place somewhere other than in the immediate vicinity of piezometer 22B; thus, the iron may precipitate at some location along the flow path (i.e., fractures) before it enters 22B. The high sodium content of the water is most likely a result of cation exchange (eqn. 5). The only other likely source of sodium

that could produce a high dissolved sodium content consistent with the observed concentration in piezometer 22B (mean Na^+ is 218.3 mg/L) is by contamination by brine. Sodium contribution by brine is highly unlikely because (1) the piezometer is situated at an elevation well above drainage where brines are usually encountered (Price and others, 1962) and (2) chloride concentrations were low (average 3.97 mg/L Cl^-) and are not consistent with the chloride concentrations that would be expected if brine contamination was occurring. Evidently the redox conditions near this piezometer are not conducive to sulfate reduction, as evidenced

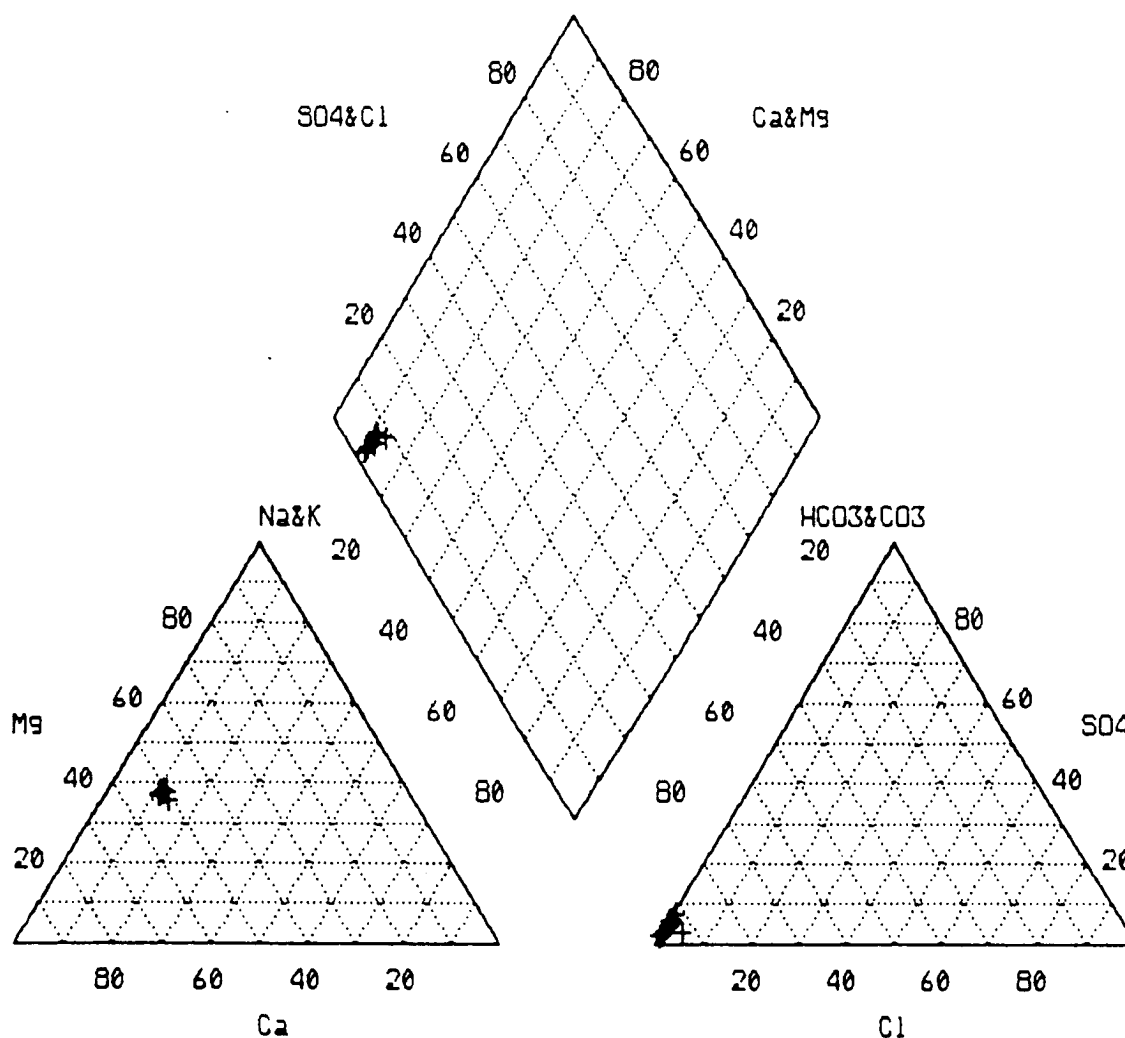


Figure 35. Chemical analyses from piezometer 12A shown on a Piper diagram.

by the high sulfate content, and H_2S was not noted during sampling.

Piezometers 11A, 22A, and 31A are $Na-HCO_3$ water types. These piezometers are set at elevations slightly below drainage in the interior area of the ridge. The water in these piezometers had to migrate through a considerable rock mass, which undoubtedly influenced the chemistry. The most likely evolutionary sequence for the generation of the $Na-HCO_3$ water type encountered in these piezometers involves cation exchange, where divalent cations are removed from water that has reacted with pyrite, calcite, plagioclase, and perhaps siderite in the shallow, fractured zones or coals near the ridge surface. In this case, water that does not move laterally and exit the ground-water system by way of the coal seams and shallow fractures would migrate vertically into the ridge core. This ground water would be in contact with the host rocks for a significant amount of time because of the low vertical hydraulic conductivities of the rocks within the ridge. This would allow time for chemical reactions such as cation exchange to proceed without interruption. Additionally, the high feldspar content of the rocks of the Breathitt Formation

(Danilchik and Waldrop, 1978) suggests that the hydrolysis of silicate minerals (eqn. 8) is likely to take place. The products of this reaction include kaolinite, along with dissolved silica, metal ions, and bicarbonate ions. Increased bicarbonate concentrations tend to occur during the hydrolysis reactions involving silicates in ground waters containing little carbon dioxide (Hem, 1985), and this reaction may aid in the creation of ground waters with a high pH. The pH of each of these three piezometers was consistently above 7.0, and above 8.0 in piezometers 11A and 22A. The highest pH measured at the site occurred in 22A, with a reading of 8.92.

Figure 48 shows the stability fields of gibbsite, kaolinite, montmorillonite, and albite as a function of pH, Na^+ , and H_4SiO_4 content. Sodium was chosen as a variable on the diagram because it is the dominant cation in the deeper piezometers. The incongruent dissolution of feldspar (K-spar) results in the formation of kaolinite (eqn. 8). Water samples from each piezometer (with the exception of 41A, which plots in the montmorillonite field) plot within the kaolinite stability field, indicating this is the most stable phase formed by the silicate weathering reactions. The stability of kaolinite with

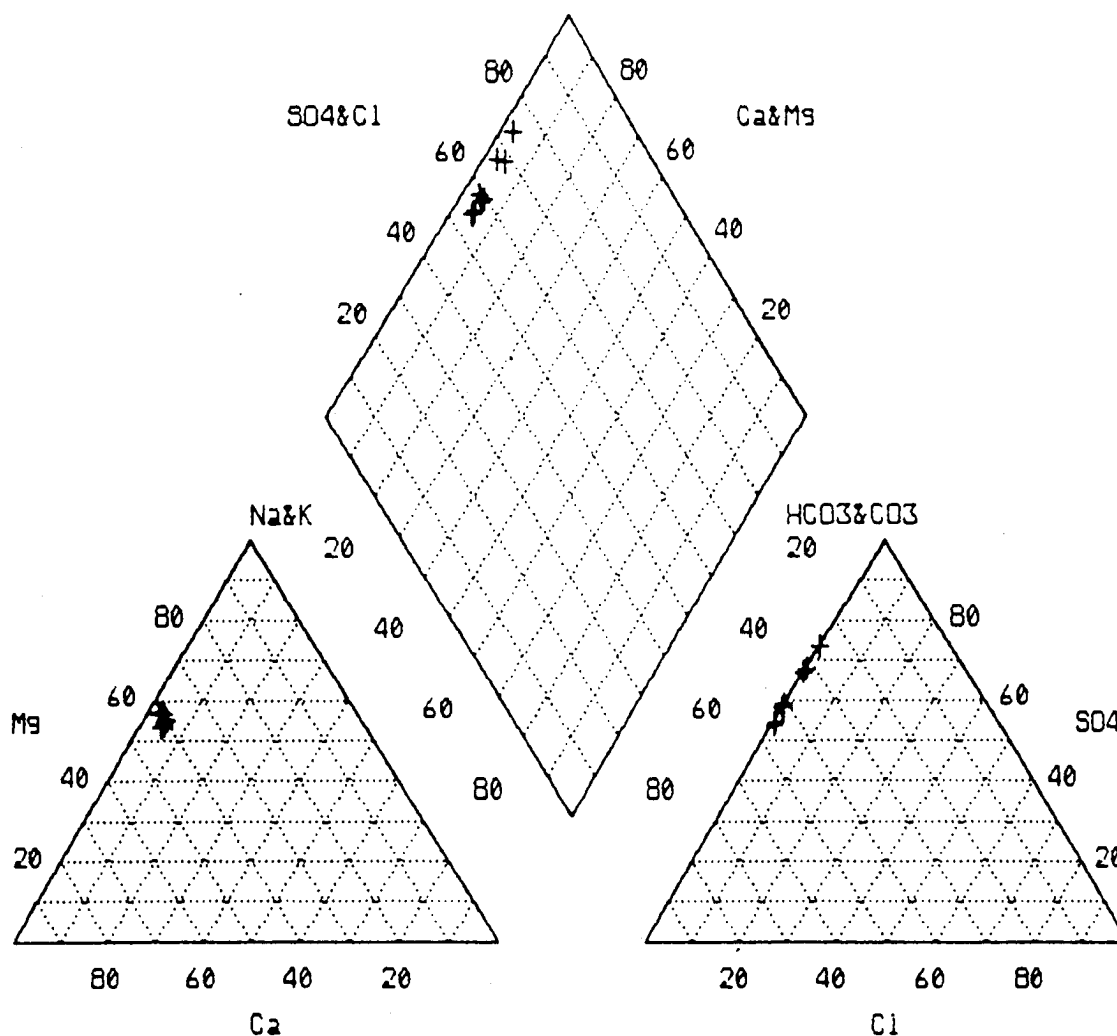


Figure 36. Chemical analyses from piezometer 14A shown on a Piper diagram.

ground water at this site is consistent with the findings of Weinheimer (1982), who reported the high occurrence of kaolinite in rocks of the Breathitt Formation.

Cation exchange (eqn. 5) most likely removes calcium and magnesium from the ground water in the ridge interior. The most likely host for the exchange reactions is kaolinite, because of its abundance. A low cation exchange capacity (CEC) (10 to 100 mmol/Kg) is usually determined for kaolinite, with the majority of exchange being pH dependant and concentrated on the edges of the clay particles (Bohn and others, 1985). Despite its relatively low CEC, kaolinite would probably have sufficient exchange capacity to accommodate the calcium and magnesium concentrations found in the relatively fresh ground waters (TDS generally less than 500 mg/L) encountered at this site. Other clay minerals, such as illite, probably also contribute to this effect. As evidence, no divalent cations are observed in high concentrations in ground water derived from the ridge interior. This suggests that ample exchange capacity exist for the adsorption of divalent cations, which are preferred over monovalent cations on exchange sites (Bohn and others, 1985). Another possible host

for cation exchange reactions may be the carboxylic acid groups found in organic matter. These radicals would most likely occur in coal. However, the stratigraphic data show that the majority of coal seams at this site occur in the upper region of the ridge, and no major coal seams occur in the ridge interior where the greatest effect of cation exchange is observed. However, carbonaceous material is common to the coal-bearing rocks in eastern Kentucky; therefore, this mechanism cannot be discounted as contributing to the net divalent cation reduction.

The chemical analyses for water samples taken from piezometers 11A and 22A show very low calcium concentrations (generally less than 5 mg/L), indicating that the cation exchange reaction (eqn. 5) has proceeded far to the right. Freeze and Cherry (1979) indicated that the cation exchange reactions will proceed to adsorb calcium as long as (1) exchange sites are available, (2) the activity product for calcium and carbonate is less than the equilibrium constant for calcite (unsaturated), and (3) as long as calcite is available for solution. Calcite has been identified as a cement in Breathitt sandstones, and isolated limestones occur within the forma

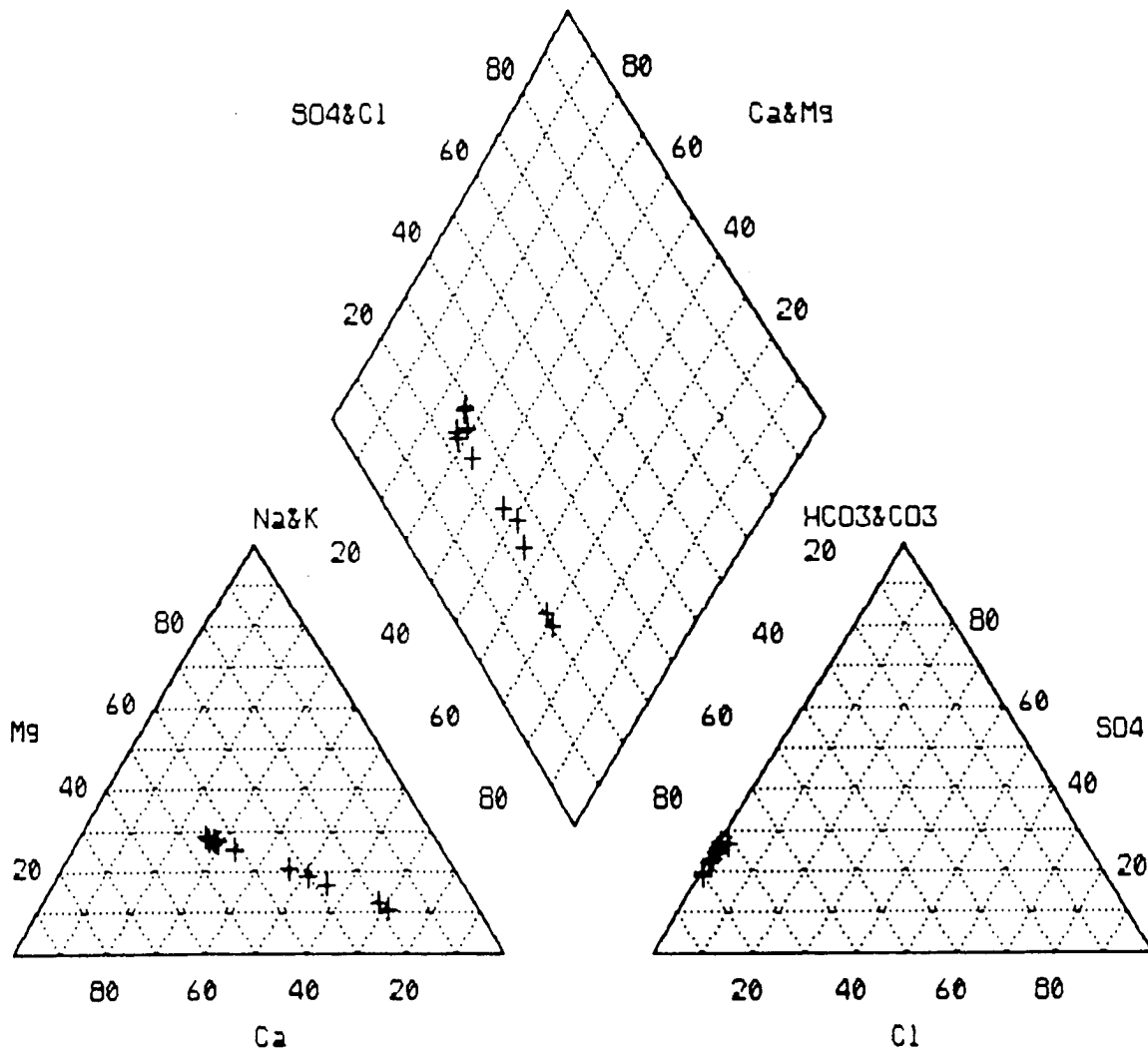


Figure 37. Chemical analyses from piezometer 31B shown on a Piper diagram.

tion (Danilchik and Waldrop, 1978; Weinheimer, 1982). As cation exchange removes calcium from solution, it allows the water to remain undersaturated with calcite; therefore, calcite continues to dissolve, which has the net effect of increasing the alkalinity by the addition of HCO_3^- (eqn. 3). Saturation indices calculated for calcite and plotted for each well are shown on Figure 49. All piezometers, with the exception of 41A, are undersaturated with respect to calcite; thus, the condition for undersaturation with calcite is met for all of the piezometers that monitor the ridge interior. Calcite dissolution will add to HCO_3^- produced by silicate hydrolysis, with the net result being an increase in the total alkalinity and pH.

The sulfate concentration is generally low in both piezometers 11A and 22A. This is most likely due to sulfate reduction mitigated by sulfur-reducing bacteria (eqn. 6). These bacteria exist under anaerobic conditions and require sulfur compounds and organic compounds such as carbohydrates, organic acids, and alcohols (Alexander, 1977) for metabolic activity. A minimum of 1.0 mg/L of organic matter is needed for sulfate-reducing bacteria to exist in the ground-water system (Perry and others, 1980). In this study, several piezometers

(22B, 22A, 11A, and 31A) contained total organic carbon in concentrations above the detection limit of 1.0 mg/L (see Appendix 6). The exact organic constituents present in this organic matter are not known, but it is likely that the necessary organic compounds to sustain bacterial activity are present. Most subsurface waters contain sufficient quantities of the necessary dissolved organic matter to sustain bacterial growth (McNabb and Dunlap, 1974).

Piezometers 11A and 22A are screened to depths at which low concentrations of dissolved oxygen would be expected to be present. The Eh values obtained for these piezometers show a mean value of 173 mV for piezometer 11A and 120 mV for piezometer 22A, which are slightly above the Eh levels where significant sulfate reduction normally occurs (Champ and others, 1979). However, the redox potential values used in this study were not measured by the determination of a redox couple at equilibrium and, therefore, may not be indicative of the actual redox conditions in the ground-water system. As indicated before, the measured redox values for ground water in this study are used in a qualitative sense for comparison purposes. A slight odor of hydrogen sulfide

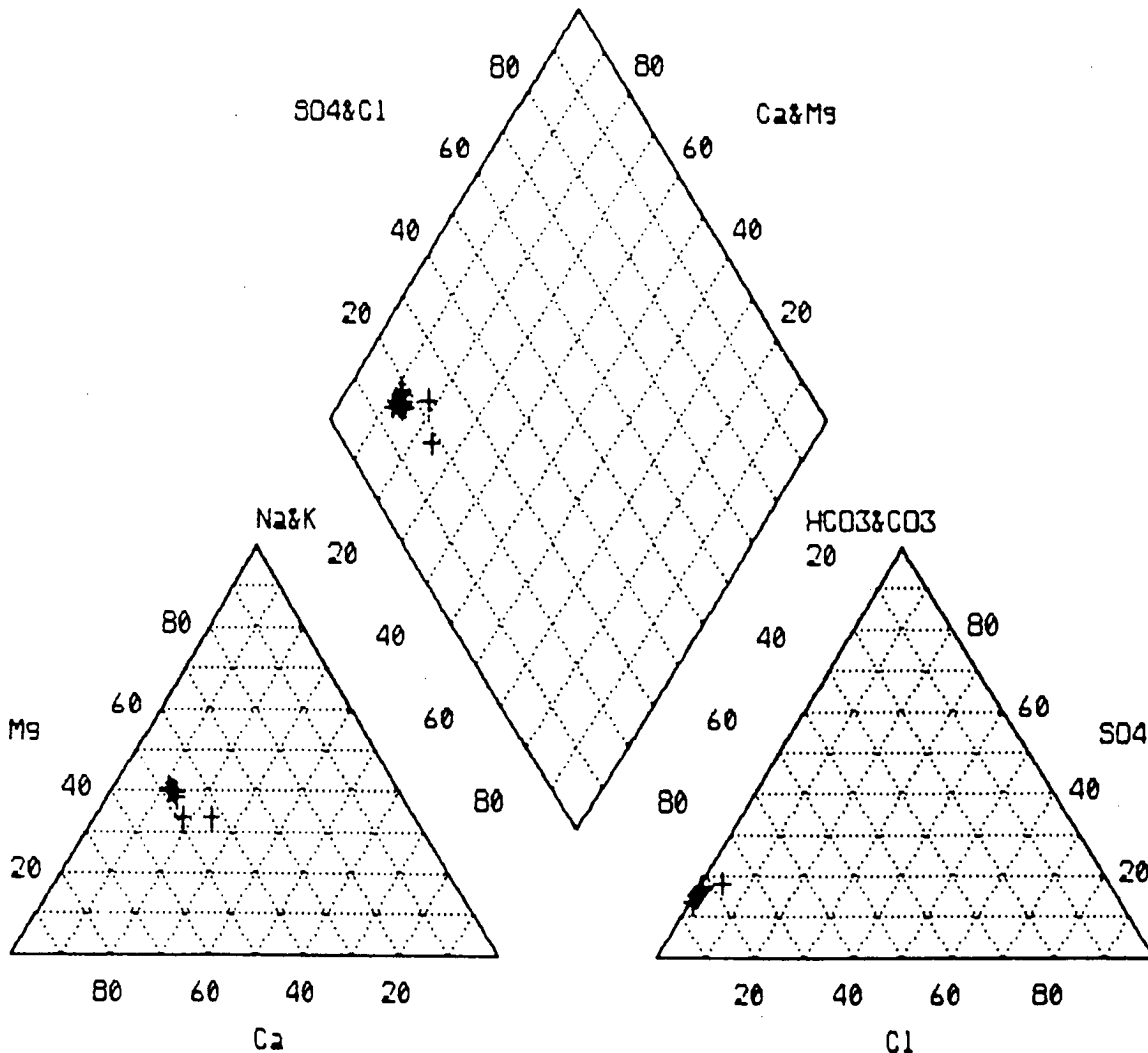


Figure 38. Chemical analyses from piezometer 11B shown on a Piper diagram.

was observed at times when sampling piezometers 11A and 22A, indicating that sulfate reduction had occurred. A field test (HACH kit) was performed on several occasions to obtain a semi-quantitative analysis of H_2S content, but these efforts were unsuccessful. Apparently, the H_2S concentration was below the detectable limits of the method (0.1 mg/L), although its presence was detectable by smell. The pH range of between 7 and 9 observed in both piezometers 11A and 22A is near the favorable pH range (6.5 to 8.5) where sulfate reduction occurs (Connell and Patrick, 1968).

On an average, the water from piezometer 31A is an $Na-HCO_3$ water type. Piezometer 31A is located down gradient of 11A and 22B and is also directly beneath 31B. The Piper plots for both 31A and 31B show that the percentage of major cations varies throughout the sampling period (see Figs. 37 and 44). The majority of variation in ion chemistry in piezometer 31B occurred in the first 5 months of the sampling period. Sodium was the major cation during this period, but gradually gave way to calcium. The relative percentages of anions remained consistent except for sulfate, which exhibited a small rise at the end of the period.

Figure 50 shows the trends in the percent of major ions in both piezometer 31A and 31B along with the monthly precipitation data. It can be seen that the percentages of ions from August through the end of the study remain quite constant in 31B, yielding a $Ca-Mg-HCO_3$ type water. The water chemistry of samples taken from this piezometer during this period is most likely controlled by the dissolution of calcite (eqn. 3) and the oxidation of pyrite (eqn. 14). This $Ca-Mg-HCO_3$ water type observed in piezometer 31B during the latter sampling times is more consistent with the water types observed in other piezometers that are set in fractures. It has been shown that $Na-HCO_3$ -type water has been associated with the piezometers located in the ridge interior, which are generally at a greater depth than 31B (e.g., 11A and 22A). Also, the water derived from the ridge interior tends to be considerably older water (based on the tritium data).

Some of the possible explanations for the cationic variation and subsequent decrease in sodium are as follows: (1) As mentioned previously, the air-rotary drilling of the borehole containing the piezometer may have temporarily altered the flow path of water entering the well by blocking fractures by

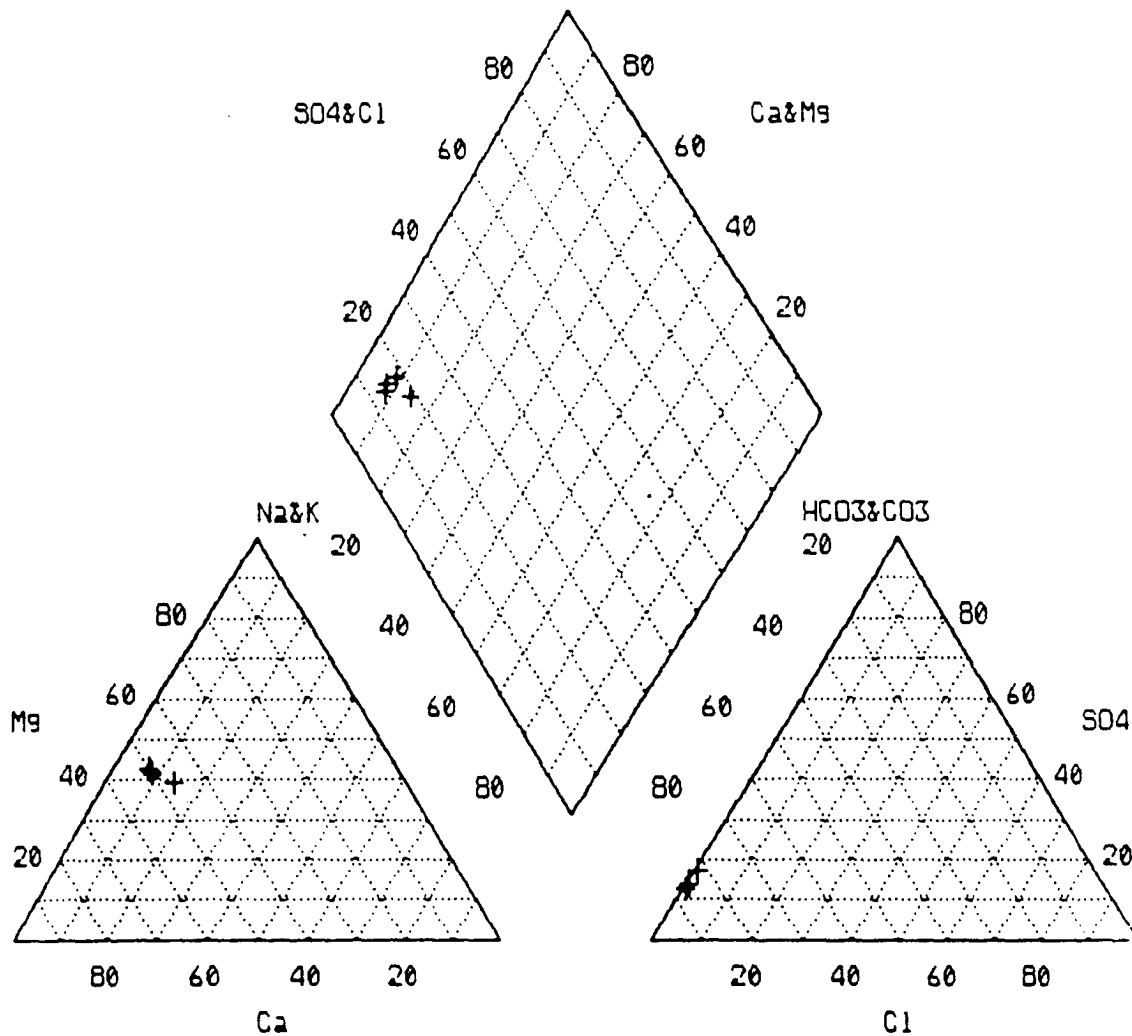


Figure 39. Chemical analyses from piezometer 13A shown on a Piper diagram.

injecting drill cuttings. Subsequently, well development of the piezometers may have reopened the pathways for ground water to enter the horizon. (2) Na-HCO₃-type water may have moved upward into the zone monitored by 31B when the borehole was left open between drilling and piezometer construction. (3) Piezometer 31B is screened into a fracture zone, and water (i.e., water containing higher calcium and magnesium) may be introduced during storm events and periods of high recharge.

Looking at simultaneous trends in the major ion concentrations in both piezometer 31B and 31A may offer insight into the variation in these piezometers. Figure 50 shows that the considerable drop in sodium and bicarbonate occurring during June 1991 in piezometer 31A correlates with a simultaneous rise in calcium, magnesium, and sulfate. The same trend is observed in June in 31B, although it is not as pronounced. During June the relative percentages of the major ions in water from 31A is very similar to the distribution observed in 31B. The bar graph (Fig. 50) showing the monthly precipitation illustrates that the highest amount of precipitation in a 1-month period occurred during June. The June pre-

cipitation may have created a pulse of recharge water that migrated downward from the surface and affected the water chemistry in 31A by adding calcium, magnesium, and sulfate while diluting the amount of sodium and bicarbonate. Eastern Kentucky experienced severe thunderstorms that created flash flooding during June of 1991. The intensity of these storms caused washouts in sections of the access roads at the site. The intrusion of ground water related to summer storm events may provide recharge in the location of these two piezometers, thereby providing water characterized by mineral reactions (e.g., calcite dissolution, pyrite oxidation) that form Ca-Mg-HCO₃ water types. This scenario may explain the prominence of calcium as the major cation for the remainder of the study period in 31B but not 31A. Subsequent storms during the remainder of the year may not have been of sufficient intensity to create the large pulse of recharge necessary to penetrate to the depth of piezometer 31A and affect its water chemistry, but were sufficient to reach 31B. This hypothesis is supported by the daily precipitation data. During the 16-day period from May 18 to June 3 (which preceded the June water sampling), four storm events

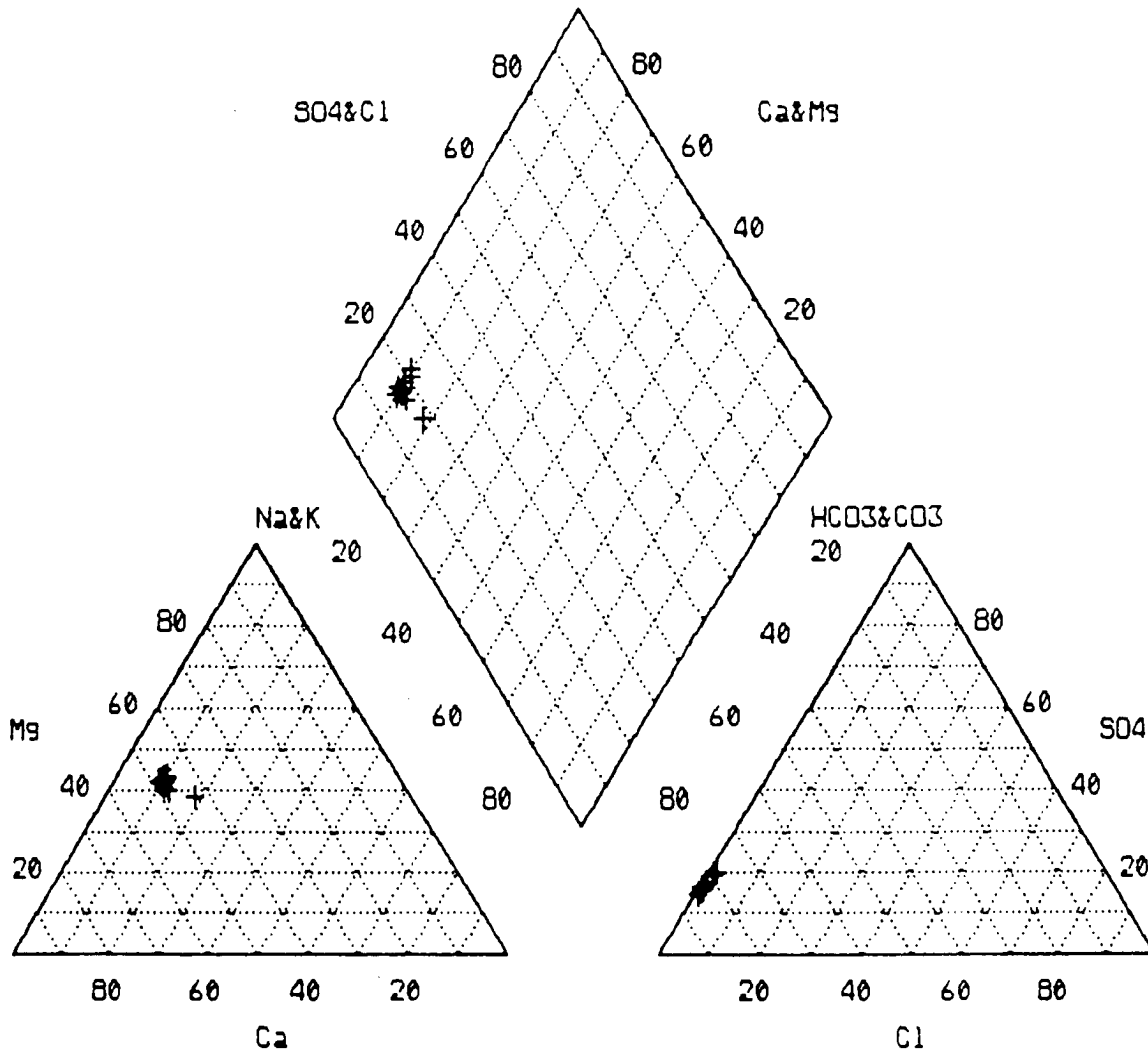


Figure 40. Chemical analyses from piezometer 21A shown on a Piper diagram.

occurred where more than 1 inch of precipitation fell (see Appendix 5). Two of these events produced more than 1.5 inches. The site did not experience this many intense events in this brief a time period during the remaining time frame of the study

Rapid infiltration in the vicinity of 31A and 31B is consistent with the earlier findings that these piezometers are situated in the area where maximum penetration of recharge enters the ridge (see Fig. 32). Additionally, although the water chemistry and the distribution of major ions found in 31A is quite similar to that found in 11A and 22A, the tritium content is significantly higher (0.32 TU for 11A, 4.64 TU for 22A, and 10 TU for 31A.), showing an increasing trend from the ridge interior outward. Although tritium is not a conservative tracer, the tritium content in 31A is more on the order of the 13 TU found in 31B, which also supports the hypothesis that ground water is migrating downward from the shallow fracture zone above 31A.

At the beginning of the sampling period the water taken from piezometer 31A showed that calcium plus magnesium represented approximately 40 percent of the cations (mille-

equivalents) but gradually dropped to less than 7 percent at the end of the study. Concurrently, the percent of anions represented by bicarbonate remained approximately the same, while chloride increased slightly. The pH also shows a steady rise from 6.78 in March to 7.73 in December of 1991. The water chemistry toward the end of the period more closely resembles the water derived from 11A and 22A, which are upgradient of 31A but screened in the same stratigraphic interval. The most likely cause for the water type found in 31A during this period is ground-water mixing by the addition of ground water from the shallow fracture zone with ground water moving down gradient from the ridge interior. As precipitation (thus, recharge) decreases at times throughout the year, the water chemistry in 31A becomes more characteristic of water from the interior (upgradient) area of the ridge. The increase in chloride content probably indicates a slight contribution of older water from depth.

Piezometer 41B is down gradient of 31A. The water type encountered in this piezometer is an Na-Ca-HCO₃. The percentage of major ions has remained stable throughout the period of study. The chloride content (mean = 27 mg/L) is five

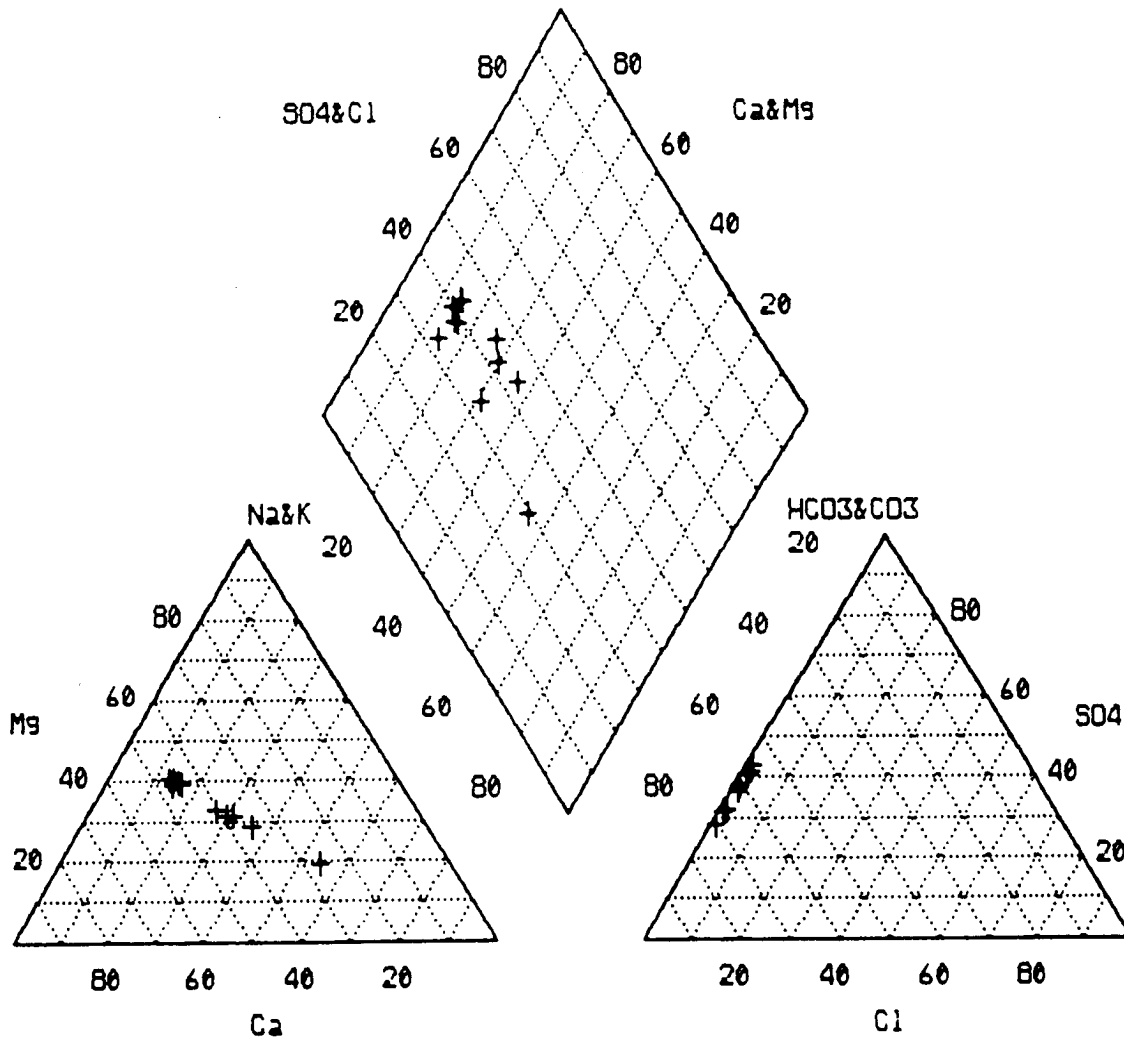


Figure 41. Chemical analyses from piezometer 11C shown on a Piper diagram.

times higher than that found in the piezometers at the same level located in the ridge interior (mean = 4.48 mg/L chloride for 11A and 4.80 mg/L chloride for 22A) and nearly twice that of 31A (mean = 17.7 mg/L chloride), which is nearest to and upgradient of 41B. Figure 51 shows the iso-concentration lines for chloride concentration along the profile of the site. The data from July 1991 are used and were chosen for the following reasons: (1) July was one of the months when the maximum number of piezometers (13 of 16) had water in sufficient quantity to sample, (2) the charge-balance error for each of the July analyses was less than 5 percent, with the mean error being 2.27 percent, and (3) the high temporal consistency in the chemical quality (as exemplified by the Piper diagrams) suggests that data from one sampling event could reasonably represent the hydrochemical conditions at the site. Subsequently, the data from July 1991 will be used in all iso-concentration plots as well as for geochemical modeling in this study.

A definite trend of increasing chloride content is shown in Figure 51, which shows iso-chloride contours along the ridge profile near Lick Branch. The higher chloride content in 41B

is probably indicative of ground-water mixing with brines that are present below in 41A. The area of high chloride concentration shown on Figure 51 is based on the available data, and this area may actually extend beneath all of the Lick Branch valley bottom.

The potentiometric heads shown by the piezometers throughout the site indicate that the valley bottom is the discharge zone for water entering the ridge. The potentiometric head measured in 41B and 41A indicate a downward gradient between the elevations monitored by these two piezometers. The brine in 41 rises to within 80 feet from ground level, which is approximately 20 feet below the water level of 41B. The head levels measured in these adjacent piezometers only represent one component of the flow field (it was shown previously that ground-water flow between the piezometers at the level is toward the southwest; see Fig. 30). The head present in 41A indicated that the brine has the potential to migrate to within 40 feet of the stream channel of Lick Branch, and perhaps even higher when the fresh water above it experiences decreased head from lack of recharge during extended dry periods. The high chemical gradient be

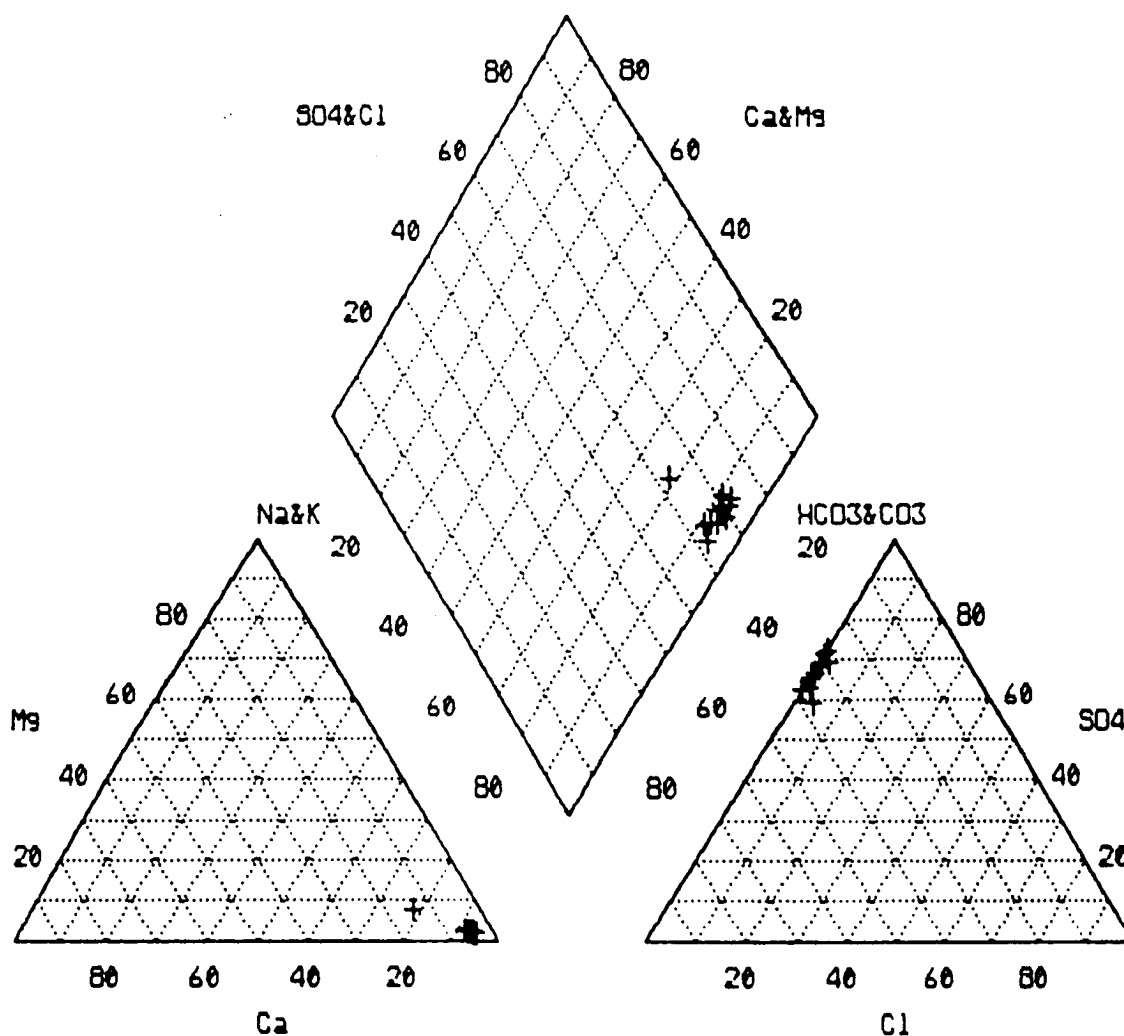


Figure 42. Chemical analyses from piezometer 22B shown on a Piper diagram.

tween the fresh water found at the surface and the concentrated brine at shallow depths below may result in the diffusion of the salt water into the fresh zone if the salt-water zone is not confined.

Examination of the conceptual models of ground-water flow presented by Harlow and LeCain (1991) and Wyrick and Borchers (1981) show that the intensity of subsurface fractures, both vertical joint patterns and bedding planes, increase in the valley bottoms. In this case, the greater intensity and interconnection of fracture planes may breach aquitards that normally separate brine and fresh water near the valley bottoms and allow for the vertical migration of brines below drainage areas. The lower occurrence of fractures in the ridge interior would probably maintain the continuity of any laterally extensive unit, such that its properties that retard the vertical movement of water would remain intact.

The brine found in piezometer 41A contains high concentrations of Na-Cl with a measured average electrical conductance of over 26,000 microsiemens (*see* Appendix 6 for chemical data). Piezometers 41B and 41A are the only two piezometers in this study that yielded water that was charac-

teristically high in barium content. Piezometer 41B had a mean barium value of 1.72 mg/L, and 41A contained 37.4 mg/L. These findings are consistent with the findings of Wunsch (1988a), where barium in ground water exhibited a strong correlation with chloride and was restricted to bedrock wells open to intervals below major drainage in valley bottoms. Additional discussion concerning barium in ground water will be covered in the following sections.

Both piezometers 41A and 41B contain ground water that is depleted in sulfate, considering the abundant sulfur sources contained in the coal-bearing rocks. Piezometer 41A has an average sulfate content of 10.9 mg/L, and 41B contains 9.1 mg/L. Often a strong odor of hydrogen sulfide gas was detected in the water from both 41A and 41B when purging took place. Wunsch (1988a-b) identified the common sulfur-reducing bacteria *Desulfovibrio* in well water in eastern Kentucky. The presence of hydrogen sulfide is common in the ground water in eastern Kentucky (Price, 1962), indicating the conditions for sulfate reduction are widespread in the area.

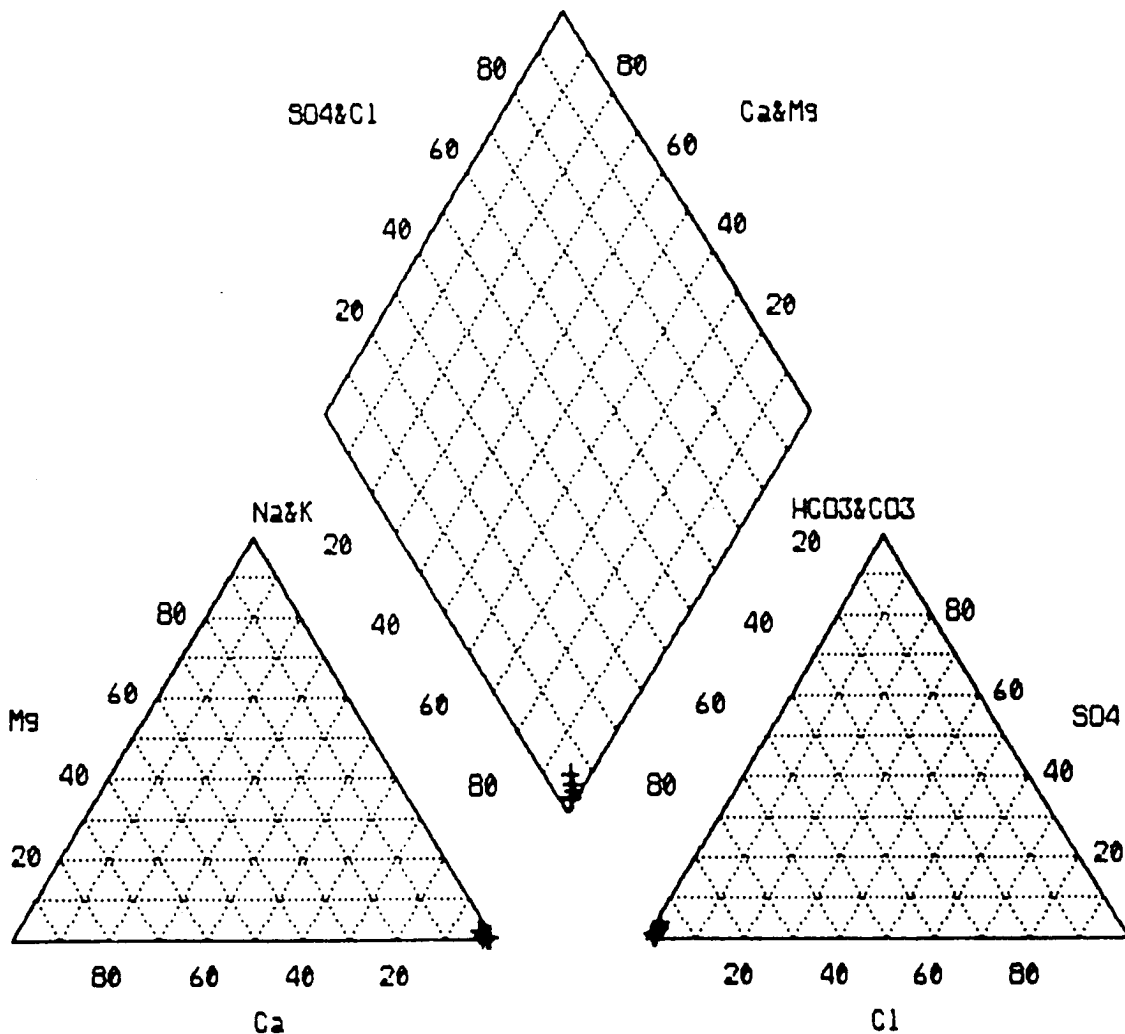


Figure 43. Chemical analyses from piezometer 11A shown on a Piper diagram.

Low Eh values are characteristic of ground water in discharge areas (Champ and others, 1978; Freeze and Cherry, 1978; Gilkeson and others, 1981). The Eh measurements found in 41A and 41B were the lowest encountered throughout the study period. At times the Eh measurements were found in the negative range, with the lowest reading being -49 mV in piezometer 41A during the December 1991 sampling. The mean Eh value for piezometer 41B (mean = 52 mV) and for 4 A (mean = 15 mV) are within the range (<100 mV) where active sulfate reduction mitigated by sulfur-reducing bacteria is likely (Connell and Patrick, 1968; Champ and others, 1978).

The total iron concentrations found in both 41A and 41B were low when compared to total iron in water from other piezometers at the site. Consistently low redox conditions in the discharge area and the near-neutral pH reading observed in both piezometers; would predict that the majority of iron in ground water in these piezometers would occur as ferrous iron (Hem, 1985). Continuous sulfate reduction in this zone results in the production of hydrogen sulfide that probably

reacts with the dissolved iron and precipitates as iron sulfides, which keeps dissolved iron concentrations low.

Geochemical Controls on Fluoride in Ground Water

Figure 52 shows the saturation indices with respect to fluorite for water samples from each piezometer at the site. All samples are undersaturated with fluorite, and no apparent trend is observed between the degree of saturation and well depth, location, or water-producing zone, suggesting that the occurrence of fluoride is not controlled by fluorite (eqn. 18). Generally, fluorite (CaF_2) is thought to be a control on fluoride concentrations in ground water that contain > 5 mg/L fluoride (Robertson, 1991). This argument is strengthened by the poor correlation ($r = .25$) of fluoride with calcium (Table 7).

Determination of fluoride concentrations in water samples from all piezometers revealed that fluoride ranged from 0.02 to 2.20 mg/L. Figure 53 shows the iso-concentration lines for fluoride concentration along the profile of the site.

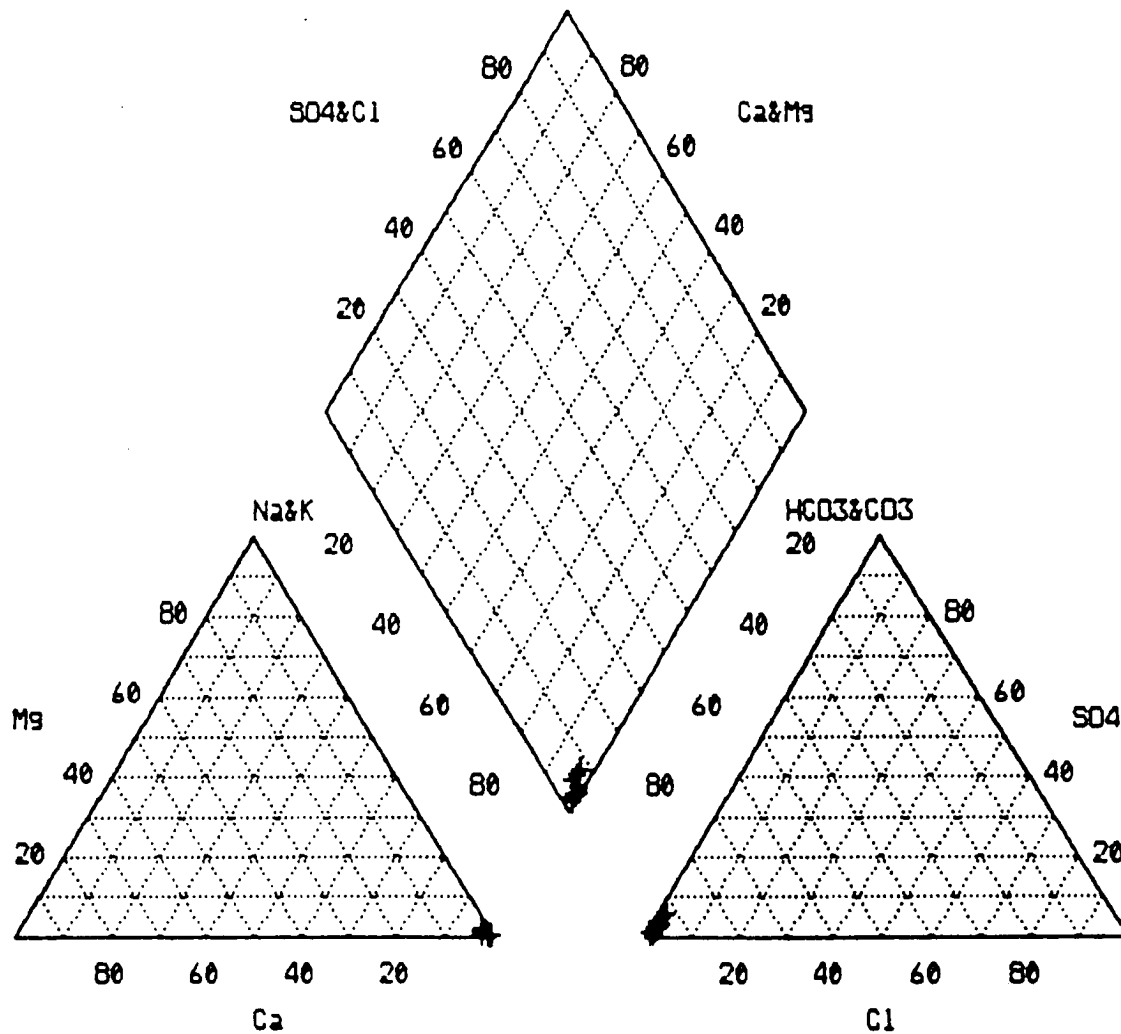


Figure 44. Chemical analyses from piezometer 22A shown on a Piper diagram.

High fluoride concentrations are restricted to the ridge interior, where the water type is predominantly Na-HCO₃ and has a high pH. A strong correlation of fluoride with pH ($r = 0.91$) at the 0.01 percent level ($p < 0.0001$) suggests that pH-dependant exchange or adsorption reactions are important in the control of fluoride concentrations. In the exchange reaction, the elevated pH of the ground water indicates that a high concentration of hydroxyl ions would be present, which would be available to exchange with fluoride (eqn. 17), resulting in increased fluoride concentrations in the ground water. Clay minerals are the likely host for the exchange reactions to occur (Bower and Hatcher, 1967); however, Bohn and others (1985) indicated strong adsorption of fluoride by goethite (FeOOH). Additional sources of fluoride may be from weathering reactions of micas and hornblende. The stability diagram based in sodium, silica, and pH indicate kaolinite is the stable clay mineral in almost all water samples; however, Weinheimer (1983) indicated the abundance of both kaolinite and goethite in rocks of the Breathitt Formation. Therefore, both of these minerals may act as hosts for anion exchange reactions. As indicated earlier, kaolinite was also suspected

as being the host for cation exchange reactions involving calcium, magnesium, and barium. Perhaps the fluoride and hydroxyl ions act to balance any net positive charge created when positively charged cations are adsorbed on the edges of clay particles. This study has not generated the types of data, nor was it a goal to determine the exact surface reactions that can account for this geochemical phenomenon. More study is needed to determine these relationships.

The decrease in fluoride content in ground water as it moves from the ridge interior to the discharge area can probably be attributed to dilution from ground-water mixing or by fluoride re-adsorption to clay minerals as the pH decreases. Decreased pH indicates a lower concentration of hydroxyl ions, thus less competition for exchange sites.

Geochemical Controls on Barium in Ground Water

Barium content in the piezometers at the site ranged from 0.024 mg/L to 48.6 mg/L. Table 7 lists Pearson product-moment correlation coefficients for several elements and pa-

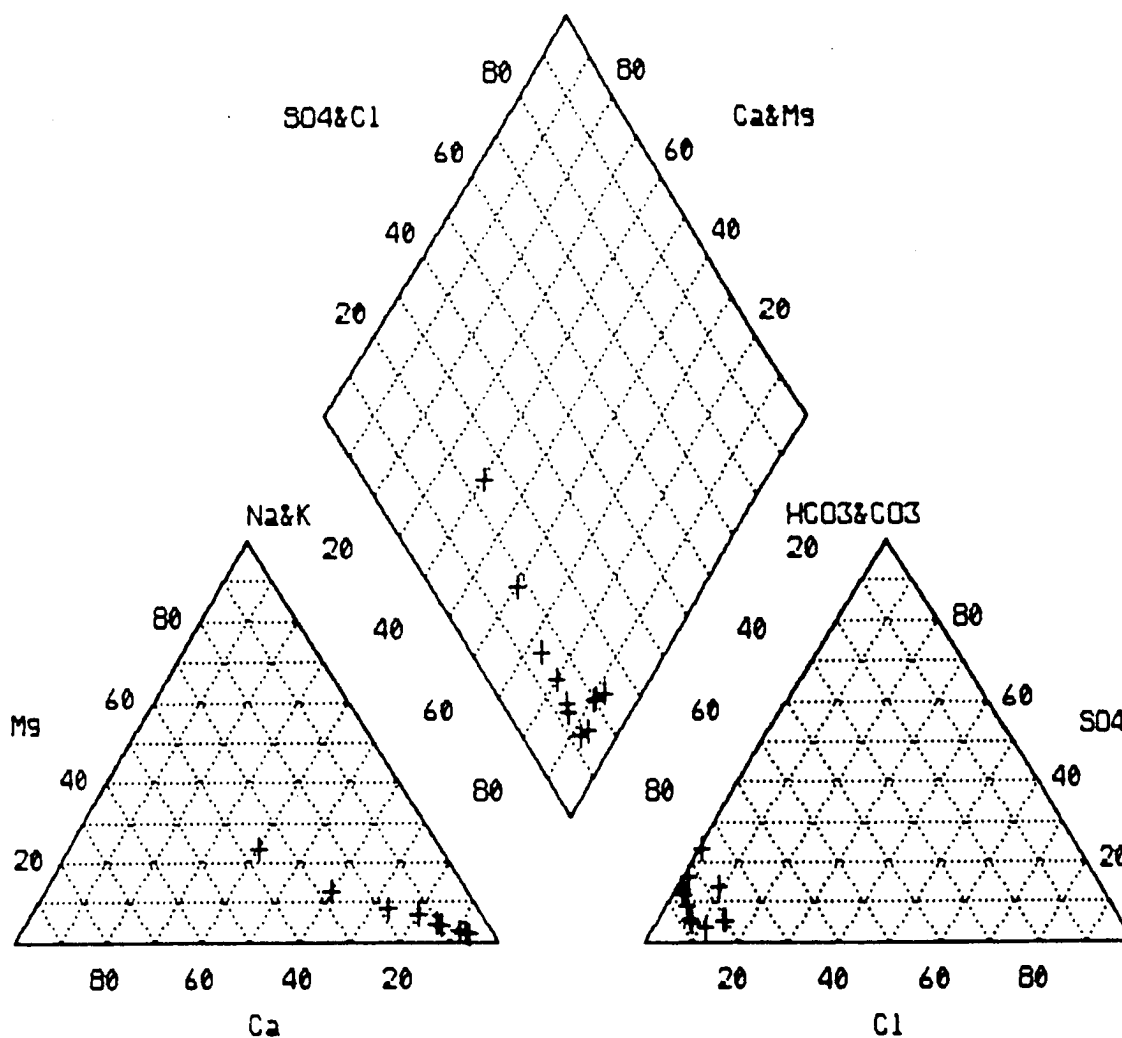


Figure 45. Chemical analyses from piezometer 31A shown on a Piper diagram.

rameters for the chemical data from all piezometers. The occurrence of barium exhibited strong positive correlations with chloride, sodium, and calcium. These findings are consistent with the findings of Wunsch (1998a), who attributed the occurrence of barium in ground water in eastern Kentucky to the mixing of fresh ground water with brines.

Figure 54 shows the saturation indices for barite plotted for each piezometer in the study. The water samples for each piezometer, with the exception of 11A, 22A, and 21A, are saturated with respect to barite. This shows piezometers with barium values less than 0.5 mg/L as well as those above 1 mg/L are saturated with respect to barite. This finding is not unexpected because of the relatively high sulfate content common to ground water in Pennsylvanian coal-bearing rocks. Sulfate can impose a solubility constraint on barium, especially under oxidizing conditions (Hem, 1985). Piezometer 21A shows a saturation index (SI) of -0.058, which is near equilibrium with barite. Of more significance to the occurrence of barium in ground water is the trend in barite stability along the flow path through piezometers 11A, 22A, 31A, and 41B. Piezometer 11A is highly undersaturated with barite.

Piezometer 22A is also undersaturated, but to a lesser degree. Moving down gradient, one observes that both 31A and 41B are supersaturated with barite (*see* Fig. 54).

Figure 55 shows a plot of the log value of the activity of select ions shown to exhibit strong correlations (Ca, Na, Cl; Table 7) with the occurrence of barium along with parameters involved with the solubility of barite (SO_4 and Eh). Eh is represented as pe for the convenience of scale on the diagram and is related to pe by the relationship Eh (volts) = pe/0.0592 (Hem, 1985). It can be seen in Figure 55 that the activity of sodium and sulfate are fairly consistent along the flow path. The activity of chloride shows a slight increase, and calcium and barium activities increase significantly from the ridge interior area (11A) to the discharge zone (41B). The pe remains consistent before exhibiting a dramatic drop in the discharge area (41B).

Wunsch (1988a) suggested that the sources of barium could be from its inclusion in brines that are encountered at shallow depth, or from cation exchange. Cation exchange appears to be an important mechanism in the occurrence of barium based on the data shown here, and is probably more

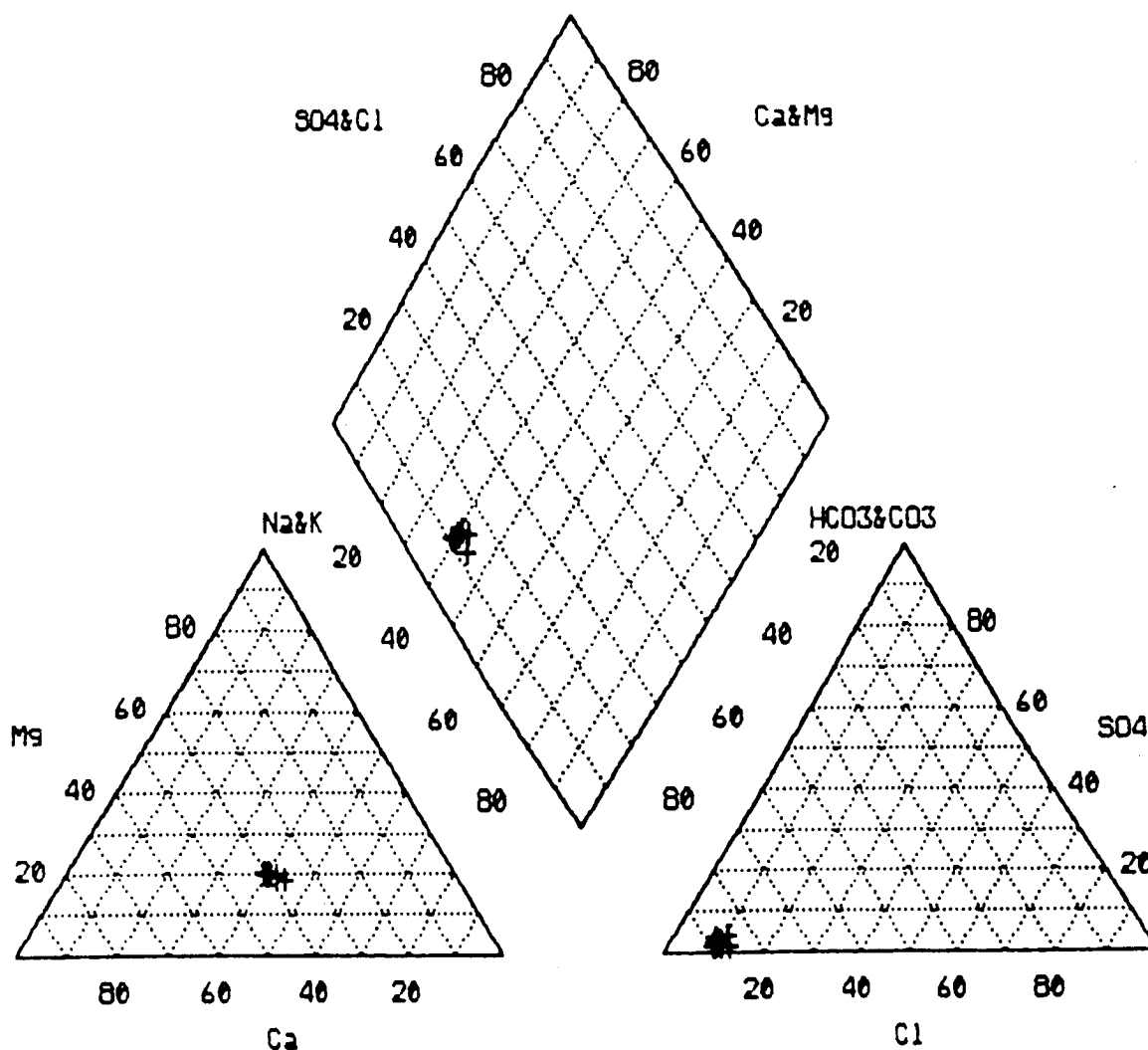


Figure 46. Chemical analyses from piezometer 41B shown on a Piper diagram.

important than the solubility constraints imposed by barite, especially at low barium concentrations (<2.0 mg/L).

The water derived from piezometer 11A shows that the sulfate concentrations are low, with a mean sulfate value of 8.34 mg/L and a mean barium concentration of 0.02 mg/L. The sulfate concentration in 11A is comparable to the sulfate found in 41B (mean = 9.1 mg/L), which consistently contains barium that exceeds 1.0 mg/L. Because the activity of sulfate is low in both 11A and 41B, and assuming the mineralogy along the stratigraphic interval monitored by these two piezometers is consistent, it would be expected that barium concentrations in 11A would be similar to those found in 41B if barite solubility was the only control on barium concentration. The ground water derived from the ridge interior is noticeably devoid of divalent cations, which suggests that cation exchange reactions are removing barium, calcium, and magnesium from solution. The lyotropic series for cations indicates that divalent cations are preferentially adsorbed by clay minerals over monovalent cations, with barium being the most preferred of these divalent ions (Bohn and others, 1985).

The chemical data show that as ground water moves from the ridge interior toward the discharge zone, an increase in calcium and magnesium in ground water is observed. As the concentration of these divalent cations increases, the competition for exchange sites increases, which may cause barium to be released into solution as the water chemistry and the exchange sites move toward equilibrium with the cations contained in solution. This scenario can explain the observed trends in the ion activities shown in Figure 55, which shows a good correlation with the increase in the activity of barium in solution as the activity of calcium increases.

The data from the barium exchange experiments indicate that calcium as well as magnesium was released from exchange sites with increased sodium solution concentration. As indicated earlier, the rock samples used for the lab experiments were taken from the same stratigraphic interval at different site locations (sites 11A and 41B). The total calcium extracted by 100 mmol Na-EDTA shows that the average total calcium released from rock samples from borehole 41B contains nearly three times the calcium compared to that de

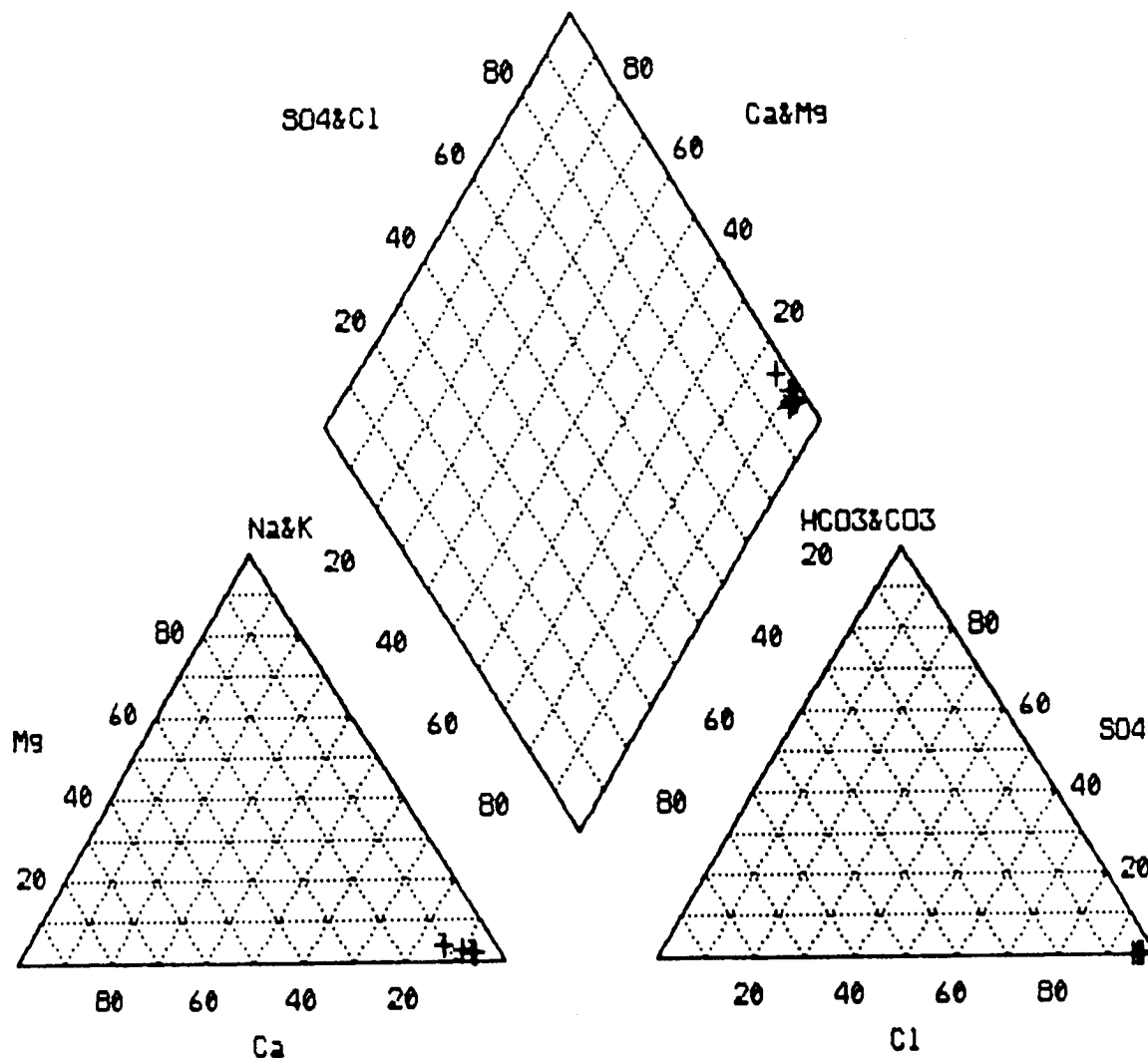


Figure 47. Chemical analyses from piezometer 41A shown on a Piper diagram.

terminated from the samples from 11A (mean = 90.6 mg/L calcium for 41B; 34.3 mg/L for 11A). Explanations for this discrepancy are (1) the clay mineralogy varies laterally from site to site, or (2) more of the exchange sites for the 41B samples have been loaded with divalent cations (principally calcium) by ground water containing higher calcium concentrations, which would be consistent with the hypothesis presented here and the observed trend shown in Figure 55. The increase in calcium from ground water moving along the flow path from the ridge area toward 41B would provide the "excess" calcium and is consistent with this analysis. This relationship suggests that barium is released from exchange sites by competition from calcium, and perhaps magnesium, and is somewhat independent of sodium concentration if the assumption is made that the total CEC for the rock samples from both sites is approximately the same. The mineral that hosts the exchange reactions within the ridge interior would have a higher percent of exchange sites containing monovalent cations, which would be available for exchange for divalent cations. This can explain why low concentrations of divalent cations are found in ground water derived from the ridge

interior. If the above scenario is accurate, ultimately the continuous loading of divalent cations on the clay mineral exchange sites in the ridge interior may reach the point when barium and other divalent cation concentration could increase in the ground water when the CEC is exceeded because of the continuous movement of calcium-loaded water into the area. Exchange experiments with a calcium-chloride solution may provide additional insight into this mechanism. Unfortunately, most of the rock samples were consumed in the original experiments.

Additional evidence for this control on the occurrence of barium in ground water is the water chemistry data for piezometer 12A. Barium concentrations for the first few months of sampling were below 1.0 mg/L. However, barium concentration increased during the study period and exceeded 1.0 mg/L in October of 1991. This trend continued, with a maximum barium concentration of 1.29 mg/L observed in December of 1991. Figure 56 show the trends in several constituents related to the controls on barium concentration found in piezometer 12A. It can be seen that the pe level drops signifi-

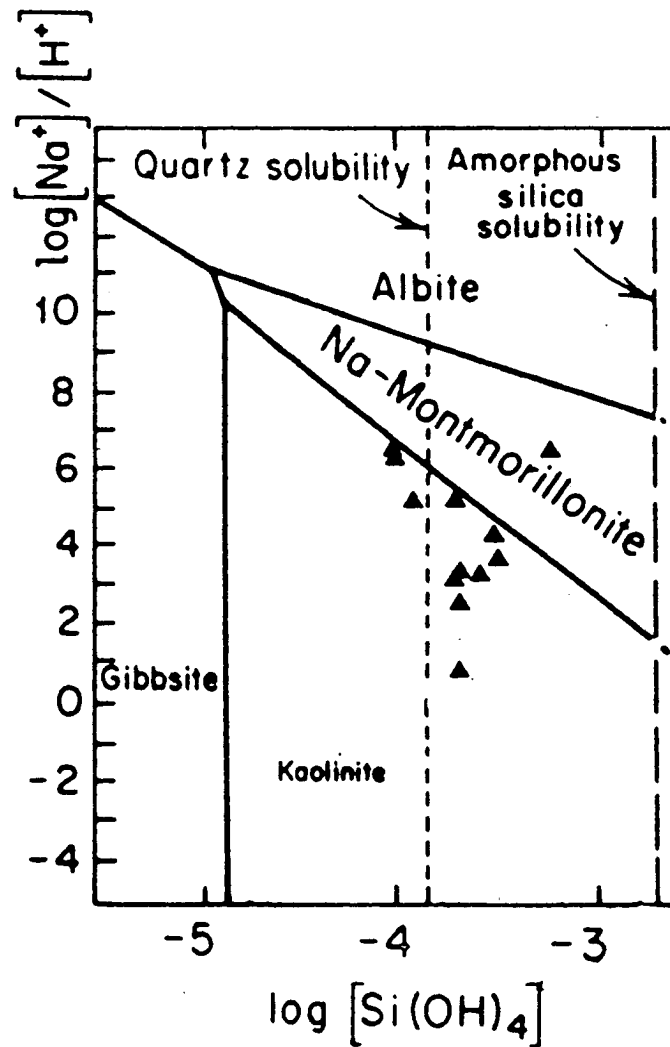


Figure 48. Water samples from each piezometer plotted on the stability fields of albite, gibbsite, sodium-montmorillonite, and kaolinite at 25°C and 1 atmosphere (stability diagram modified from Powell and Larson, 1985).

cantly during the period, which corresponds to a drop in sulfate content. Sulfate content decreases approximately fivefold from a high of 51.0 mg/L at the beginning of sampling to a low of 10.9 mg/L approximately a year later. The decrease in sulfate can be attributed to sulfate reduction by sulfur-reducing bacteria. The presence of hydrogen sulfide was noted in the purge water from 12A as the sampling schedule progressed. Also, the bicarbonate concentration increased throughout the period from 428 to 581 mg/L, which may be attributed to sulfate reduction (eqn. 6).

Piezometer 12A is the deepest piezometer that monitors a fracture zone and is at an elevation that is well above drainage. Although sulfur-reducing bacteria may not have been present initially (i.e., no H_2S odor detected, high sulfate), they may have been introduced by contaminated sampling equipment. Although sulfur-reducing bacteria from wells near valley bottoms were found to be hallophylic (Wunsch, 1988b), these bacteria are known to adapt to variations in salt content very rapidly (Alexander, 1977), and could prob-

ably establish themselves in the above-drainage environment.

The divalent cation exchange mechanism presented here may also be the cause for the enrichment of barium in eastern Kentucky brines (Heck, 1940). Brines found in the Appalachian Basin usually contain appreciable calcium (McGrain, 1953), which could exchange for barium. In addition, high chloride concentrations have an increased solubility effect on barite (Collins, 1975). The long residence time that is usually assigned to brines found in cratonic layered sedimentary rocks (Freeze and Cherry, 1979) would provide for the brine solutions to reach equilibrium with the exchangeable sites on minerals in the host rocks. The low redox conditions characteristic of old connate waters (i.e., brines) is also conducive to the activity of sulfur-reducing bacteria, which keep sulfate concentrations low (Heck, 1940) and allow for elevated barium concentrations to exist.

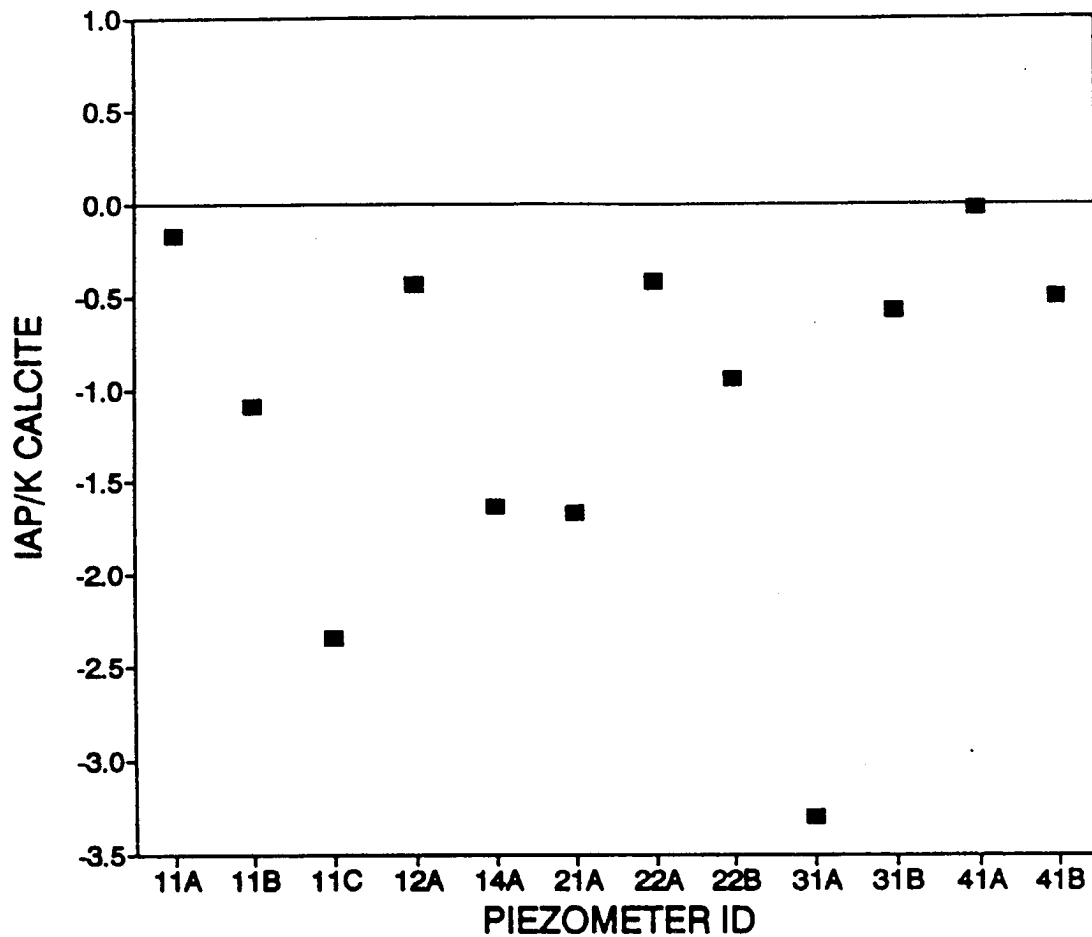


Figure 49. Saturation indices for calcite for all piezometers. Chemical data are from July 1991.

Reaction-Path Modeling Using Geochemical Models

Geochemical modeling can provide supporting evidence for the validation of the proposed reactions used to explain the chemical evolution of ground water at the site. In this study the model BALANCE was used to determine the state of solid phases (either dissolving or precipitating) in order to satisfy the mass transfer of dissolved constituents from one end member solution to another. Calibration of the model can be made by comparing the predicted state of each mineral phase used in the mass transfer model with the saturation index calculated by the equilibrium model (PHREEQE). This method does not allow for a unique solution to each reaction problem (Parkhurst and others, 1982), but it does demonstrate supporting arguments for conceptualization of groundwater evolution. Several researchers using this modeling approach also incorporated isotopic analyses of constituents into their models, which allowed them to make semi-quantitative judgements on which a particular mineral was the major contributor to the occurrence of a particular ion in solution (Powell and Larson, 1985; Wood and Low, 1988; Robertson, 1991). For example, carbon-13 determinations can be useful in determining if the source of carbon in ground water is derived from organic carbon or the dissolution of carbonates with a specific isotopic signature (Powell and Larson, 1985).

The data included in this study are limited in this respect; therefore, only supporting evidence for the plausible mineral-water reactions discussed previously can be given.

It has been proposed that ground water entering the ridge as recharge from precipitation events can travel by several paths before discharging in the area near Lick Branch in the valley bottom. Only one flow path, however, can be predicted with a degree of certainty that precludes any likely effects from ground-water mixing. This flow path is designated as precipitation entering the ground-water system at the ridge top and migrating vertically into the center or interior area of the ridge. After ground water accumulates in this area, the head gradient indicates that the ground water will move laterally toward the discharge area. Mixing is most likely to occur in these areas where recharge in the shallow fracture zone and coal seams migrates downward and mixes with ground water flowing from the ridge interior toward the valley bottom or discharges on the surface as springs and seeps.

Geochemical modeling is used to test the validity of the sets of plausible water/mineral reactions proposed in this study as controls on the ground-water geochemistry. The flow path chosen to model is one where ground water is moving vertically from the ridge top to the interior down a path parallel to borehole 11, which contains piezometers 11C, 11B, and 11A.

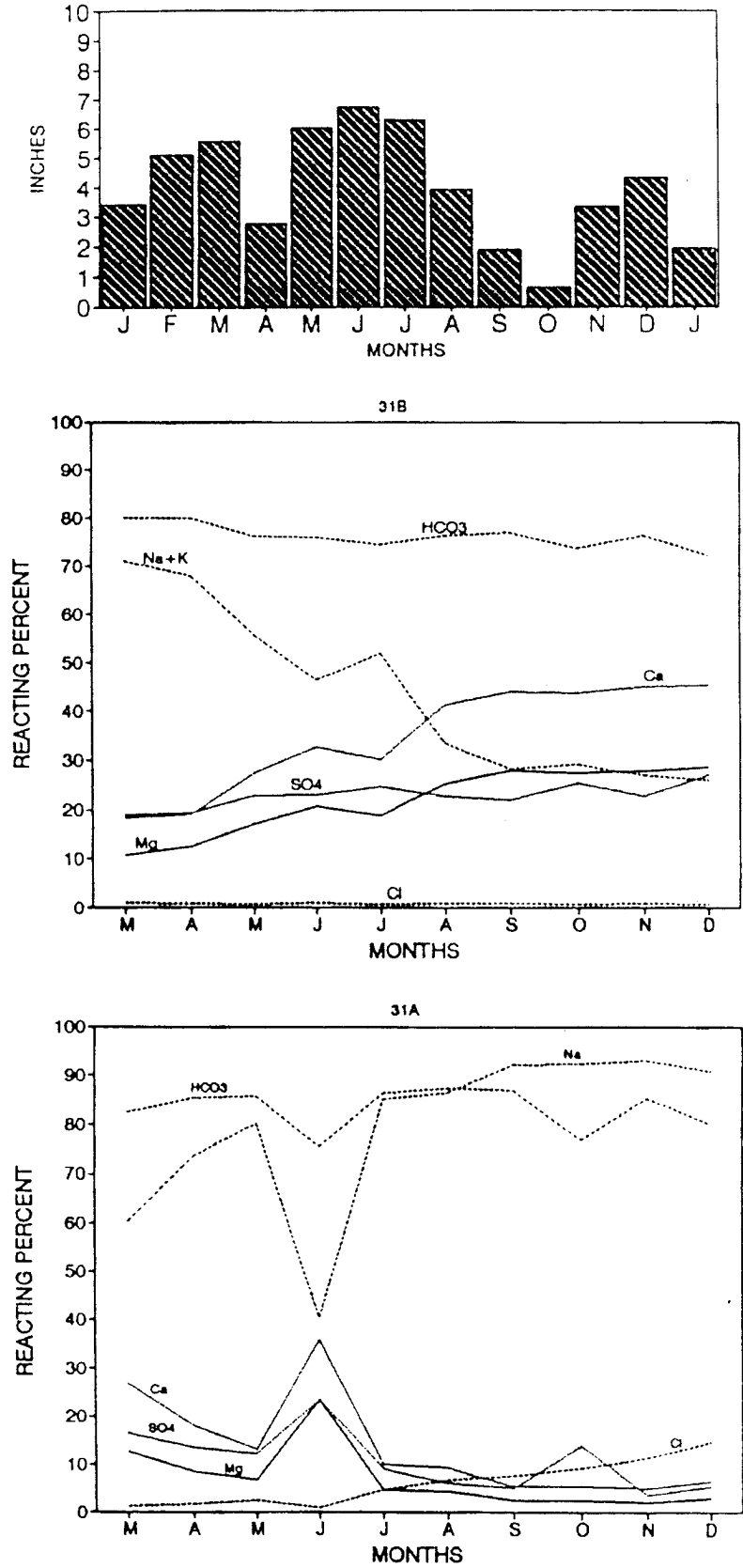


Figure 50. Profile of changes in select chemical parameters in piezometers 31A and 31B.

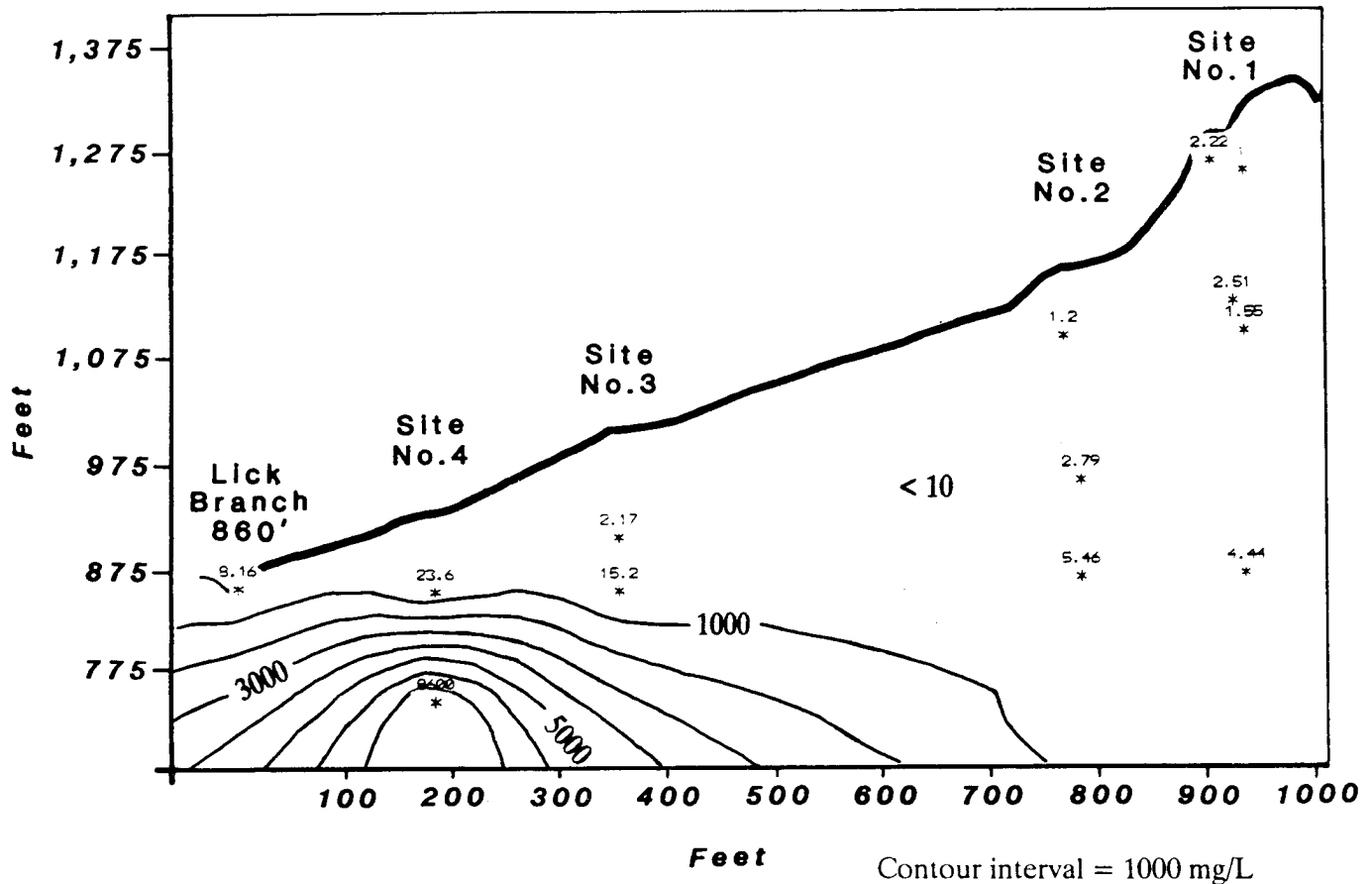


Figure 51. Contoured profile of chloride data.

These piezometers are chosen for the following reasons: (1) Piezometer 11C is directly above 11A. Assuming a vertical flow path, the water at the level of 11C would be expected to migrate to the level of 11A. (2) Piezometer 11C is screened to a shallow depth (50 feet) at the ridge top. With few exceptions, the piezometers set in the coal seams and those in the shallow fracture zones were similar in their major dissolved ion chemistry, as 11A is to the other piezometers screened into the ridge interior. The reaction paths modeled here are shown on Figure 57.

The first step of the model is to simulate the reactions encountered by precipitation as it travels through the shallow soil zone, moves through the bedrock byway of fractures and coal, and arrives at the position of piezometer 11C. The second step is the simulation of ground-water/mineral reactions as ground water migrates downward from 11C to the position of piezometer 11A (refer to Fig. 57).

The input solution is rain water, using chemical analyses from samples collected at the University of Kentucky Robinson Forest research station (Coltharp and Brooks, 1991). The mean values for constituents contained in precipitation that fell in July 1991 are used in the simulation. Chemical data for ground water are from water samples collected during July 1991.

In the first simulation, BALANCE is used to calculate the mass transfer between the incident precipitation reacting with minerals and the final water in this step, which is the water found in piezometer 11C. The assemblage of minerals and gases used were those that seem to be the most plausible based on the mineralogy contained in the rocks (Weinheimer, 1982). Calcite is assumed to be the main source of calcium and bicarbonate. Magnesium is derived from chlorite. Iron and sulfate can form from the dissolution of siderite and the oxidation of pyrite. Potassium may be derived from potassium feldspar (K-spar). Ion exchange is used to supply sodium by exchanging for calcium. Carbon dioxide gas is included because it is assumed that the system is enriched in CO_2 due to its accumulation in the soil zone from the decay of organic material (Freeze and Cherry, 1979). The data used in the models, as well as a summary of the computer output, are contained in Appendix 7.

Simulation 1 mass-balance calculations show that calcite, chlorite, pyrite, and CO_2 gas dissolve, and the ion exchange reaction where calcium is removed and sodium is released is proceeding to the right (each denoted by a positive value), but siderite is precipitating (indicated by a negative value). The reader should note that the sign convention used by BALANCE is opposite that which suggests precipitation (supersaturation) by PHREEQE. This output is inconsistent with

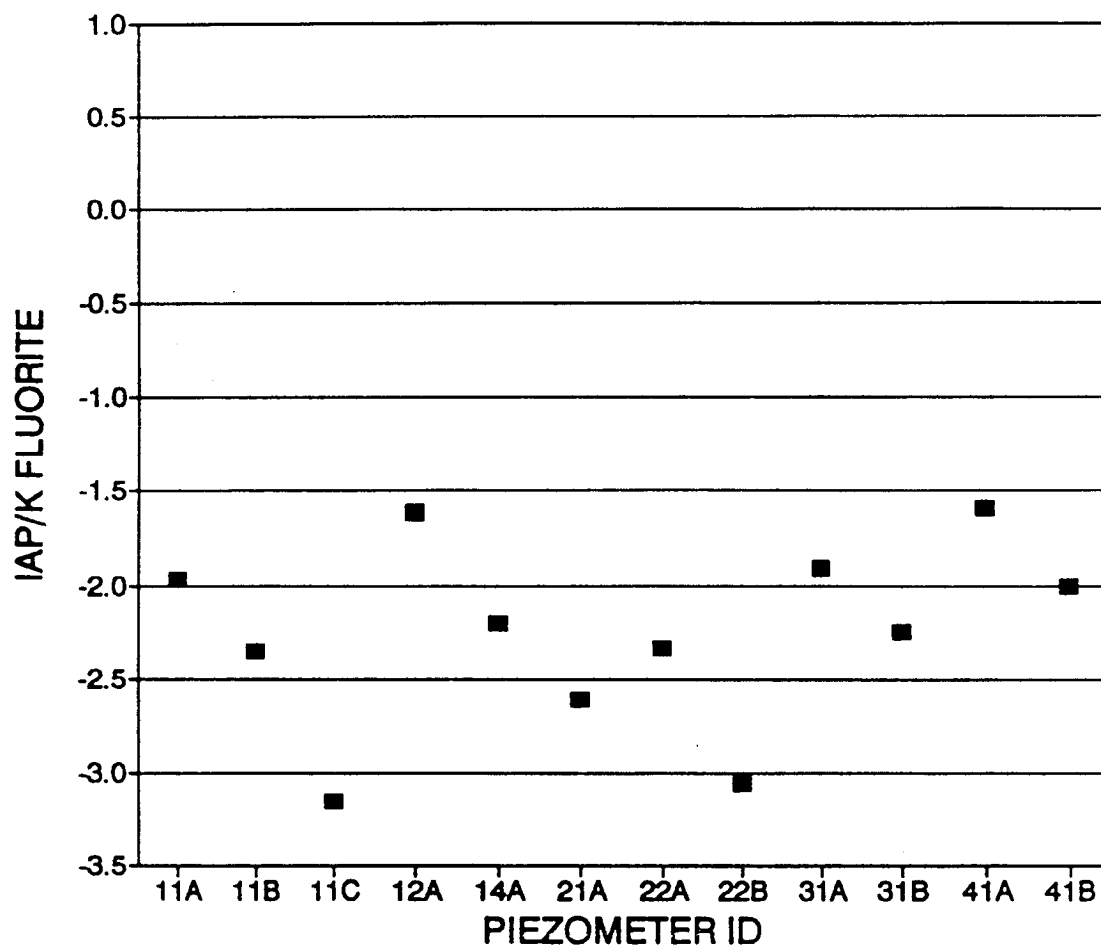


Figure 52. Saturation indices for fluorite for all piezometers. Chemical data are from July 1991.

the mineral saturation data calculated using PHREEQE, which indicates that the water in 11 C is undersaturated with siderite. Because of the oxidizing conditions of ground water near the surface, and the relatively high Eh values recorded in 11C (mean = 190 mV), iron is most likely in the ferrous state, which would result in the formation of an iron hydroxide mineral. Therefore, goethite (FeOOH) is substituted in place of siderite in simulation 2. These results are consistent with the mineral saturation data, which show that the reactions between ground water and mineral phases listed above are plausible in the evolution of water as it enters the ground as precipitation and migrates to the level of piezometer 11C. The positive delta values for the dissolved constituents used in the simulation indicate an increase in the concentration of each ion species listed.

The second modeling step consisted of calculating the mass balance resulting from the migration of the water from step I (11C) and the final water, which is the water found in 11A. The phases considered in this step are calcite, goethite, ion exchange (controlling calcium, barium, magnesium, and fluoride), siderite, goethite, iron sulfide, pyrite, hydrogen sulfide, and kaolinite. In order to maintain the input values within the operational constraints of BALANCE (number of input species = number of output phases), some phases must be dropped from consideration or substitutions made. Carbon

dioxide gas is not included in this step because it is assumed that (1) its concentration will decrease as the water moves from the soil zone, (2) the deeper ground-water zone may be a closed system to CO₂, and (3) CO₂ is consumed in reactions along the flow path.

Simulation 3 shows that calcite and siderite dissolve, whereas goethite, pyrite, and kaolinite precipitate (Appendix 7). This simulation is inconsistent with the saturation indices data, which indicate that 11A is vastly undersaturated with pyrite. Simulation 4 substitutes iron sulfide (FeS) for pyrite. The assumption here is that iron may combine with hydrogen sulfide resulting from sulfate reduction. The results for simulation 4 are in agreement with the saturation indices calculated for each mineral, with the exception of the removal of iron (as indicated by the precipitation of FeS as shown by BALANCE). The PHREEQE data show that 11A is undersaturated with FeS. Two explanations may account for the lack of mass balance for iron. By one account, the dissolution of ferroan calcite would increase the iron concentration in 11A without requiring the oxidation of an iron-sulfide mineral. Because of the lower Eh, and the assumed lack of oxygen in the deep interior area of the ridge, the oxidation of pyrite may be limited. Ferroan calcite is the dominant cementing agent and is common in Breathitt rocks (Weinheimer, 1982). The saturation index for calcite predicts that calcite (and probably fer-

Table 7.-Pearson Correlation Coefficients Calculated for Selected Constituents from all Piezometers Using July 1991 Data. Significance Level Indicates the Probability of a Correlation Relationship Occurring by Chance is Less than the Value Given.

Pearson Correlation Coefficients

	pH	mV	Ca	Mg	Na	Ba	Cl	F	SO4
pH	1.0000	0.1224	-0.2285	-0.4737	0.0194	-0.0289	-0.0217	0.9109	-0.1059
	(12)	(12)	(12)	(12)	(12)	(12)	(12)	(12)	(12)
	0.0000	0.7047	0.4750	0.1198	0.9522	0.9289	0.9466	0.0000	0.7432
mV	0.1224	1.0000	-0.6619	-0.5186	-0.6043	-0.6394	-0.6169	0.1983	0.2688
	(12)	(12)	(12)	(12)	(12)	(12)	(12)	(12)	(12)
	0.7047	0.0000	0.0190	0.0841	0.0374	0.0252	0.0326	0.5366	0.3981
Ca	-0.2285	-0.6619	1.0000	0.8915	0.9297	0.9497	0.9432	-0.2521	-0.1929
	(12)	(12)	(12)	(12)	(12)	(12)	(12)	(12)	(12)
	0.4750	0.0190	0.0000	0.0001	0.0000	0.0000	0.0000	0.4292	0.5481
Mg	-0.4737	-0.5186	0.8915	1.0000	0.7130	0.7451	0.7399	-0.3882	-0.1002
	(12)	(12)	(12)	(12)	(12)	(12)	(12)	(12)	(12)
	0.1198	0.0841	0.0001	0.0000	0.0092	0.0054	0.0059	0.2123	0.7567
Na	0.0194	-0.6043	0.9297	0.7130	1.0000	0.9969	0.9984	-0.0460	-0.1509
	(12)	(12)	(12)	(12)	(12)	(12)	(12)	(12)	(12)
	0.9522	0.0374	0.0000	0.0092	0.0000	0.0000	0.0000	0.8871	0.6396
Ba	-0.0289	-0.6394	0.9497	0.7451	0.9969	1.0000	0.9991	-0.0808	-0.1919
	(12)	(12)	(12)	(12)	(12)	(12)	(12)	(12)	(12)
	0.9289	0.0252	0.0000	0.0054	0.0000	0.0000	0.0000	0.8028	0.5502
Cl	-0.0217	-0.6169	0.9432	0.7399	0.9984	0.9991	1.0000	-0.0722	-0.1815
	(12)	(12)	(12)	(12)	(12)	(12)	(12)	(12)	(12)
	0.9466	0.0326	0.0000	0.0059	0.0000	0.0000	0.0000	0.8235	0.5724
F	0.9109	0.1983	-0.2521	-0.3882	-0.0460	-0.0808	-0.0722	1.0000	-0.2969
	(12)	(12)	(12)	(12)	(12)	(12)	(12)	(12)	(12)
	0.0000	0.5366	0.4292	0.2123	0.8871	0.8028	0.8235	0.0000	0.3487
SO4	-0.1059	0.2688	-0.1929	-0.1002	-0.1509	-0.1919	-0.1815	-0.2969	1.0000
	(12)	(12)	(12)	(12)	(12)	(12)	(12)	(12)	(12)
	0.7432	0.3981	0.5481	0.7567	0.6396	0.5502	0.5724	0.3487	0.0000

Coefficient
(Sample Size)
Significance Level

roan calcite) will dissolve in 11A, which would liberate iron and provide for the mass balance. Another possibility is simply analytical error. The difference in iron concentration between the initial (11C) and final solutions (11A) is only .007 millimole (0.41 mg/L Fe).

The positive delta phases for calcite and siderite indicate these phases dissolve. Negative delta values for goethite and kaolinite indicate these phases would precipitate. These predictions are consistent with petrographic analysis that shows authigenic kaolinite and iron-hydroxide coatings com-

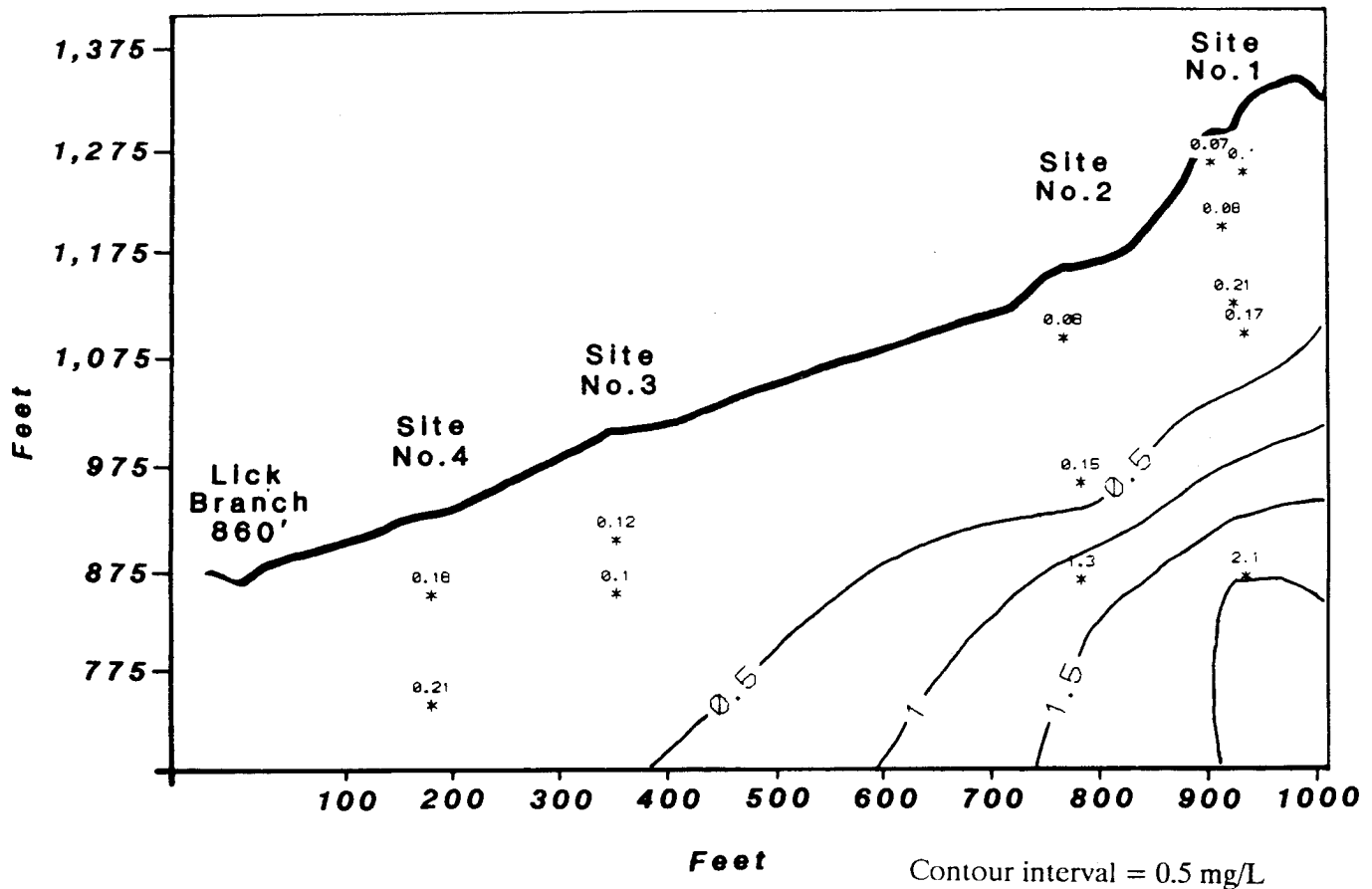


Figure 53. Contoured profile of fluoride data.

mon in Breathitt Formation rocks (Wienheimer, 1982). Positive delta values for ion exchange for the divalent cations reveal that these cations are removed from solution and sodium is released. A negative value for the ion exchange (reaction proceeds opposite to the way presented in the model simulation) for fluoride is consistent with fluoride being released into solution. Examination of the delta phases for the dissolved species from simulation 4 shows that all of the species except sodium, carbon (bicarbonate), and fluoride have negative delta values. This indicates that as the water moves along the flow path from piezometer 11C to 11A, the sodium, bicarbonate, and fluoride increase in concentration, resulting in the generation of a Na-HCO₃-type water with a high fluoride content. The findings of this modeling step are consistent with the trends in water chemistry observed in piezometers that monitor the ridge interior.

There are probably other mineral phase combinations that could produce results that are consistent with the trends found along the flow path modeled here. Still, these results indicate that the controlling geochemical reactions presented in this study represent a plausible explanation for the geochemical evolution of ground water as it flows through coal-bearing rocks in this hydrogeologic setting.

A binary mixing model using the water chemistry from piezometers 11A and 31B was used to model the mixing that would occur as water moves from the ridge interior toward the valley bottom, where it would mix with ground water stored in the shallow fracture zone. The modeling results (Appendix 7) show that a mixing ratio of 71.15 percent of water from 11A and 28.85 percent of water from 31B would create a mixture that most closely resembles the relative percent of major ions found in the water from 31A. The largest error (-77.15 percent) in the calculation occurred in the chloride content (see Appendix 7). It should be noted that chloride concentrations in these samples are very low (less than 5 mg/L), so a small variation in the concentrations results in a large percentage of error. Neither of the two end members contained sufficient chloride to account for the chloride concentration found in 31A. The higher chloride in this piezometer indicates additional mixing with other ground water containing a higher chloride content. The increase in chloride occurred as monthly sampling proceeded throughout the year, indicating that pumping of the piezometer for purging and sampling purposes may have induced the migration of water containing higher chloride. Brines are frequently found within 200 feet of the surface in eastern Kentucky (Sprinkle and oth-

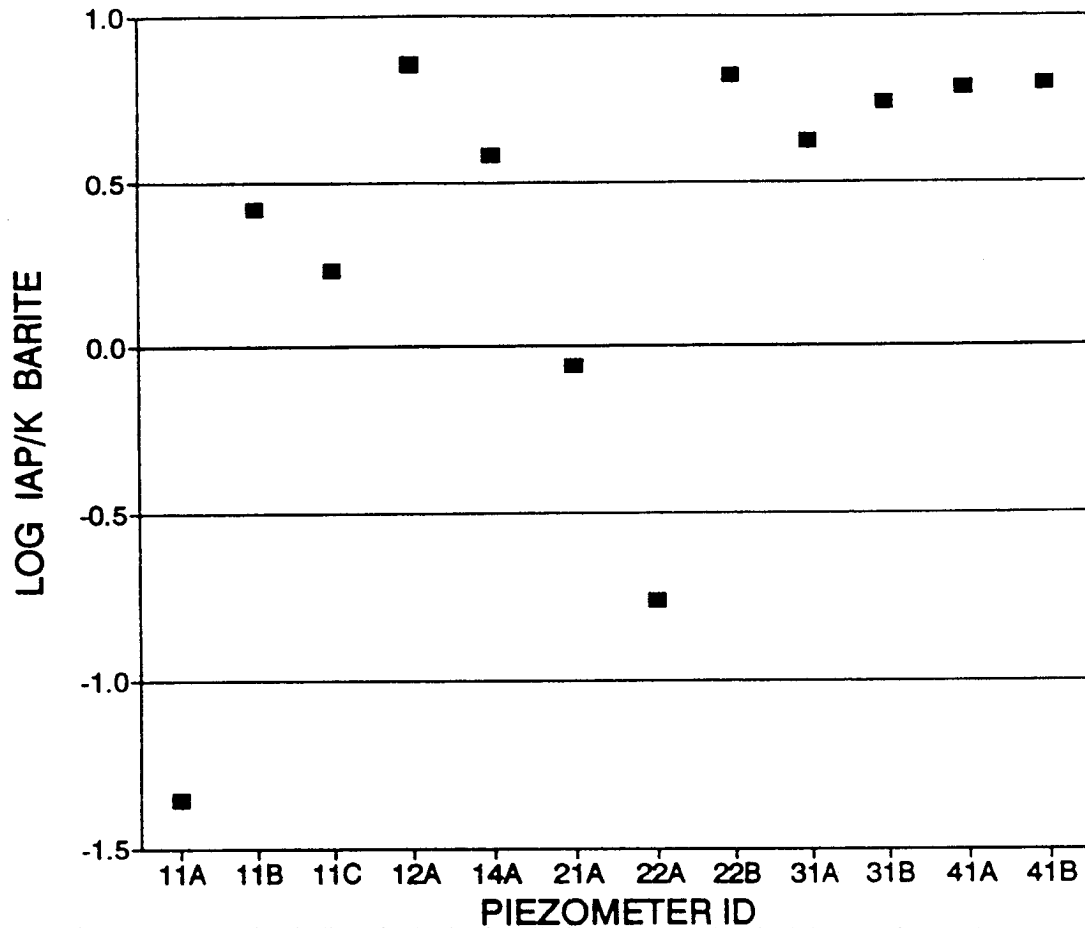


Figure 54. Saturation indices for barite for all piezometers. Chemical data are from July 1991.

ers, 1983). Brine is encountered in the study area in piezometer 41A, which is located approximately 550 feet southwest and 100 feet below 31A. The mixing zone between the brine and fresh water is not well defined in eastern Kentucky (Sprinkle and others, 1983) or at this site; therefore, pumping may draw in water containing sufficient chloride concentrations if the radius of influence induced by pumping causes migration of higher chloride water from the salt-water interface zone.

Therefore, hydrochemical trends observed in piezometer 31A can be explained by the location of this piezometer in the recharge zone where ground-water mixing or the intrusion of ground water with a different chemical signature takes place because of changes in the local flow field, which result from variation in the influx of recharge from the surface and/or changes imparted by well development and pumping.

Conceptual Model for Hydrochemical Facies

Hydrochemical facies are distinct zones that have cation and anion concentrations describable within defined composition categories (Freeze and Cherry, 1979). The data presented in this study show that the piezometers that are screened into discrete water-producing zones exhibit consistent, discernible water types that can be related to the flow system, the position of the piezometer within the ridge, and to

the elevation with respect to the adjacent major drainage stream. These observations, in conjunction with hydraulic, isotopic, and chemical data, allow for the following conceptual model to be presented, which shows areas within the ridge where the hydrochemical facies may be predicted with a reasonable amount of confidence.

Description of Hydrochemical Model Fields

Figure 58 shows the outline of the ridge with shaded fields that represent a particular hydrochemical facies. Each facies zone represents an area where a characteristic set of water types is observed and a plausible explanation can be made for its occurrence. As presented here, these facies fields represent areas where the probability is high that a combination of the cations or anions listed for that field will define the water type for a sample derived from a location within the field.

The lines separating the zones are not to be interpreted as definite or absolute boundaries. Most likely the boundaries are somewhat gradational, but may be locally abrupt where the boundary between fields coincides with a low or high permeability zone (e.g., the underclay beneath a coal or a highly fractured area). Coal seams have been shown to impart a pronounced effect on the occurrence and movement of ground water in this study area. The position of coal seams within the stratigraphic sequence of a ridge may act to expand or compress facies zones.

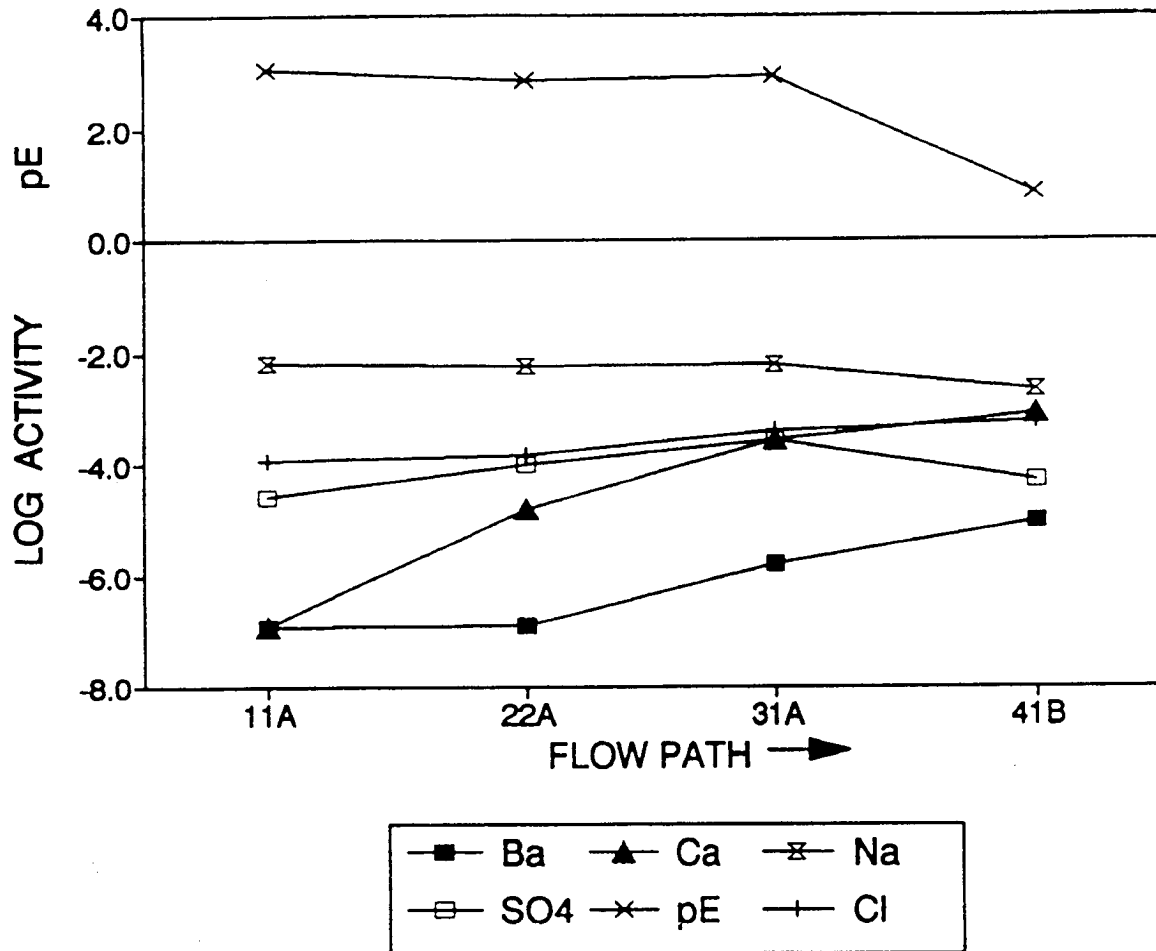


Figure 55. Trends in the activities of selected parameters along the flow path from piezometer 11A to 41 B.

The Ca+Mg, HCO_3+SO_4 facies; zone represents the area adjacent to the near-surface area of the ridge, and corresponds closely to the area where a fracture zone is most likely to occur (Wyrick and Borchers, 1983; Kipp and Dinger, 1987). In this zone, the oxidation of pyrite and the dissolution of calcite in an oxidizing environment impart the greatest influence on the chemical character of ground water. The Na, HCO_3+SO_4 zone represents the area where the dissolution of calcite, cation exchange of sodium for divalent cations, and possibly sulfate reduction control the occurrence of the major ions. The Na, Cl zone represents old, connate water that may consist of very concentrated brines (McGrain, 1953). The Na+Ca, $\text{HCO}_3+\text{SO}_4+\text{Cl}$ area represents a zone consisting of water formed when ground water from the Na, HCO_3+SO_4 zone moved from the ridge interior and mixed with water from the Ca+Mg, HCO_3+SO_4 shallow zone as water from both zones flowed toward the discharge area. Additionally, an increase in the chloride component results when additional mixing occurs with Na, Cl water near the valley bottom. Therefore, any water derived from this zone will be a water type defined by varying percentages of Na, Ca, HCO_3 , SO_4 , and Cl. A decrease in sulfate content due to sulfate reduction may be observed as the water approaches the discharge area in the valley bottom.

The Na, Cl zone is shown to be at its most shallow point beneath the valley bottom. This interpretation is based on the chloride data, and is consistent with the observations of others (Price, 1962; Sprinkle and others, 1983). Conceptual flow models for similar settings to this study site have been presented by Wyrick and Borchers (1981), Kipp and Dinger (1987), and Harlow and LeCain (1991), and each suggested that a high occurrence of fractures exists in the valley bottoms. These fractures may provide pathways for the migration of salt water to shallow depths.

Probably the most probing question not answered by this study is the exact location of the salt-water interface below the interior of the ridge. Funding and technological limitations precluded the drilling of a piezometer deep into the ridge interior that may have resolved this question. In Figure 58, the boundary of the Na, Cl zone is shown as being depressed under the ridge interior, with a question mark denoting this uncertainty. This interpretation is based on the chloride data, which shows high chloride values tend to be found in water samples taken from piezometers at or near the valley bottom. Very low chloride content is found in water samples derived from beneath the ridge at the same stratigraphic level. Also, the potentiometric head measurements from within the ridge

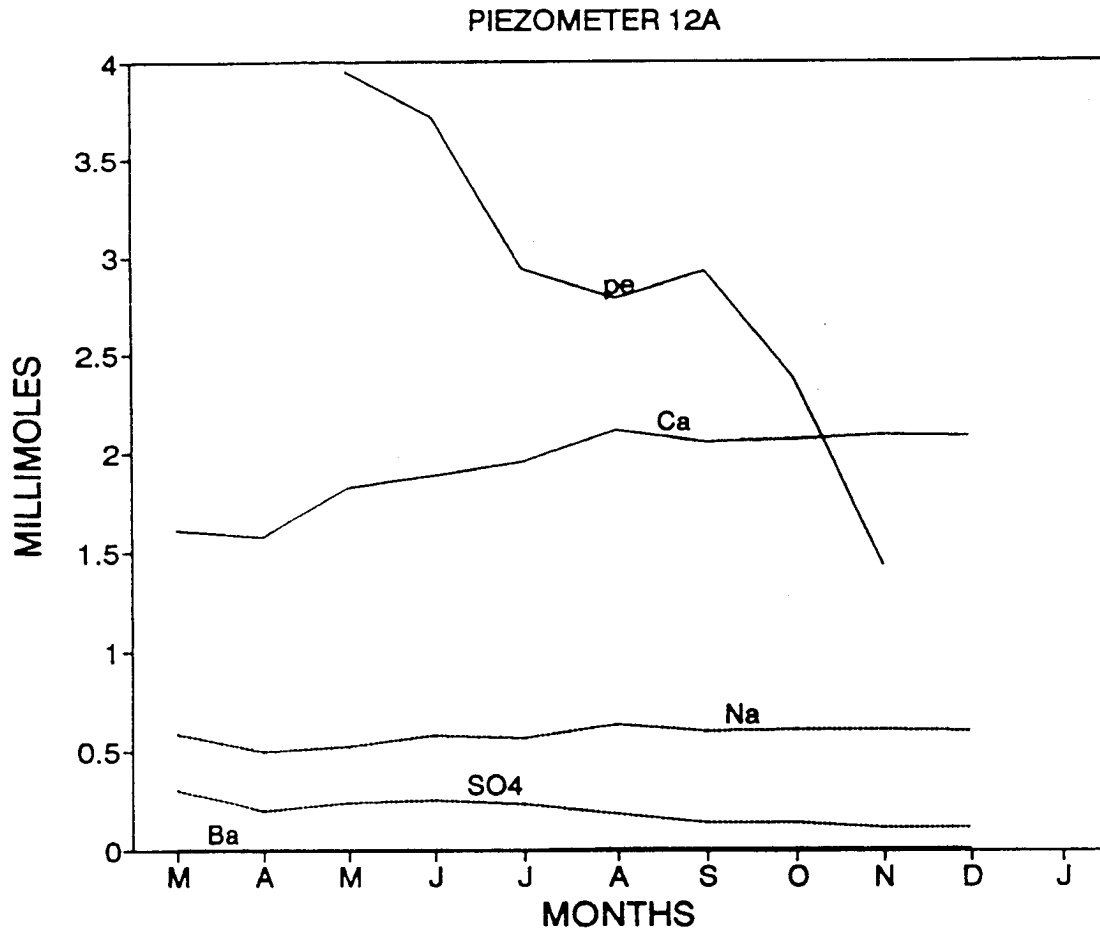


Figure 56. Temporal changes in the concentrations of selected parameters in piezometer 12A.

indicate that higher pressure heads are measured in the ridge at the same elevation (stratigraphic interval) as piezometers near the valley bottom. The higher head imparted by the fresh ground water in this area should act to depress or displace the supposed underlying saline water. Osmotic effects may also contribute to the pressure differential in this area (Freeze and Cherry, 1979). Most likely there may exist a layer or sequence of geologic stratum that may act as an aquitard to the downward movement of fresh water, or the upward movement of saline water in this area of the ridge. In this case, the saline interface may not be depressed significantly and may be encountered rather abruptly. However, if this were the case, it would be expected that over geologic time chemical diffusion would result in the occurrence of chloride content greater than the 5 mg/L or less typically found in the piezometers located in the interior area of the ridge near the assumed salt-water interface. If the actual relationship between the saline interface under the ridge presented here is accurate, it would suggest that the saline interface throughout eastern Kentucky would occur as an undulatory surface where the depressions in the interface surface would be an inverse approximation of the surface topography or potentiometric surface.

The pressure imparted upon the saline water "aquifer" by the fresh water accumulating beneath ridges would be transferred in the salt-water aquifer, causing the migration of salt water away from the high-pressure area located in the ridge interiors toward areas of lower pressure (valley bottoms). These mechanisms may provide the hydraulic pressure that drives the brines upward (relative to other areas of the brine flow system), where breaches in the rock layers that confine the salt water (presumably the highly fractured valley bottoms) exist. Further study is needed to verify these relationships.

The conceptual model described here was created using the site-specific conditions detailed in this study. The hydrochemical facies relationships represent a ridge in the Eastern Kentucky Coal Field that has not been affected by man's activities to any significant extent. In addition, this site is bordered by third- and fourth-order streams, and it is widely held that a shallow salt-water interface exists below drainages with these ranks. The salt-water interface has not been well defined in areas below streams of a lower order or intermittent streams; therefore, this model, especially in reference to the occurrence of, and the geochemical effects imparted

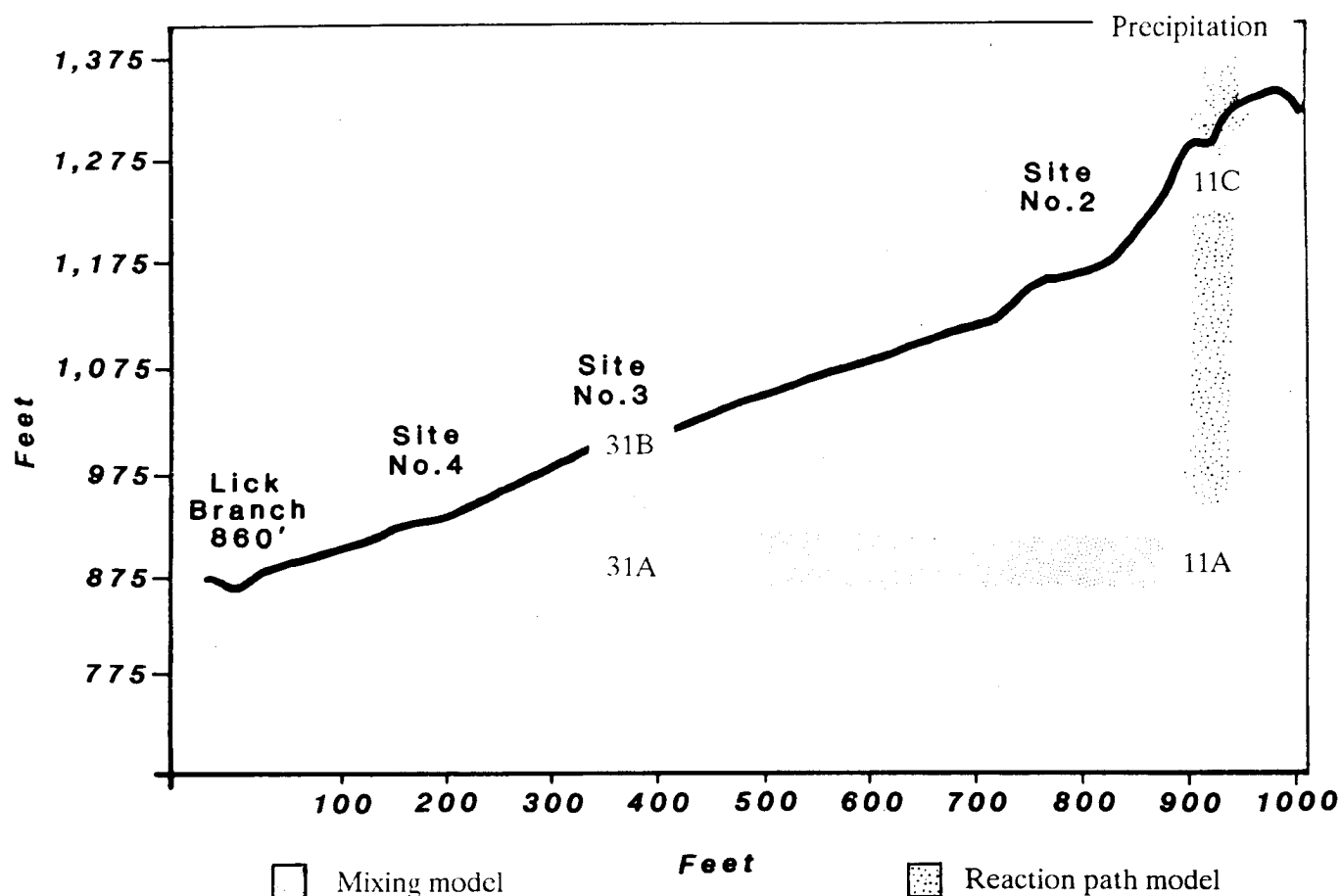


Figure 57. Reaction path of ground water modeled using PHREEQUE and BALANCE, and mixing model HC-GRAM.

by, the salt-water zone may not apply to other areas in eastern Kentucky. Also, the effects of geology, such as the stratigraphic location of highly conductive coal seams and the extent of subsurface fractures in a particular area, must be accounted for when using this model. Their presence or absence in a stratigraphic sequence may act to expand or compress the geochemical facies zones shown in this model. However, it is expected that this model will be applicable to many areas in the maturely dissected Appalachian Plateau that allow for these considerations.

CONCLUSIONS

Eight boreholes and one geologic core were drilled at various locations at the study site. Examination and description of the core, along with packer-injection tests and downhole camera observations of the boreholes indicate that the majority of ground water moving at shallow depths (generally less than 200 feet) is occurring in fracture systems and coal seams. The deepest water-producing fracture observed in this study was at 167 feet. These observations are consistent with the conceptual models that describe ground-water flow in the region. Coal seams were the lithologic units with the highest hydraulic conductivities and probably act to dewater rocks that lie above that are in hydraulic connection.

Fourteen of the total of sixteen piezometers that monitored the study site contained measurable water throughout the course of this study. Piezometers that remained dry (13B and 21A) were restricted to the upper area of the ridge, indicating that the rocks in the ridge-top area are not continuously saturated. Piezometers screened into shallow fractures and coals near ground surface exhibited the most rapid response to recharge events or periods of low precipitation. The amount of water-level fluctuation, which correlated to precipitation events, decreased with depth below the surface. This is attributed to the increased storage volume available in the rock mass with depth below the surface, which tends to buffer the rapid influx of recharge, and to the decrease in the occurrence of fractures that transmit water. Piezometers deep within the ridge contained the greatest amounts of water, and these conditions were maintained throughout the year, indicating the rocks in the core interior were saturated.

All piezometers at the site showed a decline in water level during most of the year, but most began to rebound toward the end of the study period (winter), which correlates with the return of long-term precipitation events.

Potentiometric head measurements from all piezometers at the site indicate a downward vertical gradient exists within the ridge. Although temporal fluctuation in water levels was

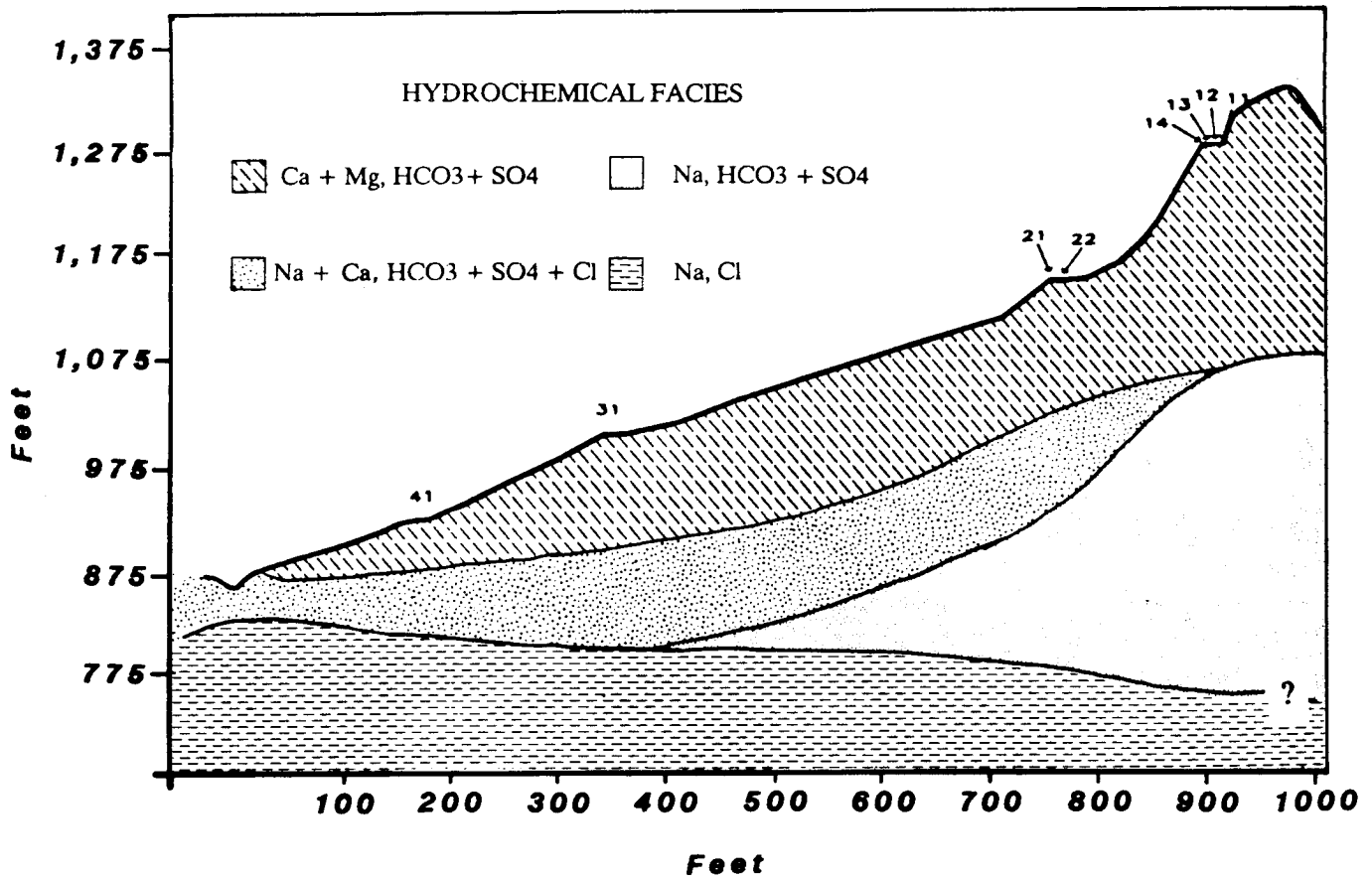


Figure 58. Conceptualized model of hydrochemical-facies zones present in the unmined ridge. Hydrochemical-facies zones indicate areas where there is a high probability that water present will have water type consisting of a combination of the ions listed for that zone.

observed in all piezometers, contoured profiles of the head data from periods when the maximum and minimum water levels were recorded showed that no significant change occurs in the flow field during the year. Water accumulates in the base of the ridge, which would form a piezometric surface that approximates the topography. Head measurements in piezometers screened at the same stratigraphic interval throughout the base of the ridge indicate ground water flows from the ridge interior toward the southwest at a gradient of 0.037.

Identification of recharge areas based on tritium data collected at the site revealed that the ground water in the crest of the ridge contained the highest tritium content, which is interpreted as having the youngest age. The oldest water, based on tritium deficiency, was found in the ridge interior and in brines in the discharge area below the elevation of the major drainage. A contoured profile of the tritium data for the site indicates a deep penetration of relatively younger water along the hillside of the ridge where the slope decreases. This area is directly below the portion of the ridge where the rocks are suspected of being de-watered by fractures and coal seams.

A conceptual model of ground-water flow at the site shows that the coals may create a "short circuit" effect to the

downward movement of ground water, which may reenter the ground-water system along the hill slope after flowing out of the coal seams as diffuse flow or as hillside springs.

The break in the degree of slope along the midsection of the ridge may result in a decrease in the velocity of surface runoff during storm events, which would allow for greater infiltration into the subsurface. Fractures along the hill slope probably provide the initial mechanism for deep penetration of young recharge water into the subsurface over extended periods of time.

The water chemistry was extremely variable at the site. The pH of water ranged from a low of 5.37 in water derived from a coal seam to a high of 8.92 in the ridge interior.

Coal seams yielded Ca-Mg-HCO₃ water types and typically contained high iron concentrations with an acidic pH. Variation in the amount of total dissolved solids was attributed to dilution from fresh-water influx, especially in piezometers set into shallow coals and fractures.

Piezometers; in fractures mainly yielded Ca-HCO₃ or Mg-SO₄ water types. One piezometer yielded water samples that showed temporal variation, mainly in the amount of calcium and sodium. This variability can be explained by intrusion by ground water associated with major storm events that infiltrated into the subsurface and mixed with the ground water

present in the system. Apparently, the fracture system has a threshold for which an intense precipitation event is necessary to produce an intrusion of fresh water to depth.

The ground water derived from the interior of the ridge was predominantly Na-HCO₃ water type with a high pH; one piezometer contained sulfate as the dominant anion. Ground water deep below the major drainage stream was an Na-Cl type. Sulfate concentrations were low in the deep interior area and in the discharge area near the valley bottom, most likely resulting from sulfate reduction. Na-HCO₃ ground water flowing down gradient from the ridge interior mixes with ground water from the near-surface fracture system (Ca- or Ca-Mg-HCO₃), which results in an increase in the calcium and magnesium concentrations along the flow path. Chloride content also increases, resulting from the gradual influence of Na-Cl brines that are nearest the surface in the valley bottoms.

Reaction path chemical modeling using the PHREEQE and BALANCE computer codes produced results that were consistent with the observed trends at the site. The chemical evolution of ground water begins with recharge entering the system as precipitation and reacting with minerals in the shallow subsurface or in fractured bedrock. The solution of calcite, the oxidation of pyrite, and the chemical weathering of chlorite, feldspars, and siderite probably exert the greatest influence on major ion chemistry in the shallow zone. Cation exchange coupled with sulfate reduction act to further alter the chemistry of the ground water as it moves downward into the interior of the ridge. Cation exchange reactions where sodium is exchanged for the more preferred divalent cations (Ca²⁺, Mg²⁺, and Ba²⁺) results in a decrease in the concentration of these ions in ground water and the formation of an Na-HCO₃ water type. Clay minerals, mostly as kaolinite, probably act as the host for exchange reactions. Sulfate reduction also occurs when ground water moves to areas where redox conditions are favorable for the activity of sulfur-reducing bacteria. Evidence of sulfate reduction is increased alkalinity, reduced sulfate concentration, and the production of hydrogen sulfide.

The solubility constraint exerted on barium concentrations by barite was not as important as the limiting effect by cation exchange reactions. Piezometers in the ridge interior contained very low concentrations of barium, although concentrations of sulfate were low. Ground water moving from the ridge interior mixes with water from the near-surface fracture zone, which has higher calcium and magnesium concentrations. These cations can compete for exchange sites on clays as the ground water continues along the flow path and comes in contact with rocks that contain barium on exchange sites. Barium is released into solution due to competition for the exchange sites, resulting in increased barium concentrations in the ground water.

The valley bottom/below drainage piezometers near major drainage consistently contained barium in excess of 1.0 mg/L. Barium concentrations as high as 48.6 mg/L were encountered in the piezometer that contained brine. Barite solubility is probably important in controlling the barium concentrations at these higher levels. Low redox conditions in the

valley bottom are conducive to the prolonged activity of sulfur-reducing bacteria, which serve to keep sulfate concentrations low. Sodium chloride ground water also may contribute to sustain high barium concentrations because of its increased solubility effect on barite.

Elevated barium concentrations did occur in a water-producing zone that was above drainage. A drop in the redox conditions, sulfate reduction, and an increase in calcium concentration correlated to the increase in barium concentration, which is consistent with the mechanism for the occurrence of barium in ground water reported here.

The occurrence of elevated fluoride concentrations is restricted to the interior ridge areas that are characterized by an Na-HCO₃ water type with a high pH. Fluoride most likely is released into solution during anion exchange reactions with hydroxyl ions on clay minerals (kaolinite) or goethite. The decrease in fluoride concentrations as the ground water moves away from the ridge interior is probably a result of dilution and/or re-adsorption.

A conceptual model (Fig. 58) can be used to show the likelihood for the occurrence of geochemical facies within the ridge. The model shows four zones where the prediction of the major cations and anions comprising the water type for a particular water sample could be predicted with a high degree of probability. The model shows a depressed salt-water interface below the ridge due to downward movement and accumulation of fresh water. The hydrostatic pressure imparted on the salt water is transmitted in the salt-water zone, causing it to rise at locations where fractures breach confining layers (valley bottoms).

The model is based on the site-specific data collected and interpreted from this site. However, this model should be applicable to other areas of the dissected Appalachian Plateau that possess a similar hydrogeologic setting. Site-specific conditions, such as the geology of the site and its proximity to surface drainage of the third order or higher, must also be considered.

ACKNOWLEDGMENTS

The author would like to express his gratitude to his graduate committee, Drs. Lyle V. A. Sendlein, James Dinger, Sue Rimmer, V. P. "Bill" Evangelou, and John Thrailkill, for their review of this report. I would like to wish Dr. Thrailkill a happy retirement, and thank him on behalf of all scientists for his many significant contributions to hydrogeology and geochemistry throughout his productive career. Special thanks go out to the administration and staff of the Kentucky Geological Survey for their help and support, especially the hydrogeologists in the Water Section. I would also like to extend my sincere thanks to Cypress Southern Realty, especially Mr. John Tate, for providing the suitable site for this study. This project could not have been performed without Jim Dinger's belief in the project and his patience and confidence in me to get it done, and for that I will always be indebted. I thank Jim Kipp for his friendship and camaraderie, and his thought-provoking discussions and critical review during several stages of this study. Page Taylor, Douglas Graham, and Shelly Minns all helped with field and computer work, and I am grateful to each of them. I sincerely hope they each found the

entire episode as great a learning experience as I have. Meg Smath helped with the editing and completion of this final document. Her patience and helpful comments throughout my tenure at KGS have helped me become a better writer. I thank Nina Wunsch for her love and support when it was needed.

Finally, this dissertation is dedicated to Theodore Wunsch, my grandfather. His patience and humility have always been an inspiration to his grandchildren. Although his education was modest, hard work provided him the means to allow his son to make a better life for himself, which ultimately allowed for his grandchildren to obtain college educations. May this dissertation serve as an inspiration to all of his descendants, present and future, to work hard to achieve their highest expectations in work, life, and love.

REFERENCES

- Alexander, Martin, 1977, Introduction to soil microbiology [2d ed.]: New York, John Wiley, p. 362-367.
- Aller, L., Petty, R., Lehr, J. H., Nielson, D., and Denne, J. A., 1989, Handbook for suggested practices for the design and construction of ground-water monitoring wells: National Water Well Association, 398 p.
- Arora, R., and Rodenbeck, S. A., 1983, Barium and radioactivity levels within groundwater of Georgia coastal plain aquifers: Geological Society of America, Southeastern Section, March 16-18, 1983.
- Banasczak, K. J., 1980, Coals as aquifers in the United States: Symposium on Surface Mining Hydrology, Sedimentology, and Reclamation, University of Kentucky, December 1-5, 1980.
- Bienkowski, L. S., 1990, Delineation and characterization of the aquifers of the Eastern Kentucky Coal Field: Ph.D. Dissertation, University of Kentucky, Lexington, 319 p.
- Bohn, H. L., McNeal, B. L., and O'Connor, G. A., 1985, Soil chemistry: New York, John Wiley, 341 p.
- Bower, C. A., and Hatcher, J. T., 1967, Adsorption of fluoride by soils and minerals: Soil Science, v. 103, p. 151-154.
- Brown, E., Skougstad, M. W., and Fishman, M. J., 1970, Methods for the collection and analysis of water samples for dissolved minerals and gases: U.S. Geological Survey Techniques of Water Resources Investigations, Book 5, 160 p.
- Caithamer, C. E., 1983, Mineralogical sources for barium in Cambro-Ordovician aquifers of northeastern Illinois: M.S. Thesis, Northern Illinois University, DeKalb, Illinois, 189 p.
- Caruccio, F. T., Geidel, G., and Pelletier, 1980, The assessment of a stratum's capability to produce acid mine drainage: Proceedings of the Symposium on Surface Mining Hydrology, Sedimentology, and Reclamation, 1980, Lexington, Kentucky.
- Champ, D. R., Gulens, J., and Jackson, R. E., 1979, Oxidation-reduction sequences in ground water flow systems: Canadian Journal of Science, v. 16, no. 1, p. 12-23.
- Collins, G. A., 1975, Geochemistry of oilfield waters: New York, Elsevier Scientific Publishing Company, 496 p.
- Coltharp, G. B., and Brooks, L. T., 1991, Incident and throughfall precipitation chemistry on a mixed hardwood watershed in eastern Kentucky [abs.]: Water Resources Symposium, University of Kentucky, Lexington, Kentucky, March 14-15, 1991.
- Connell, W. E., and Patrick, W. H., 1968, Sulfate reduction in soil: Effects of redox potential and pH: Science, v. 159.
- Corbett, R.G., and Manner, B. M., 1984, Fluoride in the ground water of northeast Ohio: Ground Water, v. 22, no. 1.
- Danilchik, W., and Waldrop, H. A., 1978, Geologic map of the Vest Quadrangle, eastern Kentucky: U.S. Geological Survey Geologic Quadrangle Map GQ-1441.
- Davis, S. N., 1986, Workbook for practical isotope hydrology: National Water Well Association, September 8-9, 1986, San Diego, California.
- Diamond, W. P., 1972, Differentiation of marine and nonmarine carboniferous environments of eastern Kentucky based on clay mineral composition: M.S. Thesis, University of Kentucky, 105 p.
- Fleischer, M., 1974, Fluorine, in Geochemistry and the environment, the relationship of selected trace elements to health and disease, v. 1: National Academy of Sciences.
- Foster, M. D., 1950, The origin of high sodium bicarbonate waters in the Atlantic and Gulf Coastal Plains: *Geochemica. et Cosmochimica Acta*, v. 1, p. 33-48.
- Freeze, R. A., and Cherry, J. A., 1979, Groundwater: Englewood Cliffs, N.J., Prentice-Hall, Inc.
- Gilkeson, R. H., Cartwright, Keros, Cowert, J. B., and Holtzman, R. B., 1983, Hydrogeologic and geochemical studies of selected natural radioisotopes and barium in ground water in Illinois: Illinois State Water Survey, Champaign, Illinois, WFIC Report 180, 93 p.
- Gilkeson, R. H., Perry, E.C., Jr., and Cartwright, Keros, 1981, Isotopic and geologic studies to identify the sources of sulfate in ground water containing high barium concentrations: Urbana-Champaign, Illinois, University of Illinois, Water Resources Center, Grant Report/Illinois State Geological Survey 1981-4, 39 p.
- Groenewold, G. H., Rehm, B. W., and Cherry, J. C., 1981, Depositional setting and groundwater quality in coal-bearing sediments and spoils in western North Dakota: SEPM Special Publication 31, p. 157-167.
- Harlow, G. E., and LeCain, G. D., 1991, Hydraulic characteristics of, and ground-water flow in, coal-bearing rocks of southwestern Virginia: U. S. Geological Survey Open-File Report 91-250.
- Heck, E. T., 1940, Barium in Appalachian salt brines: American Association of Petroleum Geologists Bulletin, v. 24, no.3, p.486-493.
- Hem, J. D., 1985, Study and interpretation of the chemical characteristics of natural water [3d ed.]: U.S. Geological Survey Water-Supply Paper 2254.

- Hendry, J.M., 1988, Do isotopes have a place in ground-water studies?: *Groundwater*, v. 26, no. 4.
- Hinrichs, E. N., 1978, Geologic map of the Noble Quadrangle, eastern Kentucky: U.S. Geological Survey Geologic Quadrangle Map GQ-1476.
- Hoefs, Jochen, 1987, *Stable isotope geochemistry* [3d ed.]: New York, Springer-Verlag, 341 p.
- Hopkins, H. T., 1966, Fresh-saline interface map of Kentucky: U.S. Geological Survey, Scale 1 in. = 8 mi.
- Kipp, J. A., and Dinger, J. S., 1987, Stress relief fracture control of ground-water movement in the Appalachian Plateaus: *Proceedings, National Water Well Association, Focus Conference on Eastern Regional Water Issues*, Burlington, Vermont, July 14-16, 1987, p. 423-438.
- Kipp, J. A., Lawrence, F. N., and Dinger, J. S., 1983, A conceptual model of ground water flow in the Eastern Kentucky Coal Field: *Symposium on Surface Mining, Hydrology, and Reclamation, 1983*, University of Kentucky, Lexington, Kentucky, p. 543-548.
- Levinson, A. A., 1980, *Introduction to exploration geochemistry*: Wilmeth, Illinois, Applied Publishing, Ltd., 923 p.
- McGrain, Preston, 1953, *Miscellaneous analyses of Kentucky brines*: Kentucky Geological Survey, ser. 9, Report of Investigations 7, 16 p.
- McIntosh, G. E., and Miler, K. P., 1989, HC-GRAM, technical support software for the graphical portrayal of hydrochemical data: U.S. Department of the Interior, *Off ice of Surface Mining*.
- McNabb, J. F., and Dunlap, W. F., 1975, Subsurface biological activity in relation to ground water pollution: *Ground Water*, v. 13, no. 19 p. 33-44.
- Moore, R. B., and Staubitz, W. W., 1984, Distribution and source of barium in ground water at Cattaraugus Indian Reservation, southwestern New York: U.S. Geological Survey Water Resources Investigations Report WRI-84-4129.
- Nordstrom, D. K., 1977, Thermochemical redox equilibria of ZoBell's solution: *Geochemica et Cosmochimica Acta*, v. 41, p. 1835-1841.
- Papp, A. R., 1982, Extractable cations in claystones and shales of the Pennsylvanian Breathitt Formation in eastern Kentucky as related to depositional environments: M.S. Thesis, Eastern Kentucky University, 153 p.
- Parkhurst, D. L., Thorstenson, D. C., and Plummer, N. L., 1980, PHREEQE, a computer program for geochemical calculations: U.S. Geological Survey Water-Resources Investigations Report 80-96, 210 p.
- Parkhurst, D. L., Plummer, N. L., and Thorstenson, D. C., 1982, BALANCE-A computer program for calculating mass transfer for geochemical reactions in ground water: U.S. Geological Survey Water-Resources Investigations Report 82-14.
- Perry, E. C., Grundl, T., and Gilkeson, R. H., 1980, Hydrogen, oxygen and sulfur isotopic study of the ground water in the Cambro-Ordovician aquifer system of northern Illinois: Northern Illinois University Press, 43 p.
- Piper, A. M., 1944, A graphic procedure in the geochemical interpretation of water analyses: *Transactions, American Geophysical Union*, v. 25, p. 914-923.
- Powell, J. D., and Larson, J. D., 1985, Relation between ground-water quality and mineralogy in the coal-producing Norton Formation of Buchanan County, Virginia: U.S. Geological Survey Water-Supply Paper 2274.
- Price, W. E., Jr., Mull, D. S., and Chabot, Kilburn, 1962, Reconnaissance of ground-water resources in the Eastern Coal Field Region-Kentucky: U.S. Geological Survey Water-Supply Paper 1607, 56 p.
- Quinones, F., Mull, D. S., York, K., and Kendall, V., 1981, Hydrology of area 14, Eastern Coal Province, Kentucky: U.S. Geological Survey Water Resources Investigation Report 81-137, 82 p.
- Robertson, F. N., 1984, Solubility controls of fluorine, barium, and chromium in the ground water basins of Arizona, in Hitchon, Brian, and Wallick, E.I., eds., *Practical applications of ground-water geochemistry: Canadian/American Conference on Hydrogeology, 1st, Banff, Alberta, Canada, June 22-26, 1984*, National Water Well Association.
- Robertson, F. N., 1991, Geochemistry of ground water in alluvial basins of Arizona and adjacent parts of Nevada, New Mexico, and California: U.S. Geological Survey Professional Paper 1406-C, 89 p.
- Robertson, F. N., and Garrett, W. B., 1988, Distribution of fluoride in alluvial basins of Arizona and adjacent parts of California, Nevada, and New Mexico: U.S. Geological Survey Hydrologic Atlas HA-665, 3 sheets.
- Schubert, J. M., 1980, Fracture flow of groundwater in coal-bearing strata: *Symposium on Surface Mining Hydrology, Sedimentation, and Reclamation*, University of Kentucky, Lexington, Kentucky, December 1-5, 1980.
- Songer, N. L., 1987, Seepage velocity in stress-relief fractures in Eastern Kentucky Coal Field: Kentucky Division of Water, Ground Water Section, Frankfort, Kentucky, MOA 006131, 87 p.
- Spengler, R. W., 1977, Geologic map of the Salyersville South Quadrangle, Magoff in and Breathitt Counties, Kentucky: U.S. Geological Survey Geologic Quadrangle Map GQ-11373.
- Sprinkle, C. L., Davis, R.W., and Mull, D.S., 1983, Evaluation of ground-water quality data from Kentucky: U.S. Geological Survey Water-Resources Investigations Report 83-4240.
- Stach, E., 1982, *Coal petrology*: Gebrüder Borntraeger, Berlin, Stuttgart, 535 p.
- Stone, R., and Snoeberger, D. F., 1978, Cleat orientation and areal hydraulic anisotropy of a Wyoming coal aquifer: *Groundwater*, v. 15, no. 6.
- U.S. Bureau of Reclamation, 1974, *The design of small dams*: Technical Publication.

- U.S. Environmental Protection Agency, 1984, Environmental radiation data report 39: U.S. EPA, July-September, EPA 520/5-85-009.
- Weast, R. C., ed., 1975, Handbook of chemistry and physics [51st ed.]: Cleveland, Ohio, Chemical Rubber Company, various pagination.
- Weinheimer, R. L., 1983, Vertical sequence and diagenesis in Breathitt sandstone of eastern Kentucky: M.S. Thesis, University of Cincinnati, Cincinnati, Ohio, 147 p.
- Winograd, I. J., and Farlekas, G. M., 1974, Problems in ^{14}C dating of waters of deltaic origin, isotope hydrology: International Atomic Energy Agency, Vienna, Austria, p. 69-93.
- Wood, W. W., and Low, W. H., 1988, Solute geochemistry of the Snake River Plain regional aquifer system, Idaho and eastern Oregon: U.S. Geological Survey Professional Paper 1408-D, 79 p.
- Wunsch, D. R., 1982, Fluoride distribution and relation to chemical character of ground water in northeast Ohio: M.S. Thesis, University of Akron, Akron, Ohio, 101 p.
- Wunsch, D. R., 1988a, High barium concentrations in ground water in eastern Kentucky: Proceedings of the Ground Water Geochemistry Conference, National Water Well Association, Denver, Colorado, February 16-18, 1988.
- Wunsch, D. R., 1988b, The effect of sulfur-reducing bacteria on high barium concentrations in ground water in eastern Kentucky: EOS Transactions, American Geophysical Union, v. 69, no. 44.
- Wyrick, G. C., and Borchers, J. W., 1981, Hydrologic effects of stress relief fracturing on an Appalachian Valley: U.S. Geological Survey Water-Supply Paper 2177, 51 p.
- Zack, A., and Roberts, I., 1988, The geochemical evolution of aqueous sodium in the Black Creek aquifer, Horry and Georgetown Counties, South Carolina: U.S. Geological Survey Water-Supply Paper 2324, 15 p.

APPENDIX 1: A Discussion on the Probable Weathering Reactions in Appalachian

Coal-Bearing Strata*

NOTE: Some of these reactions shown in this discussion include oxidation/reduction. For simplicity, only the stoichiometric equations will be represented.

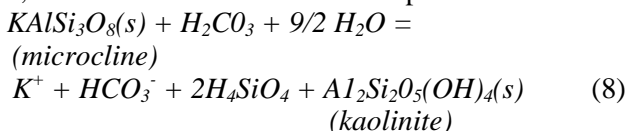
Water in contact with carbon dioxide in the atmosphere or concentrated in soil zones dissolves the gas, yielding carbonic acid by the following reaction:



Concentrations of CO_2 in the soil or shallow subsurface can reach several orders of magnitude higher than atmospheric levels (Freeze and Cherry, 1979). Ground water containing significant carbonic acid and dissolved oxygen is important in the process of chemical weathering. Some of the weathering reactions that can be expected with the minerals typical to the coal-bearing rocks in this study are as follows:

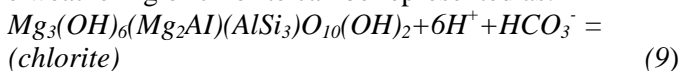
Silicate Hydrolysis

In the process of silicate hydrolysis, silicate minerals react with H^+ and produce clays, dissolved silica, metal ions, and bicarbonate ions. For example:

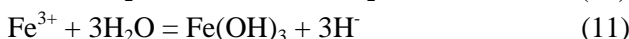
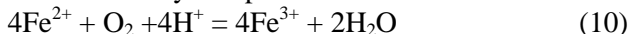


The reaction consumes H^+ and H_2CO_3 , which increases the alkalinity and pH of the water. Hydrolysis reaction may produce ground waters with a pH as high as 10 (Freeze and Cherry, 1979).

Chlorite is also an abundant mineral in coal-field rocks. The weathering of chlorite can be represented as:

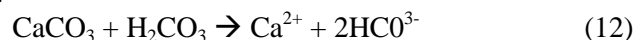


Talc is not common to the mineral suite described by Powell and Larson, and they suggest that talc reacts with additional hydrogen ions, which may add Mg^{2+} to the system. If the chlorite is iron rich, ferrous iron will be released into the system, which may be oxidized to ferric iron and produce additional hydrogen ions, thus lowering the pH. If the magnesium content is greater relative to iron, the tendency will be toward chlorite weathering to increase alkalinity and pH.



Carbonate Dissolution

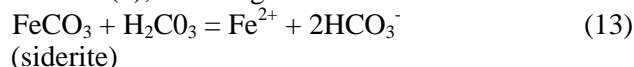
The dissolution of carbonate minerals releases metal ions (e.g., Ca^{2+} , Mg^{2+} , Fe^{2+}), bicarbonate, and raises the pH of ground water. At least two carbonate minerals are suspected of being present in the study area. The dissolution of calcite with water containing carbonic acid is:



In this reaction, 2 moles of bicarbonate ions are formed from the carbonate from the calcite plus the disassociation of the carbonic acid; therefore, this reaction can significantly increase alkalinity and pH.

The dissolution of carbonate minerals in the presence of acid generated by the weathering of sulfide minerals contributes less to alkalinity than does reaction with carbonic acid.

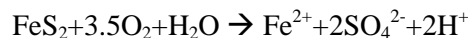
Siderite was the most abundant carbonate mineral found in the investigation by Powell and Larson. It was observed as nodules in Star Fire core 1066, and is noted as being present by Weinheimer (1983). The dissolution of siderite releases ferrous iron, which may oxidize as shown in reaction (4), releasing H^+ .



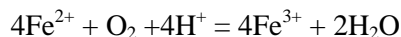
The H^+ will be neutralized by bicarbonate derived from the carbonic acid and siderite; therefore, the net effect is an increase of iron to the ground water without the large increase in acidity that the oxidation of pyrite would produce.

A common reaction in coal-field ground water systems is the oxidation of sulfide minerals (pyrite and marcasite). The products of this reaction are sulfate, ferrous and ferric iron, hydrogen ions, and amorphous iron hydroxide precipitate. The reactions are as follows:

Dissolution of Pyrite:



Oxidation of Ferrous to Ferric Iron:

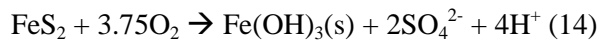


Hydration of Ferric Iron:

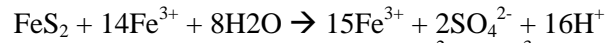


The net reaction under oxidizing conditions is then:

*Discussion largely taken from Powell and Larson (1985)

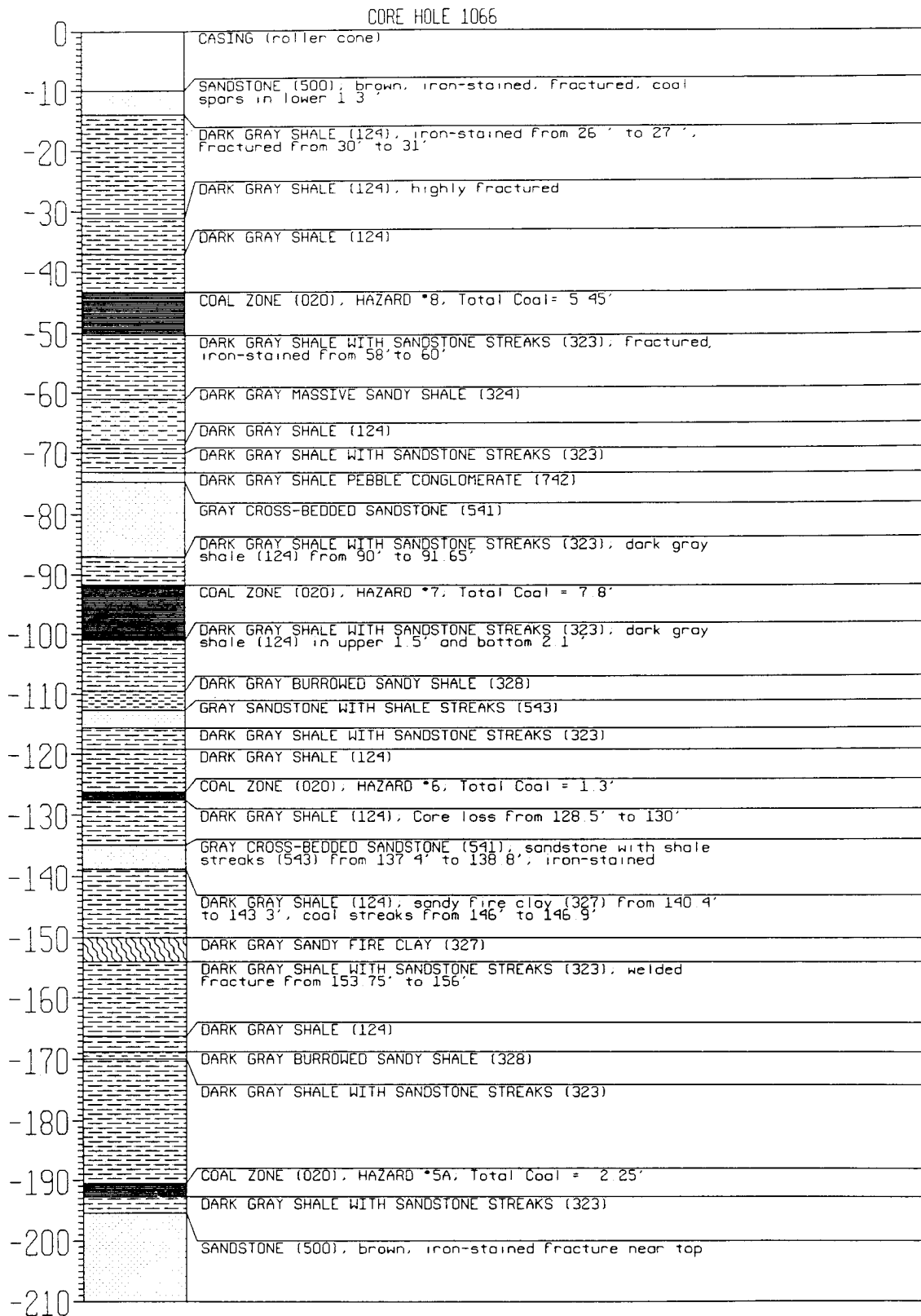


With no mineral source of sulfate (i.e., gypsum is not present) the sulfate in the ground water is a good indicator of the amount of pyrite oxidation taking place. In the case of oxygen depletion, oxidation of sulfide by ferric iron present in the water may take place. The net reaction:



In this reaction, the oxidation of Fe^{2+} to Fe^{3+} is catalyzed by bacteria such as *Thiobacillus ferrooxidans*. The activity of these bacteria is enhanced at pH less than 5.5 (Caruccio and others, 1980).

APPENDIX 2: Geologic Core Description, Piezometer Construction Specifications, Piezometer Construction Diagrams



SPECIFICATIONS FOR INSTALLATION OF PRODUCTION PIPE AND SCREEN

1. Drillers are invited to perform the installation of approximately 10 ground-water monitoring wells or until allocated grant funds are expended. Total cumulative depth of completed holes is anticipated to be approximately 1,300 feet.
2. Permanent casing will be 2 inch I.D., threaded, flush joint, PVC schedule 40. Casing shall be installed vertically in the ground such that a 6-foot bailer will pass through it without obstruction (this may necessitate the use of centralizers), extend 2 feet above ground elevation, and have a threaded removable cap. A bottom cap (plug) must be installed at the bottom of the screen to prevent sediment from entering the well. All threaded joints will have an O-ring seal. No grease or petroleum-based lubricants will be allowed. Teflon-based or other EPA-approved lubricants may be allowed at the discretion of the geologist-in-charge.
3. The monitoring wells will be completed in the following steps (see Figure 2):
 - (1) Placement of equipment over an existing borehole of suitable diameter drilled to the targeted depth,
 - (2) 1 foot of pure quartz (size FX20) sand emplaced to the bottom of the hole,
 - (3) The slotted screen (0.010 slot size) and pipe (2-inch) installed, centralizers may be installed screen to center the pipe.
 - (4) Pure quartz sand (coarse sand, 0.033 to 0.46 inch diameter) emplaced from bottom of the screen to a minimum of 3 feet above the screen,
 - (5) 3 feet of pure quartz sand (fine sand, 0.008 to 0.12 inch diameter) emplaced,
 - (6) A minimum of 3 feet of bentonite seal (consisting of bentonite pellets) emplaced,
 - (7) Bentonite slurry tremied into the hole up to an elevation that is below the chosen elevation of the next piezometer,
 - (8) 3-foot bentonite seal (bentonite pellets) emplaced. A MINIMUM OF 1 HOUR MUST ELAPSE BEFORE STEP 9 IS STARTED. This is to allow for expansion of the bentonite pellets.
 - (9) Emplace minimum of 5 feet of sand,
 - (10) Slotted screen installed,
 - (11) Start sequence over again with step
 - (12) After step 6, the bentonite slurry will be tremied or pumped into the top of the hole.

NOTE:

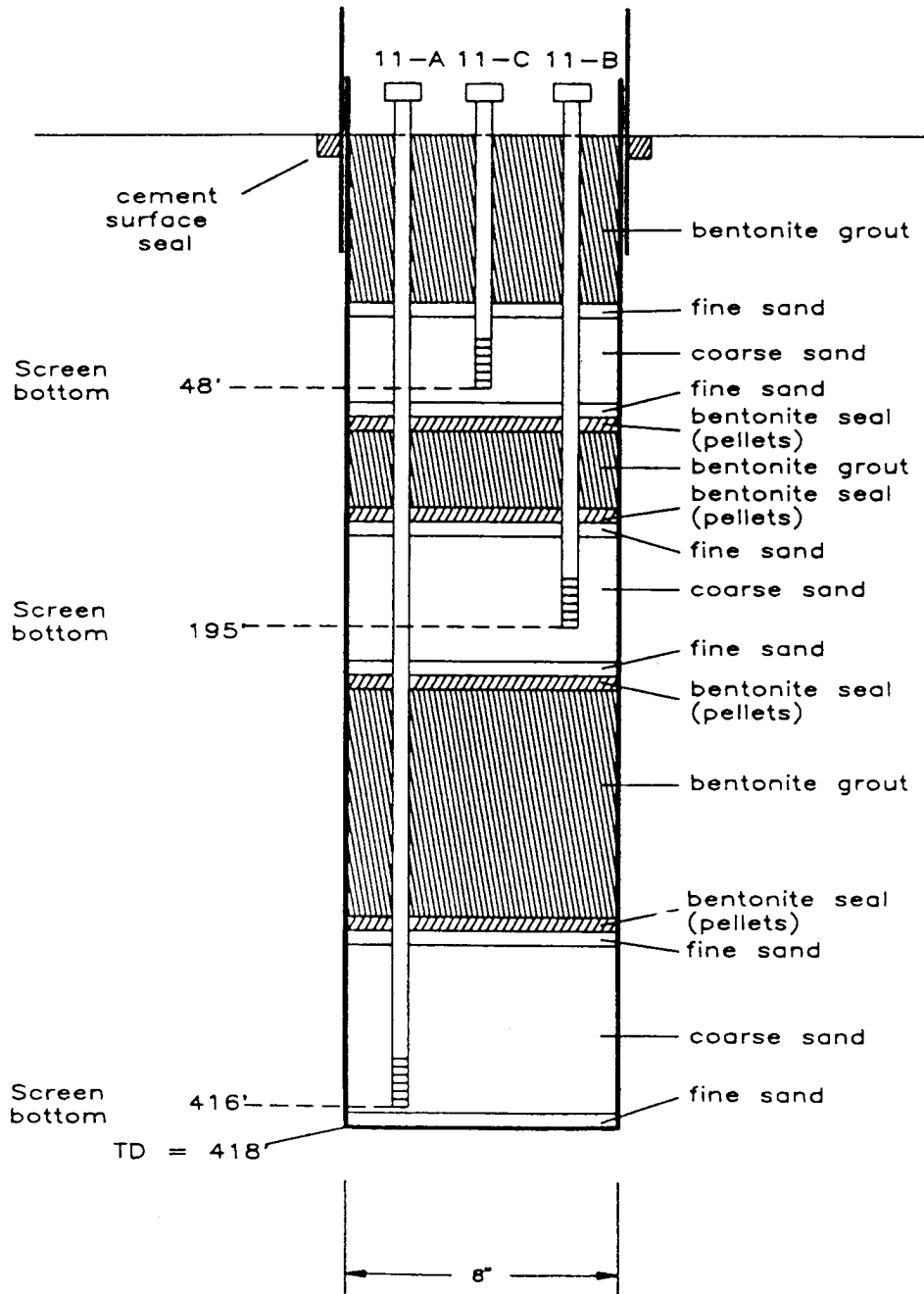
1. No bridging of bentonite, bentonite slurry, or sand will be permitted in the hole.
2. No materials such as cement that will alter the ground-water quality may be introduced into the hole.
3. All water used for slurry mixing, washing, and decontamination shall be chlorinated, potable water.
4. The delay between holes shall not be more than 1 day unless approved by the University geologist-in-charge.
5. Locations shall be cleaned up by the contractor to the satisfaction of the geologist-in-charge and cost of any damages due to acts of the contractor shall be borne by the contractor.
6. All materials connected with well installation are to be maintained in good condition. Plastic will be laid on the ground surface so that all materials that will be installed in the monitoring well such as, but not limited to, sand, well production casing, and well screens can be stored on this plastic, and plastic will cover the top of such materials to minimize contamination by foreign materials until they are installed in the well. PVC production pipe that is packaged in self-contained plastic bags or coverings will be preferred. Buckets, water tanks, tremie pipes, and other devices used to carry and emplace materials in the hole will be kept clean of foreign materials.
7. The contractor may partially complete a well by setting the deeper of the two piezometers and commence completion of an adjacent well while the bentonite and other materials are setting up in the first well.
8. All work is to be effected in a diligent manner using standard acceptable techniques. Equipment is to be maintained in good working order.
9. Access rights to the property will be obtained by the Kentucky Geological Survey. Suitable drilling pads will be the responsibility of the Kentucky Geological Survey.

STAR FIRE PROJECT
BEDROCK WELL SITES

Well identification 11
Piezometers 11A, 11B, 11C
Surface casing...8 5/8" steel
Production pipe...Schedule 40 pvc,
Flush joint
Screen slot size...0.01"

Coordinates
N. Latitude 37° 22' 27.85"
W. Longitude 83° 06' 48.99"
Well Elevation 1283.7'
(Top of Surface casing)

Schematic Well Construction Diagram

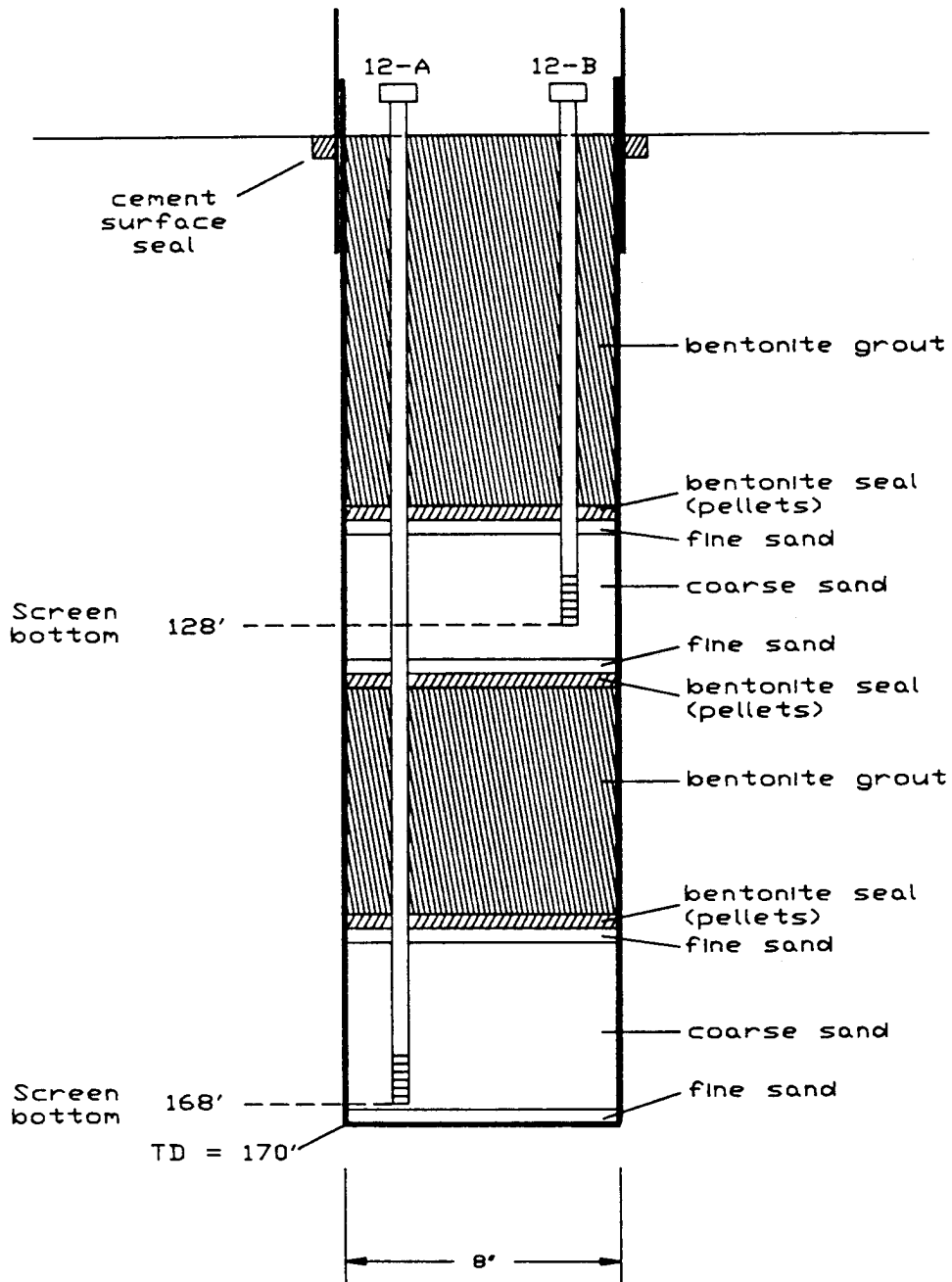


STAR FIRE PROJECT
BEDROCK WELL SITES

Well Identification 12
Piezometers 12A, 12B
Surface casing...8 5/8" steel
Production pipe...Schedule 40 pvc,
Flush joint
Screen slot size...0.01"

Coordinates
N. Latitude 37° 22' 28.00"
W. Longitude 83° 06' 49.68"
Well Elevation 1283.8'
(Top of Surface casing)

Schematic Well Construction Diagram

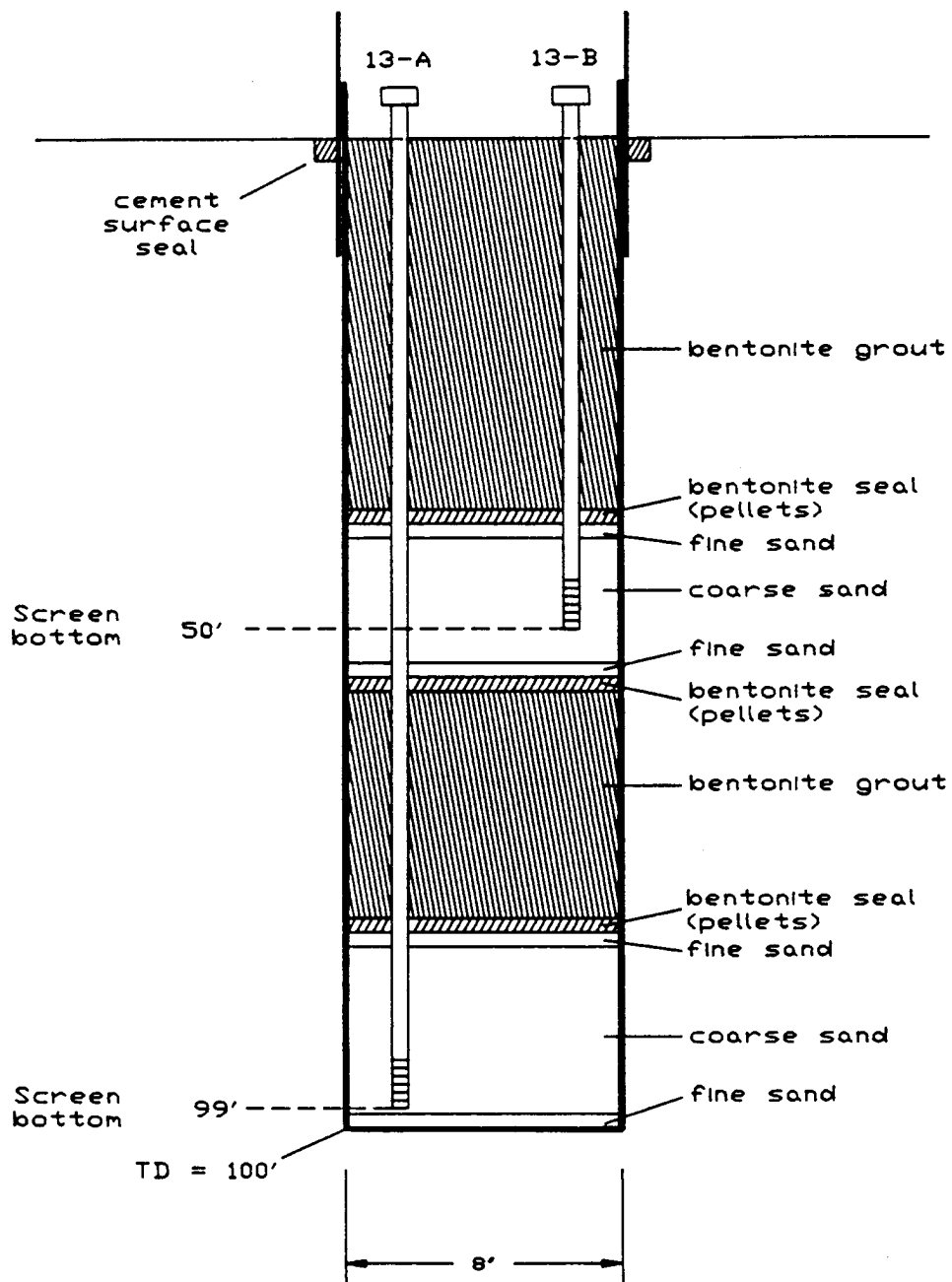


STAR FIRE PROJECT
BEDROCK WELL SITES

Well identification 13
Piezometers 13A, 13B
Surface casing...8 5/8" steel
Production pipe...Schedule 40 pvc,
Flush joint
Screen slot size...0.01"

Coordinates
N. Latitude 37 22' 28.09"
W. Longitude 83 06' 50.10"
Well Elevation 1284.7
(Top of Surface casing)

Schematic Well Construction Diagram

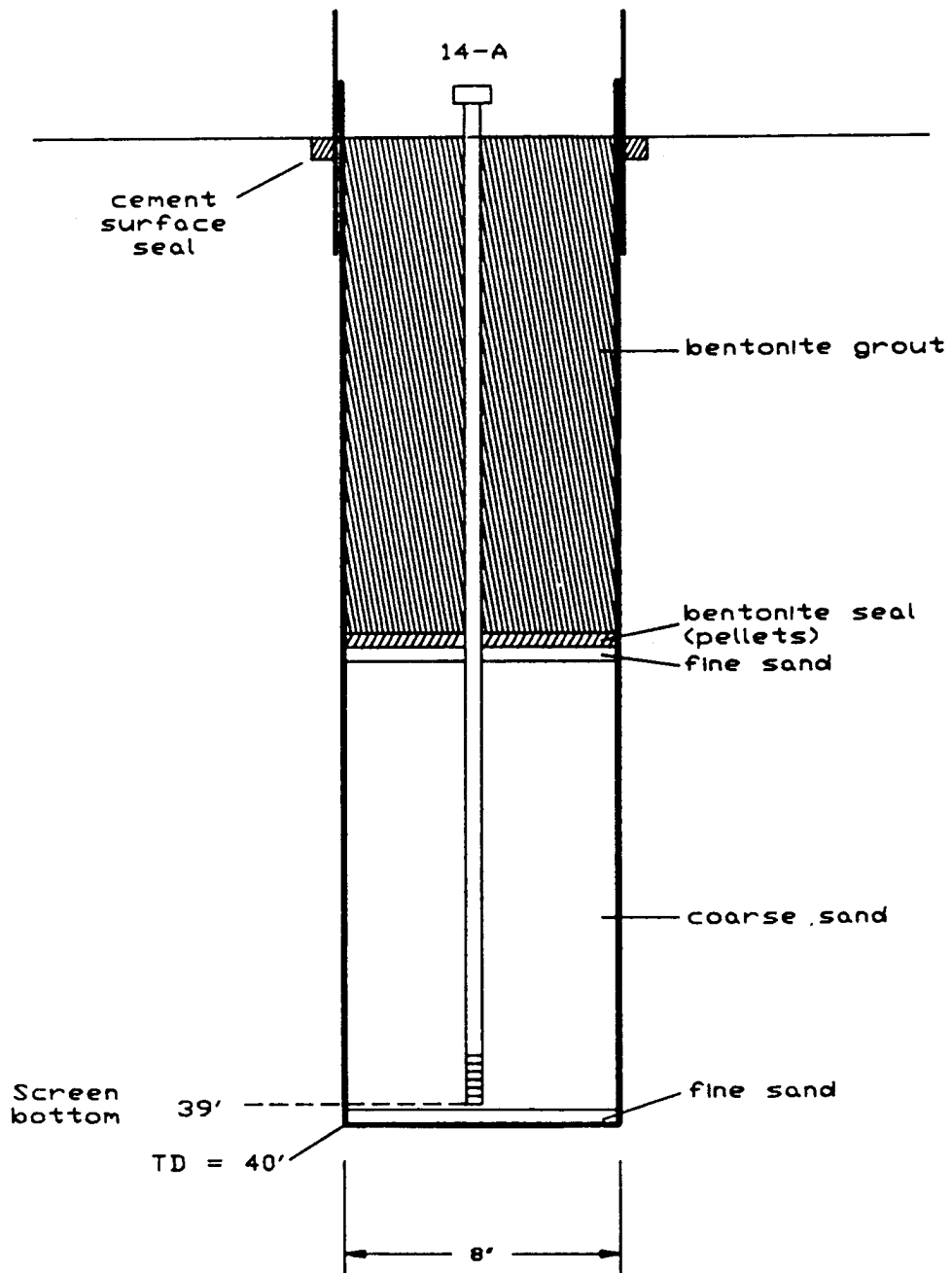


STAR FIRE PROJECT
BEDROCK WELL SITES

Well identification	14
Piezometers	14A
Surface casing...8 5/8" steel	
Production pipe...Schedule 40 pvc	
Flush joint	
Screen slot size...0.01"	

Coordinates	
N. Latitude	37° 22' 28.10"
W. Longitude	83° 06' 50.42"
Well Elevation (Top of Surface casing)	1284.2'

Schematic Well Construction Diagram

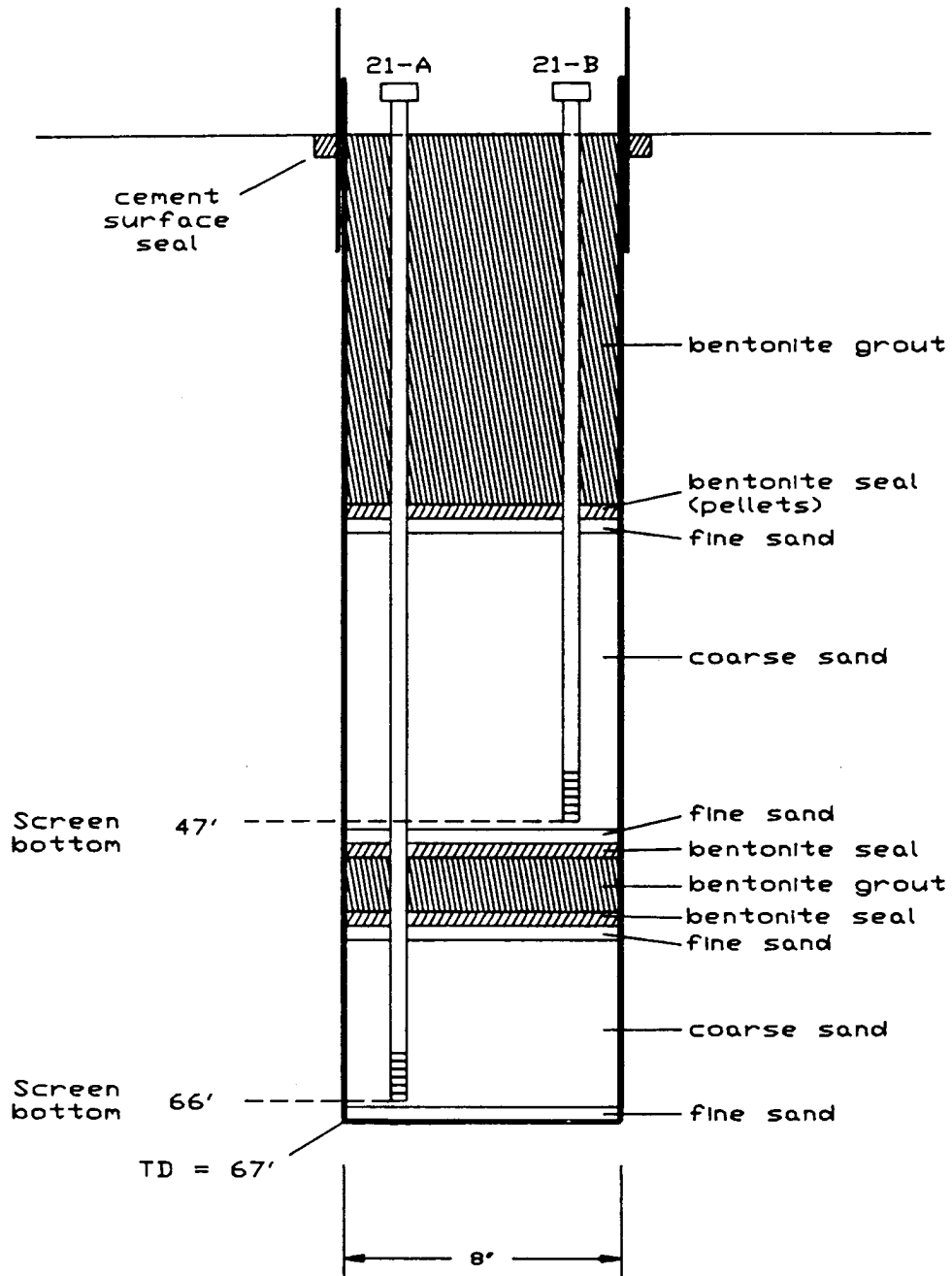


STAR FIRE PROJECT
BEDROCK WELL SITES

Well Identification 21
Piezometers 21A, 21B
Surface casing...8 5/8" steel
Production pipe...Schedule 40 PVC
Flush joint
Screen slot size...0.01"

Coordinates
N. Latitude 37° 22' 31.43"
W. Longitude 83° 06' 50.39"
Well Elevation 1152.1
(Top of Surface casing)

Schematic Well Construction Diagram

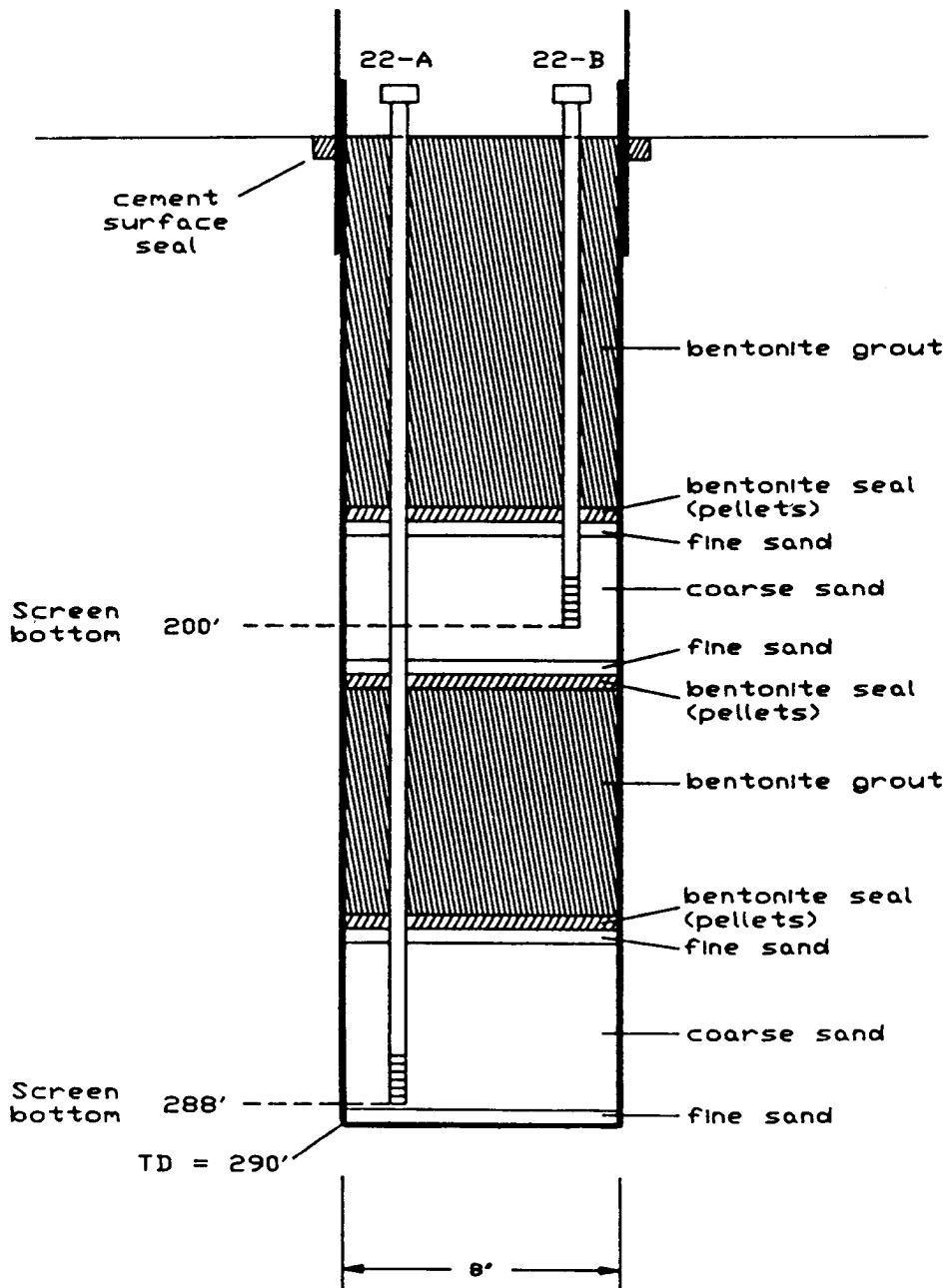


STAR FIRE PROJECT
BEDROCK WELL SITES

Well identification	22
Piezometers	22A, 22B
Surface casing...	8 5/8" steel
Production pipe...	Schedule 40 pvc, Flush joint
Screen slot size...	0.01"

Coordinates	
N. Latitude	37 22' 31.38"
W. Longitude	83 06' 50.19"
Well Elevation (Top of Surface casing)	1152.9'

Schematic Well Construction Diagram

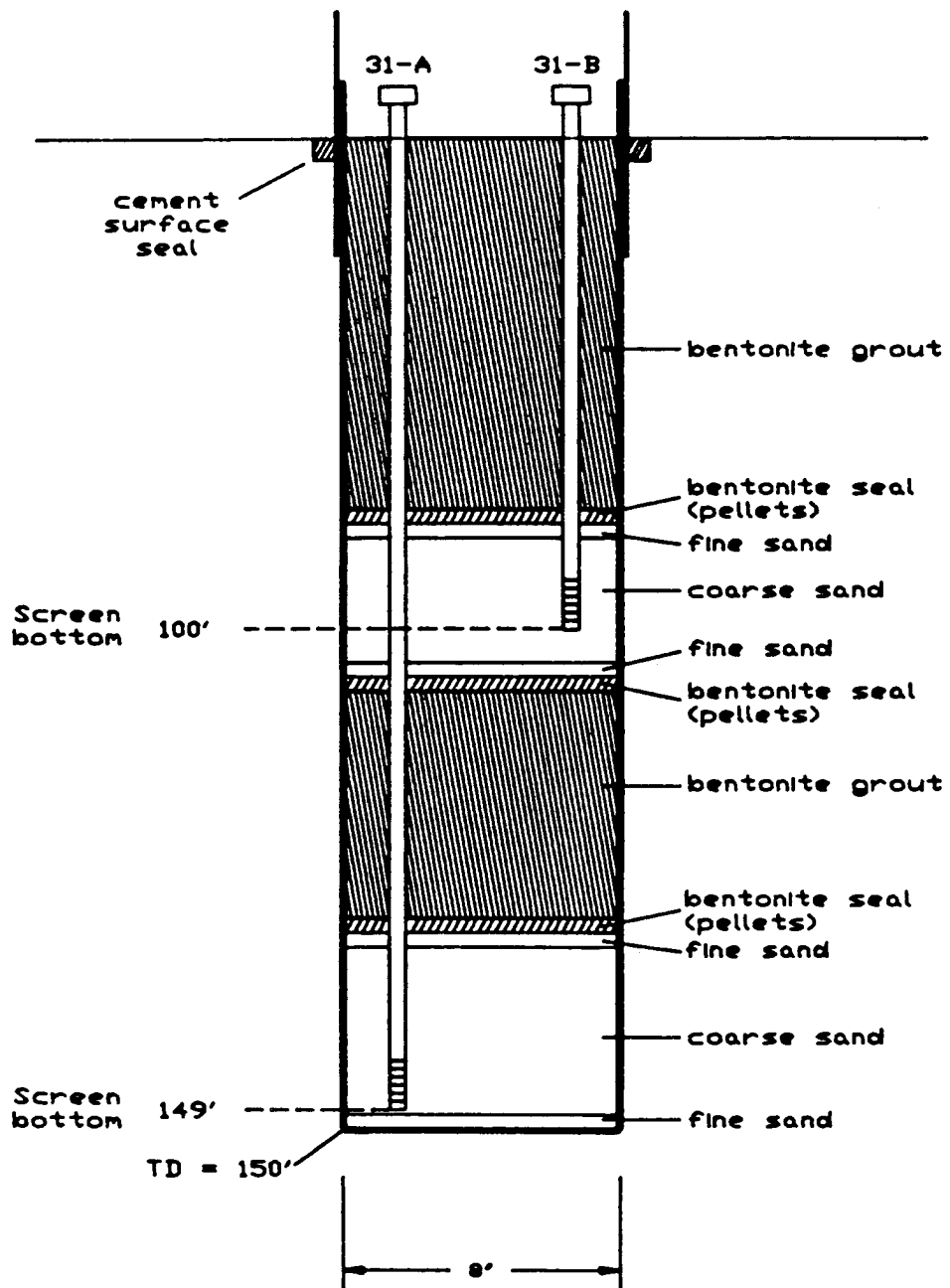


**STAR FIRE PROJECT
BEDROCK WELL SITES**

Well Identification 31
 Piezometers 31A, 31B
 Surface casing 8 5/8" steel
 Production pipe Schedule 40 pvc
 Flush joint
 Screen slot size .01"

Coordinates
 N. Latitude 37° 22' 29.10"
 V. Longitude 83° 06' 41.98"
 Well Elevation (Top of Surface casing) 1003.7'

Schematic Well Construction Diagram

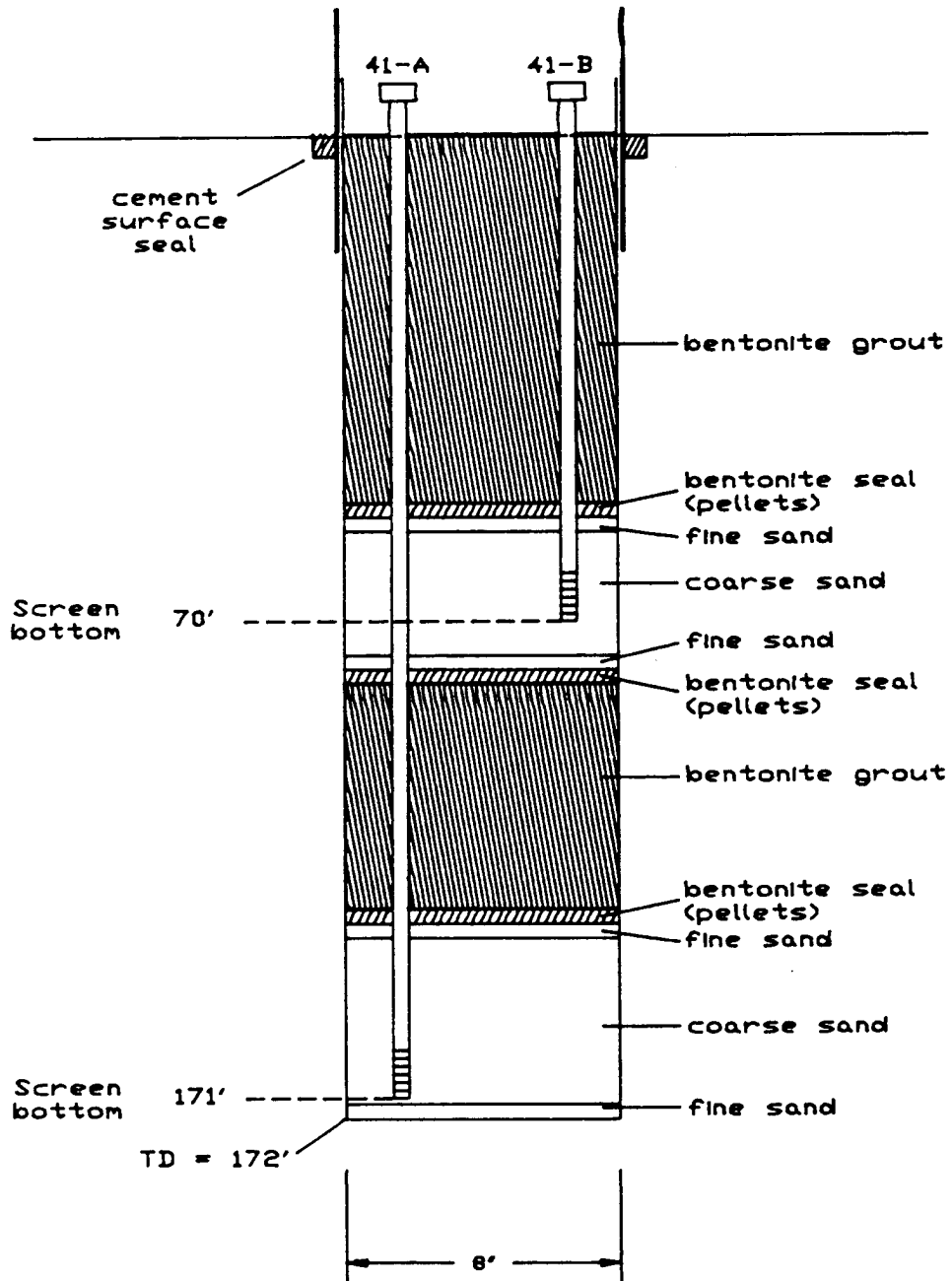


STAR FIRE PROJECT
BEDROCK WELL SITES

Well identification 41
Piezometers 41A, 41B
Surface casing...8 5/8" steel
Production pipe...Schedule 40 pvc
Flush joint
Screen slot size...0.01"

Coordinates
N. Latitude 37 22' 24.96"
W. Longitude 83 06' 38.34"
Well Elevation 925.0'
(Top of Surface casing)

Schematic Well Construction Diagram



APPENDIX 3: Analytical Laboratory Methods, Methods for Tritium Collection, Description of Geochemical Models

KENTUCKY GEOLOGICAL SURVEY Computer and Laboratory Services Section Analysis Parameters

INORGANIC-METAL

Method: EPA 200.7a-Inductively Coupled Plasma (ICP)

<i>Element</i>	<i>DML µg/L</i>	<i>Element</i>	<i>MDL µg/L</i>
Aluminum	18.0	Magnesium	29.0
Antimony	42.0	Manganese	2.0
Arsenic	58.0	Nickel	20.0
Barium	0.40	Phosphorus	77.0
Beryllium	0.60	Potassium	926
Boron	27.0	Selenium	52.0
Cadmium	4.0	Silicon	34.0
Calcium	20.0	Silver	4.0
Chromium	5.0	Sodium	21.0
Cobalt	10.0	Strontium	0.30
Copper	3.0	Sulfur	29.0
Gold	8.0	Thallium	34.0
Iron	4.0	Tin	99.0
Lead	36.0	Vanadium	5.0
Lithium	75.0	Zinc	4.0

Method: EPA 200.9 GFAA Methods

<i>Element</i>	<i>MDL µg/L</i>	<i>Element</i>	<i>MDL µg/L</i>
Arsenic	1.70	Cadmium	1.90
Chromium	1.60	Copper	1.45
Lead	1.36	Nickel	2.11

INORGANIC-NONMETAL

<i>Parameter</i>	<i>Method</i>	<i>MDL mg/L</i>
Acidity	EPA 305.1	8.00
Alkalinity	EPA 310.1	3.00
Bicarbonate	Calculated	3.00
Bromide	EPA-300.0 (IC)	1.00
Carbonate	Calculated	1.00
Chloride	EPA-300.0 (IC)	1.00
Conductance	EPA 120.1	0.001
Fluoride	EPA-340.2	0.020
pH	EPA-150.1	0.001
Sulfate	EPA-300.0 (IC)	5.00
Total Hardness	Calculated	1.00
Oxygen (Dissolved)	EPA 360.1	0.010

ADVICE ON SAMPLING

REVISED 20 September 1985

SAMPLING OF ENVIRONMENTAL WATER FOR LOW-LEVEL TRITIUM ANALYSIS

A. Explanation

Tritium in environmental samples will be determined with a limit of detection of 0.1 T-units (JU) (0.0003 pCi/ml). Water vapor of the open air varies from 2 to 100 TU. Indoors, the atmospheric humidity may reach 10,000 TU from various luminescent dials. Exposure of the water to such air at any temperature might give badly erroneous tritium results.

B. Sample bottles

For lowest level of tritium samples we recommend using 1 liter (1 quart) glass bottles with "PolySeal," conical inset caps. The bottles should be clean and dry, preferably factory fresh. If transfer is to be made indoors, the dry bottles should first be filled with argon gas. See below.

If the very lowest detection level is not needed, heavy-wall plastic bottles may be acceptable. Must have good caps. Hold a filled bottle upside down and squeeze hard. No leakage is allowed. Remember that there are large pressure changes in air transport.

C. Sampling procedures

1. Sample transfer should be done outdoors, unless a specially vented room is available with *ban on wristwatches*.
2. THE PERSON PERFORMING THE SAMPLE TRANSFER IS NOT ALLOWED TO WEAR A WRISTWATCH, COMPASS, OR SIMILAR WITH LUMINESCENT DIALS OR SO-CALLED "BETA" LIGHTS.
3. Fill the bottle close to the neck with sample. Do not rinse. Overflow is not desirable.
4. Replace and screw cap on tightly.
5. Record bottle numbers on original field data sheets, and fill in information on bottle label.
6. If sampling indoors, never let the water be exposed to the air. Pipe the sample water into the middle of an argon-filled bottle (below the argon level). Do not pour the argon out before by tilting an open bottle.

Mass Balance Modeling Using BALANCE

The model BALANCE (Parkhurst and others, 1982) calculates the mass transfer (amount of materials or phases entering or leaving the liquid phase) necessary to account for the observed changes in ground-water composition collected at two points along a flow path (Deutsch and others, 1991). A phase can be a mineral solid, gases, ion exchangers, and aqueous solutions. The model calculates the amount of each phase needed to solve the following equation:

$$\text{INITIAL SOLUTION}(A) + \text{REACTANT PHASES} = \text{FINAL SOLUTION} + \text{PRODUCT PHASES}$$

A series of simultaneous equations using initial and final water compositions and selected mineral or gas phases define the changes in molality of each constituent along a flow path by determining reaction coefficients for the specified mineral stoichiometry or gas compositions (Robertson, 1991). The

mass transfer is defined as the number of millimoles per kilogram H₂O of reactant or product phase that enter or leave the aqueous phase. The number of phases used in the model must be equal to the number of elements in the chemical composition of the water used.

The model input requires the concentrations of the end-member solutions (in molar concentrations), the proposed mineral phases, and the stoichiometric coefficient of the ions contained with a mineral. The model output produces a set of values that indicate if a particular mineral phase is dissolving (positive) or precipitating (negative).

Geochemical Calculations Using PHREEQE

PHREEQE (Parkhurst and others, 1980) is a computer program designed to model geochemical reactions. PHREEQE stands for pH-Redox-Equilibria, and was created by merging parts of three previously developed models, WATEQF, WATEQ2, and MIX2. This model calculates the activities and concentrations of the solution species entered into the model, along with calculating the partial pressures of dissolved gases, and mineral saturation indices (Deutsch and others, 1991). Saturation indices are defined in terms of the saturation index (SI):

$$SI = \text{Log}(IAP / K)$$

where IAP is the ion activity product and K is the equilibrium constant. If the IAP is less than zero, the solution is undersaturated with respect to a given mineral, and the mineral may dissolve. If the SI is equal to zero, the solution is in equilibrium; if the SI is greater than zero, the solution is saturated or supersaturated, and the mineral would be expected to precipitate from the solution. However, the model does not take into account kinetic factors or stability effects of a particular mineral in the presence of others. Therefore, it cannot be absolutely determined if a species does indeed precipitate or dissolve as predicted.

Reaction-Path Modeling

When using a reaction-path model to describe the changes in water chemistry along a flow path, the state of the phases (i.e., either dissolving or precipitating) determined by the mass-transfer model must be consistent with the equilibrium model (Robertson, 1991). Most likely there may be several possible scenarios that satisfy the conditions described by the BALANCE model and PHREEQE; thus, a unique solution may not be found. However, through a process of elimination, solutions containing suites of phases that satisfy the conditions set forth by the two models can most likely be determined, giving way to possible scenarios of geochemical reactions between rocks and minerals in the system that may be useful in understanding of the hydrogeochemical evolution of water moving along a flow path.

The suite of minerals used in this study was postulated from the following sources of information: (1) those used by Powell and Larson (1985) because, as discussed previously, the geologic and geomorphic setting of the area used in their study of

ground water in coal-bearing rocks in Virginia is very similar to this study site, (2) published mineralogical data from the literature (e.g., Weinheimer, 1983), and (3) minerals that are pertinent to this study that may impose solubility controls on ions of interest (i.e., barite and fluorite). In a modeling scenario presented here, usually the number of possible phases or minerals exceeds the number of constituents (Plummer and others, 1983; Robertson, 1991). Therefore, the approach taken here will be to form a "best fit" model, where reactions that are most compatible with the water chemistry data and minerals present, along with solubility and kinetic considerations, will be used.

Binary Mixing Using HC-GRAM

HC-GRAM (McIntosh and Miller, 1989) is a program designed to graphically display water-quality data using either Piper trilinear diagrams or Stiff diagrams. The program allows for up to 400 water samples to be entered at one time.

Binary mixing of two water samples is one of the options available in the program. The program will calculate a straight-line mix between the two water samples, with the user choosing the acceptable tolerance from a straight line used in calculations. The smaller the number, the less tolerance from a straight line will be searched for in the mix. The output shows the percent of major ions (in millequivalents) of the input samples and a calculated mix of the two at the specified tolerance. A percent error for the resultant mix water and the actual sample chemistry is also calculated.

APPENDIX 4: Description of Drill Cuttings, Borehole Diagnostics from Downhole Camera Investigations, Geophysical Logs

WELL 11		
<i>Feet</i>	<i>Description</i>	<i>Remarks</i>
0		
200		
214	tan medium gray sandstone	
220	brown medium gray sandstone with coal flakes	
225	gray, fine grained sandstone, micaceous	
230	gray shale and sandstone mixed (shale, with sandstone chips)	
235	gray shale	
240	gray sandy shale	dry
245	gray siltstone	
250	gray shale	
255	gray shale	
260	dark gray shale	damp, water
265	gray shale	dry
270	dark gray shale with carbonaceous material	
275	dark gray shale	slightly damp
280	dark gray shale, methane odor	
285	dark gray shale with carbonaceous material	
290	dark gray shale	
295	dark gray shale	
300	coal with shale	water, dust cut a lot
305	fine sandstone with coal pieces	
310	light brown shale	
315	light brown micaceous shale, somewhat silty	
320	dark gray shale	
325	gray silty shale, methane smell	
330	gray silty shale, little carbonaceous	
335	micaceous shale, greenish-gray	
340	dark gray shale with greenish-gray shale	
345	greenish-gray shale, micaceous	
350	interbedded dark gray and light greenish-gray shale, micaceous	
355	interbedded dark gray and light greenish-gray shale, micaceous	
360	dark gray shale (Magoffin?)	damp cuttings
365	dark gray shale, harder	
370	dark gray shale, carbonaceous	
375	gray shale with some siltstone	slightly damp
380	gray shale with some siltstone	dust cut at 350 feet
385	dark gray shale	
390	dark gray shale	
395	dark gray shale	dust cut at 397 feet
400		

WELL 11		
<i>Feet</i>	<i>Description</i>	<i>Remarks</i>
405	3 to 4 feet thick dark shale with coal in cuttings	dust cut some
410	medium gray shale, micaceous	dust still cut at 412 feet, methane smell
415	gray siltstone with shale	dust still cut
420	bottom	

WELL 21		
<i>Feet</i>	<i>Description</i>	<i>Remarks</i>
0		
50	brown siltstone	
55	brown siltstone, at 57 feet dark gray carbonaceous shale	
60	dark gray carbonaceous shale, at 64 feet 1-foot-thick brown siltstone atop 2-foot-thick coal	
66	gray siltstone, carbonaceous	
67	bottom	

WELL 22		
<i>Feet</i>	<i>Description</i>	<i>Remarks</i>
0		
66	top of 2-foot coal	
68	gray siltstone, micaceous	
78	gray siltstone	
80	brown sandstone, micaceous	
83	brown sandstone, micaceous	
95	gray sandstone	
110	gray sandstone, shale	
130	gray carbonaceous shale, soft, friable	
150	gray carbonaceous shale, soft, friable	
170	gray shale	
191	coal (approximately 1 foot thick), gray shale	
195	coal (less than 1 foot thick)	
200	could be underclay in this interval	
215	gray siltstone	
220	interbedded gray shale and gray siltstone	
225	gray shale	
230	gray shale	
235	gray siltstone	
240	interbedded gray siltstone and shale	
245	gray shale	
250	gray shale, coal pieces in cumulative cuttings	water added
259	water	
290	bottom	

WELL 31		
<i>Feet</i>	<i>Description</i>	<i>Remarks</i>
0		
20	gray shale	
35	coal (approximately 6 inches)	
45	coal (approximately 6 inches)	
60	dark carbonaceous shale	
70	dark shale, coal (approximately 1.5 feet thick)	
95	coal (approximately 6 inches)	
108	coal (approximately 2 feet thick)	
130	fine gray sandstone	no dust, no water present
140	silty shale with white chips	
145	silty shale with white chips	
150	bottom	

WELL 41		
<i>Feet</i>	<i>Description</i>	<i>Remarks</i>
0		
26	gray shale	
40	brown siltstone	
45	white friable sandstone, quartz	moist
48	brown friable sandstone	
50	white mottled sandstone	
60	coal (approximately 8 inches), shale below	
70	dark carbonaceous shale	dry
80	light gray, fine grained sandstone	
90	gray sandstone with coal flecks	water present
95	hard carbonaceous gray sandstone	
100	gray sandstone with coal pieces	
110	mix of gray sandstone, shale, and coal chips	
120	fine grained gray sandstone, friable, with coal chips	
130	fine sandstone, carbon streaks	H ₂ S odor, more water present
140	fine gray sandstone, micaceous, carbon streaks	20 gpm total
150	dark gray shale with light gray sand grains	
160	dark gray shale, hard	20 gpm, H ₂ S odor
170	dark grayish-black shale, hard	20 gpm, H ₂ S odor
173	bottom	

Downhole Camera Diagnostics Monitoring Well 11

Hole Depth in Feet	Observations
0	- Top of Hole, 10 Feet of Casing
	- 25 Feet, Minor—Minor Amount of H ₂ O Entering Hole
	- 46 Feet, Coal w/ H ₂ O Entering Hole Fe-Hydroxide Stains
	- 62 Feet, Fractures, Fe-Hydroxide Stains Well Bore Wash Out
100	- 95 Feet, Coal, H ₂ O Entering Hole
	- 101 Feet, Fractures, Minor Coal w/ H ₂ O
	- 147 Feet, Fracture w/ Fe-Hydroxide Stains
	- 168 Feet, Thin Coal Seam
	- 193 Feet, Fractures, Fe-Hydroxide Stains, H ₂ O?
200	- 210 Feet, Brown Sandstone
	- 234 Feet, Static Water Level Lost Visibility
300	
418	

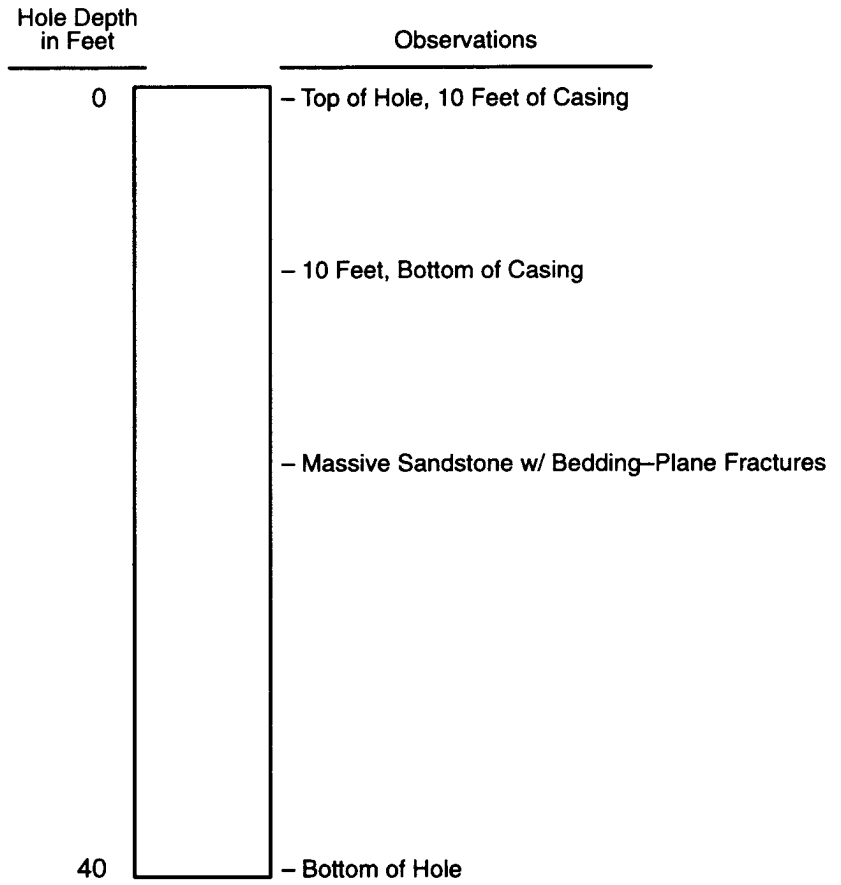
Downhole Camera Diagnostics Monitoring Well 12

Hole Depth in Feet	Observations
0	- Top of Hole, 10 Feet of Casing
	- 20.5 Feet, H ₂ O Entering Hole Through Fracture
	- 46 Feet, Coal
	- 82 Feet, Coal
	- 93 Feet, Coal, Fe-Hydroxide Stains
	- 154 Feet, Static Water Level, Lost Visibility
170	- Bottom of Hole

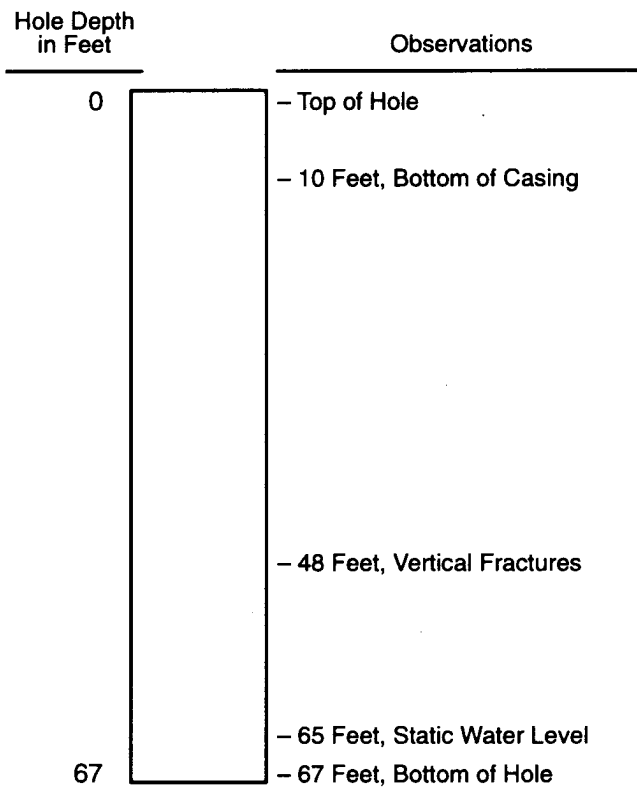
Downhole Camera Diagnostics Monitoring Well 13

Hole Depth in Feet	Observations
0	- Top of Hole, 10 Feet of Casing - 10 Feet, Bottom of Casing
	- 29-31 Feet, Fracture w/ Clay Oozing Out
	- 47 Feet, Vertical Fractures w/ Fe-Hydroxide Stains
102	- 100 Feet, Static Water Level - Bottom of Hole

Downhole Camera Diagnostics Monitoring Well 14



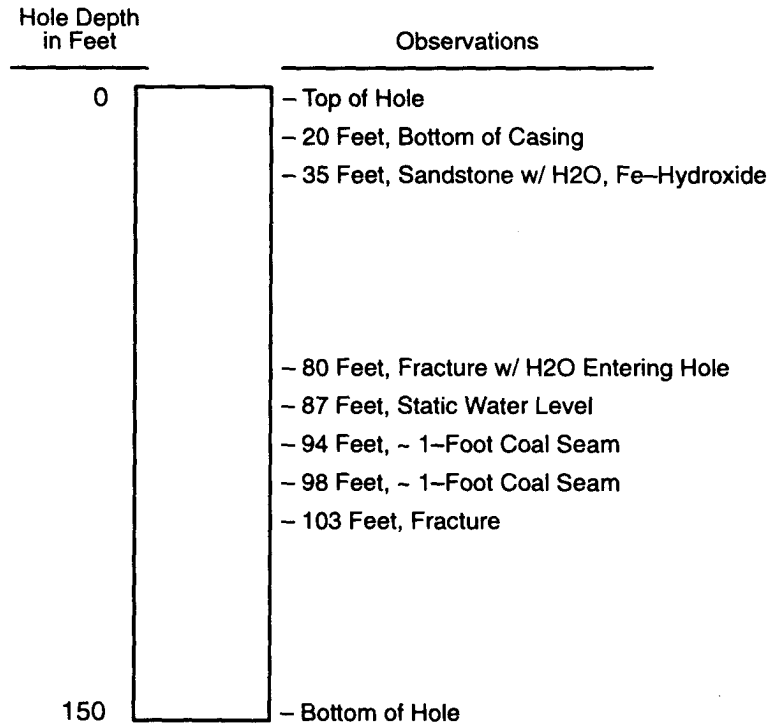
Downhole Camera Diagnostics Monitoring Well 21



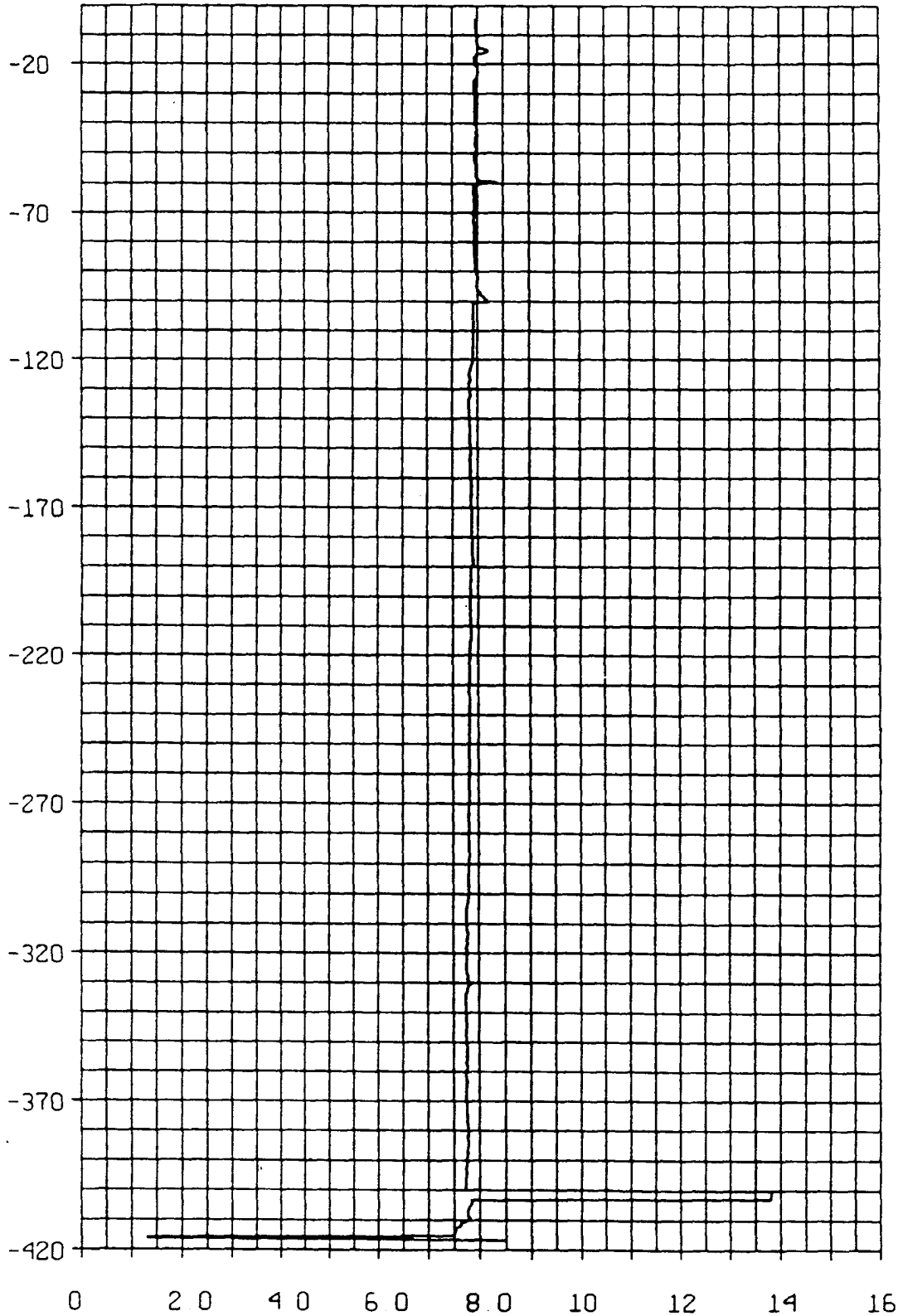
Downhole Camera Diagnostics Monitoring Well 22

Hole Depth in Feet	Observations
0	- Top of Hole
	- 10 Feet, Base of Casing
	- 19 Feet, Wet Zone, Fe-Oxide Stains
	- 69 Feet, Static Water Level, Thin Coal Seam Fe-Oxide Suspended in Water
	- 86 Feet, Lost Visibility
290	

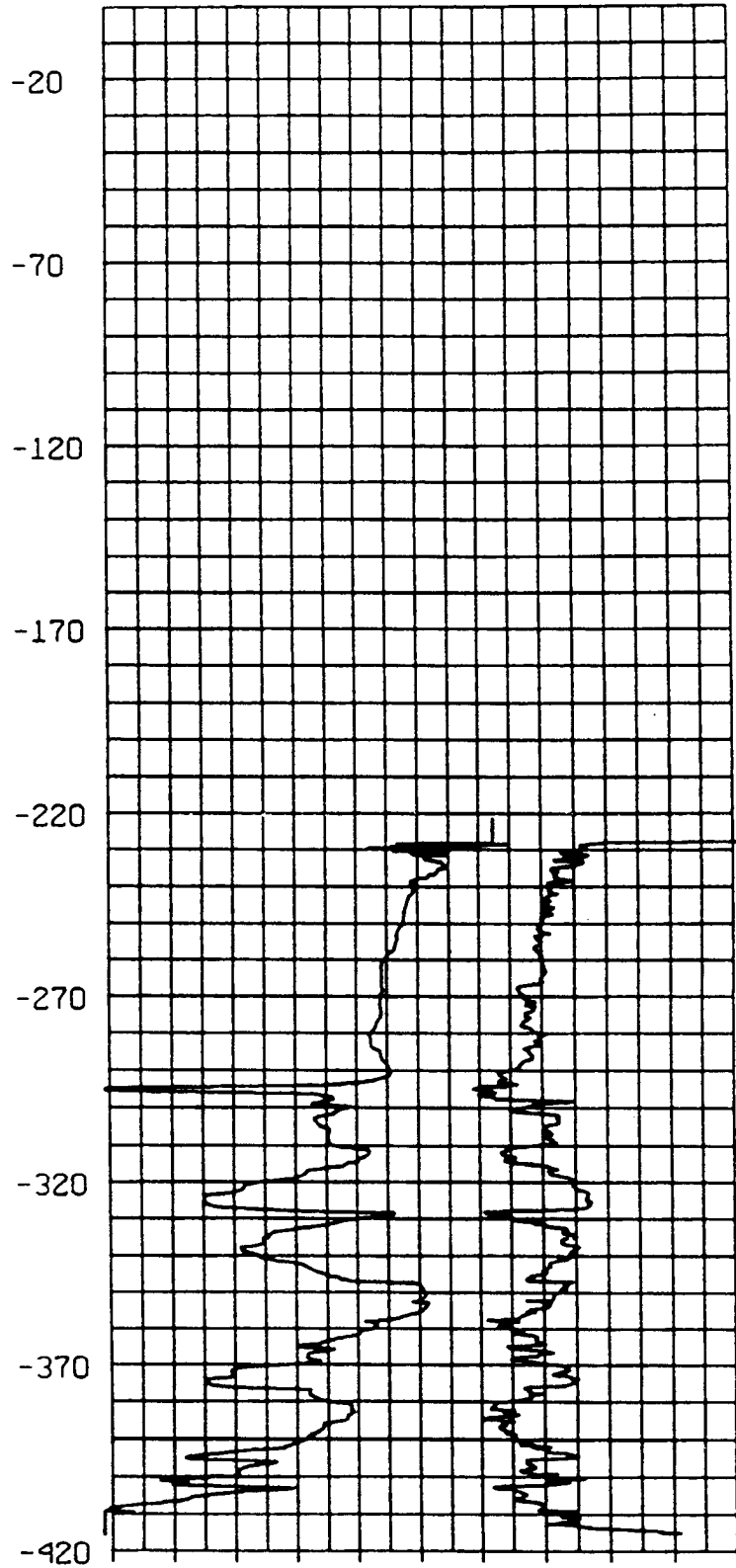
Downhole Camera Diagnostics Monitoring Well 31



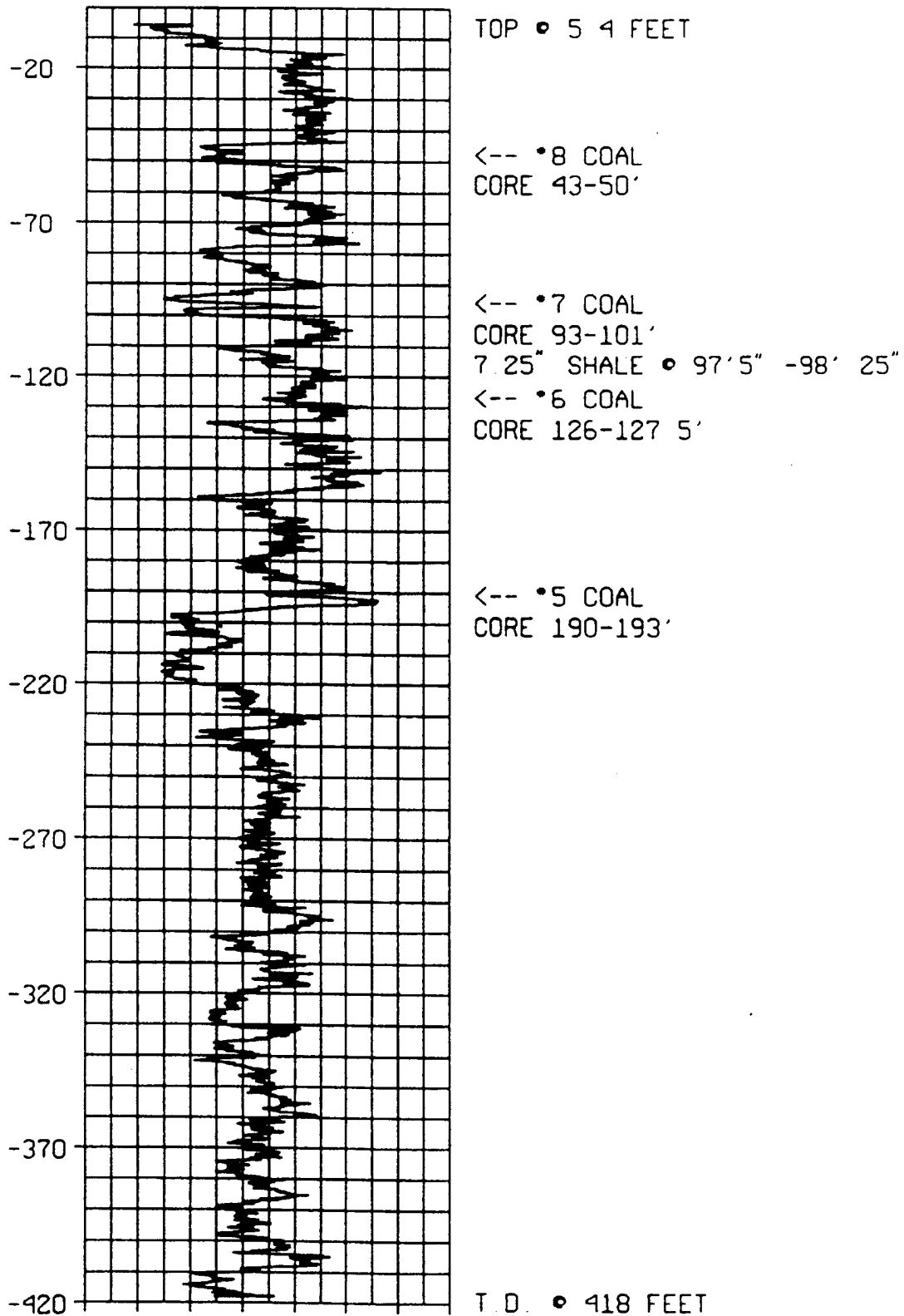
SF MONITORING WELL 11
CALIPER LOG (INCHES)
11/29/90



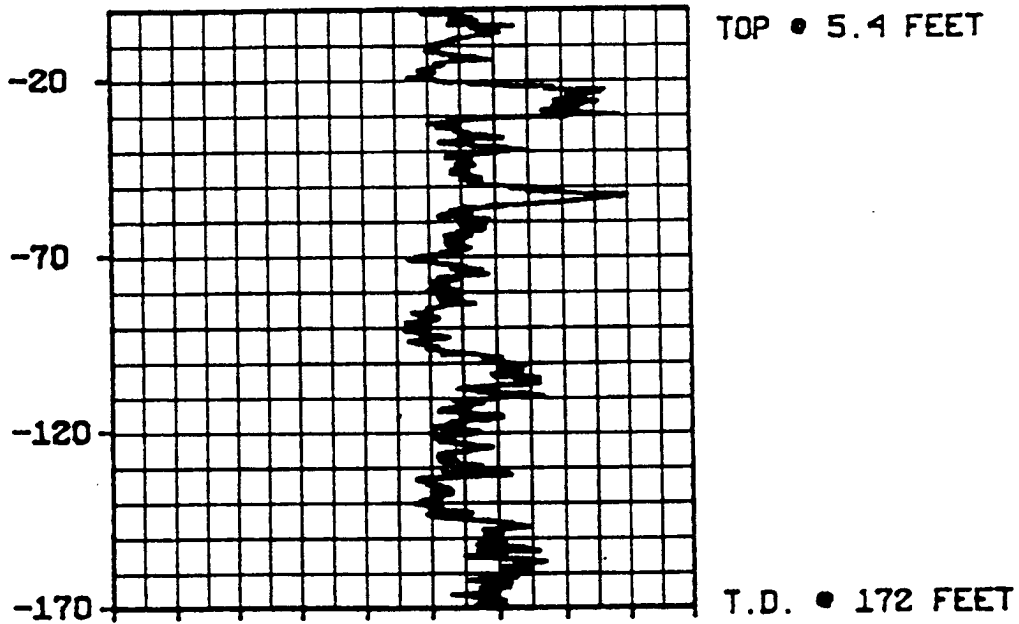
SF MONITORING WELL 11
SP/RESISTIVITY LOGS
11/29/90



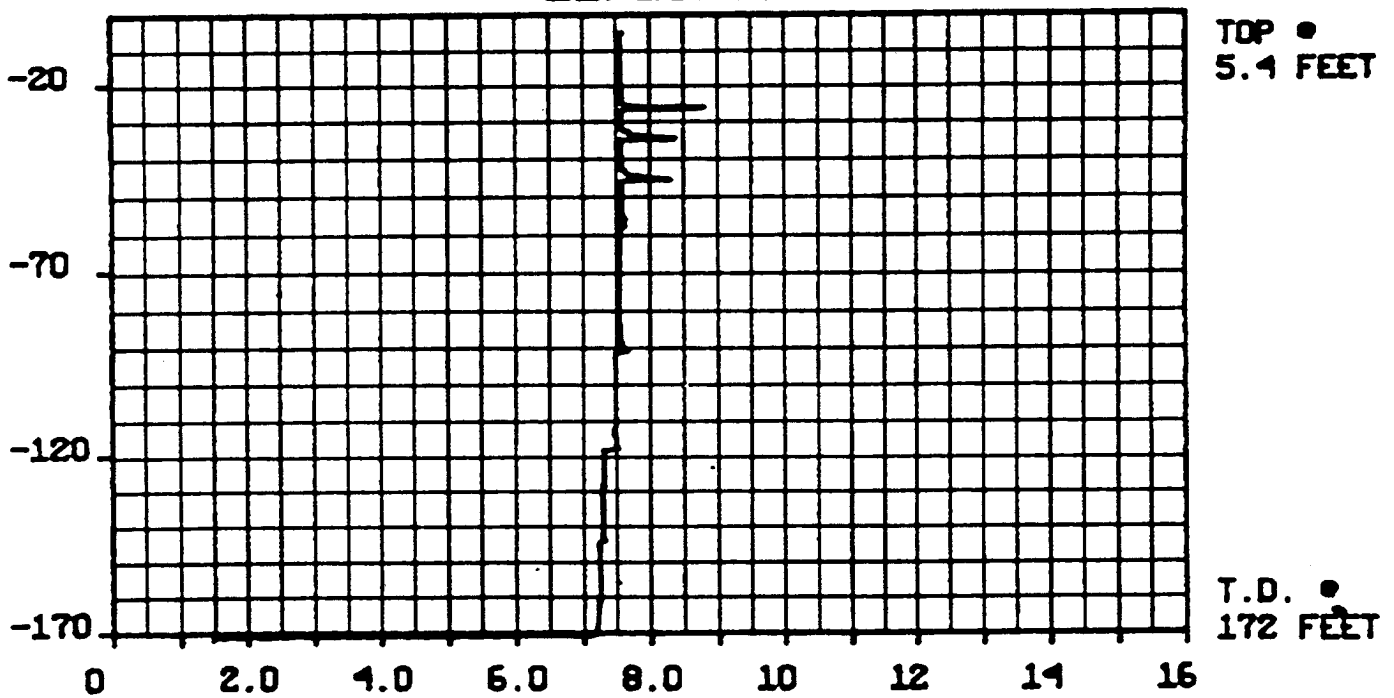
SF MONITORING WELL 11
GAMMA LOG
11/29/90



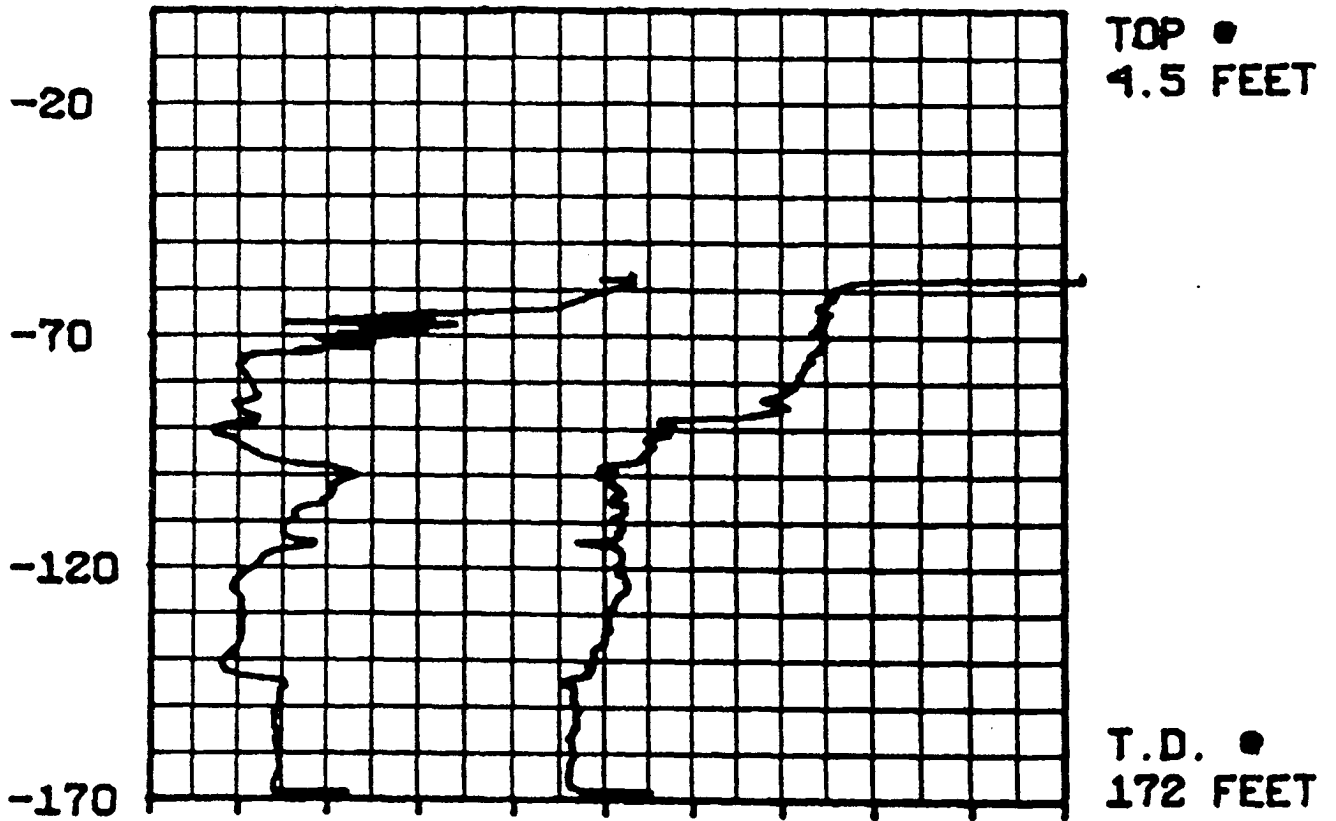
SF MONITORING WELL 11
GAMMA LOG
11/29/90



SF MONITORING WELL 41
CALIPER LOG (INCHES)
11/29/90



SF MONITORING WELL 11 SP RESISTIVITY LOGS 11/29/90



APPENDIX 5: Daily Precipitation Data, Robinson Forest Precipitation Data

DAILY PRECIPITATION DATA

Date:	1991 January	February	March	April	May	June	July	August	September	October	November	December	1992 January
1	0	0	0.087	0	0	1.181	0.022	0	0	0	0	0.350	0
2	0	0	0.066	0	0.087	0.284	0.044	0	0	0	0	0	0.022
3	0	0	0.700	0	0	1.247	0.022	0	0.262	0	0	0	0.328
4	0	0	0.022	0	0	0	0	0	0.087	0	0	0	0.022
5	0	0.197	0.066	0.328	0	0.022	1.400	0	0.131	0.197	0	0	0.022
6	0.481	1.072	0.262	0	0.394	0	0	0.044	0	0	0	0	0
7	0.940	0.066	0	0	0	0	0	0.940	0	0	0	0	0
8	0.066	0	0	0	0	0	0.328	0	0	0	0	0	0
9	0.087	0	0	0.372	0.569	0	0.022	1.531	0	0	0	0.984	0.131
10	0.547	0	0	0	0	0	0.656	0.022	0.109	0	0.109	0	0.05
11	0.087	0	0	0	0.678	0	0.044	0	0	0	0.022	0	0
12	0.087	0	0.328	10.262	0	0.087	1.378	0	0	0	0.022	0	0.02
13	0	0.612	0.306	0.262	0	0	0.372	0.394	0	0	0	0.940	0.04
14	0	0.437	0.175	0	0	0	0	0	0	0	0	0	0.37
15	0.044	0	0	0.831	0	0	0	0	0	0.459	0	0	0
16	0.153	0	0	0	0	0.219	0.022	0	0	0	0.022	0	0
17	0	0.481	0.350	0	0	0.044	0.022	0.175	0.700	0	0	0	0
18	0	0.634	0.109	0.022	1.618	0.328	0	0.262	0.066	0	0	0	0
19	0	1.290	0	0.634	0.109	0.328	0	0.219	0.044	0	0	0	0
20	0.109	0.197	0	0	0.306	0	0	0	0	0	0	0	0
21	0	0	0	0.022	0.044	0.044	0	0	0	0	0.744	0.394	0
22	0	0	0.744	0	0	1.837	0	0	0	0	1.968	0	0
23	0	0	0.612	0	0	0	1.181	0	0.022	0	0	0.394	0.46
24	0	0	0	0	0	0.022	0.262	0	0.262	0	0	0	0.46
25	0	0.066	0	0	0	1.115	0	0	0.175	0	0	0	0.03
26	0	0.066	0.087	0	0	0	0	0	0	0	0	0	0
27	0.109	0	0.219	0.044	0.525	0	0	0	0.044	0	0	0	0
28	0.109	0	0	0	0	0	0.547	0	0	0	0	0.219	0
29	0		1.270	0	1.728	0	0	0.306	0	0	0	0.219	0
30	0.612		0.022	0	0	0	0	0.044	0	0	0.481	0	0
31	0		0.153		0	0	0	0		0		0	0
Monthly Totals	2.71	5.118	4.133	2.777	4.33	6.758	5.775	3.587	1.902	0.656	2.887	3.062	1.955

Robinson Forest Precipitation Quality

<i>Month</i>	<i>Day</i>	<i>Year</i>	<i>Cond.</i>	<i>SO₄</i>	<i>Mg</i>	<i>Ca</i>	<i>K</i>	<i>Na</i>	<i>Alk.</i>	<i>pH</i>	<i>NO₃</i>	<i>PO₄</i>
4	29	91	17.5	0	0.07	1.48	0.15	0.09		6		0.05
5	6	91	21	0	0.04	0.21	0	0.03	17	4.4		0.02
5	13	91	12	0	0.02	0.11	0.01	0.03	25	4.6		0.05
5	20	91	8.5	0.6	0.01	0.09	0.01	0.03	33	4.7		0.02
5	27	91	0	0	0	0	0	0		0		0
5	28	91	23	0	0.02	0.12	0.03	0.04	22	4.3		0.05
6	3	91	17	0	0.05	1.26	0.43	0.25		5		0.02
6	12	91	0	0	0	0	0	0		0		0
6	17	91	25	0	0.01	0.04	0.02	0	23	4.2		0.05
6	24	91	40	2.4	0.03	0.12	0.05	0.05	26	4		0.05
7	1	91	0	0	0.08	1.21	0	0.43		0		0
7	8	91	37.5	1.8	0.04	0.16	0.04	0.01	26	4.1		0.02
7	15	91	24	1.8	0.05	0.27	0.05	0.01	15	4.3		0.02
7	22	91	0	0	0	0	0	0		0		0
8	12	91	20	2.4	0.03	0.78	0.05	0.13	18	4.4		0.02
8	19	91	30.5	3.5	0.06	0.25	0.01	0.07	37	4.3		0.06
8	26	91	39	3	0.05	0.59	0.05	0.02	37	4		0.06
9	3	91	56	2.4	0.06	0.24	0.09	0.24		3.8		0

Mean July Data

15.4 1.8 0.06 0.55 0.05 0.15 20.5 4.1 0.01

APPENDIX 6: QA/QC Chemical Data, Water-Quality Tests of Well Construction Materials, Water-Sample
Chemical Analyses

Duplicate Samples—Chemical Data																				
Date	Sam- ple ID	Time	Temp (C)	pH	Eh (mV)	Cond.	Ca	Mg	Na	K	Cl	F	Fe	SO ₄	HCO	CO ₃	Ba	Br	TDS*	TOC
7/11/91	11-A	1200	14.4	8.68	174	730	1.07	0.24 3	168	1.38	4.13	1.36	0.02 9	< 5	562	—	0.0218	< 1	744	—
8-7-91	31-A	1053	15.6	7.52	207	821	15.7	4.25	165	3.7	15.6	0.3	0.004	36.8	538	—	0.207	< 1	780	—
9-18-91	31-B	1102	17.0	6.82	118	671	60.1	23.2	40.6	6.91	2.2	0.16	0.013	91	387	—	0.102	< 1	611	56
10-7-91	11-A	1500	13.2	8.64	190	729	1.22	0.934	165	1.88	4.54	1.74	3.87	< 5	558	—	0.0414	< 1	742	< 1
11-11-91	22-A	1820	12.0	8.92	89	588	0.596	0.206	150	0.948	5.9	1	0.043	< 5	527	6	0.0314	< 1	697	—
12-10-91	12-A	1425	12.1	6.7	117	744	85.1	37.3	14	11.8	< 1	0.3	0.051	< 11.8	582	—	1.35	—	745	—
1-23-92	21-A	1115	12.0	6.05	—	234	27.2	14.9	5	2.31	< 1	0.1	0.006	25.6	161	—	0.0681	< 1	237	—

Chemical Analyses of Sand-Pack Solute in mg/L			
Date	3-08-91	6-06-91	1-14-92
Al	< 0.018	< 0.018	< 0.015
Sb	< 0.038	< 0.042	< 0.037
As	< 0.043	< 0.058	< 0.059
Ba	0.0027	0.0435	0.0014
Be	< 0.0006	< 0.0006	< 0.001
B	< 0.016	< 0.027	< 0.014
Cd	0.003	0.004	< 0.004
Ca	0.047	0.272	0.036
Cr	< 0.005	< 0.005	< 0.004
Co	≤ 0.006	< 0.01	< 0.006
Cu	< 0.003	< 0.003	< 0.003
Au	< 0.008	< 0.008	< 0.008
Fe	< 0.004	< 0.008	0.007
Pb	< 0.031	< 0.004	< 0.04
Li	< 0.002	< 0.036	< 0.002
Mg	< 0.021	< 0.075	< 0.018
Mn	< 0.001	0.053	< 0.002
Ni	< 0.021	< 0.002	< 0.018
P	< 0.062	< 0.02	< 0.052
K	< 0.622	< 0.077	< 0.722
Se	< 0.098	< 0.926	< 0.067
Si	1.11	< 0.052	1.7
Ag	< 0.005	< 0.004	< 0.004
Na	0.466	5.58	0.324
Sr	0.003	0.054	< 0.0009
S	0.088	0.335	0.12
Tl	< 0.034	< 0.034	< 0.055
Sn	< 0.035	< 0.099	< 0.073
V	< 0.006	< 0.005	< 0.003
Zn	< 0.003	0.008	< 0.003
Cl	< 1		
Fl	< 0.1		
SO ₄	< 5		
HCO ₃	4		
Br	< 1		

Piezometer 11A—Chemical Data

Date	Time	Temp (C)	pH	Eh (mV)	Cond.	Ca	Mg	Na	K	Cl	Fe	F	SO ₄	HCO ₃	CO ₃	Ba	Br	TDS*	TOC
2-4-91	1700	13.5	7.52	—	604	9.96	3.15	104	1.98	4.94	0.044	0.45	49.7	381	—	0.117	1	555.98	—
3-6-91	1240	14.0	7.82	—	670	2.74	1.55	148	1.57	3.94	0.018	1.12	16.0	501	—	0.022	1	677.38	—
4-2-91	1510	13.5	8.10	—	748	1.80	0.652	130	0.622	4.57	0.146	1.52	12.7	529	—	0.028	1	682.52	—
5-7-91	1740	14.1	8.37	191	708	1.27	0.336	154	1.76	5.19	0.004	1.50	10.7	554	0.54	0.030	1	730.21	—
6-4-91	1545	14.8	8.64	190	738	1.21	0.258	169	1.31	4.50	0.029	2.10	7.31	555	7.8	0.029	1	749.65	—
7-11-91	1200	14.4	8.68	174	730	1.43	0.335	168	1.31	4.44	0.043	1.32	5	550	—	0.024	1	733.12	—
8-6-91	1114	14.9	8.65	160	758	1.06	0.266	171	1.15	4.12	0.035	1.43	5	562	13.8	0.019	1	761.30	—
9-17-91	1203	14.8	8.72	191	747	1.15	0.364	166	1.14	4.17	0.019	1.96	5	572	13.8	0.020	1	766.80	1
10-7-91	1500	13.2	8.64	190	729	1.23	0.317	165	1.07	4.92	0.035	1.78	5	566	3.6	0.023	1	750.06	1
11-11-91	1502	12.5	8.82	118	696	1.01	0.245	169	1.15	3.83	0.029	1.50	5	565	7.2	0.016	1	754.84	—
12-10-91	1215	13.0	8.77	159	660	0.777	0.188	161	1.01	3.56	0.024	1.56	5	545	7.2	0.021	—	725.68	—
1-24-92	1131	11.8	8.65	—	653	0.862	0.19	154	0.95	3.63	0.036	1.34	5	531	16.8	0.032	—	713.54	—
n**		11	11	8	11	11	11	11	11	11	11	11	11	11	8	8	—	11	—
max		14.90	8.82	191	758	2.74	1.55	171	1.76	5.19	0.15	2.10	16.00	572	16.80	0.03	—	766.80	—
min		11.80	7.82	118	653	0.78	0.19	130	0.62	3.56	0.004	1.12	5.00	501	0.00	0.02	—	677.38	—
mean		13.73	8.53	172	712	1.32	0.43	160	1.19	4.26	0.038	1.56	7.43	548	8.84	0.02	—	731.37	—
std		1.02	0.31	26	38	0.55	0.39	12	0.30	0.52	0.037	0.29	3.91	21	5.97	0.00	—	30.07	—
CV		7.44	3.65	15	5.28	41.29	91.99	8	25.72	12.17	98.42	18.45	52.70	4	68	16.95	—	4.11	—

* Total Dissolved Solids (TDS) calculated
 ** Data from 2-5-91 not used in calculations

Piezometer 11B—Chemical Data

Date	Time	Temp (C)	pH	Eh (mV)	Cond.	Ca	Mg	Na	K	Cl	F	Fe	SO ₄	HCO ₃	CO ₃	Ba	Br	TDS*	TOC
2-4-91	1715	13.0	6.82	—	449	18.9	8.33	45.7	3.03	2.21	< 0.1	0.403	55.7	251	—	0.083	< 1	386.78	—
3-6-91	1445	13.0	6.35	—	420	39.3	14.4	18.4	2.13	1.53	0.21	0.619	39.4	243	—	0.217	< 1	350.99	—
4-2-91	1540	13.0	6.25	—	376	26.5	11.1	10.9	0.94	7.14	0.31	0.659	38.4	210	—	0.086	< 1	306.88	—
5-7-91	1815	13.5	6.56	180	367	33.2	16.3	10.0	2.35	1.83	0.03	0.559	37.7	251	—	0.273	< 1	354.56	—
6-4-91	1610	14.1	6.77	143	401	35.8	18.4	10.5	2.52	1.43	0.17	0.650	36.7	245	—	0.168	< 1	352.56	—
7-11-91	1324	14.1	6.64	93	390	37.5	19.3	10.8	2.37	1.55	0.16	0.956	39.1	249	—	0.137	< 1	361.75	—
8-6-91	1145	14.3	6.66	85	420	38.7	19.8	11.4	2.59	1.51	0.17	0.923	35.6	250	—	0.118	< 1	361.91	—
9-17-91	1305	14.5	6.92	78	416	37.4	19.3	9.10	2.46	1.26	0.18	0.866	34.9	250	—	0.144	< 1	356.71	< 1
10-7-91	1545	12.6	6.68	50	389	35.2	18.0	9.57	2.29	1.36	0.21	0.866	35.6	250	—	0.146	< 1	354.36	< 1
11-11-91	1535	11.9	6.78	-8	348	37.4	19.1	9.03	2.04	1.44	0.17	0.898	34.4	276	—	0.116	< 1	381.31	—
12-10-91	1321	12.5	6.75	1	409	35.7	18.4	8.69	2.48	1.18	0.18	0.808	34.3	249	—	0.125	—	350.74	—
1-24-92	1154	11.3	6.64	—	365	39.2	19.9	9.45	2.74	< 1	0.18	0.831	33.4	251	—	0.139	—	358.16	—
n**		11	11	8	11	11	11	11	11	11	11	11	11	11	—	11	—	11	—
max		14.50	6.92	180	420	39.2	19.9	18.4	2.74	7.14	0.31	0.96	39.4	276	—	0.27	—	381.31	—
min		11.30	6.25	-8	348	26.5	11.1	8.7	0.94	1.00	0.03	0.56	33.4	210	—	0.09	—	306.88	—
mean		13.16		78	391	35.2	17.6	10.7	2.26	1.93	0.18	0.79	36.3	248	—	0.15	—	353.63	—
std		1.04		64	25	3.8	2.7	2.7	0.48	1.74	0.06	0.14	2.1	15	—	0.05	—	17.70	—
CV		7.90		83	6	10.92	15.40	25.15	21.25	90.23	36.14	17.66	5.71	6	—	34.31	—	5.01	—

* Total Dissolved Solids (TDS) calculated

** Data from 2-5-91 not used in calculations

Piezometer 11C—Chemical Data

Date	Time	Temp (C)	pH	Eh (mV)	Cond.	Ca	Mg	Na	K	Cl	F	Fe	SO ₄	HCO ₃	CO ₃	Ba	Br	TDS*	TOC	
2-4-91	—	—	—	—	—	—	—	—	—	—	—	—	—	—	—	—	—	—	—	—
3-6-91	1510	12.5	5.57	—	275	13.6	6.65	15.1	1.65	1.72	0.1	0.115	48.3	83	—	0.105	1	171.3	—	
4-2-91	1550	12.5	5.37	—	204	17.0	8.67	5.61	0.946	1.45	0.10	1.28	39.5	71	—	0.080	1	146.40	—	
5-7-91	1832	13.2	5.86	225	151	14.3	7.56	3.75	1.75	1	0.02	0.742	36.9	74	—	0.071	1	141.51	—	
6-4-91	1630	14.6	5.96	215	189	16.9	9.16	4.84	2.17	1.34	0.14	0.567	39.3	71	—	0.086	1	146.26	—	
7-11-91	1340	15.7	6.19	167	188	15.0	8.08	5.27	1.93	1	0.10	0.446	38.1	79	—	0.075	1	150.30	—	
8-6-91	1202	15.3	5.86	172	222	16.7	9.01	5.72	1.74	1.36	0.10	0.348	36.8	79	—	0.078	1	152.16	—	
9-17-91	1325	17.2	6.08	173	203	13.3	7.17	3.86	1.75	1.11	0.11	0.022	30.3	82	—	0.066	1	140.43	1	
10-7-91	1555	12.1	6.34	—	193	12.6	6.33	10.7	2.15	1.59	0.12	0.091	35.6	94	—	0.164	1	164.29	1	
11-11-91	1239	14.0	6.42	—	182	10.0	4.54	22.8	2.25	1.35	0.13	0.546	35.8	115	—	0.038	1	193.13	—	
12-10-91	1335	11.9	6.10	—	176	12.9	6.31	10.2	1.98	1	0.1	0.123	36.9	82	—	0.060	1	151.31	—	
1-24-92	1221	10.7	6.33	—	153	14.4	7.08	9.85	1.85	1	0.1	0.255	38.9	77	—	0.071	—	150.37	—	
n**		11	11	5	11	11	11	11	11	11	11	11	11	11	—	11	—	11	—	
max		17.2	6.42	225	275	17.0	9.16	22.80	2.25	1.72	0.14	1.28	48.3	115	—	0.164	—	193.13	—	
min		10.7	5.37	167	151	10.0	4.54	3.75	0.95	1.00	0.02	0.02	30.3	71	—	0.038	—	140.43	—	
mean		13.6		190	194	14.2	7.32	8.88	1.83	1.27	0.10	0.41	37.9	82	—	0.081	—	155.22	—	
std		1.9		27	34	2.1	1.38	5.83	0.36	0.26	0.03	0.37	4.3	12	—	0.032	—	15.54	—	
CV		14.24		14	18	14.91	18.80	65.65	19.38	20.51	30.05	89.49	11.34	15	—	39.48	—	10.01	—	

* Total Dissolved Solids (TDS) calculated
 ** Data from 2-5-91 not used in calculations

Piezometer 12A—Chemical Data

Date	Time	Temp (C)	pH	Eh (mV)	Cond.	Ca	Mg	Na	K	Cl	F	Fe	SO ₄	HCO ₃	CO ₃	Ba	Br	TDS*	TOC
2-5-91	930	12.0	6.41	—	697	65.9	28.6	12.6	12.1	3.39	0.1	0.066	51.0	428	—	0.260	1	603.236	—
3-6-91	1420	12.5	6.43	—	665	64.7	27.6	13.3	11.1	2.42	0.1	0.004	29.4	468	—	0.675	1	618.78	—
4-2-91	1630	12.5	6.36	—	714	63.3	29.0	11.3	11.0	1.98	0.20	0.046	19.5	493	—	0.436	1	630.64	—
5-7-91	1555	13.2	6.74	234	707	73.2	33.4	12.0	11.8	1	0.03	0.442	23.2	476	—	0.583	1	632.46	—
6-4-91	1715	13.7	6.84	220	729	75.4	34.3	13.2	11.3	2.49	0.21	0.027	24.5	477	—	0.702	1	640.15	—
7-11-91	1420	14.4	6.72	174	747	77.9	34.4	12.8	11.7	2.51	0.28	0.017	22.9	503	—	0.847	1	666.99	—
8-6-91	1313	13.9	6.76	165	798	84.3	36.7	14.4	11.9	2.81	0.24	0.004	18.2	534	—	0.928	1	704.84	—
9-17-91	1408	14.2	6.83	173	813	82.1	36.3	13.6	11.4	1.87	0.26	0.041	13.7	556	—	1.030	1	717.62	1
10-7-91	1651	12.4	6.82	140	788	82.6	36.2	13.7	11.6	2.05	0.35	0.027	13.5	569	—	1.110	1	730.66	1
11-11-91	1611	11.8	6.81	85	750	83.3	36.4	13.7	11.2	1.80	0.30	0.033	10.9	581	—	1.290	1	740.64	—
12-10-91	1425	11.7	6.03	116	856	83.0	36.5	13.9	11.4	1.00	0.30	0.059	11.1	578	—	1.340	—	736.88	—
1-24-92	1312	11.4	6.71	—	746	77.6	33.6	12.8	10.6	1.00	0.30	0.078	7.02	590	—	1.310	—	734.79	—
n**		11	11	8	11	11	11	11	11	11	11	11	11	11	—	11	—	11	—
max		14.4	6.84	234	856	84.3	36.7	14.4	11.9	2.81	0.35	0.442	29.4	590	—	1.340	—	740.64	—
min		11.4	6.03	85	665	63.3	27.6	11.3	10.6	1.00	0.03	0.004	7.0	468	—	0.436	—	618.78	—
mean		12.9		163	756	77.0	34.0	13.2	11.4	1.90	0.23	0.071	17.6	530	—	0.932	—	686.77	—
std		1.1		50	54	7.4	3.1	0.9	0.4	0.65	0.10	0.125	6.9	47	—	0.312	—	49.20	—
CV		8.19		30.46	7	9.57	9.11	6.78	3.4	34.42	40.75	176.9	39.4	9	—	33.46	—	7.16	—
											2								9

* Total Dissolved Solids (TDS) calculated
 ** Data from 2-5-91 not used in calculations

Piezometer 13A—Chemical Data

<i>Date</i>	<i>Time</i>	<i>Temp (C)</i>	<i>pH</i>	<i>Eh (mV)</i>	<i>Cond.</i>	<i>Ca</i>	<i>Mg</i>	<i>Na</i>	<i>K</i>	<i>Cl</i>	<i>Fe</i>	<i>F</i>	<i>SO₄</i>	<i>HCO</i>	<i>Ba</i>	<i>Br</i>	<i>TDS*</i>	<i>TOC</i>
2-5-91	—	—	—	—	—	—	—	—	—	—	—	—	—	—	—	—	—	—
3-6-91	1620	12.5	5.67	—	278	25.4	13.1	3.69	1.81	1	< 0.004	< 0.1	21.2	181	0.096	1	246.9596	—
4-2-91	1440	12.5	6.71	—	274	26.4	13.7	3.76	1.43	1	0.072	0.09	21.6	168	0.071	1	236.483	—
5-7-91	1620	13.0	6.19	—	218	23.2	11.8	3.64	1.75	1	< 0.004	< 0.02	25.1	151	0.108	1	217.90	—
6-4-91	1745	14.0	6.42	—	294	26.6	13.6	7.83	2.32	1.17	0.030	0.08	27.0	162	0.203	1	241.093	—
n**		4	4	—	4	4	4	4	4	4	4	4	4	4	4	—	4	—
max		14	6.71	—	294	26.6	13.7	7.83	2.32	1.17	0.07	0.10	27.0	181	0.203	—	246.96	—
min		12.5	5.67	—	218	23.2	11.8	3.64	1.43	1.00	0.00	0.02	21.2	151	0.071	—	217.90	—
avg		13	6.25	—	266	25.4	13.1	4.73	1.83		0.03	0.07	23.7	166	0.119	—	235.61	—
std		0.7071	0.44	—	33	1.6	0.9	2.07	0.37		0.03	0.04	2.8	12	0.058	—	12.56	—
CV		5.4393	7.04	—	12	6.1	6.7	43.71	20.15		116.7	49.6	11.8	7	48.422	—	5.3	—

* Total Dissolved Solids (TDS) calculated
 ** Data from 2-5-91 not used in calculations

Piezometer 14A—Chemical Data

Date	Time	Temp (C)	pH	Eh (mV)	Cond.	Ca	Mg	Na	K	Cl	Fe	F	SO ₄	HCO	Ba	Br	TDS*	TOC
2-4-91	1640	12.5	6.10	—	973	96.1	74.3	7.80	7.56	1.77	0.597	< 0.1	450	183	0.028	1	821.25	—
3-6-91	1130	15.0	6.12	—	647	54.4	43.7	4.77	5.55	1.78	0.277	< 0.1	226	134	0.027	1	470.80	—
4-2-91	1350	12.5	6.10	—	597	46.4	38.0	3.79	4.43	1	0.518	0.11	172	156	0.031	1	422.44	—
5-7-91	1430	13.2	6.03	194	593	53.6	41.9	4.08	5.06	2.33	0.709	0.02	175	185	0.024	1	468.16	—
6-4-91	1810	13.2	6.01	200	627	52.6	44.3	5.79	4.54	1	1.22	0.07	190	166	0.028	1	465.47	—
7-11-91	1455	13.8	6.10	158	708	53.6	45.3	4.62	4.71	2.22	1.48	0.18	205	211	0.048	1	528.22	—
8-6-91	1340	14.4	6.12	168	686	54.9	44.9	4.84	4.44	2.07	0.528	0.12	189	201	0.041	1	502.14	—
9-17-91	1440	14.2	6.18	131	793	66.0	57.1	4.32	4.84	1.80	1.45	0.15	248	223	0.056	1	606.98	1
10-7-91	1720	11.8	6.32	—	862	68.9	59.9	4.49	4.94	1	2.39	0.15	295	232	0.070	1	668.64	4
12-10-91	1452	11.7	6.03	116	856	83.8	70.7	4.33	4.95	1.39	0.413	0.21	332	183	0.029	—	680.82	—
1-24-92	1335	10.4	6.37	—	853	81.8	70.3	4.5	4.66	1	2.40	0.12	330	251	0.031	—	746.13	—
n**		10	10	6	10	10	10	10	10	10	10	10	10	10	10	—	10	—
max		15.0	6.37	200	862	83.8	70.7	5.79	5.55	2.33	2.40	0.21	332	251	0.070	—	746.13	—
min		10.4	6.01	116	593	46.4	38.0	3.79	4.43	1.00	0.28	0.02	172	134	0.024	—	422.44	—
mean		13.0		161	722	61.6	51.6	4.55	4.81		1.14	0.12	236	194	0.038	—	555.98	—
std		1.4		28	110	13.0	12.0	0.54	0.34		0.79	0.05	62	36	0.015	—	111.40	—
CV		10.939		17	15	21.0	23.2	11.76	7.04		69.2	44	26	19	39.68	—	20.03742	—

* Total Dissolved Solids (TDS) calculated

** Data from 2-5-91 not used in calculations

Piezometer 21A—Chemical Data

Date	Time	Temp (C)	pH	Eh (mV)	Cond.	Ca	Mg	Na	K	Cl	F	Fe	SO ₄	HCO ₃	CO ₃	Ba	Br	TDS*	TOC
2-5-91	1320	13.5	6.54	—	417	43.1	20.7	6.40	4.48	3.80	< 0.1	0.142	70.5	218	—	0.062	1	367.664	—
3-7-91	1155	11.3	5.94	—	354	26.1	13.9	4.53	2.80	1.43	< 0.1	0.033	30.6	178	—	0.138	1	257.751	—
4-3-91	1210	15.0	6.44	—	371	30.9	16.2	5.92	3.65	1	0.09	0.193	30.2	192	—	0.068	1	279.761	—
5-8-91	1208	14.6	6.54	255	289	23.6	12.1	5.82	2.21	1.55	< 0.02	0.209	26.2	176	—	0.053	1	247.442	—
6-5-91	955	13.6	6.41	232	244	28.3	15.1	4.86	2.32	1	0.08	0.024	25.6	170	—	0.064	1	246.928	—
7-11-91	1600	14.0	6.36	198	286	26.1	14.2	11.3	2.57	1.2	0.14	0.029	26.7	165	—	0.059	1	247.00	—
8-6-91	1421	14.1	6.37	193	308	28.2	15.4	5.79	2.70	1.33	0.12	0.016	26.0	177	—	0.061	1	256.517	—
9-17-91	1615	14.6	6.49	140	337	28.5	16.1	6.01	2.77	1.34	0.14	0.008	27.7	189	—	0.068	1	271.736	1
10-8-91	1025	11.5	6.41	157	287	26.5	15.1	5.27	2.69	1.21	0.12	0.018	27.6	182	—	0.069	1	260.357	< 1
11-11-91	1709	6.1	6.44	—	254	27.8	15.4	5.37	2.49	1.50	0.11	0.027	27.4	203	—	0.065	1	282.682	—
12-10-91	1700	12.0	6.62	—	257	26.0	14.5	5.32	2.41	1.36	0.12	0.016	28.6	182	—	0.072	—	260.178	—
1-23-92	1115	12.0	6.05	—	234	26.5	14.5	4.77	2.62	1.66	0.10	0.004	25.4	155	—	0.057	—	230.547	—
n**		11	11	6	11	11	11	11	11	11	11	11	11	11	—	11	—	11	—
max		15.0	6.62	255	371	30.9	16.2	11.3	3.65	1.66	0.14	0.209	30.6	203	—	0.138	—	282.682	—
min		6.1	5.94	0	234	23.6	12.1	4.53	2.21	1	0.02	0.000	25.4	155	—	0.053	—	230.547	—
avg		12.618		196	293	27.136	14.77	5.91	2.66	1.33	0.1036	0.052	27.5	179	—	0.070	—	258.3	—
std		2.55		43	46	1.8896	1.15	1.86	0.38	0.21	0.0335	0.074	1.8	13	—	0.023	—	15.5	—
CV		20.18		22	16	7.0	7.8	31.43	14.25	15.93	32	143	6.4	7	—	33.038	—	6.0	—

* Total Dissolved Solids (TDS) calculated
 ** Data from 2-5-91 not used in calculations

Piezometer 22A—Chemical Data

Date	Time	Temp (C)	pH	Eh (mV)	Cond.	Ca	Mg	Na	K	Cl	F	Fe	SO ₄	HCO ₃	CO ₃	Ba	Br	TDS*	TOC
2-5-91	1335	13.0	7.43	—	1064	22.8	9.21	193	3.18	4.94	0.36	0.087	293	355	—	0.055	<1	881.652	—
3-7-91	1040	12.0	7.95	—	719	2.19	1.03	139	1.10	3.66	0.88	0.036	20.2	479	—	0.030	<1	647.586	—
4-3-91	1230	14.0	8.00	—	775	2.12	1.35	138	1.64	3.43	1.00	0.468	15.4	522	—	0.030	<1	685.60	—
5-8-91	1035	14.8	8.19	216	416	1.53	0.353	77.5	1.56	3.82	0.04	0.004	13.5	283	—	0.020	<1	381.367	—
6-5-91	1105	16.7	8.29	189	711	1.14	0.425	168	1.33	3.80	1.30	0.111	10.0	542	5	0.036	<1	733.222	—
7-11-91	1830	14.3	8.64	162	673	0.994	0.318	150	1.42	5.46	1.02	0.052	13.3	473	10	0.025	<1	656.149	—
8-6-91	1622	14.4	8.59	153	736	1.02	0.434	153	1.44	7.23	1.08	0.171	12.9	523	5	0.028	<1	705.483	—
9-17-91	1725	14.4	8.69	137	708	0.75	0.289	155	1.32	6.94	1.42	0.037	10.4	529	12	0.026	<1	717.662	8
10-8-91	1135	13.0	8.70	130	755	0.759	0.300	166	1.79	4.73	1.40	0.017	9.18	561	7	0.032	<1	752.608	2
11-11-91	1820	12.0	8.92	89	588	0.709	0.244	150	0.96	4.14	1.00	0.034	5	527	6	0.034	<1	690.161	—
12-10-91	1635	12.6	8.85	98	618	0.713	0.286	150	1.18	3.23	1.09	0.034	5	522	11	0.040	—	689.533	—
1-23-92	1220	12.5	8.93	—	666	0.689	0.225	167	1.13	2.01	1.20	0.031	5	558	25	0.037	—	755.062	—
n**		11	11	8	11	11	11	11	11	11	11	11	11	11	7	11	—	11	2
max		16.7	8.93	216	775	2.19	1.350	168	1.79	7.23	1.42	0.468	20.20	561	25	0.040	—	755.062	8
min		12.0	7.95	89	416	0.69	0.225	78	0.96	2.01	0.04	0.004	0.0	283	5	0.020	—	381.367	2
avg		13.7		147	670	1.15	0.478	147	1.35	4.40	1.0391	0.090	9.53	502	11	0.031	—	674.039	—
std		1.4		77	101	0.56	0.365	25	0.25	1.58	0.3742	0.134	6.81	78	7	0.006	—	103.171	—
CV		10.466		53	15	48.7	76.5	17.1	18.54	35.92	36	148.1	71.4	15	62.9	18.943	—	15	—

* Total Dissolved Solids (TDS) calculated
 ** Data from 2-5-91 not used in calculations

Piezometer 22B—Chemical Data

Date	Time	Temp (C)	pH	Eh (mV)	Cond.	Ca	Mg	Na	K	Cl	F	Fe	SO ₄	HCO ₃	CO ₃	Ba	Br	TDS*	TOC
2-5-91	1340	12.0	—	—	—	—	—	—	—	4.36	<0.1	—	605	511	—	—	1	1120.64	—
3-7-91	1140	12.0	8.20	—	1728	5.59	1.92	153	2.57	2.57	<0.1	0.254	602	379	—	0.047	1	1147.47	—
4-3-91	1110	14.8	7.90	—	1846	8.60	2.88	269	2.09	1.86	0.19	0.431	564	321	—	0.064	1	1170.0	—
5-8-91	1110	16.2	7.17	215	1732	18.1	5.45	326	5.31	1	0.03	0.004	559	285	—	0.079	1	1200.5	—
6-5-91	1245	15.8	7.51	172	1675	14.1	4.53	317	4.60	3.65	0.15	0.469	542	303	—	0.059	1	1189.1	—
7-11-91	1726	18.3	7.33	175	1499	13.0	3.95	276	3.78	2.79	0.16	0.058	479	277	—	0.046	1	1055.7	—
8-6-91	1650	19.8	7.32	159	538	4.12	1.15	83.5	1.06	1.70	0.12	0.059	282	190	—	0.032	1	564.1	—
9-17-91	1825	19.1	7.39	127	826	24.0	7.75	150	3.65	12.8	0.75	0.017	252	203	—	0.093	1	653.6	24
10-8-91	1255	14.3	7.36	83	1230	8.22	2.39	147	2.69	5.26	0.31	0.055	321	233	—	0.058	1	720.0	3
11-11-91	1045	15.0	7.28	96	1296	9.35	2.74	243	3.07	4.11	0.30	0.074	422	321	—	0.046	1	1005.6	—
12-10-91	1740	14.1	7.5	95	1402	9.48	2.83	249	2.85	1.85	0.20	0.004	458	293	—	0.040	—	1017.1	—
1-23-92	1414	15.2	7.23	—	1479	11.0	3.19	260	3.12	1	0.17	0.021	492	290	—	0.064	—	1060.9	—
n**		11	11	8	11	11	11	11	11	11	11	11	11	11	—	11	—	11	—
max		19.8	8.2	215	1846	24.00	7.75	326.0	5.31	12.80	0.75	0.469	602	379	—	0.093	—	1200.5	—
min		12.0	7.2	83	538	4.12	1.15	83.5	1.06	1.00	0.03	0.004	252	190	—	0.032	—	564.1	—
avg		15.9	7.5	140	1386	11.41	3.53	224.9	3.16	3.51	0.23	0.131	452	281	—	0.057	—	980.4	—
std		2.3	0.3	47	402	5.71	1.84	78.9	1.16	3.35	0.19	0.172	120	55	—	0.018	—	227.6	—
CV		14.751	4.16	34	29	50.0	52.2	35.1	36.81	95.61	85	131	27	20	—	31.08	—	23.21	—

* Total Dissolved Solids (TDS) calculated
 ** Data from 2-5-91 not used in calculations

Piezometer 31A—Chemical Data

Date	Time	Temp (C)	pH	Eh (mV)	Cond.	Ca	Mg	Na	K	Cl	F	Fe	SO ₄	HCO ₃	CO ₃	Ba	Br	TDS*	TOC
2-5-91	1515	13.0	6.24	—	493	37.3	11.1	50.2	5.81	2.42	< 0.1	0.126	49.7	287	—	0.33	1	443.79	—
3-7-91	1340	12.5	6.78	—	607	30.0	8.54	73.5	5.00	2.96	< 0.1	0.004	53.0	338	—	0.295	1	511.34	—
4-3-91	1458	14.0	6.99	—	706	24.5	7.03	112	5.30	4.35	0.18	0.136	48.5	403	—	0.267	1	604.86	—
5-8-91	1354	17.5	7.39	198	717	17.4	5.54	122	3.71	7.44	< 0.02	0.004	49.8	453	—	0.157	1	658.69	—
6-5-91	1400	14.2	6.56	194	686	49.0	19.2	58.8	6.44	2.5	0.10	0.073	89.4	365	—	0.127	1	590.42	—
7-12-91	1117	16.8	7.50	168	786	16.6	4.58	157	4.09	15.2	0.40	0.009	40.0	488	—	0.220	1	726.10	—
8-7-91	1053	15.6	7.52	207	821	15.9	4.38	166	3.80	23.2	0.44	0.004	27.8	517	—	0.214	1	759.02	—
9-18-91	1036	16.9	7.57	112	816	8.52	2.22	164	2.64	27.8	0.51	0.004	24.2	543	—	0.109	1	772.90	1
10-8-91	1350	19.2	7.52	123	905	8.73	2.29	170	2.63	35.9	0.64	0.018	72.4	515	—	0.146	1	807.59	1
11-12-91	1135	13.4	7.52	120	782	8.06	2.05	174	2.02	40.1	0.52	0.004	16.7	522	—	0.128	1	765.74	< 1
12-11-91	1030	13.4	7.73	141	770	10.9	2.87	175	2.59	44.3	0.53	0.004	22.5	516	—	0.185	—	774.94	—
1-23-02	1600	13.3	7.41	—	862	13.5	3.68	187	3.04	60.7	0.61	0.010	13.1	666	—	0.221	—	828.08	—
n**		11	11	8	11	11	11	11	11	11	11	11	11	11	—	11	—	11	—
max		19.20	7.73	207	905	49.00	49.00	187	6.44	50.7	0.64	0.14	89.4	556	—	0.30	—	828.08	—
min		12.50	6.56	112	607	8.06	8.06	59	2.02	2.5	0.02	0.00	13.1	338	—	0.11	—	511.34	—
avg		15.16		158	769	18.46	18.46	142	3.75	23.1	0.36	0.02	41.6	474	—	0.19	—	709.06	—
std		2.16		39	85	12.23	12.23	44	1.37	17.8	0.22	0.04	24.0	74	—	0.06	—	102.40	—
CV		14.25		24	11	66.26	66.26	30.8	36.41	77.03	60.3	171.9	57.8	16	—	32.2	—	14.4	—

* Total Dissolved Solids (TDS) calculated

** Data from 2-5-91 not used in calculations

Piezometer 31B—Chemical Data

Date	Time	Temp (C)	pH	Eh (mV)	Cond.	Ca	Mg	Na	K	Cl	F	Fe	SO ₄	HCO ₃	CO ₃	Ba	Br	TDS*	TOC	
2-5-91	—	—	—	—	—	—	—	—	—	—	—	—	—	—	—	—	—	—	—	—
3-7-91	1430	13.0	6.54	—	753	20.8	7.32	90.7	2.83	3.03	<0.1	0.199	79.6	425	—	0.229	1	629.37	—	
4-3-91	1425	16.0	6.48	—	832	26.3	10.4	103	7.48	2.68	0.12	1.96	82.4	429	—	0.163	1	663.94	—	
5-8-91	1433	18.5	6.85	233	729	37.8	14.3	84.4	6.24	2.23	0.15	0.303	92.8	392	—	0.158	1	630.00	—	
6-5-91	1430	19.6	6.65	199	740	46.5	17.9	71.9	6.31	3.15	0.12	0.056	90.9	382	—	0.15	1	618.85	—	
7-11-91	1130	17.2	6.81	148	730	54.6	20.8	53.2	6.84	2.17	0.17	0.020	102	389	—	0.149	1	629.13	—	
8-6-91	1112	16.8	6.64	160	688	59.3	22.1	51.1	6.84	2.48	0.15	0.045	87.4	372	—	0.14	1	601.66	—	
9-17-91	1102	17.0	6.82	118	671	57.7	22.2	38.6	6.62	2.34	0.19	0.019	83.9	372	—	0.12	1	583.79	—	
10-8-91	1410	15.6	6.62	140	732	60.2	22.9	41.6	7.33	2.32	0.2	0.010	103	378	—	0.141	1	615.90	—	
11-11-91	1158	12.1	6.62	119	671	60.3	22.7	38.1	6.43	2.88	0.17	0.026	92.2	394	—	0.102	1	616.97	—	
12-10-91	1119	10.9	6.63	135	583	60.6	23.2	36.3	6.71	1.61	0.17	0.029	89.6	371	—	0.093	—	589.19	—	
1-23-92	1600	12.8	6.87	—	615	62.4	23.8	37.9	6.71	1	0.16	0.049	96.5	381	—	0.103	—	609.26	—	
n**		11	11	7	11	11	11	11	11	11	11	11	11	11	—	11	—	11	—	
max		19.60	6.87	233	832	62.4	23.8	103.0	7.48	3.15	0.20	1.960	103.0	429	—	0.229	—	663.94	—	
min		10.90	6.48	118	583	20.8	7.3	36.3	2.83	1.00	0.10	0.010	79.6	371	—	0.093	—	583.79	—	
avg		15.41		160	704	49.7	18.9	58.8	6.39	2.35	0.15	0.247	90.9	390	—	0.141	—	617.10	—	
std		2.81		43	69	14.9	5.7	24.4	1.24	0.63	0.03	0.576	7.5	20	—	0.038	—	22.020	—	
CV		18.25		27	10	29.97	30.26	41.5	19.43	26.62	19.9	233.1	8.3	5	—	26.9	—	3.6	—	

* Total Dissolved Solids (TDS) calculated
 ** Data from 2-5-91 not used in calculations

Piezometer 41B—Chemical Data

Date	Time	Temp (C)	pH	Eh (mV)	Cond.	Ca	Mg	Na	K	Cl	F	Fe	SO ₄	HCO ₃	CO ₃	Ba	Br	TDS*	TOC
2-5-91	1740	13.0	6.48	—	659	46.1	13.0	510	4.57	27.9	< 0.1	0.182	15.5	426	—	4.03	1	—	—
3-7-91	1650	12.0	6.61	—	658	47.2	14.4	58.3	3.74	30.0	0.2	0.004	14.9	405	—	1.75	1	575.53	—
4-3-91	1655	14.0	6.56	—	690	40.4	12.3	54.8	1.76	23.6	0.19	0.110	13.1	410	—	1.54	1	557.72	—
5-8-91	1540	18.3	6.70	151	604	46.8	14.3	53.6	3.37	27.4	0.05	0.299	9.32	405	—	1.73	1	561.91	—
6-5-91	1515	17.4	6.71	107	595	46.9	14.6	53.1	2.96	26.2	0.18	0.151	9.58	403	—	1.70	1	557.97	—
7-12-91	1235	17.4	6.86	49	621	50.0	15.3	55.5	3.79	23.6	0.22	0.539	8.62	407	—	1.88	1	566.93	—
8-7-91	1155	18.0	6.92	40	640	49.5	15.0	55.2	3.61	26.3	0.30	0.703	7.12	421	—	1.73	1	580.36	—
9-18-91	1215	18.2	6.97	13	635	47.6	14.5	51.1	3.58	24.4	0.23	0.372	6.35	425	—	1.55	1	574.24	—
10-8-91	1457	15.7	6.85	30	656	47.2	14.7	54.7	3.35	35.2	0.34	0.863	6.73	428	—	1.77	1	593.07	—
11-12-91	1240	12.6	6.86	-25	623	48.5	14.6	53.1	3.38	26.4	0.27	0.940	6.11	426	—	1.80	1	580.88	—
12-11-91	1231	14.2	6.93	-49	565	49.9	15.1	55.6	3.71	21.2	0.28	0.822	< 5	421	—	1.78	—	569.29	—
1-23-92	1630	12.4	6.90	—	584	48.5	14.4	53.7	3.69	24.4	0.25	0.762	< 5	416	—	1.74	—	563.46	—
n**		11	11	8	11	11	11	11	11	11	11	11	11	11	—	11	—	11	—
max		18.30	6.97	151	690	690	15.3	58.3	3.79	35.2	0.34	0.940	14.90	428	—	1.88	—	593.07	—
min		12.00	6.56	-49	565	565	12.3	51.1	1.76	21.2	0.05	0.004	0.00	403	—	1.54	—	557.72	—
avg		15.47		40	625	625	14.5	54.4	3.36	26.2	0.23	0.506	7.44	415	—	1.72	—	571.03	—
std		2.51		65	36	36	0.8	1.8	0.58	3.8	0.08	0.334	4.60	9	—	0.10	—	10.99	—
CV		16.20		165	165	5.83	5.44	3.39	17.34	14.35	33.7	66.1	61.8	2.3	—	5.83	—	1.93	—

* Total Dissolved Solids (TDS) calculated
 ** Data from 2-5-91 not used in calculations

Piezometer 41A—Chemical Data

Date	Time	Temp (C)	pH	Eh (mV)	Cond.	Ca	Mg	Na	K	Cl	F	Fe	SO ₄	HCO ₃	CO ₃	Ba	Br	TDS*	TOC
2-5-91	1700	13.5	6.73	—	12200	115	29.8	2400	19.4	4370	0.32	0.166	38.7	456	—	17.2	25	—	—
3-7-91	1600	13.0	7.20	—	23700	251	59.9	4230	31.4	7990	0.27	0.317	13.8	414	—	27.5	39	13018	—
4-3-91	1620	16.0	7.09	—	23700	273	58.9	3980	20.1	6600	0.27	0.244	24	311	—	27.4	37	11295	—
5-8-91	1616	17.4	6.91	48	27000	223	55.6	4950	24.0	8970	0.04	0.116	11.1	415	—	30.2	48	14679	—
6-5-91	1650	16.4	7.03	14	25500	271	67.4	5300	33.0	8553	0.21	0.004	15.8	420	—	44.5	49	14682	—
7-12-91	1307	17.2	7.01	41	27100	266	67.3	5350	34.2	8600	0.28	0.251	5.0	426	—	43.2	47	14792	—
8-7-91	1237	17.5	7.17	21	21500	189	48.1	3840	17.3	6200	0.39	0.181	11.8	482	—	26.5	35	10815	—
9-18-91	1255	17.1	7.04	24	30000	278	70.3	5380	31.3	9440	0.33	0.041	5.0	427	—	44.4	62	15676	< 1
10-8-91	1600	16.9	7.19	-17	30800	292	74.0	5720	31.1	9660	0.45	0.208	6.7	427	—	48.6	81	16260	< 1
11-12-91	1326	15.4	7.06	-28	25300	265	65.0	5100	25.7	9380	0.33	0.266	5.0	432	—	44.7	102	15318	—
12-11-91	1356	17.5	7.23	-22	19100	193	48.9	4070	22.0	6720	0.50	0.372	—	481	—	31.7	—	11567	—
1-23-92	1700	15	7.2	—	19900	233	56.6	4710	25.5	6360	0.50	0.473	—	488	—	39.3	—	11913	—
n**		11	11	7	11	11	11	11	11	11	11	11	11	11	—	11	9	11	—
max		17.50	7.23	48	30800	292	74.0	5720	34.2	9660	0.50	0.473	0.50	488	—	48.6	49	16260	—
min		13.00	6.91	-28	19100	189	48.1	3840	17.3	6200	0.04	0.004	0.04	311	—	26.5	27	10815	—
avg		16.31		15	24873	249	61.1	4785	26.9	8041	0.32	0.225	0.32	429	—	37.1	37	13638	—
std		1.39		28	3790	35	8.5	656	5.7	1335	0.14	0.138	0.14	48	—	8.5	8	1961	—
CV		8.54		191	15	14	13.9	14	21.1	17	41.8	61.5	41.8	11	—	22.8	23	14	—

* Total Dissolved Solids (TDS) calculated
 ** Data from 2-5-91 not used in calculations

CR1—Chemical Data

Date	Time	Temp (C)	pH	Eh (mV)	Cond.	Ca	Mg	Na	K	Cl	F	Fe	SO ₄	HCO ₃	CO ₃	Ba	Br	TDS*
5-8-91	1610	21	7.91	—	2240	237	162	18.5	10.4	8.76	0.02	0.207	1170	312	—	0.0815	< 1	1919

APPENDIX 7: Geochemical Modeling Data

	<i>I1A</i>	<i>I1B</i>	<i>I1C</i>	<i>I2A</i>	<i>I4A</i>	<i>I21A</i>	<i>I22A</i>	<i>I22B</i>	<i>I31A</i>	<i>I31B</i>	<i>I41A</i>	<i>I41B</i>
<i>Barite</i>	-1.3568	0.4204	0.2323	0.8568	0.5854	-0.0580	-0.7616	0.8240	0.6253	0.7441	0.7893	0.7983
<i>Calcite</i>	-0.1717	-1.0887	-2.3431	-0.4295	-1.6395	-1.6752	-0.4201	-0.9414	-3.2978	-0.5711	-0.0255	-0.4991
<i>Goethite</i>	6.5848		2.1709	2.3947		1.9426	7.0082	4.7779	4.4696	2.3474		2.2590
<i>Fluorite</i>	-1.9634	-2.3424	-3.1533	-1.6133	-2.1998	-2.6033	-2.3276	-3.0596	-1.9035	-2.2391	-1.5937	-2.0024
<i>Pyrite</i>	-109.7100		-63.2006	-75.2881		-74.7670	-104.21	-83.0406	-86.3723	-69.6129		-47.0622
<i>Silica</i>	-1.1839	-0.7855	-0.8787	-0.9254	-0.9271	-2.7710	-1.2025	-1.1195	-1.1195	-0.7824	-0.4693	-0.7431
<i>Kaolinite</i>	5.3273	5.5889	5.8530			5.8613	5.4508	5.4367	5.4367	6.7342	9.3109	6.2120
<i>Feldspar</i>	1.2286	0.3767	-0.1990			0.0291	1.2495	0.7424	0.7424	1.5898	4.2900	1.2070
<i>Chlorite</i>	-1.2421	-12.049	-17.5763			-15.2773	-1.6262	-6.1751	-6.1751	-8.3475	-2.1236	-8.7574
<i>Siderite</i>	-1.8465		-2.0057	-2.1654		-2.7710	-1.1907	-4.6715	-4.6715	-2.1229		-0.5829
<i>CO₂(g)</i>	-3.1249	-1.4292	-1.4300	-1.2137	-0.9606	-1.3213	-3.1467	-5.0269	-5.0269	1.3780	-1.6534	-1.4090
<i>O₂(g)</i>	-39.8931	-53.8334	-49.9292	-47.7331	-51.5286	-47.6156	-40.9264	-44.2715	-44.2715	-48.2945	-54.9309	-54.8997

Saturation indices for selected minerals and gases in water samples calculated by PHREEQE.

Values greater than 0 indicate solution is supersaturated.

Values less than 0 indicate solution is undersaturated.

Reaction Path Simulation 1

<i>Precipitation and IIC</i>		
Ca	0.374	0.016
Mg	0.332	0.002
S	0.397	0.019
C	1.08	0.336
Na	0.229	0.006
Fe	0.008	0.000
K	0.049	0.001
Calcite	Ca 1.0	C 1.0
Siderite	Fe 1.0	C 1.0
Chlorite	Mg 3.0	
Pyrite	Fe 1.0	S 2.0
CO ₂ gas	C 1.0	
Ion Exchange	Ca -1.0	Na 2.0
K-spar	K 1.0	
<i>Delta Phases</i>		
Calcite		.4695
Siderite		-.1810
Chlorite		.1100
Pyrite		.1890
CO ₂ gas		.4555
Ion Exchange		.1115
K-spar		.0480

Reaction Path Simulation 2

<i>Precipitation and IIC</i>		
Ca	0.374	0.016
Mg	0.332	0.002
S	0.397	0.019
C	1.08	0.336
Na	0.229	0.006
Fe	0.008	0.000
K	0.049	0.001
Calcite	Ca 1.0	C 1.0
Goethite	Fe 1.0	
Chlorite	Mg 3.0	
Pyrite	Fe 1.0	S 2.0
CO ₂ gas	C 1.0	
Ion Exchange	Ca -1.0	Na 2.0
K-spar	K 1.0	
<i>Delta Phases</i>		
Calcite		.4695
Goethite		-.1810
Chlorite		.1100
Pyrite		.1890
CO ₂ gas		.2745
Ion Exchange		.1115
K-spar		.0480

Reaction Path Simulation 3

<i>Sample PZ 11C and 11A</i>		
Ca	0.036	0.374
Mg	0.014	0.332
S	0.038	0.397
C	7.57	1.08
Na	7.31	0.229
Fe	0.001	0.008
Ba	0.002	0.005
F	0.007	0.005
Si	0.104	0.21
Calcite	Ca 1.0	C 1.0
Goethite	Fe 1.0	
Ion Exchange	Mg 1.0	Na 2.0
Siderite	Fe 1.0	C 1.0
FeS ₂	Fe 1.0	S 2.0
Ion Exchange	Ca -1.0	Na 2.0
Ion Exchange	Ba -1.0	Na 2.0
Ion Exchange	F -1.0	
Kaolinite	Si 2.0	Al 2.0
<i>Delta Phases</i>		
Calcite		2.8815
Goethite		-3.4360
Ion Exchange		.3180
Siderite		3.6085
FeS ₂		-.1795
Ion Exchange		3.2195
Ion Exchange		.0030
Ion Exchange		-.0020
Kaolinite		-0.530

Reaction Path Simulation 4

<i>Sample PZ 11C and 11A</i>		
Ca	0.036	0.374
Mg	0.014	0.332
S	0.038	0.397
C	7.57	1.08
Na	7.31	0.229
Fe	0.001	0.008
Ba	0.002	0.005
F	0.007	0.005
Si	0.104	0.21
Calcite	Ca 1.0	C 1.0
Goethite	Fe 1.0	
Ion Exchange	Mg -1.0	Na 2.0
Siderite	Fe 1.0	C 1.0
FeS	Fe 1.0	S 1.0
Ion Exchange	Ca -1.0	Na 2.0
Ion Exchange	Ba -1.0	Na 2.0
Ion Exchange	F -1.0	
Kaolinite	Si 2.0	Al 2.0
<i>Delta Phases</i>		
Calcite		.28815
Goethite		-3.2565
Ion Exchange		.3180
Siderite		3.6085
FeS		-.3590
Ion Exchange		3.2195
Ion Exchange		.0030
Ion Exchange		-.0020
Kaolinite		-.0530

<i>Ion</i>	<i>31B</i>	<i>11A</i>	<i>Calculated Mix</i>	<i>31A</i>	<i>Percent Error</i>
Concentration	11.72	11.63	11.66	12.67	-8.01
Mg	1.71	0.03	0.39	0.38	3.99
Ca	2.72	0.07	0.65	0.83	-22.08
Na + K	2.49	7.34	6.29	6.93	-9.27
HCO ₃ + CO ₃	5.31	7.81	6.74	6.65	1.34
SO ₄	2.12	0.08	0.95	0.83	13.85
Cl	0.06	0.13	0.10	0.43	-77.15
Mixing factors	28.85%	71.15%			

Output from HC-Gram binary mixing model. Concentrations are in equivalents per million.